1. Report No.	2. Government Accession No.	3. Recipient's Catalog No.
FHWA/LA.09/448		

4. Title and Subtitle	5. Report Date
Transport, Speciation, Toxicity, and Treatability of Highway Stormwater Discharged to Receiving Waters in Louisiana	January 2013
	6. Performing Organization Code LTRC Project Number: 01-3ENV State Project Number: 736-99-0922

7. Author(s)	8. Performing Organization Report No.
Dr. John Sansalone, Dr. Frank Cartledge	

9. Performing Organization Name and Address	10. Work Unit No.
Department of Civil and Environmental Engineering Louisiana State University Baton Rouge, LA 70803	11. Contract or Grant No.

12. Sponsoring Agency Name and Address:	13. Type of Report and Period Covered
Louisiana Department of Transportation and Development P.O. Box 94245 Baton Rouge, LA 70804-9245	Final Report, 04/27/04 – 02/17/11
	14. Sponsoring Agency Code

15. Supplementary Notes

16. Abstract

Stormwater from transportation land uses is a complex heterogeneous mixture of particulate matter, nutrients (phosphorus and nitrogen), heavy metals, inorganic, and organic compounds with variations in flow and mass loadings by orders of magnitude during a single hydrologic event. To effectively manage stormwater, the transport, toxicity, and viability of treatment must be examined. Management is particularly challenging in Louisiana where many transportation-related discharges are directly to receiving waters. This study investigated: (1) transport and treatability of particles and phosphorus in urban rainfall-runoff on an event-basis, (2) influence of hydrology on rainfall-runoff metal element speciation, (3) toxicity of particulates in urban rainfall-runoff, (4) event-based treatability with hydrodynamic separation, and (5) gravimetric evaluation of hydrodynamic separation. With respect to transport and treatability of particles and phosphorus in urban rainfall runoff, a screened hydrodynamic separator (HS) was used on a test site draining the bridge deck on the I-10 over City Park Lake in Baton Rouge, Louisiana. Mass separation efficiencies (from 38 percent to 70 percent for particles and 8 percent to 49 percent for total phosphorus) of the screened HS and coarse particle size distributions (d_{50m} of 270 to 2202 μm) exhibited very large variability. Regarding the influence of hydrology on rainfall runoff metal element speciation, it was found that Cd and Zn dominated the dissolved species, while Pb was predominately associated with dissolved organic matter and Cu was predominately associated with carbonate species or DOM. The toxicity of particulates in runoff is a concern because many chemicals are bound to particles and transported through the aquatic environment. Early post-larvae life stages are more sensitive to toxicity from runoff containing particulates. Testing of screened HS units revealed that suspended sediment concentration treatment efficiency were generally less than 50 percent even when units were cleaned after every treatment event to ensure no scour. Treatment is a function of surface loading rate, screen size, and scour. After extensive testing of screened HS units, results indicated that treatment and maintenance requirements were not sustainable and, therefore, four additional green infrastructure treatment designs were examined. These results indicated that either Buoyant Adsorptive Media (BAM) filters in the lake or cementitious permeable pavement (CPP) with a BAM network met treatment requirements, were sustainable, and provided context-sensitive implementation.

17. Key Words	18. Distribution Statement
Stormwater, runoff, toxicity, green infrastructure, particulate matter, permeable pavement	**Unrestricted. This document is available through the National Technical Information Service, Springfield, VA 21161.**

19. Security Classif. (of this report)	20. Security Classif. (of this page)	21. No. of Pages	22. Price
None	None	250	

Project Review Committee

Each research project has an advisory committee appointed by the LTRC Director. The Project Review Committee is responsible for assisting the LTRC Administrator or Manager in the development of acceptable research problem statements, requests for proposals, review of research proposals, oversight of approved research projects, and implementation of findings.

LTRC appreciates the dedication of the following Project Review Committee Members in guiding this research study to fruition.

LTRC Manager

Chester G. Wilmot

Special Studies Research Manager

Members

Ed Bodker

Gregory du Cote

Curtis Fletcher

Vince Russo

Directorate Implementation Sponsor

William B. Temple

Transport, Speciation, Toxicity, and Treatability of Highway Stormwater Discharged to Receiving Waters in Louisiana

by

John Sansalone, Ph.D.
Frank Cartledge, Ph.D.

Department of Civil and Environmental Engineering
Louisiana State University
Baton Rouge, LA 70803

LTRC Project No. 01-3ENV
State Project No. 736-99-0922

conducted for

Louisiana Department of Transportation and Development
Louisiana Transportation Research Center

January 2013

EXECUTIVE SUMMARY

Stormwater from transportation land is a complex heterogeneous mixture of particulate matter, nutrients (phosphorus and nitrogen), heavy metals, inorganic and organic compounds with variations in flow, and mass loadings by orders of magnitude during a single hydrologic event. This complexity has made stormwater challenging to understand and manage. To ensure effective management in light of the recent National Pollutant Discharge Elimination System (NPDES) Phase II stormwater regulations and total maximum daily loads (TMDLs), issues associated with the transport and toxicity as well as viability of treatment and cost/benefit alternatives must be examined. Management is particularly challenging in Louisiana where many transportation-related discharges are directly to receiving waters. This final report is separated into five chapters. These chapters are: (1) transport and treatability of particles and phosphorus in urban rainfall-runoff on an event-basis; (2) influence of hydrology on rainfall-runoff metal element speciation; (3) toxicity of particulates in urban rainfall-runoff; (4) event-based treat-ability with hydrodynamic separation, and (5) gravimetric evaluation of hydrodynamic separation. These chapters are summarized below.

1) Transport and Treatability of Particles and Phosphorus in Urban Rainfall Runoff

This study examined the event-based removal performance of a small footprint screened hydrodynamic separator (HS) for particulate matter and phosphorus (P) transported in eight actual rainfall-runoff events. The studied urban source area was (1088-m^2) located underneath I-10 City Park Lake Bridge in Baton Rouge, LA. Mass separation efficiencies (from 38% to 70% for particles; and 8% to 49% for total phosphorus) of the screened HS and rainfall-runoff particle size distributions (d_{50m} of 270 to 2202 μm) exhibited very large variability. Overall particle separation efficiency (PSE) of the screened HS was compartmentalized into higher separation capability for sediment fraction (> 75 μm) of particulate matter ranging from 76% to 94%. The PSE was much lower and highly variable from 3% to 57%, and 1 to 43% for settleable (25 – 75 μm) and suspended (1 – 25 μm) fractions respectively. Similar removal trends were demonstrated for total phosphorus. The higher removal efficiencies occurred for sediment-bound P (approximately 60%), lower removal efficiency for settleable-bound P (mostly 30 to 60%) and the lowest removal efficiency for suspended bound P and dissolved P (10% or less, at times statistically insignificant from 0). Particle and phosphorus separation performance of a screened

HS was far more strongly affected by influent particle size distribution (PSD) than by hydrologic and hydraulic conditions. The results of PSDs for the screened HS particles also illuminated the fundamental differences in the role of screened and volute area of the screened HS for overall particle and phosphorus separation performance. Frequent maintenance is required for this system to ensure against scour and reducing redox conditions and hydrologic control is not provided by the screened HS.

2) Influence of Hydrology on Rainfall-Runoff Metal Element Speciation

Examination of speciation for metal elements transported in urban rainfall-runoff events is critical when evaluating the potential fate, bioavailability, and effective control of such constituents. In many urban areas anthropogenic activities result in rainfall pH levels that are acidic and low in alkalinity. As a result, finely abraded metallic components and exposed metal infrastructure can be leached into the rainfall-runoff. This study examined the influence of hydrology on stormwater metal element speciation at the upper end of a Portland cement concrete (PCC) small urban watershed. This study focused on lead (Pb), cadmium (Cd), copper (Cu), and zinc (Zn); metal elements commonly found in urban and transportation land uses. For this site, partitioning results demonstrated that Cd and Cu partitioned nearly equally between particulate and dissolved phases, while Zn was generally particulate-bound and Pb was highly particulate-bound. Utilizing water quality analyses, measured ion balances, and speciation modeling, results for Cd and Zn indicated that divalent ionic forms of these metals dominated the dissolved species for all events, while Pb was predominately associated with dissolved organic matter (DOM), and Cu was predominately associated with carbonate species or DOM. Of the three events examined, only the mass-limited events demonstrated a change in speciation during the passage of the hydrograph. Results from this study indicate that effective control of stormwater metal elements at the upper end of the urban watershed requires unit operations and processes that account for the ionic, complexed, and particulate-bound species and account for the hydrology at the upper end of the urban watershed.

3) Toxicity of Particulates in Urban Rainfall Runoff

Particulate matter transported by the urban rainfall-runoff is a hetero-disperse mixture of particles. These particles are a potential concern not only because of the environmental and ecological issues related to particles, but also since many contaminants are bound to the surface of particles and transported through the aquatic environment. This study examined rainfall-runoff events captured from an instrumented MS4 watershed. In this study, the early life stage aquatic species of fathead minnows and channel catfish were utilized. The early post-larvae life stages are more sensitive to toxicity from runoff containing particulates. The possible routes for toxicant entry in fish include direct uptake across the gills, uptake by the skin, and through ingestion of particles. Post-larvae stages may ingest the proper size fine particles which could cause secondary exposure through the intestine. For the juvenile and adult fish, ingestion is not likely as an exposure pathway for fine particles. But the epithelial tissues in gills are able to trap the suspended particles which are less than 25 μm. As the species matures these particles become less acutely toxic to juvenile and adult stage fish. Untreated runoff (as opposed to filtered runoff) containing suspended, settleable, and sediment particles can result in acute and chronic toxicity in addition to dissolved contaminants such as metals which are readily bioavailable.

A dynamic partitioning process occurred between dissolved and particulate phases all the time and it was very difficult to separate them or consider each of them alone. Untreated runoff had higher accumulative mortalities than runoff treated through only physical filtration, indicating the role of particulates on toxicity since the sand filter material did not reduce the soluble contaminant concentrations. LT_{50} and NOET values indicated that higher particulate loads associated with mass-limited events were most toxic; and for mass-limited events that toxicity decreased across the event. Soluble and particulate-bound metals had a toxicity impact on early-life stage aquatic species since these species are potentially exposed to particulate and particulate bounded chemicals through gill and ingestion. Fine particles with size range less than 25 μm were easily trapped by gill tissue. Oxygen consumption results indicate as total particulate concentrations increase, the suspended particles were more toxic than settleable and sediment particles. The adverse effect on gill function

including abrasion, coughing, hyperventilation or increase metabolism energy demand was not recoverable. No difference of aquatic species oxygen consumption rate under settleable and sediment loads suggested that settleable and sediment particles was not sufficient to significantly impact gill function. Information in this paper is helpful in selecting better BMPs for controlling the particulate quality of runoff through a unit operation and process design for toxicity reduction.

4) Testing of the Hydrodynamic Separator (HS) "L-Unit"

From April 2004 through June 2004, a standard full-scale HS "L-Unit" with a 2400-μm screen was tested on rainfall runoff from the I-10 bridge over City Park Lake in Baton Rouge, Louisiana. Testing was based on the December 23, 2003, New Jersey memorandum. In addition to the New Jersey testing requirements, examinations included a 10% steady-flow operating rate, measured particle gradations for the effluent and "L-Unit" captured particles, treatment run mass balances, turbidity analyses, particle density, and total dissolved solids. All gradations were generated from the same sub-batches of US silica materials and suspended and tested with potable tap water.

Results indicate that the Total Suspended Solids (TSS) (expressed as suspended sediment concentration, SSC) treatment efficiency ranged from 22 to 44% across all influent loadings. While a decrease in treatment efficiency was consistently observed with increasing flowrate for the specified influent particle size gradation, regardless of influent gravimetric concentration (100-300 mg/L), the decreasing trend was relatively weak given the range of flow rates tested (10-125% of 150 gallons/minute). Interestingly, these relatively consistent treatment efficiency results indicated that lower influent gravimetric concentrations resulted in higher treatment efficiency for the "L-Unit." Given the fine particle size gradation, the small footprint standard "L-Unit" with a 2400-μm screen trapped coarse particles over a wide range of flow rates without screen blinding. The two washout runs with clean influent tap water indicated that (1) re-suspension and elution of captured sump particles occurs without a larger capacity sump and/or shear/baffle plates, and (2) a full sump results in far greater elution for a given flow rate and gradation than a sump that was half-full.

5) Gravimetric Evaluation of a PMSU20_20 Hydrodynamic Separator

From September 2005 through December 2005, a PMSU20_20 hydrodynamic separation unit with the 2400-μm screen, the 4700-μm screen, and control (no screen) was tested at the Baton Rouge test site. The testing evaluations involved loadings at 10, 25, 50, 75, 100 and 125% of design flow (1.1 cfs). Examinations included measured particle gradations for influent, effluent, captured screen area and volute area particles, treatment run material balance error by mass, hydraulic profiles and turbidity analyses. All particle gradations were generated from the same sub-batches of US Silica materials and generated the same tested size gradation. Particle gradations were suspended and tested in potable water.

The total of 66 performance tests were conducted for a PMSU20_20 in three configurations consisting of 60 in., 72 in., and 84 in. diameters, respectively, at constant flows from 10 to 125% of design flow rate, at nominal influent concentrations of 100, 200, 300 mg/L with the New Jersey Corporation for Advanced Technology (NJCAT) tested gradation and potable water, for a nominal volumetric loading of 7,500 gallons. Full measured mass balances were performed for each evaluation at a required material balance error of < 10% by dry mass.

The results presented in this report demonstrate that the performance of the PMSU20_20 was mainly dependent on the surface loading rate, the screen size, and the coarseness and hetero-dispersivity of the gradation. A decrease in treatment efficiency was consistently observed with increasing flow rate for all tested diameters for the specified influent particle size gradation, regardless of influent gravimetric concentration (100-300 mg/L), and particles less than 250 μm were eluted from the unit. Equal weighting of incremental efficiencies resulted in a calculated arithmetic mean efficiency for the 60-in. PMSU20_20 of 51.5% over the tested flow range of 26 gpm to 338 gpm. Given the PMSU20_20 configurations with 60, 72, 84 in. diameters, and loading conditions; 50% separation efficiency of SSC occurred at 168, 232, and 372 gpm, respectively.

This evaluation leads to several observations: (1) volute area (50% to 80% of captured mass) contributed significantly to overall SSC removal for the tested

configuration and conditions although this dependence on volute area for particle separation varies depending on unit diameter and screen aperture size; (2) the 2400 µm screen enhanced the performance of the screen area and reduced the dependence on volute area for overall SSC removal; and (3) particle separation performance by screen area was a function of operating flow rates. Results illustrate the role of volute area and the improvements provided by smaller screen aperture. Overall performance of the PMSU20_20 can be improved through use of a 500- to 1200-µm screen, larger volute, a sediment weir, a larger sump volume, and frequent maintenance to reduce scour and changing water chemistry in the sump between events.

6) Green Infrastructure Design and Synthesis for Implementation

Management of urban rainfall-runoff (stormwater) represents a significant challenge requiring economic resources equal to or greater than domestic wastewater. The complexity and challenges of urban stormwater management, beyond mitigating flooding, are now recognized as embodied in current debates over total maximum daily loads (TMDLs) and discharge criteria for nutrients, metals, particulate matter (PM), pathogens, and emerging constituents. While managing stormwater from at-grade pavement systems is challenging, management of elevated pavement systems such as the I-10 bridge represents an even more difficult challenge. Southeastern states, in particular coastal and the expansive inland receiving waters of peninsular Florida and South Louisiana, have been traversed by contemporary transportation infrastructure often elevated with direct discharges to receiving waters. Nutrients, metals, and PM are directly discharged to receiving waters with the potential to generate acute and chronic toxicity. Conventional stormwater designs typically require detention/retention, are land-intensive, and can be at odds with the context-sensitive nature of land-water interfaces that require innovative design solutions.

By utilizing this context, design alternatives are illustrated. These designs were focused on nutrients, metals, and particulate matter (PM) management from a typical interstate bridge on I-10, discharging rainfall-runoff to City Park Lake in Baton Rouge. As an urban crown jewel, the lake drives surrounding up-scale redevelopment in the local area. Four treatment designs were examined: (1) conventional clarification and filtration, (2) engineered oxide-admixture cementitious

permeable pavement (CPP), (3) a network of Buoyant Adsorptive Media (BAM) filters in the lake, and (4) CPP and a BAM network. The high maintenance, scour potential, deteriorating inter-event water chemistry, and lower inter-event treatment efficiency of the screened hydrodynamic separator units did not make such units viable treatment solutions compared to the four treatment designs illustrated. The metrics that characterize the preferred design treatment solution demonstrated that the selected option provided a significant reduction in total nitrogen (TN), total phosphorus (TP), metals, and PM loading to the receiving water while meeting regulatory criteria at a lower cost/benefit ratio with respect to design alternatives. However, it was important to note that, in a popular recreational area, the aesthetic benefit of low footprint treatment options was also of significant value as a context-sensitive attribute. Based on data analysis and process modeling, the BAM network was the most economical solution, followed by CPP. Treatment and load reduction targets are achieved for the recommended BAM design and CPP with BAM network. Costs are lower than conventional treatment or current treatment databases. While BAM filters were preferred to CPP in terms of economics, BAM filters are preferred to conventional treatment as they provided a smaller footprint. In addition, a portion of the BAM filters were hidden from view below the water surface. The CPP combined with the BAM filters provided both primary and secondary treatment adding redundancy to the system, providing a higher total treatment. The reduction in TP, TN, and PM loading provided by the BAMs network closely followed by the 2 in. of CPP design options reduce eutrophication, turbidity, and metal discharges into City Park Lake, thereby providing aesthetic and water chemistry benefits. In addition, the removal of nutrients will help return the lake towards the ecological diversity of Bayou Duplantier. Although this design illustrated results for TN and TP, the BAM and CPP were also effective adsorptive systems for dissolved and particulate-bound metals. The integration of manganese oxide as a media coating for the BAMs and as an admixture in the CPP provided significant metal adsorption capacity as well as filtration by these design options. The adsorption of metals, such as Zn, Cu, and Cd, whether in the BAM filters or the CPP, will benefit the ecology of the lake and prevent bio-magnification of metals. Detailed design options, feasibility, and costs are illustrated for the I-10 bridge over City Park Lake. There are over 10,000 bridges in Louisiana of which over 80% are over water, providing significant potential for extensibility of these design results to infrastructure crossing land-water interfaces across Louisiana.

ABSTRACT

Stormwater from transportation land uses is a complex heterogeneous mixture of particulate matter, nutrients (phosphorus and nitrogen), heavy metals, inorganic, and organic compounds with variations in flow and mass loadings by orders of magnitude during a single hydrologic event. To effectively manage stormwater, the transport, toxicity, and viability of treatment must be examined. Management is particularly challenging in Louisiana where many transportation-related discharges are directly to receiving waters. This study investigated: (1) transport and treatability of particles and phosphorus in urban rainfall-runoff on an event-basis, (2) influence of hydrology on rainfall-runoff metal element speciation, (3) toxicity of particulates in urban rainfall-runoff, (4) event-based treatability with hydrodynamic separation, and (5) gravimetric evaluation of hydrodynamic separation. With respect to transport and treatability of particles and phosphorus in urban rainfall runoff, a screened hydrodynamic separator (HS) was used on a test site draining the bridge deck on the I-10 over City Park Lake in Baton Rouge, Louisiana. Mass separation efficiencies (from 38 percent to 70 percent for particles and 8 percent to 49 percent for total phosphorus) of the screened HS and coarse particle size distributions (d50m of 270 to 2202 μm) exhibited very large variability. Regarding the influence of hydrology on rainfall runoff metal element speciation, it was found that Cd and Zn dominated the dissolved species, while Pb was predominately associated with dissolved organic matter and Cu was predominately associated with carbonate species or DOM. The toxicity of particulates in runoff is a concern because many chemicals are bound to particles and transported through the aquatic environment. Early post-larvae life stages are more sensitive to toxicity from runoff containing particulates. Testing of screened HS units revealed that suspended sediment concentration treatment efficiency were generally less than 50 percent even when units were cleaned after every treatment event to ensure no scour. Treatment is a function of surface loading rate, screen size, and scour. After extensive testing of screened HS units, results indicated that treatment and maintenance requirements were not sustainable and, therefore, four additional green infrastructure treatment designs were examined. These results indicated that either Buoyant Adsorptive Media (BAM) filters in the lake or cementitious permeable pavement (CPP) with a BAM network met treatment requirements, were sustainable, and provided context-sensitive implementation.

IMPLEMENTATION STATEMENT

Restraints should be exercised while implementing results from this work, especially when attempting to compare the performance of the screened Hydrodynamic Separator (HS) to other structural Unit Operations and Processes (UOPs), or to another screened HS with different internal configurations and/or unit dimensions. The reasons are that watersheds of concern may also have substantially different parameters such as demographic, traffic, pavement surface and runoff characteristics, sources of particulate matter with different physical and chemical nature, and dissimilar hydrologic and hydraulic transport patterns. This would highlight the importance of influent particle size distribution analyses in order to make an accurate assessment of separation performance for any Best Management Practice (BMP) in interest, especially for the ones whose separation mechanisms are largely or in part dependent on gravitational settling (i.e., detention/retention pond, dry/wet basin).

Rainfall-runoff transports a wide range of particulate matter (from 1^{-} µm to $10{,}000^{+}$ µm). Phosphorus and metals not only distributes among all sizes of particles but also partitions between the particulate bound phase and solution phase. While screened hydrodynamic separation was considered in early field studies, results indicated that this treatment option would not be a viable solution. Therefore four treatment designs were examined in detail as part of this study. The high maintenance, scour potential, deteriorating inter-event water chemistry and lower inter-event treatment efficiency of the screened hydrodynamic separator units did not make such units viable treatment solutions compared to the four treatment designs illustrated. The metrics that characterize the preferred design treatment solution demonstrated that the selected option provides a significant reduction in TN, TP, metals and PM loading to the receiving water while meeting regulatory criteria at a lower cost/benefit ratio with respect to design alternatives.

However, it is important to note that, in a popular recreational area, the aesthetic benefit of low footprint treatment options is also of significant value as a context-sensitive attribute. Based on data analysis and process modeling, the BAM network is the most economical solution, followed by CPP. Treatment and load reduction targets are achieved for the recommended BAM design and CPP with BAM network. Costs are lower than conventional treatment or current treatment databases. While BAM filters are preferred to CPP, BAM filters are preferred to conventional treatment as they provide a smaller footprint. In addition, a portion of the BAM filters are hidden from view below the water surface. The CPP

combined with the BAM filters provides both primary and secondary treatment adding redundancy to the system and providing a higher total treatment.

TABLE OF CONTENTS

LIST OF TABLES

LIST OF FIGURES

INTRODUCTION

Receiving water quality degradation due to urban rainfall-runoff has received increasing attention over the last a few decades. Consequently, implementation of various structural treatment controls is becoming more widespread (James, 1999). This implementation has been further accelerated in the United States by the application of March 2003 enactment of NPDES Stormwater Phase II Regulations.

While a number of separation mechanisms occur in stormwater controls, gravitational sedimentation continues to be a predominant unit operation for urban stormwater. Previous studies have reported solids reductions measured as total suspended solids (TSS) as a result of extended detention range from 50-70 percent (Hartigan, 1989). However, rapid urbanization and expansion of urban land uses cause restrictive urban infrastructure condition or limited land area for unit operations and processes (UOPs) to control pollutants from urban rainfall-runoff. The increasing cost of urban land, in part, also has led to consideration of stormwater pollutant load reductions by smaller structured UOPs. One class of stormwater control systems, requiring small urban surface areas while providing a required water quality benefit, is screened hydrodynamic separator (HS). By 2003, over 2,500 screened HS stormwater units, including combined sewer overflow (CSO) units, were installed worldwide with approximately 1,300 units throughout the United States and Canada. Despite the increasing application of these systems, their performance is rarely examined other than through event mean gravimetric results due to highly unsteady urban rainfall-runoff with variable granulometry. Literature reviews also illustrate that independent, peer-reviewed published results and in-depth analysis beyond a “black-box” examination of these systems are rare.

The entrainment and transport of anthropogenic constituents such as metal elements is controlled by dry depositional processes (Wu et al., 1998), physiochemical interactions between water and the various phases of solids, suspension of constituents by turbulent water flow, and aquatic chemistry (Deletic and Maksimovic, 1998). The interaction of these processes dictates the phase of each runoff constituent. Dissolved metals are of particular concern for acute impacts since dissolved metals can be readily assimilated by aquatic biology (Yousef et al., 1985). However, once metals partition into the particulate phase, they have long-term potential of accumulation in waterways and can be transported through the aquatic environment with the potential for repartitioning to the dissolved phase (Sansalone,

2002). Due to the relatively acidic nature of rain in many urban areas, metals have the potential to leach into the dissolved phase at the upper end of the urban watershed as a function of residence time, pH, alkalinity and the nature and extent of entrained solids (Sansalone et al., 1997; Revitt et al., 1987). Previous research has suggested that the Pb and Cu species leached after contact with acidic rain are complexed by organic matter or partition to suspended solids, while Cd and Zn remain primarily in solution (Morrison et al., 1990). In contrast to asphalt pavement, the acidic rain may be quickly buffered to a relatively neutral pH (ranging from 6.7 to 7.5) upon contact with the Portland cement concrete (PCC) pavement, potentially reducing the overall ionic metal species in runoff (Sansalone et al., 1997). Dissolved metal complexes are often categorized as electrochemically available, chelex removable and strongly bound. The chelex removable species are readily taken up by aquatic biota and include ionic species of metals as well as weakly bound organic species (Morrison et al., 1989). Strongly bound metals are less toxic, forming complexes with hydroxides, carbonates and dissolved organic matter (DOM), which acts as a biogenic chelator (Ammann, 2001).

Toxicity of particulate matter in stormwater runoff causes increasing concern not only because of the environmental and ecological issues related to solid itself, but also since many contaminants are bounded on the surface of these particles and transported through the aquatic environment (Sansalone, 2002). Anthropogenic activities and infrastructure, in particular, transportation and maintenance regimes are significant contributory sources of particulate matter ranging from sub-micron particles to gravel size material (Sansalone et al., 1998; Muschack, 1990). Particulate contaminants in the water column are toxic to fish and other aquatic life. Improper highway construction practices created episodes of muddy water in karst springs, which caused a large number of trout deaths due to clogged fish gills (Werner, 1983). Construction of an interstate in West Virginia resulted in large quantities of silt and clay washing into a system of caverns, resulting in killing a large number of trout due to silt build-up on their gills (Garton, 1977). Particulate matter is also a significant reservoir for both chemical constituents and toxicity (Gjessing et al. 1984; Makepeace 1995). In addition to increasing the turbidity in receiving waters, suspended solids may act as a substrate on which toxic materials may be absorbed, transported, and released into receiving waters (McKenzie and Irwin, 1983). Particulate matter entrained as suspended or bed load material in runoff may settle in receiving waters interacting with natural sediment in the deposition and re-suspension cycles of streams, impact biota, and deplete dissolved oxygen while reducing conveyance capacities and increasing dredging frequencies (Breault and

Granato, 2000). Binding to sediment particles alters the bioavailability and toxicity of contaminants. Although a contaminant dissolved in interstitial water may affect biota similarly to dissolved contaminants in the water column, the toxicity of the same contaminant when particle-bound is poorly understood. A primary difficulty in examining the relative toxicity of interstitial versus particle-bound contaminants has been the inability to manipulate their concentration separately. Some studies have inferred the relative toxicity of particle-bound contaminants from indirect evidence (Langston, 1984; Swartz et al., 1985a).

Adverse effects on aquatic ecosystems may result from toxicant exposure that directly causes the death of an organism (acute effects) or produces sublethal effects on the organism's ability to develop, grow, and reproduce in the ecosystem (chronic effects). To identify and control toxic inputs to aquatic systems requires that laboratory toxicity tests be performed and that pollutant levels are extrapolated from these laboratory-derived data that can be deemed "safe" for aquatic ecosystems. Although there have been many studies on the toxic effects of pollutants in the dissolved phase, the action of particulate matter has received less attention, especially for the particles from stormwater runoff. This approach utilizes two economically and ecologically important species, freshwater fathead minnows (*Pimephales promelas*) and channel catfish (*Ictalurus punctatus*), to address toxicity of particulate matter in urban stormwater. Information of this study is critical for effective treatability for toxicity reduction, control and regulatory frameworks for stormwater discharges, and the receiving environment.

OBJECTIVE

The primary objective of this study was to gain a greater understanding of transport, treatability, speciation, and toxicity of highway stormwater discharged to receiving waters in Louisiana. Under such an umbrella, this final report addresses: (1) transport and treatability of particles and phosphorus in urban rainfall-runoff, (2) the influence of hydrology on rainfall-runoff metal element speciation, (3) toxicity of particulates in urban rainfall-runoff, (4) the testing of the hydrodynamic separator (HS) "L-Unit," and (5) the gravimetric evaluation of the hydrodynamic separator Precast Manhole Stormwater Unit (PMSU20_20).

Transport and Treatability of Particles and Phosphorus in Urban Rainfall-runoff

The main goal was to evaluate the screened HS performance in separating particulate matter and phosphorus. The first objective was to evaluate the transport and treatment of rainfall-runoff by capturing the entire event volume, which is quality assured and controlled by statistically enough numbers of full flow cross-sectional manual sampling. The second objective was to examine the event-based separation performance of the screened HS on particles (size gradations from 1^{-} to $10{,}000^{+}$ μm) and phosphorus transported by rainfall-runoff. The third objective was to differentiate the transport and treatability of varying fractions of phosphorus and particle fractions (sediment, settleable, and suspended) to the screened HS. The last objective was to examine the impact of influent particle gradation on the performance of the screened HS under dynamic conditions of real rainfall-runoff event.

Influence of Hydrology on Rainfall-runoff Metal Element Speciation

There were three objectives of this part of the study. The first objective included the summarization and compilation of water quality data at an I-10 experimental site in Baton Rouge, a site typical of the Gulf Coast area. The second objective was to examine temporal partitioning of heavy metals (Pb, Cd, Cu, and Zn) at the experimental site as a function of hydrology. Water quality analysis required for partitioning and speciation investigations included pH, conductivity, redox potential, temperature, alkalinity, dissolved and particulate metal concentrations, PO_4^{-3}, NO_3^{-}, SO_4^{-2}, Cl^{-}, dissolved organic carbon (DOC), suspended solids concentrations (SSC), and total dissolved solids (TDS). Flow rates, rainfall intensity and traffic counts were recorded during each storm event to examine delivery of metal

elements. The final objective was to examine the speciation of Cd, Cu, Pb, and Zn as a function of time for each event to investigate hydrologic influences. Metal speciation was studied using a computer-aided model simulating the formation of metal complexes under specified rainfall-runoff conditions.

Toxicity of Particulates in Urban Rainfall-runoff

This study measured toxicity of solids transported in lateral pavement sheet flow from a heavily traveled urban roadway (I-10) in Baton Rouge. There were six objectives in this part of study: (1) to determine sampling representatives and the toxicity change with the hydrograph, (2) to determine the lethal effect of suspended and settleable solids, (3) to determine the function of particulate matter in runoff on toxicity, (4) to determine the size range of the solid affect fish gill function, (5) to determine the oxygen consumption rate of fish change with solid exposure, and (6) to determine the recovery ability of fish gill function.

Testing of the Hydrodynamic Separator (HS) "L-Unit"

This study investigated the particle removal performance of the hydrodynamic separator (HS) "L-Unit" under the simulated stormwater conditions.

Gravimetric Evaluation of Hydrodynamic Separator Precast Manhole Stormwater Unit (PMSU20_20)

This study investigated the particle removal performance of the hydrodynamic separator (HS) PMSU20_20 under the simulated stormwater conditions.

SCOPE

This report focuses on treatment performance of particles and phosphorus by a screened hydrodynamic separator, metal speciation, and particulate toxicity in urban rainfall-runoff. The studied rainfall-runoff originated from a small source area of urban highway transportation land use.

METHODOLOGY

Experimental Site Description

City Park Lake is a shallow (mean depth of 4 to 5 ft.), 57-acre lake located in urban Baton Rouge, Louisiana. Originally a cypress swamp known as Bayou Duplantier, City Park Lake was created in 1929 when the site was dredged by the Works Progress Administration. Known as the crown jewel of Baton Rouge, City Park Lake is highly regarded as a symbol of local beauty around which many upscale residences in Baton Rouge have been built. The lake is used extensively for recreational purposes. A USEPA (1991) assessment of the City Park Lake system indicated that 56 percent of people surveyed utilize the lake for walking or running, 44 percent for bird watching, 40 percent for bicycling, and 12 percent for fishing. Due to urban rainfall-runoff loadings the lake is hyper-eutrophic. For nearly four decades, a heavily traveled portion of Interstate 10 has spanned the northern end of the lake, as shown in Figure 1. The concrete bridge deck is loaded with an average daily traffic (ADT) of 70,400 vehicles in each direction (east and west). With 58 in. of annual rainfall, runoff from the bridge transports significant nutrient, PM and metal loads directly into the lake (Sansalone et al., 2005, Ying et al., 2008).

Figure 1
Aerial view of City Park Lake environs

The Louisiana Administrative Code (LAC) provides water quality criteria for fresh water bodies. According to Title 33, Part IX, Chapter 11 of the LAC, the purpose of the criteria is to "establish water quality standards that provide for protection of the waters, public health, and serve the objectives of the Louisiana Water Control Law and Federal CleanWater Act." Located in USEPA Ecoregion X, City Park Lake is used for indirect water contact activities, such as canoeing and fishing and is classified as a "Secondary Contact Lake." This classification requires that metal concentrations meet the USEPA criteria. While P and N criteria are currently under development by the Louisiana Department of Environmental Quality (LDEQ), the USEPA has regionally-based recommended nutrient criteria levels (USEPA, 2002). Table 1 summarizes these criteria for Ecoregion X.

Direct discharges from bridges to water bodies are not commonly monitored, however if such data exist it is important to compare the water chemistry of the I-10 bridge to other bridges of similar hydrologic and traffic fluxes in order to illustrate that such discharge loadings are reasonably similar. McKenzie et al. (1983) monitored the I-95 bridge north of State Rd 836 in Miami, FL. The bridge is 1,048 ft. long with an ADT of 70,000 in each direction. Annual rainfall is similar to Baton Rouge, ~ 58 in. A comparison for specific water chemistry constituents is made in Table **1**2.

Table 1
USEPA-recommended nutrient criteria for Ecoregion X

Parameter	Criteria
Total Phosphorus, TP [µg/L]	60
Total Nitrogen, TN [µg/L]	570
Chlorophyll-a [µg/L]	5.5
Secchi Depth [m]	0.8

Table 2

Comparison of Miami (I-95) and Baton Rouge (I-10) bridge discharge concentrations

Constituent	Monitored Data as Site Mean Concentrations		Annual Baton Rouge (I-10) Loadings to Lake (kg)
	Miami (I-95)	Baton Rouge (I-10)	
Total Cu [µg/L]	54	27	0.5
Total Zn [µg/L]	370	220	4
TP [µg/L]	170	340	6
TN [µg/L]	4,100	11,000	195
PM as TSS [mg/L]	81	110* (SSC = 330)	5,862

The experimental catchment site consisted of both sections of the east- and west-bound lanes of I-10 City Park Lake Bridge in Baton Rouge, Louisiana. The total elevated highway bridge span over the lake is 886 ft. The concrete-paved catchment area consisted of two lanes that are 146 ft. long and 40 ft. wide, with a total area of 11,706 ft^2. Rainfall-runoff generated from the catchment was in a form of lateral pavement sheet flow and drained through the east-most expansion joint of the bridge and was captured in a collection trough where it combined with the downspout flow from the bridge catchment before the experimental facility. Details of site description and characteristics are available elsewhere (Sansalone et al., 2005).

A screened hydrodynamic separator (HS) unit was installed in the experimental catchment site. The screened HS was plumbed into the existing rainfall-runoff capture, delivery and monitoring system. Experimental set-up and the screened HS testing system including hydrologic data and sample collection are illustrated in Figure 2.

Sample Collection Method

Prior to each rainfall-runoff event, the screened HS unit, drop box, and Parshall flume at the experimental site were cleaned and set up. Rainfall-runoff from 11,706 ft^2 of total catchment area was eventually routed through a 2-in. Parshall flume followed by a drop box from which influent samples were taken. The free fall from the downstream of Parshall flume was the influent sampling location. It allowed a sample collection across the entire cross sectional area of flow, including the coarser bed load particles. Upon rainfall-runoff observation in the drop box, influent sample collection was immediately started for each actual rainfall-runoff

event. Free fall from the 8 in. diameter PVC pipe downstream of the screened HS was the effluent sampling location. Influent and effluent sampling locations are described in Figure 2. Around 14-17 influent samples and 13-15 effluent samples were taken for each rainfall-runoff event depending on its duration with the exception of one short event. Such a sampling strategy assured a reasonable estimate of temporal particulate concentrations (McBean et al., 1997).

Judgments for sampling intervals were made based on a prior knowledge of the seasonal weather patterns and information compiled from local and national radar imagery systems. Typically more frequent sampling intervals (1-3 minutes) were employed in the beginning of the event. Then, sampling intervals were spaced out to 5 minutes or longer depending on the duration of the event.

At each sampling time, replicate 3.2 gal (12 L) and 0.26 gal (1 L) samples were manually taken using wide-mouth polypropylene containers. The 3.2-gal samples were used to recover sediment fraction, and the 0.26 gal samples were utilized for the measurement of settleable and suspended particle concentrations.

Sample Collection Classification

To evaluate the transport and treatability of particles and phosphorus, eight discrete rainfall-runoff events between March 14, 2004 and October 3, 2005 were monitored and treated by the screened HS at the Baton Rouge I-10 experimental site. To examine the influence of hydrology on metal speciation, four separate events between April and June in 2002 were collected and analyzed. To study the particle toxicity in rainfall-runoff, another four discrete events between April 2004 and April 2005 were measured.

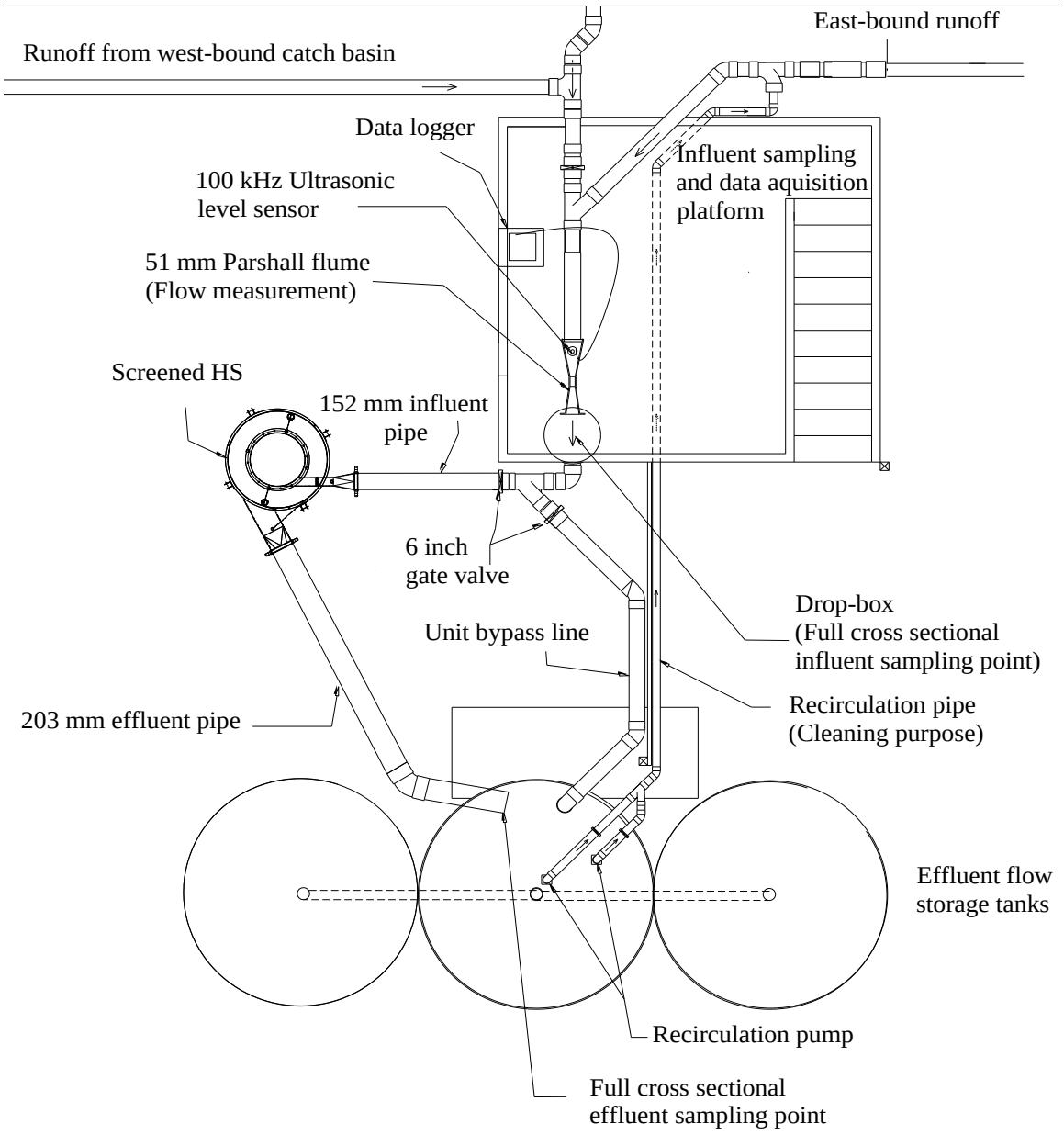

Figure 2
Schematic plan view of experimental setup

Rationale for Manual Sampling

The wide gradation of particles was observed in rainfall-runoff from colloidal-size to gravel-size material (Sansalone et al., 1998). It was found that from an entire gradation of particles deposited on pavement surface, 34 percent were larger than 420 μm (Shaheen, 1975). However, a mechanical device for sample collection such as an automatic sampler does not appear to be capable of collecting the entire gradation of particles, especially large grain size particles in runoff. This is because automatic peristaltic pumps employed to draw samples often are not capable of sampling larger material entrained in stormwater (Bent et al., 2000), which would result in a gross underestimation of the total solids load. In addition, automatic samplers tend to miss the initial runoff of an event because samplers are typically initiated by a certain allowable minimum volume of flow. Therefore, to ensure the collection of the entire gradation of particles, manual sampling through the cross-sectional area of flow was performed in this study.

Hydrologic Data Collection

Rainfall was recorded with a tipping bucket gauge in increments of 0.01 in. A 70 kHz ultrasonic level sensor was mounted 10 in above the bottom surface of Parshall flume to measure flow depths. Flow levels were transmitted to the datalogger of American Sigma (1994) every second and averaged over one minute to provide a single average flow level for each minute. The one-minute flow level average value was calibrated to the flow rate using the upstream head-discharge calibration curve for the 2 in Parshall flume. The upper limit of flow height of the flume is 13 in, which corresponds to 405 gpm flow capacity. The lower limit of the flume and ultrasonic sensor is 0.03 in, which corresponds to 0.3 gpm flow capacity.

Particle Fraction Analyses

Particulate matter in stormwater ranges from micrometer-sized colloidal organic material to millimeter-sized sand, silt, and gravel, more than six-order of magnitude. In the present study, particulate matter indicates particles larger than nominal size of 1.2 μm and is categorized into three fractions by size: suspended, settleable, and sediment fraction.

The "sediment" fraction includes all particle sizes larger than 75 μm, which is consistent with published classifications that separate "coarse" from "fine" particles and silt from sand at 75 μm (ASTM 1993). This fraction includes not only coarse sand (inorganic particulates) but also litter (i.e., paper, plastic, metal, glass, etc) and debris (i.e., leaves, twigs, and grass). The "settleable" fraction is defined as part of particulate matter settled out in 1-hour Imhoff cone according to the Standard Method 2540F (Standard methods, 1995). Those particles remaining in Imhoff suspension after one hour are defined as the "suspended" fraction (or non-settleable particle) (Standard methods, 1995).

The three particulate fractions (suspended, settleable, and sediment) were analyzed separately for each replicate discrete influent and effluent sample. Analysis methods include ASTM and Standard Method (#2540 F) protocols (Standard methods, 1995). The separation effectiveness of the screened HS for each particle-size fraction was examined in order to identify effectiveness based on particle size classes of suspended (1 – 25 μm), settleable (25 – 75 μm) and sediment (> 75 μm). These results may allow the development of sample measurements to infer treatability behavior for these particle size classes for a given combination of separation system and loading.

Separated HS Particles

At the end of each event, particles captured by the screened area of the screened HS unit were recovered separately for further analyses. First, particles in the screened HS were allowed to settle for at least 12 hours but no more than 24 hours from the end of each runoff event. The time frame of settling for particles in screened HS unit was set up to provide enough time for particles to settle but at the same time to prevent the occurrence of anoxic conditions which could cause re-suspension of particles. The unit supernatant was then siphoned. Particles from screened and volute areas at the end of the event were separately recovered through the drainage pipes at the bottom of the unit and transported to the lab for air-drying at 40°C in a temperature-controlled isolation room. Once dried, the particles were disaggregated and granulometric distributions of screened and volute particles were separately determined by mechanical sieve analysis following the modified procedure ASTM D422 (ASTM 1993). Using a total of 17 standard stainless steel sieves ranging from 9.5 mm (#3/8) through 25 μm (#500), 18 particle size classes were separated and stored in separate round-glass specimen jars for the measurement of mass and specific gravity (ASTM 1994).

Influent Particle Size Distribution

Influent particulate matter transported by rainfall-runoff ended up either trapped by the screened or volute area in the HS at the end of event or discharged from the screened HS throughout an event. Under the constraint of the mass balance error, event-based influent PSD was calculated by the summation of each measured size distribution for screened, volute, and effluent particles.

Size distributions for screened and volute particles are measured by sieve analyses as previously described. It is indicated by standard methods that determination of particle sizes smaller than 75 μm by sieving analysis is not recommended. This is because, unlike the larger particles, fine particles (< 75 μm) behave cohesively and form smaller agglomerates that do not easily desegregate into their original sizes of discrete particles during the standard ASTM dry sieve analysis process. In addition, effluent particles are expected to be mainly composed of sub 75 μm particles. Therefore, a laser diffraction type of particle analyzer LISST Portable (Sequoia Tech Inc.) was used to analyze the particle size distribution for the effluent discrete samples. The range of measurable size by the laser analyzer covers from 1.25 to 250 μm.

Influent particle gradation for each event was then calculated by the summation of PSDs for the screened, volute, and effluent particles. This methodology ensures the characterization of the full range of influent PSD from 1 μm to larger than 9,500 μm size. Total mass of screened, volute, and effluent load particles should be within 10 percent of calculated influent mass load.

Event Mean Concentration (EMC)

Since the concentration of particulate matter transported in rainfall-runoff can vary by orders of magnitude during a storm event, an EMC is often used to characterize the concentration for a specific parameter of concern for an entire event (Huber, 1993) and is computed as follows:

$$EMC = \frac{M}{V} = \overline{C} = \frac{\sum_{i=0}^{n} \overline{C}(t_i)\overline{Q}(t_i)\Delta t}{\sum_{i=0}^{n} Q(t_i)\Delta t} = \frac{\sum_{i=0}^{n} M(t_i)}{\sum_{i=0}^{n} V(t_i)} \quad (1)$$

where, $\overline{Q}(t)$ and $\overline{C}(t)$ = average flow rate and the average concentration during the time interval; n = time coinciding with the last sample collection; $\Sigma M(t)$ = total mass of particulate matter over entire event duration (M); and $\Sigma V(t)$ = total runoff volume treated by the screened HS over entire event duration (L).

Particle Separation Efficiency

To assess the particle separation performance of best management practices (BMPs), there are four techniques according to Strecker et al. (2001). These include the statistical characterization of influent and effluent concentrations, sum of loads, storm by storm comparison, and regression of loads. In the presented study, all of these methods are utilized to make an accurate assessment of the particle separation ability for the screened HS.

Statistical characterization defines removal as the ratio between influent and effluent EMC as follows:

$$\Delta Particle\ (\%) = \left[\frac{EMC_{in} - EMC_{out}}{EMC_{in}} \right] \times 100 \tag{2}$$

The sum of loads method takes the ratio of the total influent and effluent loads of the monitored events as follows.

$$\Delta Particle\ (\%) = \left[\frac{M_{in} - M_{out}}{M_{in}} \right] \times 100 \tag{3}$$

$$M_{in} = \sum_{i=0}^{n} M_{in}(t_i) \quad \text{and} \quad M_{out} = \sum_{i=0}^{n} M_{out}(t_i)$$

where, ΔParticle = Particle separation efficiency (%); M_{in} = total mass of influent particulate matter over entire event duration (M); and M_{out} = total mass of effluent particulate matter over entire event duration (M).

Percent reductions in the concentration and load are calculated for particulate matter and three different size classes of particles (sediment, settleable, and suspended particles) by the integration of measured particle concentrations of influent and effluent discrete samples and flow rate.

Particulates Total Phosphorus (TP) Analysis

There are numerous analytical procedures for TP reported in the literature. Currently employed methods are adapted from methods used for soil, solid waste, and wastewater quality analyses (Standard methods, 1995). The ascorbic acid method was used to detect orthophosphate as recommended by other researchers. The persulfate digestion was used to measure TP by converting all forms of phosphorus to orthophosphate. Measurement of particle-bound phosphorus in rainfall-runoff involves three steps: (1) particulate matter separated from solution; (2) acid digestion and conversion particulate bound phosphorus to dissolved phosphate; and (3) analytical measurement of the dissolved phosphate using colorimetric reagent.

Particulate/Solution Separation

Wet and dry sieving are commonly used methods of separating and fractionating particles from a solution. Wet sieving was utilized to separate sediment (> 75 μm) from the 1-L and 12-L containers for each discrete rainfall runoff sample. After sediment was removed from the 1-L samples, settleable (25-75 μm) and suspended (< 25 μm) particles were fractionated by the Imhoff Cone protocol. The sediment, settleable, and suspended fractions were then analyzed and quantified for the TP associated, respectively.

Acid Digestion and Conversion of Particulate P to Phosphate

Replicate samples of a precisely-measured dry particulate mass (approximately 1 g) were obtained from sediment, settleable, and suspended fractions. Particles were mixed with up to 80 mL of de-ionized water. Each of these replicate solutions were separately digested to convert all particulate-bound phosphorus (primarily polyphosphates and organic P) to dissolved phosphate using the Persulfate Digestion Method (Standard methods, 1995).

Analytical Measurement of the Dissolved Phosphate

Phosphorus was measured by the HACH DR/2000 Spectrophotometer using PhosVer 3 Ascorbic Acid Method (Standard methods, 1995). The ascorbic acid method was used to detect orthophosphate, and a persulfate digestion was used to convert any other forms of

phosphorus to orthophosphate. The overall sample of total phosphorus concentration is the summation of sediment bound, settleable bound, suspended bound, and dissolved phosphorus concentrations.

Metal analysis–ICP/MS

Metal analysis was conducted with an inductive coupled plasma mass spectrometer (ICP-MS) (Elan 6000, Perkin-Elmer Science). The ions produced in the plasma gas are introduced into a mass spectrometer, which separates ions according to their mass-to-charge ratios. For dissolved metals analysis, the sample is filtered with a 0.45 micron filter; the filtrate is preserved with acid and analyzed by the previously mentioned method. For particle bound metals analysis, water samples containing particles are digested in nitric, perchloric acid to dissolve all metals. Particulates remaining in the digestate are removed by filtration.

Metal Speciation Modeling

Metal speciation was modeled using MINTEQ. MINTEQ utilizes aqueous ionic constituents, water pH, redox potential and ionic strength to determine the concentration of each aqueous species formed under specified conditions. For MINTEQ to perform a complete charge balance, all major dissolved ionic measurements were required. Each sample was fractionated prior to analysis. Nitrates, sulfates, phosphates and chlorides were determined by colorimetric analyses. Respective reagents were combined with 25-mL of sample to determine concentrations of NO_3^--N, SO_4^{-2}, PO_4^{-3}-P, and Cl^-.

DOC was measured using a Shimadzu TOC-5050A analyzer. Prior to analysis, samples were fractionated into their dissolved phases and acidified to a pH of 2 using trace metal sulfuric acid. The TOC concentrations measured by this procedure were actually DOC concentrations. All particulate organic carbon was removed during fractionation. Any inorganic carbon was removed during the purging step. Samples were purged at room temperature to remove inorganic carbon such as carbonates and hydrogen carbonates. Once purged, 40 μL of sample was injected into a combustion tube containing an oxidation catalyst and heated to 680°C. Analyses were conducted in triplicate. Statistical analyses carried out on the results revealed no significant error (< 10%). A four-point standard curve was developed for calibration.

To model the behavior of DOC in the stormwater, the DOM sub model of MINTEQ was utilized. DOC acts as a negatively charged ligand that has a high affinity for positively charged ions such as ionic metals. MINTEQ utilizes a Gaussian model to statistically determine the extent of proton binding in solution. The Gaussian DOM model derives complexation at a multi-dentate site and applies this behavior to the entire ligand, assuming site heterogeneity. The Gaussian model requires the assumption that ligands of the DOM mixture are normally distributed with respect to their log K value (Allison et al., 1991). All reactions assume a 1:1 stoichiometry between complexing anions and ligands. MINTEQ offers up to three types of surface binding entities for a complex representation of the DOM surface chemistry. However, this research will use a monodentate model that utilizes a carboxylic binding site subset (Allison et al., 1991).

The two dominant parameters influencing complexation reactions are pH and ligand concentrations (Hoins et al., 1993). As previously stated, the major ligand components include DOC, $Cl^{-,}$ SO_4^{-2}, NO_3^- , PO_4^{-3}, and HCO_3^-. Due to the number of species possible under these conditions, the results will be categorized into the five most dominant species of each target metal. The concentrations of these complexes will be plotted as a function of time for the duration of the storm event. By determining speciation as a function of time, we are examining the impacts of the hydrograph on the formation of metal complexes.

Equilibrium and Partitioning Kinetics

The model used to predict metal speciation assumes that the aqueous system is in equilibrium. However, rainfall-runoff events are dynamic processes that exhibit changes in constituent concentrations that can vary by an order of magnitude throughout the duration of an event. From the instant that a raindrop impacts the impervious surface to the time it is discharged into the environment, the various phases of constituents are subjected to processes that can alter their partitioning and speciation. While partitioning and speciation changes throughout the event, samples were taken, rapidly fractionated, stabilized and preserved. Therefore partitioning was measured at discrete points in time during the event and speciation modeled given the measured water quality analyses at these discrete points in time.

Acute Lethal Toxicity Test

For three 8-L samples, which represent the first flush, one hour flush, and end flush, four liters were taken from each one and passed through the TSS filter. Each of the filtered samples was separated into two 2-L sub-samples that were filtered (0.45 μm) and then poured into clean, labeled, pre-rinsed glass beakers. The same occured for the non-filtered samples except passing the filters.

The test fish were then introduced into glass test beakers, and there was no change of water for the duration of the test. The loading of the fish into the test beakers was limited to ensure that the concentrations of dissolved oxygen and test substance do not fall below acceptable levels, concentrations of metabolic products do not exceed acceptable levels, and the test organisms are not stressed because of aggression or crowding. Fish were transferred by using a soft, fine mesh nylon screen. Aeration was provided to keep the level of dissolved oxygen at least 4.0 mg/L. The test began when the test organisms were first placed in test beakers containing test solutions.

Mortalities were recorded one hour after test initiation and hourly or every five hours thereafter depending on fish behavior. Fish were considered to be dead when they do not respond to gentle prodding at caudal peduncle. Dead fish were removed to prevent fouling of the test solution. Samples were siphoned or gently poured off into a separate container for the measurement of water analysis every 24 hours.

Oxygen Consumption Test

Selected gradation of dry solids collected from previous storm events with a different size was used to differentiate the sediments (coarse particles > 75 μm), settleable solids (25-75 μm), and suspended solids (< 25 μm). For each representative size solid, researchers used clean tap water to soak 500 mg for at least 2 hours. The soaked solids were introduced into a 1000 mL beaker with tap water to reach an approximate TSS concentration around 500 mg/L. These solutions were used in the following oxygen consumption test.

Composite runoff samples collected from the Baton Rouge site were separated into two groups. Group one was transferred into the Imhoff cone for 60 minutes quiescent settling to remove the settleable and sediment fractions. Group two was the raw sample without any

treatment. Both groups were well mixed by using a stirrer bar and replicate samples were taken at 0 hour, 2 hour, and 6 hour intervals after the test started with the fish exposed.

The test fish were introduced into the test media and were not given any feed during the test. Light mineral oil (paraffin oil, light, Fisher Scientific, Fair Lawn, New Jersey) was added into the bottle to form a 2-cm oil layer in order to isolate the oxygen from the water surface. The systems were allowed to reach the ambient temperature of 22^{o}C (room temperature) two hours prior to the initiation of the test. The Orion 810A+ oxygen meter was used to record the dissolved oxygen concentration at specific time interval until it reached the death point. The oxygen consumption of the fish remaining in the 500 mL glass beaker after each sampling interval was measured and corrected after all the fish body weights were known at the end of each test. The fish were assumed to be the only oxygen consumers in these closed systems. Changes in bacteria oxygen consumption were small (< 5%) over 24 to 48 hours even though they did propagate, and these changes were ignored in the calculation of oxygen uptake.

Calculation and Analysis

At the end of the test, fish oxygen consumption was calculated according to the following equation:

$$O_{uptake} = \frac{(DO_{t_x} - DO_{t_0}) \times V}{W \times (t_x - t_0)} \tag{4}$$

where, O_{uptake} = Oxygen uptake (mg); DO_{tx} = Dissolved oxygen concentration in the water at time x (mg/L); DO_{t0} = Dissolved oxygen concentration in the water at the beginning (mg/L); W = total body weight of fish used (kg); t_x = time x after initiation of test (h); and t_0 = the initiation of test (h).

Regression analysis was used to model the relationship between the oxygen consumed per gram fish (Wo) and the time (t) used for the oxygen consumption:

$$\ln(W_O) = a + b\ln(t) \tag{5}$$

The oxygen consumption rate (λ_O) was determined by the differentiation of time variable:

$$\frac{dW_O}{dt} = \lambda_O = (b \times e^a) \times t^{b-1} \quad (6)$$

COANOVA regression analysis and pairwise t-test were used in the statistical analysis to evaluate and compare the difference of the impact, 0.05 will be the critical value in all statistical analysis.

Mass Balance and QA/QC

A mass balance (MB) error analysis was conducted after each event to ensure mass conservation and QA/QC. MB error was determined by the following equation where particulate matter loads of influent (M_{in}) and effluent (M_{out}), dry mass of recovered screened ($M_{screened}$), and volute particles (M_{volute}) are used. Mass balance errors were within the range of ± 10%.

$$MB\ error(\%) = \left[\frac{M_{in} - (M_{out} + M_{screen} + M_{volute})}{M_{in}} \right] \times 100 \quad (7)$$

Experimental Test Procedure of HS "L-unit"

The HS "L-Unit" was installed into the existing outdoor covered laboratory and bolted to the existing concrete slab of the test site located in Baton Rouge. The "L-Unit" was plumbed into the existing rainfall-runoff capture, delivery, and monitoring system. Details of the site configuration and setup are illustrated in Figure 4. Calibration of the flow monitoring system consisting of a 2-inch Parshall flume, 70 kHz ultrasonic sensor, and flow appurtenances is provided in the lower plot of Figure 4 over the full range of flow rates. Since the system was also connected to the overhead storm drains from the 11,706 ft^2 pavement drainage area over the laboratory site, any storm flows were diverted away for the New Jersey testing system. The bridge over the laboratory also kept the experimental test site dry during wet weather. The outdoor laboratory was powered by 220-V and 110-V AC power. Potable water for the testing was provided through a fire hydrant tap connection located 100-ft. from the 1000-gallon batch mixing tank shown in Figure 4. In addition to the HS "L-Unit," the New Jersey (NJCAT) testing setup consisted of two 1000-gallon batch tanks, one for mixing the NJCAT gradation with tap water to produce the required influent particle gradations and gravimetric loadings and the other for collecting all effluent from the HS." The unit was cleaned after

each run to ensure no scour.

Five different test gradations of silica particles were obtained from the US Silica Company and each of the five test gradations were first sieved to separate too coarse and too fine particles between specific sieve increments. These sieved gradations were combined to meet the specified New Jersey test gradation. Once combined and mixed, the 5-sieved final particle components of the final gradation were sieved again down to 25-μm, and the fraction finer than 25-μm was analyzed using laser diffraction. Measured (sieved) results were then compared to the target NJCAT gradation and to calculation. Results of the NJCAT target gradation, the calculated gradation, and the measured gradation are summarized graphically in Figure 3 and in a tabular manner in Table 3 and Table 4. Particle densities are summarized in Figure 5. Error bars in Figure 3 represent standard deviations of replicate measurements in either one or both directions (the case for flow rate calibration). Once the NJCAT target gradation was generated and replicate testing was carried out to verify the gradation for the test runs, the dry mass required for each gravimetric concentration (nominally 100-mg/L, 200-mg/L, and 300-mg/L) was determined, and this dry mass of known gradation was utilized in batch testing at flow rates ranging from 10 to 125% of the "L-Unit" design flow of 150 gallons/minute (gpm).

In the field laboratory, the testing process involved the following steps. Prior to starting an actual test, the tanks, HS "L-Unit," and recirculation systems were thoroughly cleaned using potable tap water. The valves on the recirculation system were calibrated with tap water and set to the given flow rate (either 10%, 25%, 50%, 75%, 100%, and 125% of the "L-Unit" design flow rate and either 100-mg/L, 200-mg/L, or 300-mg/L) through the use of either one or two 110-gpm recirculation pumps. Calibrated flow measurements were made throughout each run. The 1000 gallon mixing tank was then filled with a batch of 1000 gallons of tap water and well-mixed using one of the three 110 gpm sewage pumps in the batch mixing tank. The NJCAT particle mixture mass (based on 1000 gallons of influent for treatment) of measured gradation (measured NJCAT gradation in Figure 3) was introduced into the batch mixing tank and well-mixed in the nominal 1000-gallons of tap water. After 15 minutes to ensure sufficient mixing, the well-mixed batch influent was pumped into the "L-Unit" at a constant given flow rate. The "L-Unit" was filled with tap water. Sampling intervals for influent and effluent were calculated based on the operating flow rate. Flow was diverted to the HS unit, and the military time was noted as "Time 0." The full volume of influent was

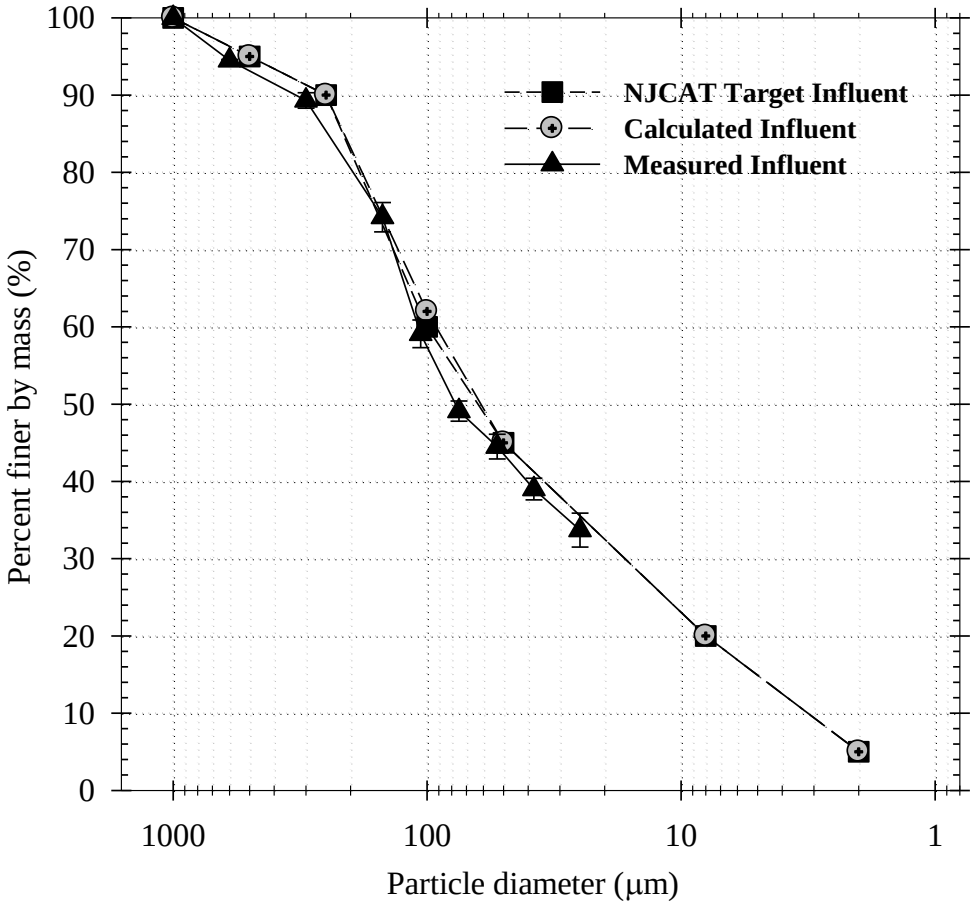

Figure 3

Plots of NJCAT target influent particle size distribution, the calculated and measured gradation utilizing 5 different silica particle gradations supplied by US Silica Company

pumped through the "L-Unit" at a constant flow rate, and the full volume of effluent (equal to influent since the "L-Unit" was filled with water before time 0) was captured and recovered in the 1000-gallon effluent tank (excepting the sample volume). All influent and effluent samples were taken across the full cross-section of flow. Influent was sampled at the drop box which is located upstream of the "L-Unit" and downstream of the 2-in. Parshall flume as shown in the upper plot of Figure 4. Effluents were sampled immediately downstream of the "L-Unit" at the entrance of the effluent tank. The influent and effluent samples consisted of 10 individual replicated (A and B) 1-L sample bottles. The total sample volumes were 20-L

Table 3

Particle size distribution (by mass) calculated based on product sheets provided US Silica Company to follow the proposed NJCAT gradation

Particle Size	Silica particle gradations						Mass Fraction
	20/30	H-85	scs-250	scs-51	mus-10	SUM	
(microns)	(g)	(g)	(g)	(g)	(g)	(g)	(%)
500-1000 (coarse sand)	20.2	1.9	0	0	0	22.1	**5**
250-500 (medium sand)	0	20	0	0	0	20	**5**
100-250 (fine sand)	0	79.8	38	0	0	117.8	**28**
50-100 (very fine sand)	0	18	46	6.6	0	70.6	**17**
8-50 (silt)	0	0.2	16	83.4	4	103.6	**25**
2-8 (silt & clay)	0	0.2	0	37.5	26	63.7	**15**
1-2 (clay)	0	0	0	10.5	10	20.5	**5**
SUM	**20.2**	**120.2**	**100**	**138**	**40**	**418.4**	**100**

Table 4

Comparison of NJCAT target particle size distribution with calculated and measured gradation using five different silica particle gradations

Particle Size (microns)	Sandy Loam (percent by mass)		
	NJCAT Target	Calculated	Measurement
500-1000 (coarse sand)	5	5	5
250-500 (medium sand)	5	5	5
100-250 (fine sand)	30	28	35
50-100 (very fine sand)	15	17	15
8-50 (silt)	25	25	22
2-8 (clay)	15	15	13
1-2 (clay)	5	5	5
Sum	100	100	100

each for influent and effluent samples, respectively. Since the flow rate was constant for each run, samples were taken at equal time intervals across the entire duration of each run. Furthermore, 100 gallons of effluent were captured and recovered in 55-gallon polypropylene tanks, filled by taking samples at equal time intervals across the duration of each run at the same sampling frequency as the 1-L samples. The 100 gallons were taken across each run in order to recover sufficient particle mass to carry out particle gradations.

Lab analyses were conducted from replicate composite influent and effluent samples consisting of 10 individual replicate (A or B) samples from across the entire testing time. The lab analyses consisted of turbidity analyses (ISO method 7027) using a Hach 2100AN-IS turbidimeter and total dissolved solids (TDS) measurements using an Orion 2908 Probe. Total suspended solids (TSS) were measured as suspended sediment concentration (SSC) using 1-L samples. Particles captured by the "L-Unit" from each run were completely recovered as a wet slurry from the sump chamber (inner annular volume inside the 2400-μm screen) and also as a wet slurry from the volute chamber (outer annular volume outside the 2400-μm screen). These particle slurries were completely dried, separately, at 40 °C and then sieved using mechanical sieves to obtain the required particle gradations. The mechanical sieves were comprised of the #30, #50, #100, #140, #200, #270, #400, #500, and the pan. Mass balances were determined for each mechanical sieve analysis and mass balance errors were in the range of 1 to 2% by mass.

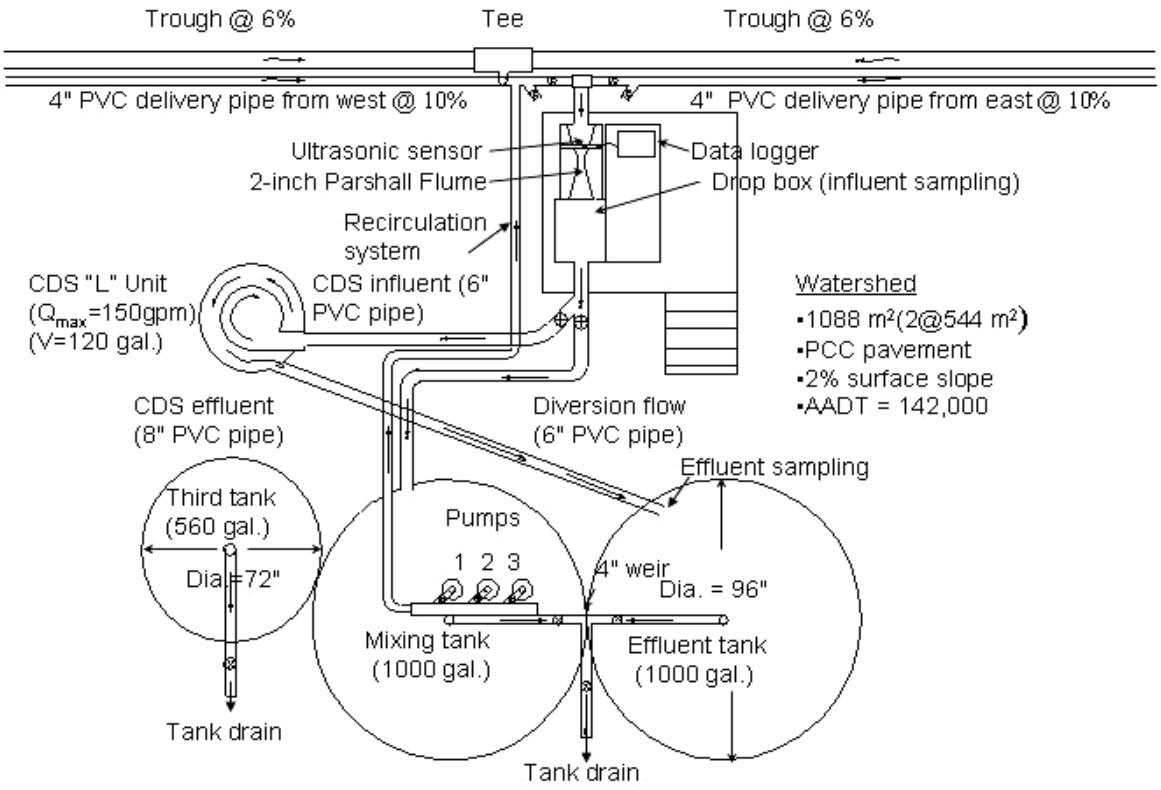

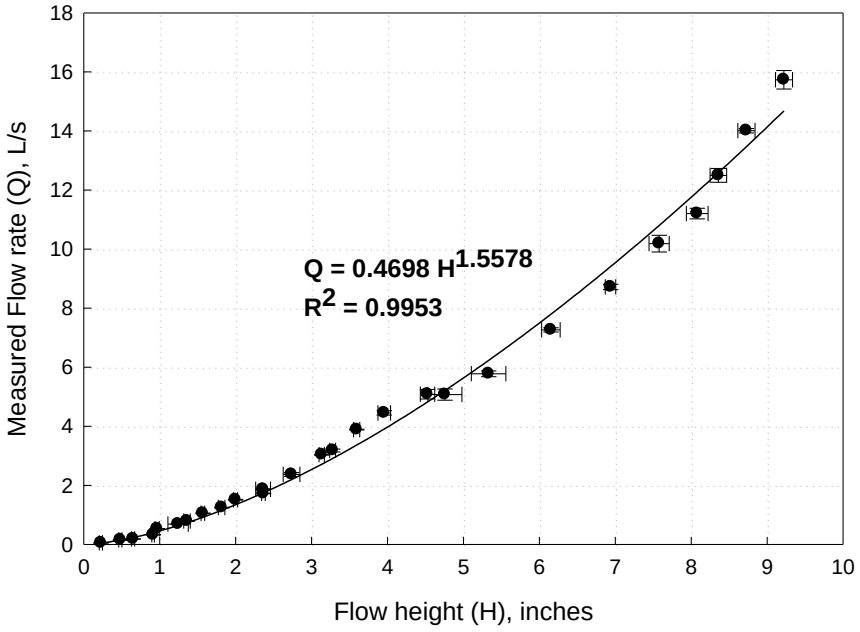

Figure 4

Plan view of experimental site and setup for New Jersey testing illustrated in upper plot. The calibration for the Parshall flume and untrasonic depth sensor are shown in the lower plot

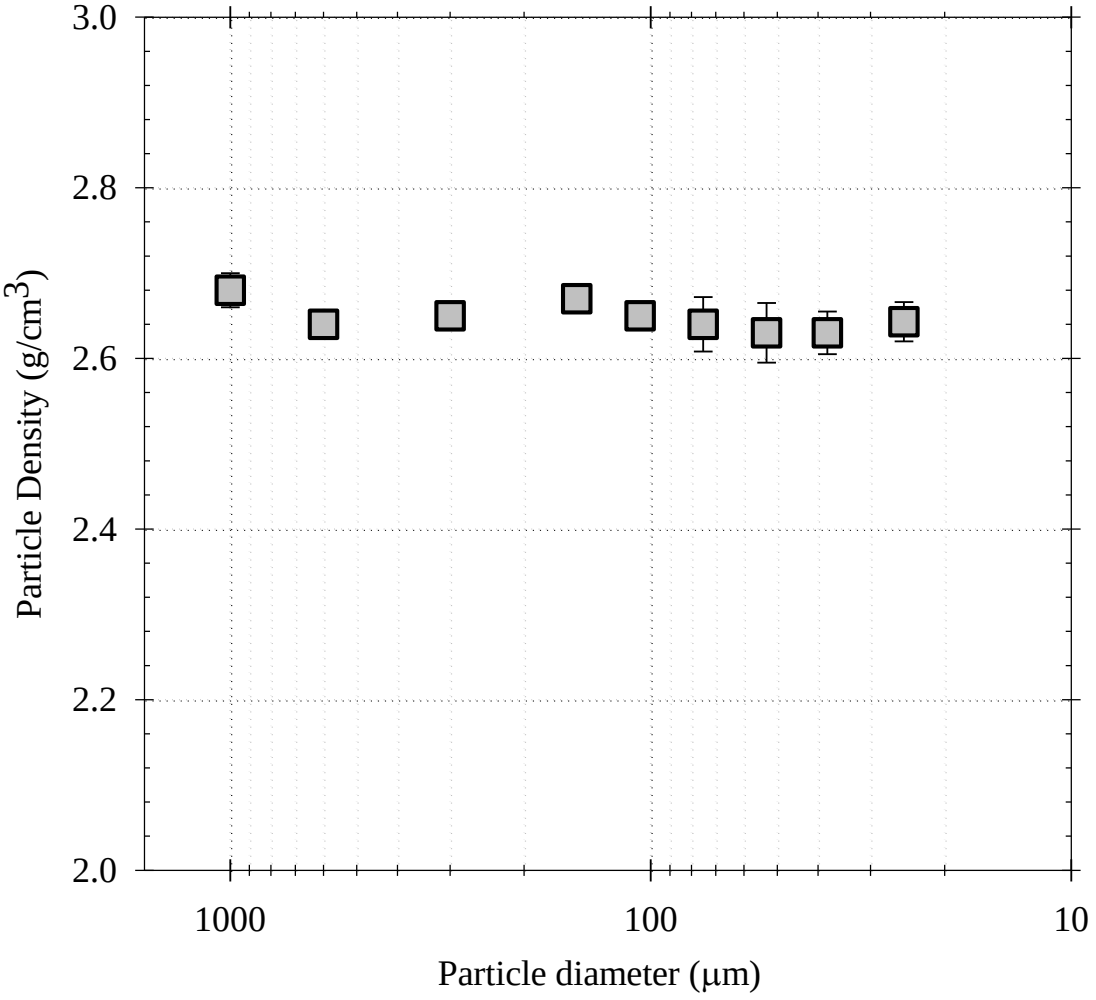

Figure 5
Particle density of influent particle gradation prepared based on NJCAT target gradation utilizing five different silica particle gradations supplied by US Silica Company

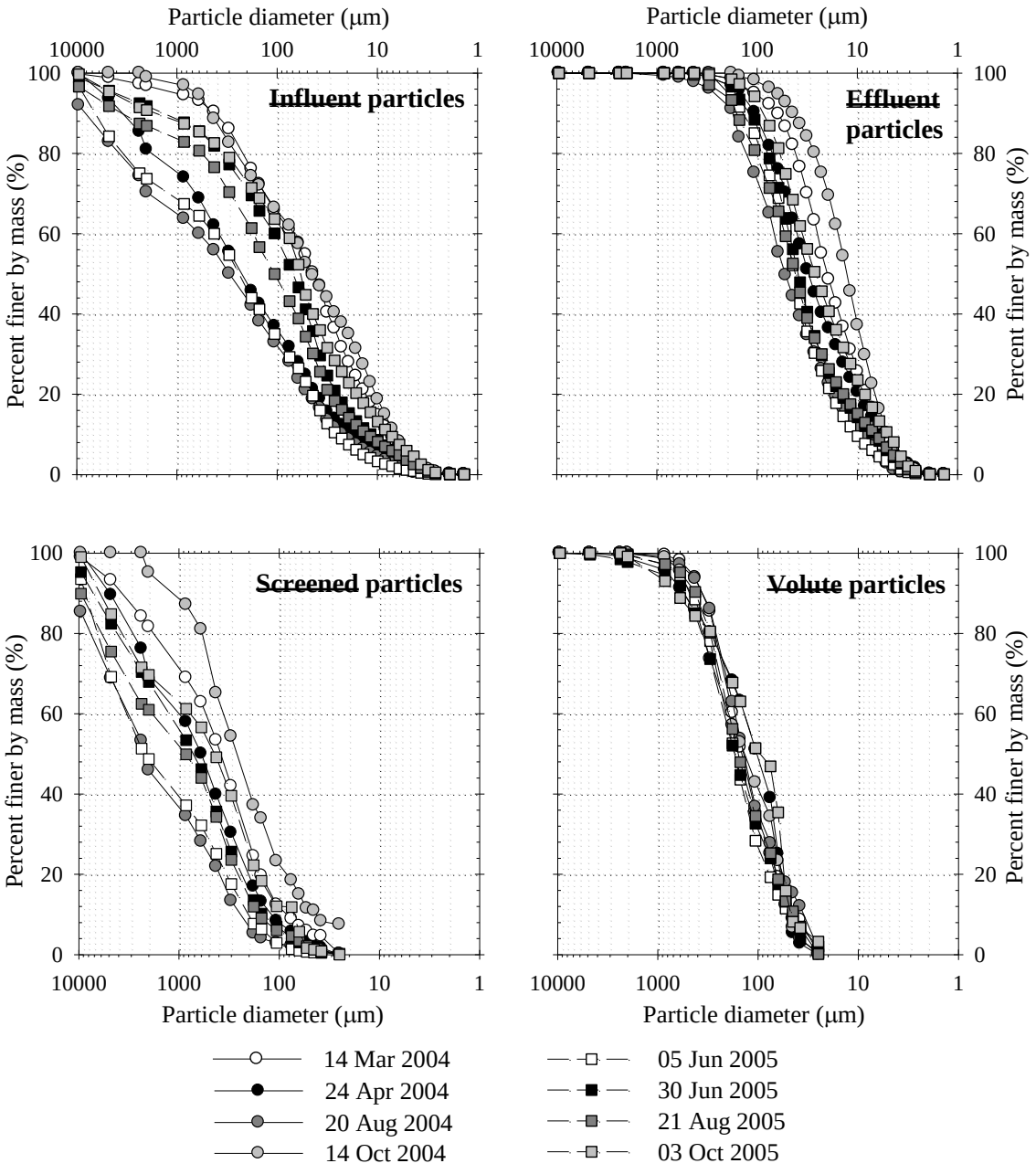

Figure 6

Event representative influent, screened, volute, and effluent PSD for eight runoff events treated by screened HS

Table 5

Summary of hydrologic and sampling based indices for eight events analyzed for the I-10 experimental catchment site (1088-m^2 of pavement) over East Lakeshore Drive

Rainfall Runoff Event	Hydrologic, Rainfall TDP and Sampling based indices								
	PDH[1] (hrs)	Rainfall[2] Duration (min)	Runoff[3] Duration (min)	Total Precip.[4] (mm)	Total Flow[5] (L)	Q_p[6] (L/s)	t_p[7] (min)	Rainfall TP[8] [mg/L]	IPRT[9] (min)
14-Mar-2004	204	413	408	26.2	24076	6.38	295	0.023	8
24-Apr-2004	313	184	215	7.2	7288	1.78	116	0.027	16
20-Aug-2004	26	29	59	17.3	12307	17.5	23	0.025	12
14-Oct-2004	86	179	197	2.6	1672	0.58	60	0.022	48
05-June-2005	117	53	51	7.1	5856	9.35	13	0.021	6
30-June-2005	143	72	71	19.1	15117	13.75	21	0.026	8
21-Aug-2005	94	112	106	51.1	50002	17.32	36	0.024	7
3-Oct-2005	217	9	14	3.81	2615	12.1	5	N/A	2

Notes:

1: PDH: Previous dry hours: Time between current and last event that accumulated at least 0.02 in. of rainfall.

2: Rainfall Duration: The time spanning between the start and stop of effective rainfall for each event.

3: Runoff Duration: The time spanning between the start and stop of runoff for each event.

4: Total Precipitation: The total amount of precipitation recorded on site for each event.

5: Total Flow: The total amount of runoff generated from the experimental section of I-10 for each event.

6: Q_p: The measured peak flow of runoff for each event.

7: t_p: The time spanning between start of effective runoff and the peak flow for each event.

8: Rainfall TP: Rainfall total phosphorus concentration.

9: IPRT: Initial pavement residence time = time between start of effective rainfall and observable runoff.

Table 6

The event-based separation performance of the screened HS for sediment, settleable and suspended particle and total particulate matter transported by eight independent rainfall-runoff events

Rainfall-runoff event	Particle fraction	Sediment particle	Settleable particle	Suspended particle	Total particulate matter	Mass balance error[4]	Particle transport distribution
MAR 14, 04 event	Inf. Mass Load (g)	2325	1424	1201	4949	9.3%	Mass-Limited[2]
	Eff. Mass Load (g)	220	1135	1184	2539		
	ΔParticle (%)[1]	91%	20%	1%	49%		
APR 24, 04 event	Inf. Mass Load (g)	1738	1010	471	3219	-0.8%	Mass-Limited
	Eff. Mass Load (g)	97	475	404	976		
	ΔParticle (%)	94%	53%	14%	70%		
AUG 20, 04 event	Inf. Mass Load (g)	7186	2357	1048	10592	-4.0%	Mass-Limited
	Eff. Mass Load (g)	1501	1858	946	4305		
	ΔParticle (%)	79%	21%	10%	59%		
14 Oct 04 event	Inf. Mass Load (g)	52	125	368	544	2.4%	Mass-Limited
	Eff. Mass Load (g)	3	54	210	267		
	ΔParticle (%)	94%	57%	43%	51%		
JUN 05, 05 event	Inf. Mass Load (g)	3161	1211	386	4758	4.2%	Mass-Limited[2]
	Eff. Mass Load (g)	192	1050	339	1580		
	ΔParticle (%)	94%	13%	11%	67%		
30 Jun 05 event	Inf. Mass Load (g)	1961	1366	717	4044	-3.2%	Mass-Limited
	Inf. Mass Load (g)	470	1321	703	2495		
	ΔParticle (%)	76%	3%	2%	38%		
21 Aug 05 event	Inf. Mass Load (g)	4480	2997	1361	8838	-7.8%	Mass-Limited
	Eff. Mass Load (g)	1003	2586	1296	4884		
	ΔParticle (%)	78%	14%	5%	45%		
03 Oct 05 event	Inf. Mass Load (g)	291	251	197	738	7.5%	Flow-Limited[3]
	Eff. Mass Load (g)	32	181	173	386		
	ΔParticle (%)	89%	28%	12%	48%		
Overall	Inf. Mass Load (g)	21194	10741	5749	37684	-1.3%	-
	Eff. Mass Load (g)	3518	8660	5207	17385		
	ΔParticle (%)	83%	19%	9%	54%		

Note: 1. Calculated by using equation (3).
2. For mass-limited events, mass delivery is skewed towards the initial portion of the event.
3. For flow-limited events, mass delivery tends to follow the hydrograph.
4. Calculated by using equation (4).

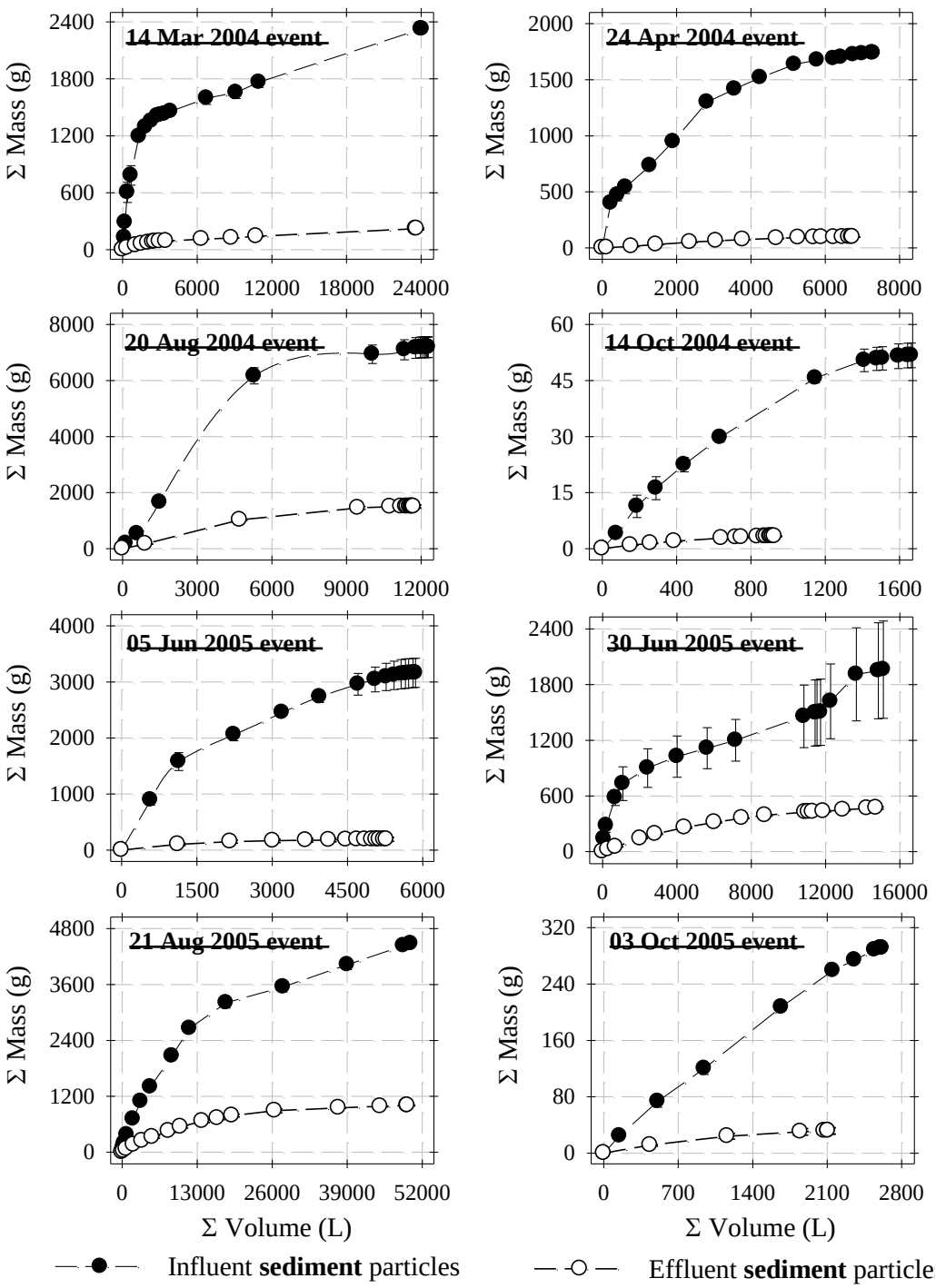

Figure 7
Mass delivery of sediment fraction particulate matter in influent and effluent runoff volume for the eight urban rainfall-runoff events treated by the screened HS unit

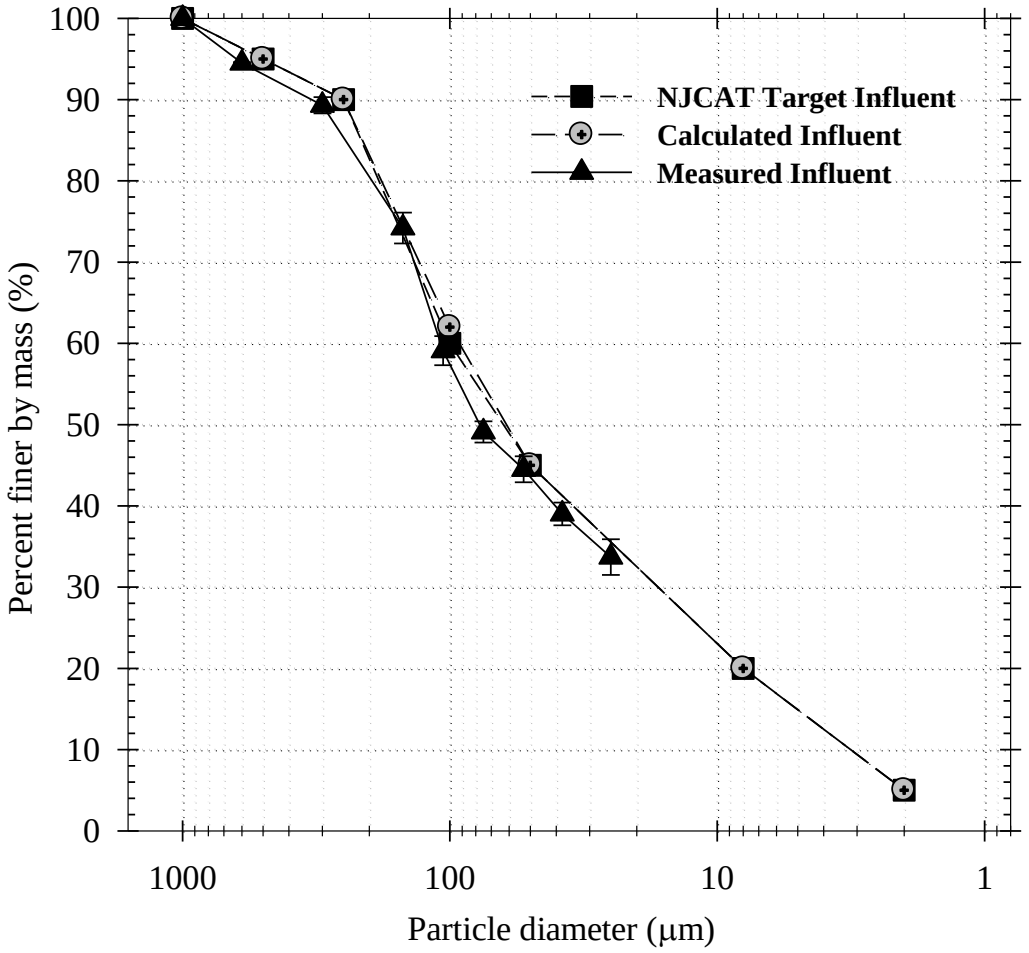

Figure 8
Plots of NJCAT target influent particle size distribution, the calculated and measured gradation utilizing 5 different silica particle gradations supplied by US Silica

Experimental Test Procedure of HS PMSU20_20

Site Set Up and Configuration

The testing test site employed for this evaluation was located under the I-10 bridge overpass of City Park Lake at East Lakeshore Drive in Baton Rouge, Louisiana. The bridge decks over the laboratory area kept the test facility dry during wet weather, yet served as an elevated catchment for capture and treatment of rainfall-runoff. A commercial PMSU20_20 with a 2400 μm (and an additional 4700 μm screen) was installed on the existing concrete slab of the testing facility as illustrated in Figure 9. The PMSU20_20 unit supplied to the researchers had the flexibility of a three-diameter configuration; 60 in., 72 in. and 84 in. This report

includes the results from all three sizes of diameter configurations. Within this unit, a 25½-in. diameter screen was eccentrically located with respect to the center of the unit. Details of the site configuration, setup and dimensions are illustrated in Figure 9 and Figure 10. Influent flow depth measurements were conducted with a Warminster Plastics nested Parshall flume that was installed upstream of a drop box that was used for full cross-sectional flow sampling. The bottom and flow invert of the drop box was steeply-sloped (> 10%), and the bottom of the drop box was also steeply-sloped to the center flow invert so all flow and entrained particulate matter remained mixed and funneled into a 10-in. PVC pipe that connected the outlet of the drop box to the PMSU20_20 inlet section.

The flow monitoring system consisted of a 6-in. Parshall flume, 100 kHz-ultrasonic sensor, and flow appurtenances that are illustrated in Figure 10. The flow monitoring system was calibrated over a wide range of flow rates, from a minimum flow rate of 51.7 gpm to a maximum flow rate of 590.7 gpm (from 10.5% to 119.7% of design flow rate). A diesel pump with a capacity of 1100 gpm and a recirculation system were used to reach the flow-rates tested. Potable water for the testing was provided through a fire hydrant tap connection located 100 ft. from the 10,000 gallon influent Baker tank. The unit was cleaned after each run to ensure there was no scour.

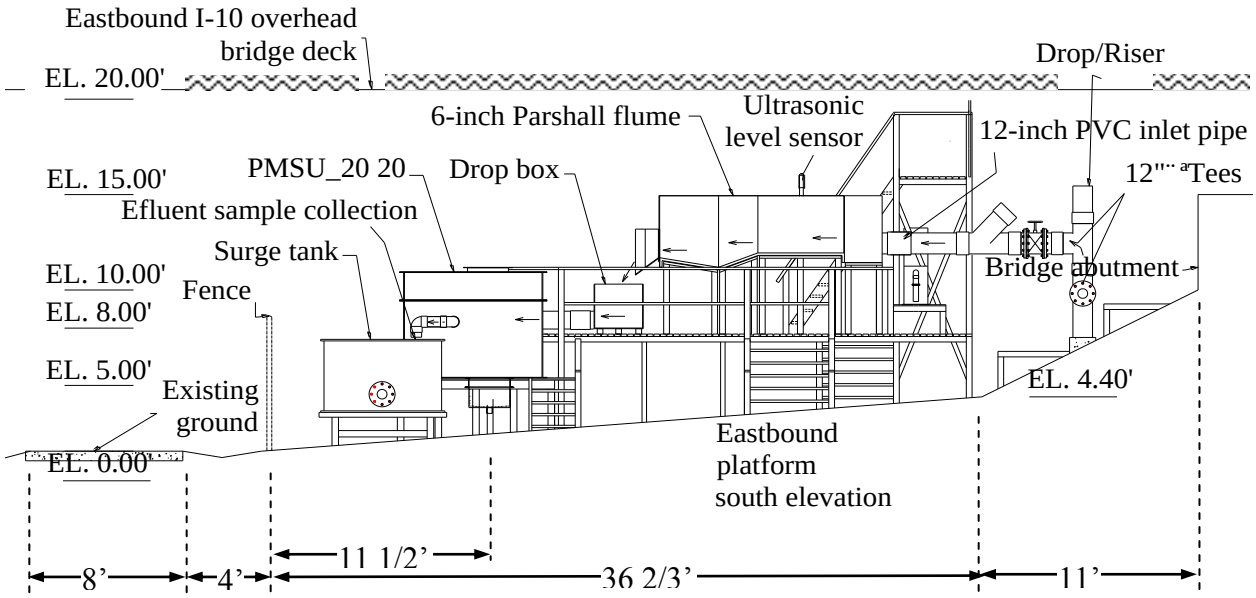

Figure 9

Overall side view and elevation layout of the PMSU20_20 testing facility

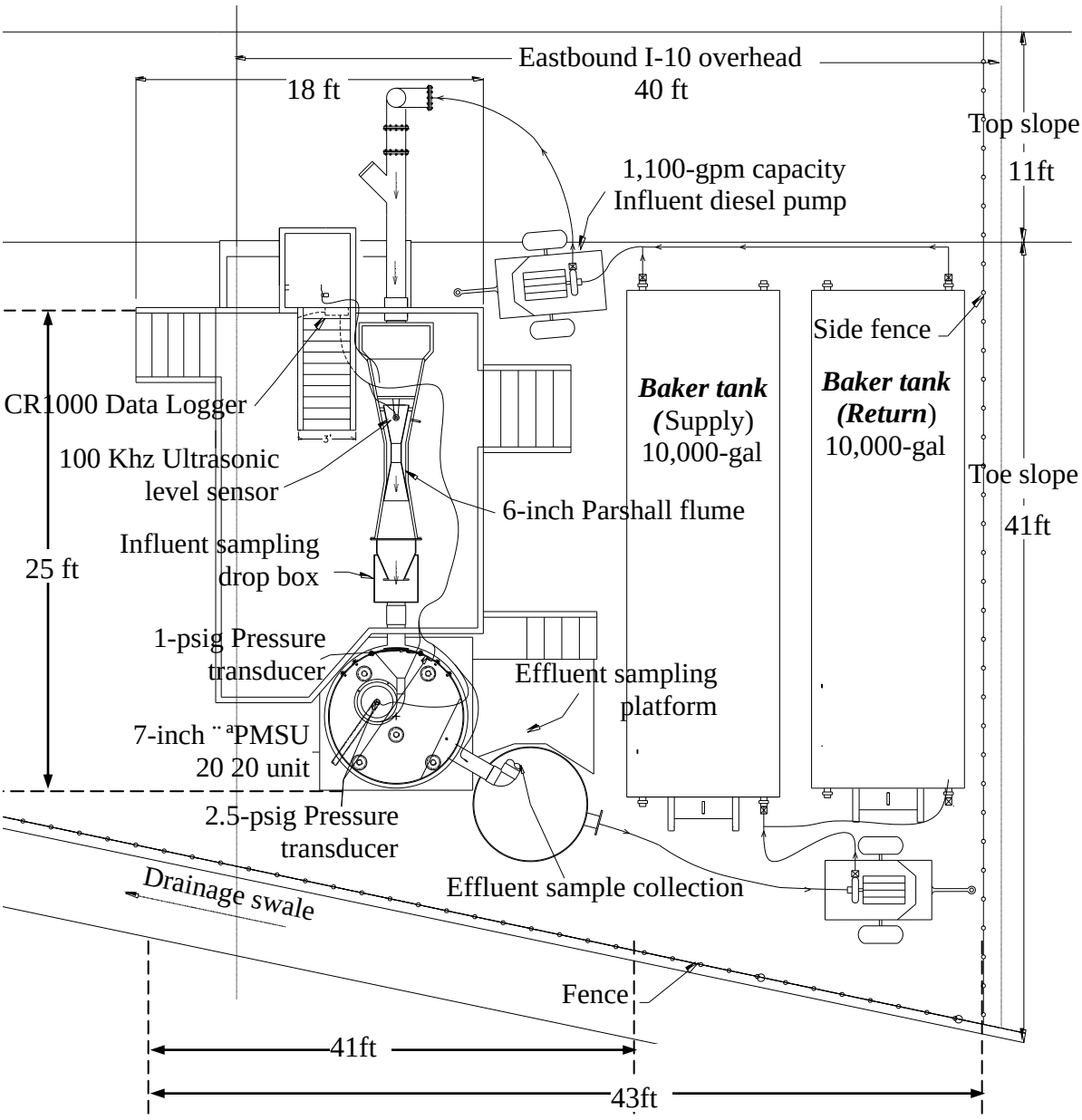

Figure 10

Overall schematic plan view of experimental setup and PMSU20_20 testing system

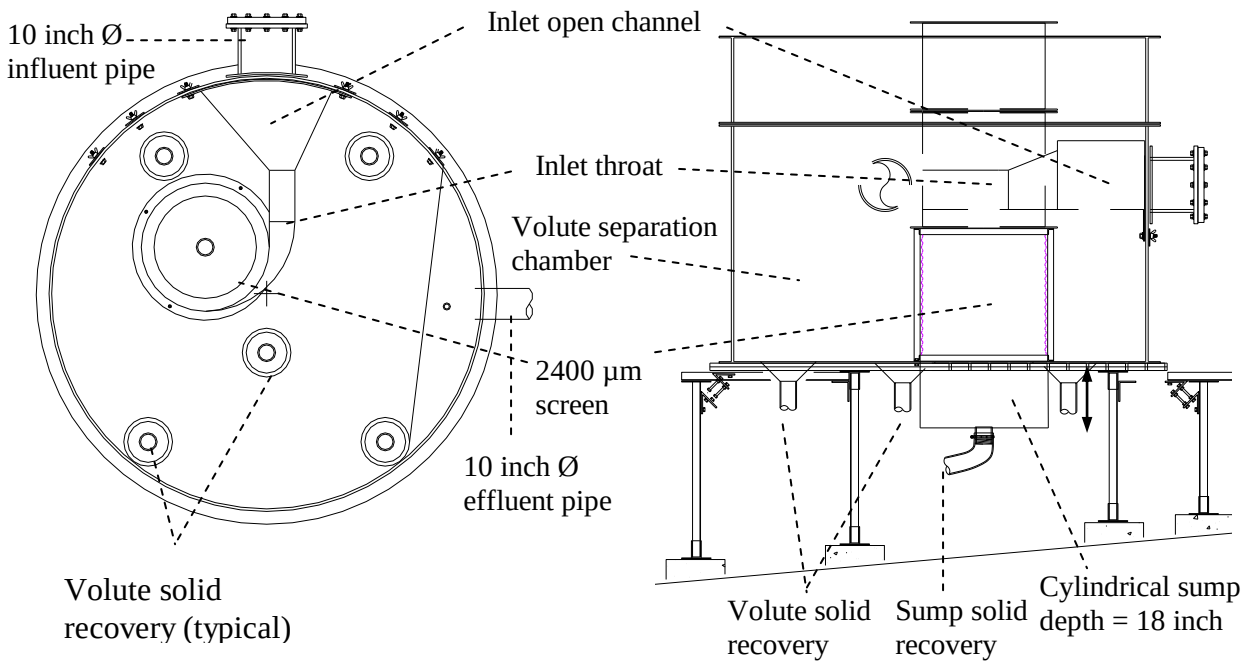

PMSU20_20 unit	Dimensions
Unit Diameter	2.133 m
Unit height	1.676 m
Effective volume of unit (5.0 ft. dia.)	1.580 m^3
Effective volume of unit (6.0 ft. dia.)	2.212 m^3
Effective volume of unit (7.0 ft. dia.)	2.959 m^3
Volume of cylindrical sump	0.145 m^3
Diameter of sump chamber	0.635 m
Diameter of effluent pipe	0.254 m
Diameter of influent pipe	0.254 m
Inlet throat area (Ta)	0.026 m^2
Diameter of screen	0.647 m
Screen vertical surface area (Sa)	1.273 m^2
Sa/Ta	49.3
Volute area (VA) – 7.0 ft. dia. unit	3.244 m^2
Screen horizontal area (SA)	0.331 m^2
SA/VA – 7.0 ft. dia. Unit	0.10
SA/VA – 6.0 ft. dia. Unit	0.14
SA/VA – 5.0 ft. dia. Unit	0.22
Overall unit surface area	3.575 m^2

Figure 11

Diagrammatic cutaway and plan view of 7.0 ft. diameter PMSU20_20 and loading dimensions of the unit

Data Acquisition and Management

The following data were collected as part of this study:

1. Water depths in inlet, screen, and volute area of a PMSU20_20 unit were measured with pressure transducers manufactured by Druck, Inc. Depth measurements were made with three ranges of pressure transducers: 1 psi for inlet water height, and 2.5 psi each for screen area and volute area, respectively. The exact locations of the pressure transducers in the inlet, screen area, and volute area are indicated in Figure 12.
2. Ultrasonic depth sensor: A Shuttle® 100 kHz ultrasonic sensor (measuring range up to 3 ft. with accuracy of ± 0.04 in.) manufactured by MJK North America was used to measure real-time depth of flow in the 6-in. Parshall flume.

Installation and calibration procedures and locations for each pressure transducer and ultrasonic depth sensor will be described in further detail in the next section of report (Calibration Procedures for Water Depth and Flow Measurement Devices).

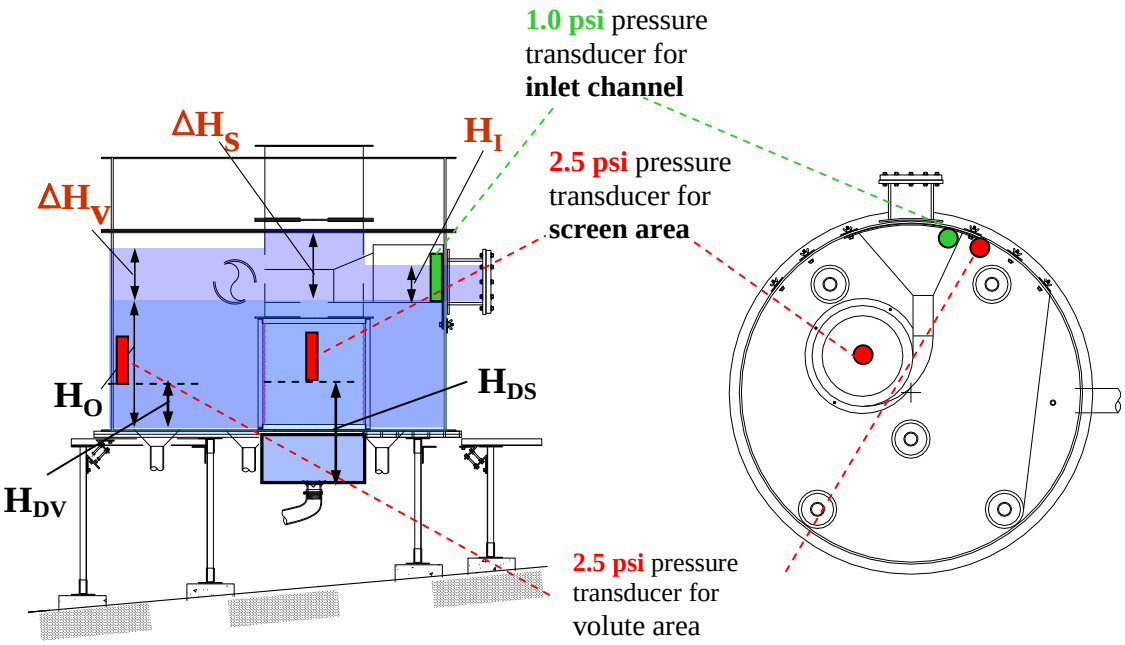

Figure 12
Graphical description of locations of pressure transducers

ΔH_S = H_S (Pressure head from the invert of sump) - H_O

ΔH_V = H_V (Pressure head from the invert of volute chamber) - H_O

H_I = Pressure head in inlet open channel

H_O = Depth of quiescent water under no inflow

H_{DS} = Default height of 2.5 psi pressure transducer from the invert of sump

H_{DV} = Default height of 2.5 psi pressure transducer from the invert of volute chamber

A CR1000 datalogger, manufactured by Campbell Scientific Inc., was used as the real-time data monitoring and data collection unit. The pressure transducers and the ultrasonic sensor were hard-wired to the CR1000 datalogger. The CR1000 datalogger was configured to enable data-monitoring with 1-s sampling intervals and was powered for constant operation by 110-V AC power for continuous data logging. Data was transferred from the datalogger to a data acquisition notebook computer via a data transfer cable. LoggerNet v3.0, a data monitoring and acquisition program compatible with the CR1000 datalogger was installed on the data acquisition notebook computer. LoggerNet v3.0 provides a graphical user interface (GUI) with which the testing personnel were able to communicate with the datalogger. Each sensor utilized in the study was assigned appropriate multipliers and offsets in order to obtain data in the required depth formats (inch or ft.). The multipliers and offsets were inserted in the main program associated with the CR1000 datalogger with the help of an associated module of LoggerNet v3.0, the CRBasic module. Data was retrieved from the CR1000 datalogger by utilizing the LoggerNet v3.0 program after each individual test as required. A QA/QC check was performed after each data download to ensure that the acquired data was valid. This was done by routinely checking for any outliers, spikes, or questionable values in the data that could indicate erroneous measurement.

Calibration Procedures for Water Depth and Flow Measurement Devices

Calibration of Pressure Transducers

The CS420-L pressure transducers with 1 psi and 2.5 psi range (Model PDCR 1830-8388) manufactured by Druck, Inc. were connected to the CR1000 datalogger (Campbell Scientific, Inc.). The data acquisition notebook computer was connected to the CR1000 datalogger for real-time data monitoring. The pressure data measured by each pressure transducer was

reported as millivolts (mV) as raw data acquired by the computer through the CR1000 data logger.

In order to convert voltage (as mV) readings to depth results (ft.), a calibration curve for each pressure transducer was developed. The calibration also helped quantify the accuracy of measurement. The pressure transducer was placed in a clean container filled with discrete depths of water under static conditions. The depth of water in the container was physically measured using an engineering scale at 20 ^{o}C.

This physical depth measurement was coupled to the mV reading obtained from each pressure transducer through the datalogger. After the mV readings were plotted as a function of physically-measured depth data, a linear regression procedure provided the necessary multiplier, m_n (slope), and offset, b_n (intercept) parameters. The significance of these parameters and their inclusion in the data acquisition computer program (LoggerNet) is explained in detail in the succeeding text. The multiplier and offset parameters were input into the data acquisition program in order to obtain data in depth units (ft.). These parameters were included in the section of the program where all governing constants were declared. Specifically, in lines of the program that read:

Const DepthM_n = m_n
Const DepthB_n = b_n

where, n = 1,2,3 and corresponds to the designated enumeration for the corresponding sensor.

The previous procedure was repeated for each individual pressure transducer that was utilized in this study. Each sensor was scaled with respect to the expected depth being measured. For instance, the 1 psi sensor at the inlet of the PMSU 20_20 was expected to measure no more than 1.8 ft. of head, and thus calibrated for the expected measurement range.

The method suggested by the manufacturer to calculate the multiplier and offset involved the following steps. It was recommended that the multiplier should be calculated as:

- M = {1}/{Sensitivity (mV/V/psig)}, if the sensitivity values provided in the

calibration certificate by the manufacturer are in mV/V/psig).

- M = {Range (psig)}/ {(Sensitivity (mV)/Supply Voltage (v)}, if the sensitivity values provided in the calibration certificate by the manufacturer are in mV.

The offset was to be the difference in the staff gage measurement of depth compared with the measured depth by the sensor (Druck models PDCR 1830 and 1230 pressure transducers instruction manual).

The previous method was treated with caution, and each pressure transducer was recalibrated on site to account for any changes in sensitivity due to factors, such as shipping, handling, and temperature changes. That is, each sensor was recalibrated in-situ, and the multipliers and offsets obtained from the corresponding linear regression techniques were used in favor of a standard calibrated relationship provided by manufacturer data sheets. The monitored data was modeled with a linear regression and the slope and intercept obtained were used as the multiplier and the offset, respectively, in the data acquisition program. This recalibration provided an individual in-situ corrected monitor to measure the depth curve for each transducer, which was then used in all corresponding analyses. Calibration curves for the pressure transducers used are provided in **Error! Not a valid bookmark self-reference.** for the single 1 psi pressure transducer and each of the two 2.5 psi transducers utilized. The resolution and measured depth ranges of the sensors were as follows. The 1 psi sensor was used to measure depths up to 20 in. with a resolution of around 0.01 in. The 2.5 psi sensors were each used to measured depths up to 30 in. with a resolution of around 0.02 in.

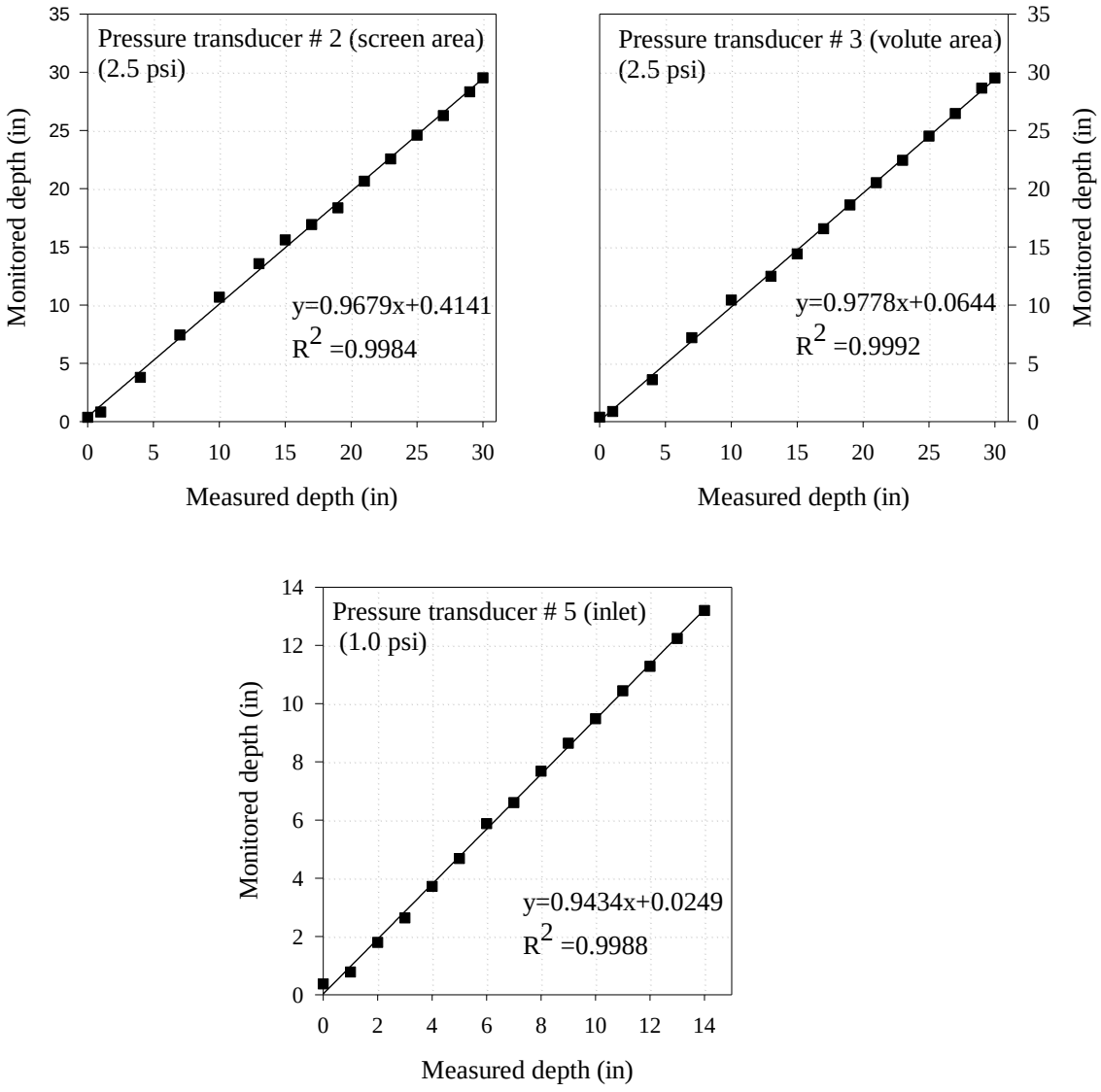

Figure 13
Calibration curves for 2.5 psi and 1.0 psi pressure transducers

Calibration of Influent Reservoir (Baker Tank)

A ¼ inch thick carbon steel tank with the nominal capacity of 10,000 gallons, simply called a "Baker tank," was used as the reservoir for volumetric calibration of the 6-in. Parshall flume and as the reservoir for treatment runs. Although the manufacturer provided geometric and dimensional data for the tank, the stage-storage relationship was established through calibration and validation processes in order to ensure the validity of the stage-storage relationship. The influent reservoir tank was filled to a known depth. The depth was noted from the calibrated pressure transducer measurement displayed in the real-time datalogger program (LoggerNet v3.0) on the data-acquisition notebook computer. LoggerNet v3.0 software provided program generation, editing, data retrieval, and real-time monitoring. The influent reservoir was then allowed to discharge by gravity flow into a calibrated 1000-gallon cylindrical HDPE storage tank of known diameter (used later as a surge tank during the test process). The volume of water discharged by the Baker tank for the given decrease in head was calculated from the volume stored in the HDPE storage tank. The volume of quiescent water in the 4 in.-diameter discharge line was also included in the overall volume calculation. Six replicate measurements were made for each trial. Figure 72 indicates the stage-storage relationship in the Baker tank.

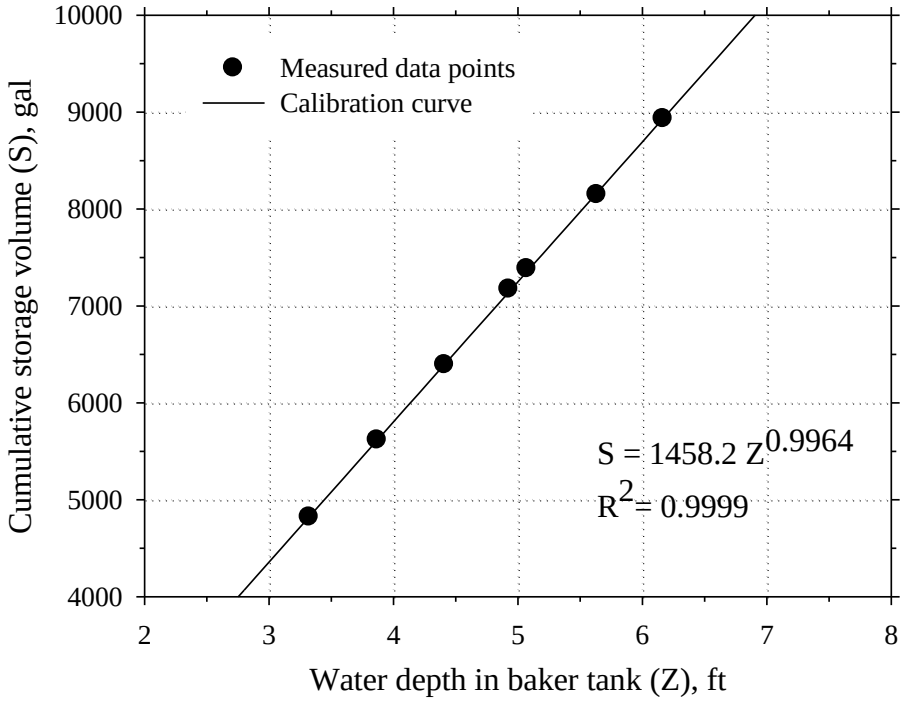

Figure 14
Stage-storage relationship in the Baker tank

Calibration of MJK Ultrasonic Sensor for Flow Depth Measurements

A Shuttle® 100-kHz Ultrasonic sensor (*Unit #2094)* manufactured by Branom Instrument Company was mounted 30 in. above the invert surface of the 6-in. nested Parshall flume and at the 2/3(A) location on the flume. The ultrasonic sensor had a measuring range up to 3 ft. and an accuracy of ± 0.04 in. The sensor was connected to the CR1000 datalogger and delivered an analog voltage output signal (mV) to the CR1000.

In order to convert the voltage signal to depth, a calibration procedure between voltage and depth was followed. First, the invert surface of the 6-in. Parshall flume was cleaned and dried. Once the surface had been prepared, a sensor measurement was obtained. This measurement provided the voltage reading from the MJK ultrasonic sensor, as observed from the data acquisition notebook computer. This measurement was noted to be the zero depth or control reading. The distance from the point that the signal emanated from the mounted sensor to dry, clean invert was also physically measured. Any effect of background vibrations, due to the site characteristics (vehicle-generated vibrations), were taken into effect by an extended observation period to account for any fluctuation in voltage signals. These fluctuations were addressed by analyzing data recorded by the datalogger across periods of time corresponding with typical testing periods of the day to account for traffic variations. Typical fluctuations due to mechanical vibrations were found to be negligible (< ± 0.05%), and were, therefore, assumed to have an insignificant effect on overall accuracy of measurement.

Once voltage signal and depth pair of measurements were recorded for the dry, clean invert, measurement pairs (voltage, height) at a series of discrete depths were made for the expected range of flow depths in order to produce a calibration curve for the Parshall flume. Rectangular wooden blocks of measured height were placed on the clean, dry invert of the flume to a known (measured) height, directly underneath the ultrasonic sensor, and corresponding voltage readings were noted. Depths were measured from 0.5 in. to 12 in., in 10 increments, utilizing appropriately-sized wooden blocks. The depths of these wooden blocks were 1.063 in., 1.875 in., 2.063 in., and 3.563 in.

Once this series of measurement pairs was completed, a calibration curve was developed to establish a relationship between the analog voltage output signal and the distance from the sensor to the surface of the block, and therefore to the actual depth in the Parshall flume since the distance between the sensor and Parshall flume invert was known. Duplicated

readings were made and standard deviation from duplicated readings is indicated by error bars in Figure 15. Following a continuous power law regression procedure, a calibration curve was developed for the ultrasonic sensor monitored depth (reported as voltage, mV) as a function of measured depth.

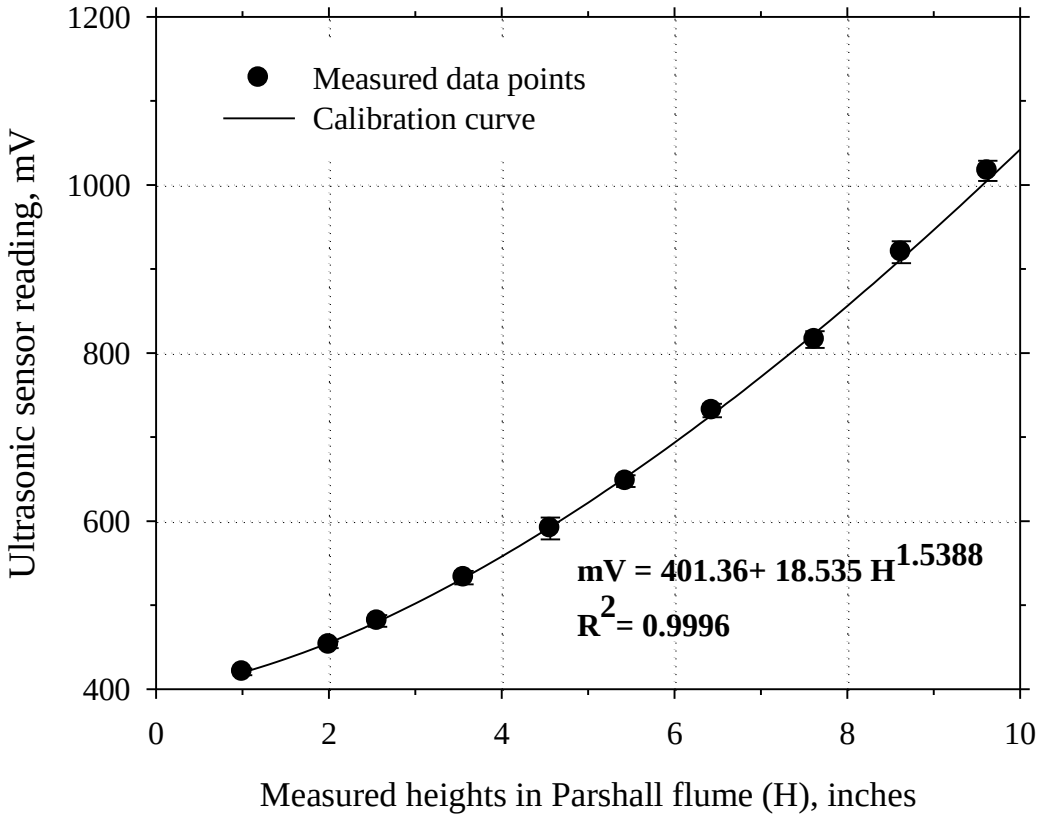

Figure 15
Calibration curve for 100-kHz ultrasonic sensor mounted in 6-in. Parshall flume

The values for the multiplier (m_n) and offset (b_n) for input into the data acquisition program were chosen as 1 and 0, respectively, in the section of the program where all governing constants were declared. Specifically, in lines of the program that read:

Const $VoltM_n = m_n$
Const $VoltB_n = b_n$

Depth (in.) values corresponding to voltage (mV) output from the ultrasonic sensor were calculated from the continuous power law model calibration curve, indicated in Figure 15.

Calibration of Parshall Flume

A dual range (nested) fiberglass Parshall flume (manufactured by Warminster Fiberglass) was installed as the primary flow measurement device for testing 7.0 ft. diameter PMSU20_20. A 6 in. width of throat size was nested inside a 12 in. flume to accommodate the range of tested flow rates and increase precision. The installed Parshall flume was volumetrically calibrated. The volumetric calibration procedure for each flow rate is described as follows.

The Baker tank used for supply water was filled to capacity using potable water from the nearby fire hydrant located approximately 100 ft. from the influent Baker tank. The data acquisition notebook computer was connected to the CR1000 datalogger, and real-time data were monitored on the LoggerNet v3.0 software and the graphical user interface.

Prior to a series of calibration runs, trial flow rate management runs were also performed to obtain a better sense of the relationship between the extent of opening for each valve (4 in. influent discharge valves and 4 in. recirculation valve) and rpm (revolutions per minute) of the influent pump and achievable flow rate so that it enabled the experimenters to achieve and maintain target flow rate quickly and effectively. After influent discharge valve and 4-in.-recirculation valve were opened to an approximate predetermined level (from trial flow rate management runs), the 1,100-gpm capacity diesel pump was started. Flow rates were further adjusted by operating the discharge and recirculation valve on the 4-in. diameter discharge line and the butterfly valve on the 12-in. diameter feed line, immediately upstream of the Parshall flume as depicted in Figure 10. The effluent diesel pump downstream of the effluent surge tank was started when the surge tank volume was close to 50 percent of its total capacity. The flow rate of effluent pump was also manually adjusted to a level of

influent flow rate so that the surge tank can retain approximately 50 percent of its total capacity at all times. It was noticed that the typical time taken for the flow to reach steady state conditions at a desired flow rate was less than 60 seconds. The steady state conditions were checked by monitoring the real-time data from the data acquisition program to ensure that the fluctuation of depth reading from MJK ultrasonic sensor is within ± 10 mV for at least 20 seconds.

When the flow reached a steady state, at a chosen flow rate, starting time for a calibration run was recorded. Elapsed run time was determined in the range of 3 minutes to 30 minutes based on operating flow rate (in the range of 50 gpm to 600 gpm) and the constraint of available water volume in the influent reservoir. At least 1,500 gallons of water were used at each calibration run for a target flow rate. At the end of the predetermined run time (3 ~ 30 minutes), the influent pumps were turned off and two valves (the influent discharge valve and 4-in. recirculation valve) were immediately closed. Several minutes later, the effluent pumps were also turned off. Depth data in flume electronically measured by ultrasonic sensor were downloaded from the datalogger. The volumetric flow rate for the corresponding depth in the Parshall flume was calculated based on the total volume of water (available from change of water depth in the Influent baker tank) and elapsed run time (available from stop-watch).

The above procedure was repeated for a calibration range of 1.7 in. to 9.3 in. which correspond to flow rates of 51.7 gpm to 590.7 gpm. A calibration curve was developed for the Parshall flume, and compared to that provided by the manufacturer (ASTM 1991; ISO 1992) as indicated in Figure 16. Measurement pairs (voltage and depth) for each flow rate in the Parshall flume was made in pairs. Error bars represent the standard deviation from duplicated readings, and they were within ± 13 mV. The volumetric calibration procedure yielded a curve that fit the rating curve provided by the manufacturer ($R^2 = 0.9985$).

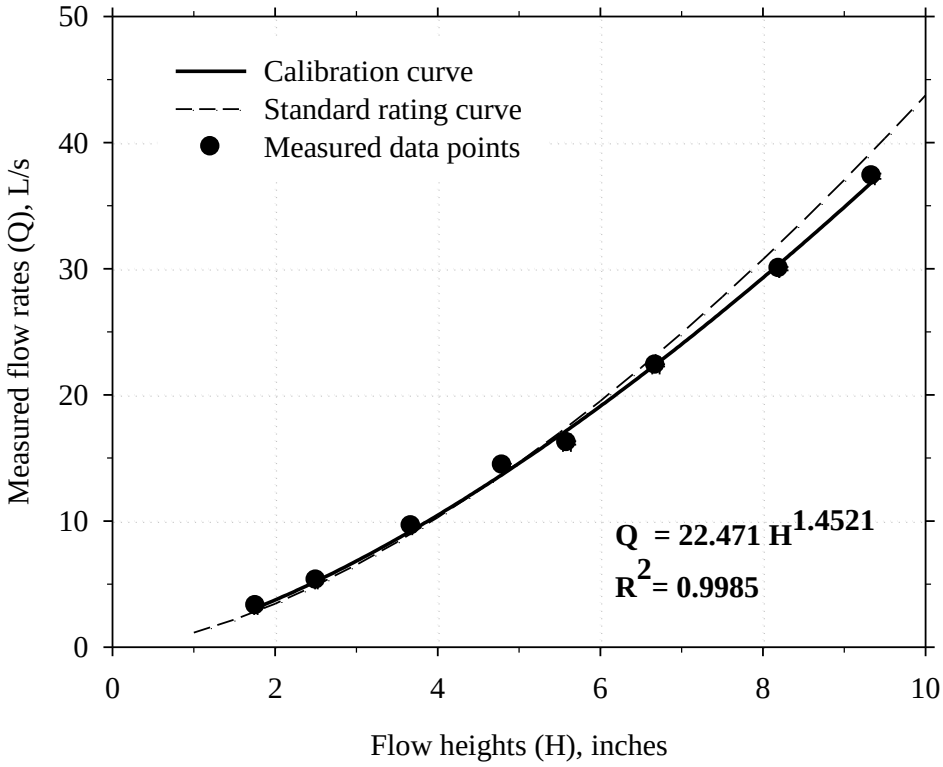

Figure 16
Calibration curve for 6-in. Parshall flume

Experimental Design for PMSU20_20

The parameters selected in the experimental design matrix included:

1. particle concentration (100 mg/L, 200 mg/L and 300 mg/L);
2. flow rate (10%, 25%, 50%, 75%, 100%, and 125% of the given design capacity of 1.1 cfs);
3. screen aperture size (4700 μm and 2400 μm);
4. diameter of volute separation chamber (5.0 ft., 6.0 ft., 7.0 ft.); and
5. an influent particle gradation based on an NJCAT gradation, a non-uniform, and a non-cohesive sandy-silt (USCS designation as opposed to a Φ_{50} classification).

The three concentrations of NJCAT influent particles, 100 mg/L, 200 mg/L, and 300 mg/L were used to examine the effect of particle concentration on the separate performance of the

PMSU20_20 with a 2400 um and 4700 μm screen under the selected hydraulic loadings. It was hypothesized that the hydraulic characteristics and particle separation mechanisms were different in the screen area and the volute area of the PMSU20_20. It is a subject of our continued evaluation as to how the overall particle separation performance will be affected if screen area is increased (or decreased) while total horizontal surface area of unit remains constant at a given operating flow rate and loading conditions (influent PSD and concentration). In other words, how will particle separation efficiency of PMSU20_20 be influenced by changing relative ratio of screen area to volute area while total area, the summation of screen and volute area, remains unchanged. In order to answer this question, a unit needs to have flexibility that diameter and location of the screen can be changed while overall unit diameter is kept constant. The PMSU20_20 unit provided by HS Technologies for this study was a commercial unit and conformed to the specifications of PMSU20_20 units that are manufactured and distributed. It was designed with the flexibility that outer diameter of volute sections can be changed to three different sizes (60, 72, and 84 in.). However, the location and size of the screen in the tested PMSU20_20 are not changeable as illustrated in Figure 11.

In order to answer this question at least indirectly given the fact that only the diameter of volute area can be changed, the same SLR (surface loading rate, sometimes called "overflow rate") was applied to each diameter (60, 72, and 84 in.) of PMSU20_20, which will simulate the condition mentioned above where the effect of relative ratio of screen and volute area on separation performance can be investigated. The tested ranges of flow rates for each diameter of units that were set up to provide the same SLR (Surface Loading Rate). As summarized in the table at the bottom of Figure 11, the relative dominance of volute area with respect to screen area increases as the diameter of volute area increases from 5.0 ft. to 7.0 ft. This is noticed by the increase of ratio of screen area to volute area from 0.10 to 0.22. 1.1 cfs (494 gpm, 31.2 L/s) that was used as a design flow rate for a 7.0-ft. diameter unit and 10 – 125% of 1.1 cfs (49.4 – 617.2 gpm) was the range of flow rate tested for 7.0 ft. diameter. The design flow rates for a 5.0-ft. and 6.0-ft. diameter unit were set up as 0.81 cfs (362.7 gpm) and 0.56 cfs (251.9 gpm), both of which provide the same surface overflow rate (0.87 cm/sec) as a 7.0 ft. unit at 100% of 1.1 cfs.

The experimental matrices for a 5.0 and 6.0-ft. diameter PMSU20_20 unit with the 2400 μm screen and the 7.0 ft. diameter unit with 2400 μm and 4700 μm are summarized in Table 7, Table 8, Table 9, and Table 10, respectively, along with corresponding performance results.

Table 7

Summary of treatment run results for 5.0 ft. diameter PMSU20_20 with a 2400 µm screen aperture loaded by NJCAT gradations under 100, 200, and 300 mg/L and various operating flow rates

Run	Flow rate [gpm]	Influent conc. [mg/L]	Influent mass [g]	Volute mass captured [g]	Volute/ Influent [%]	Sump mass captured [g]	Sump/ Influent [%]	SSC Removal efficiency [%]	Mass balance check [%]	Turbidity Removal [%]
3	314.9	200	3145	745.2	23.7	369.2	11.7	35.4	-0.7	19.9
2	251.9	200	3145	811.8	25.8	448.2	14.3	40.1	-2.3	14.7
1	188.9	200	3145	856.0	27.2	590.1	18.8	46.0	-2.3	23.4
4	125.9	200	3145	1047.4	33.3	780.6	24.8	58.1	-4.5	24.0
5	63.0	200	3145	1020.2	32.4	952.7	30.3	62.7	-4.7	38.8
1'	25.2	200	3145	1051.4	33.4	1053.2	33.5	66.9	-3.0	45.3
6	314.9	100	1573	352.2	22.4	196.6	12.5	34.9	-6.9	16.5
7	314.9	300	4718	1113.3	23.6	509.5	10.8	34.4	-2.8	22.0
8	188.9	100	1573	441.9	28.1	289.3	18.4	46.5	3.8	20.1
9	188.9	300	4718	1262.0	26.8	802.4	17.0	43.8	-4.6	26.9
10	63.0	100	1573	491.4	31.2	504.5	32.1	63.3	-6.2	29.0
11	63.0	300	4718	1421.5	30.1	1408.2	29.9	60.0	-5.8	39.5

Table 8

Summary of treatment run results for 6.0 ft. diameter PMSU20_20 with a 2400 µm screen aperture loaded by NJCAT gradation under 100, 200, and 300 mg/L and various operating flow rates

Run	Flow rate [gpm]	Influent conc. [mg/L]	Influent mass [g]	Volute mass captured [g]	Volute/ Influent [%]	Sump mass captured [g]	Sump/ Influent [%]	SSC Removal efficiency [%]	Mass balance check [%]	Turbidity Removal [%]
12	453.4	200	4536	1248.9	27.5	479.9	10.6	38.1	-8.5	18.7
13	362.7	200	4536	1408.9	31.1	523.1	11.5	42.6	-3.0	14.8
14	272.0	200	4536	1524.0	33.6	573.2	12.6	46.2	-8.6	18.3
15	181.4	200	4536	1735.4	38.3	755.5	16.7	54.9	1.9	22.9
16	90.7	200	4536	1672.1	36.9	1119.0	24.7	61.5	-2.5	35.7
17	36.3	200	4536	1703.0	37.5	1398.2	30.8	68.4	3.7	39.7

18	453.4	100	2268	632.8	27.9	222.3	9.8	37.7	-3.1	15.4
19	453.4	300	6804	1857.5	27.3	734.8	10.8	38.1	-7.9	25.0
20	272.0	100	2268	791.6	34.9	330.3	14.6	49.5	0.1	15.3
21	272.0	300	6804	2258.9	33.2	823.3	12.1	45.3	-6.6	28.5
22	90.7	100	2268	852.8	37.6	564.7	24.9	62.5	-2.9	28.5
23	90.7	300	6804	2585.5	38.0	1639.8	24.1	62.1	0.3	31.3

Table 9

Summary of treatment run results for 7.0 ft. diameter PMSU20_20 with a 2400 µm screen aperture loaded by NJCAT gradation under 100, 200, and 300 mg/L and various operating flow rates

Run	Flow rate [gpm]	Influent conc. [mg/L]	Influent mass [g]	Volute mass captured [g]	Volute/ Influent [%]	Sump mass captured [g]	Sump/ Influent [%]	SSC Removal efficiency [%]	Mass balance check [%]	Turbidity Removal [%]
24	617.2	100	2800	904.2	32.3	315.2	11.3	43.6	-2.7	26.0
25	493.7	100	2800	923.6	33.0	271.9	9.7	42.7	-6.5	26.2
26	370.3	100	2800	966.3	34.5	398.2	14.2	48.7	-6.5	25.0
30	246.9	100	2800	1125.2	40.2	439.2	15.7	54.4	-5.2	20.7
28	123.4	100	2800	1158.0	41.4	701.3	25.0	66.4	-0.5	41.9
31	49.4	100	2800	1201.8	42.9	762.5	27.2	70.2	4.0	39.7
32	617.2	200	5600	1746.4	31.2	621.2	11.1	42.3	-7.7	19.1
29	493.7	200	5600	1828.4	32.7	632.4	11.3	43.9	-9.8	16.3
33	370.3	200	5600	1898.4	33.9	722.4	12.9	46.8	-7.7	23.2
27	246.9	200	5600	2123.4	37.9	809.1	14.4	52.4	-8.0	17.7
34	123.4	200	5600	2156	38.5	1321.6	23.6	62.1	-7.9	32.1
35	49.4	200	5600	2346.4	41.9	1573.6	28.1	70.0	-2.6	40.1
36	617.2	300	8400	2511.6	29.9	840	10.0	39.9	-6.1	23.1
37	493.7	300	8400	2679.6	31.9	912.4	10.9	42.8	-6.3	27.3
38	370.3	300	8400	2709.4	32.3	1070.2	12.7	45.0	-4.3	27.0
39	246.9	300	8400	3150	37.5	1268.4	15.1	52.6	-1.1	32.6
40	123.4	300	8400	3183.6	37.9	2009.4	23.9	61.8	-5.2	45.3
41	49.4	300	8400	3628.8	43.2	2360.4	28.1	71.3	-5.0	47.3

Table 10

Summary of treatment run results for 7.0 ft. diameter PMSU20_20 with a 4700 µm screen aperture loaded by NJCAT gradation under 100, 200, and 300 mg/L and various flow rates

Run	Flow rate [gpm]	Influent conc. [mg/L]	Influent mass [g]	Volute mass captured [g]	Volute/ Influent [%]	Sump mass captured [g]	Sump/ Influent [%]	SSC Removal efficiency [%]	Mass balance check [%]	Turbidity Removal [%]
45	617.2	100	2800	901.7	32.2	191.5	6.8	39.0	-4.4	18.7
44	493.7	100	2800	966.8	34.5	200.2	7.2	41.7	-4.5	36.4
43	370.3	100	2800	994.2	35.5	250.1	8.9	44.4	-4.6	21.2
42	246.9	100	2800	1169.6	41.8	256.5	9.2	50.9	-8.0	16.7
46	123.4	100	2800	1248.2	44.6	397.4	14.2	58.8	-2.8	24.5
47	49.4	100	2800	1205.6	43.1	699.5	25.0	68.0	8.8	26.2
49	617.2	200	5600	1752.5	31.3	411.8	7.4	38.6	-7.1	12.9
50	493.7	200	5600	1863.4	33.3	449.2	8.0	41.3	-7.5	24.4
48	370.3	200	5600	1931.5	34.5	586.4	10.5	45.0	0.4	17.3
51	246.9	200	5600	2383.5	42.6	503.2	9.0	51.5	5.0	22.1
52	123.4	200	5600	2423.2	43.3	855.3	15.3	58.5	-7.9	32.2
53	49.4	200	5600	2387.2	42.6	1476.2	26.4	69.0	4.6	34.1
54	617.2	300	8400	2494.2	29.7	582.3	6.9	36.6	-8.9	23.3
55	493.7	300	8400	2725.2	32.4	601.6	7.2	39.6	-5.8	24.9
56	370.3	300	8400	2794.2	33.3	803.0	9.6	42.8	-7.7	26.6
57	246.9	300	8400	3429.7	40.8	820.1	9.8	50.6	5.8	31.9
58	123.4	300	8400	3744.7	44.6	1492.2	17.8	62.3	5.0	44.2
59	49.4	300	8400	3616.8	43.1	2068.5	24.6	67.7	0.9	46.5

Field Testing Procedure

Prior to starting each test all testing equipment including the tanks, PMSU20_20, and the entire flow transport system were thoroughly cleaned using potable water delivered from a fire hydrant outlet with a 2-in. diameter and 50 lb/in.^{2} to the 100 ft. of 2 in.-diameter flexible fire hose. This cleaning involved manual sweeping and flushing with clean potable water throughout the entire system and was intended to ensure that were no deposited particles or external materials in any component of the experimental system. Once the entire system was cleaned, the 10,000-gallon influent Baker tank was then filled with potable water. This cleaning procedure was utilized consistently immediately before each experiment. Water

temperature was checked every two days. The average temperature of tap water remained consistent at around 21^{o}C with a standard deviation of ± 2^{o}C.

Before the start of each testing run, the clean Baker tank was filled to capacity (nominally 10,000 gallons) using potable water and a clean PMSU20_20 was filled with particle-free potable water. The data acquisition notebook computer was connected to the CR1000 datalogger, and sensor data was monitored in real time on the LoggerNet v3.0 software and graphical user interface. The data measured are detailed in the section of data acquisition and management.

The 4-in. influent discharge valve and 4-in. recirculation valve were opened to an approximate predetermined level (determined from trial flow rate management runs). Following this step, the 1,100-gpm capacity diesel pump was started and the flow rate was adjusted by operating the combination of discharge and recirculation valve on the 4-in. diameter discharge line and the butterfly valve on the 12-in. diameter feed line, immediately upstream of the Parshall flume as depicted in Figure 10. Operating flow rate was checked by monitoring the MJK ultrasonic sensor data from LoggerNet v3.0, a data monitoring and acquisition program. When target water depth in the Parshall flume was achieved and the fluctuation of depth reading from MJK ultrasonic sensor was within ± 10 mV for at least 20 seconds, the test was started. Influent particle slurry prepared based on NJCAT gradation started to be directly injected into the drop box after a theoretical residence time which was calculated based on operating flow rate and the unit effective volume. The effective volume of a unit indicates the volume occupied by stagnant water when there is no influent flow. 5.0, 6.0 and 7.0 ft. diameter of the PMSU20_20 have 1436, 2067 and 2814 L of effective volume, respectively as summarized in Figure 11. The drop box is located immediately downstream of the 6 in. Parshall flume and connected to the inlet of PMSU20_20 by the section of a 10 in. diameter PVC pipe. Dry mass of particle mixture required to achieve three levels of gravimetric concentrations (nominally 100 mg/L, 200 mg/L and 300 mg/L) was calculated based on 28,000 L (7407 gallons) of total influent volume. The rate of particle injection was consistent across the period of test run on a gravimetric and granulometric basis. Details about granulometric characteristics and preparation of NJCAT gradation are presented later in the section of PMSU20_20 influent particulate material.

Duration of each test run was pre-determined by target operating flow rate and constrained by the available volume of the influent Baker tank reservoir. Overall influent treated volume

was approximately 7,400 gallons regardless of tested operating flow rates. Sampling design and methodology will be further detailed in the next section of this report. The number of turnover volumes, which indicates the ratio of total volume of influent to the total volume of the PMSU20_20 unit as operated at a given flow rate was always lower than 10 and decreased as the operated flow rate increased because the volumetric depth of water in the PMSU20_20 unit also increased as the flow rate increased. Figure 17 describes the storage relationship in the 84-in. diameter and turn-over volume as a function of operating flow rates. At the end of predetermined run time (12 ~ 150 minutes), which will be detailed in the next section, the influent pumps were turned off and two valves (influent discharge valve and 4 in. recirculation valve) were immediately closed. After a couple of minutes later, effluent pumps were also turned off. Following this, depth data in flume electronically, measured by an ultrasonic sensor for the test time period, were downloaded from the datalogger. A known amount of coagulant (ferric chloride) was added to screen and volute area of the PMSU20_20 unit and the four 55-gallon polypropylene tanks to accelerate the settling process of particles. Forty 2-L effluent sample bottles (20 discrete replicated 2 L samples) were transported to the laboratory for water quality and SSC analyses.

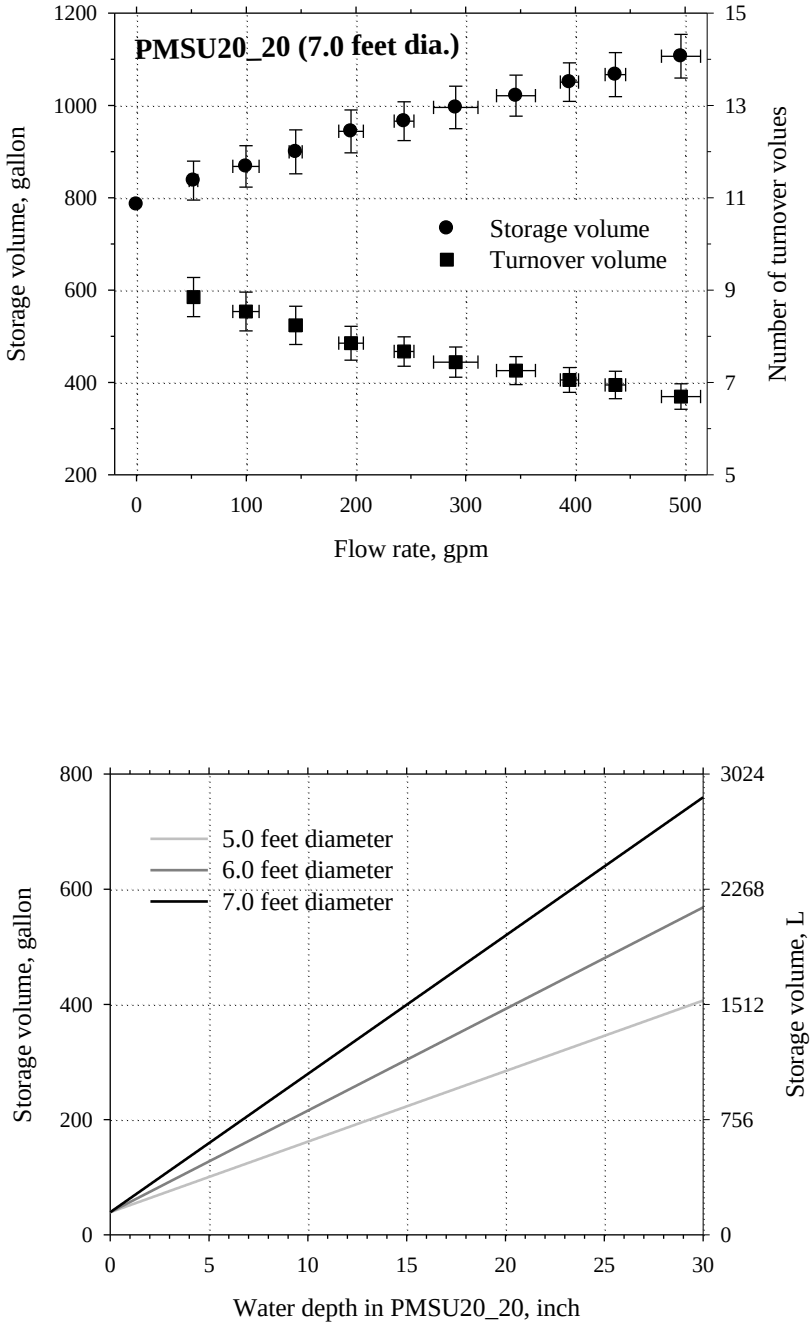

Figure 17
Storage volume-flow rates relationship in 7.0 ft. diameter PMSU20_20 under steady flow rate conditions

Sampling Design and Methods

PMSU20_20 Effluent Particulate Material

Total treatment run time was determined based on the steady state target flow rate and total treated influent volume (~ 7,500 gallons) which was determined based on the volume capacity (~ 10,000 gallons) of influent, volume of water consumed during the target flow generation time and the minimum volume (~ 1,000 gallons) that the influent bucket has to retain in order to prevent any sudden flow rate drop. Treatment run times at 10, 25, 50, 75, 100, and 125% of 1.1 cfs flow rates were 120, 60, 30, 20, 15, and 12 minutes, respectively. Twenty discrete replicated (A and B) 2 L effluent samples were collected in 2 L wide-mouth volumetric sample bottles for water quality and SSC analyses at consistent sampling time intervals throughout the duration of each test run. These sampling interval times were calculated based on treatment run times and were in the rage of 450 sec to 35 sec for the range of operating flow rates from 10% to 125% of design flow rate of each PMSU20_20 diameter.

Effluent samples were taken from a free outfall nappe that discharged from the 10 in. effluent pipe into a lower surge tank to ensure full cross-sectional sampling for each sample. This unique sample collection method was utilized to eliminate any bias in the measurement of particle mass concentration due to the segregation of particles of differing size and mass in the effluent cross-section.

In addition to the discrete samples described in the preceding paragraph, nominally 200 gallons of effluent were captured and recovered in four of 55-gal polypropylene tanks. The 200 gallons of effluent volume was generated by taking multiple 10.0 L samples at equal time intervals across the duration of each run at the same sampling frequency as the 2.0 L samples described above. The 200 gallons were captured across each run in order to recover sufficient particle mass to carry out gravimetric particle gradation analyses for the effluent.

PMSU20_20 Captured Particulate Material

After each run, a known amount of coagulant (ferric chloride) was added to screen and volute area of the PMSU20_20 unit to accelerate the settling process of particles. At least 5 hours of settling time was allowed before slurry recovery.

The slurry recovery process was started by setting up siphoning hoses in the PMSU20_20

unit to drain supernatant. Particle mass loss through the siphoning process was approximately less than 0.5 percent of the total influent mass load by measuring particle concentration in drained supernatant. At the end of the siphon, particles captured by the PMSU20_20 unit from each run were completely recovered as wet slurry from the sump chamber and as wet slurry from the volute chamber (outer annular volume outside the screen). Effluent particles captured in two 55-gallon polypropylene tanks were also recovered as wet slurry. The entire slurry recovery process was done manually.

As illustrated in Figure 11, the screen area is the cylindrical volume within the section of cylindrical screen that holds the screened particles, and the volute area indicates the outer annular volume outside the screen and inside the outer unit diameter of the PMSU20_20 unit. The particle separation mechanisms of each of these areas are distinct, and therefore the sampling methodology required separate sampling and particulate material recovery from each area separately.

Particle slurry recovered from the PMSU20_20 unit was temporarily stored in three to four 55- gallon barrels for approximately 12 hours to facilitate further quiescent settling. This served the purpose of further concentrating the recovered slurry by draining the supernatant. Screen and volute particle slurry were finally transported to 5-gallon containers separately for the delivery to the laboratory. Two sets of particle slurries (screen and volute slurry) that were transported were completely dried at 40°C in glass trays followed by mechanical sieve analyses to obtain the required particle gradations. Sieve analysis is described in the next section.

Laboratory Analyses

Twenty of the replicated 2 L effluent samples transported from the field were mixed into replicated (A and B) 40 L composite containers. Laboratory analyses were conducted from these replicate composite effluent samples consisting of 20 individual replicate (A or B) samples taken at consistent sampling time intervals across the entire run time. The lab analyses consisted of turbidity analyses (ISO 1999) using a Hach 2100AN-IS turbidimeter, suspended sediment concentration (SSC) (ASTM 1999), and sieve analyses following standard procedure ASTM D422 (ASTM 1993).

SSC Analyses. An SSC analysis was performed to quantify particle concentration for each effluent composite sample as captured from each treatment run and to calculate the

effluent mass load by integrating with operating flow rates. Since discrete effluent samples were taken at consistent sampling time intervals and a steady flow rate condition across the entire run time, particle concentration in composite samples can represent effluent particle concentration. This methodology would incorporate a certain extent of experimental and sampling error associated with SSC analyses and instrumental error associated with flow rate measurement. These errors were part of a 10 material balance error criteria as a QA/QC. Previous work has demonstrated that in contrast to TSS (total suspended solids) the method for determining SSC produces relatively reliable results for samples of natural water, regardless of the amount or percentage of sand-size material in the samples (Gray et al., 2000). Therefore, a SSC analysis was done by filtering the entire volume (40 L) of replicate composite samples through a 1.2 µm fiberglass filter (ASTM 1999).

Sieve Analyses. All particle slurries recovered from the PMSU20_20 unit were completely dried in an electrical oven and maintained isothermally at 105 ^{o}C, and the screen area particles were weighted separately from the volute particles. The dry disaggregated particles were then sieved using mechanical sieves to obtain the required particle gradations. The individual mechanical sieves were #60 (250 µm), #80 (180 µm), #100 (150 µm), #140 (106 µm), #200 (75 µm), #230 (63 µm), #270 (53 µm), #325 (45 µm) and the pan (< 45 µm). The sieve analysis follows the standard procedure ASTM D422 (ASTM 1993). Particle size is defined by sieve diameter, which is the width of the minimum square aperture through which the particle passes (Allen, 1990). Dry solids separated on each of the stainless steel sieves were weighed and stored separately in round clear sample bottles. Mass balances were determined for each mechanical sieve analysis, and mass balance errors were in the range of 1 to 2 percent by dry mass. All analyses were conducted on a dry weight basis.

PMSU20_20 Influent Particulate Material

Three different silica sand gradations of silica sand particles, the #1 Dry (65), SCS-106, and 20/40 Oilfrac, were used to prepare the specified NJCAT gradation. These silica particles were obtained from the US Silica Company and were combined based on calculated mass ratios. Mass ratio of silica sands for the influent particle mixture was determined based on the particle size distribution of each individual silica sand gradation provided by the manufacturer to meet the specified NJCAT test gradation as summarized in Table 11.

Table 11

Particle size distribution (by mass) calculated based on product data sheets provided by US Silica Company for NJCAT component gradations

Particle Size		Silica particle gradations				Mass Fraction	Total % finer by mass
		1 #Dry (65)	scs-106	20/40 Oilfrac	Total		
(microns)		(g)	(g)	(g)	(g)	(%)	(%)
> 850	(coarse sand)	0.0	0.0	0.1	0.1	**0.0**	**100.0**
600~850	(coarse sand)	0.4	0.0	5.0	5.4	**0.5**	**100.0**
425~600	(coarse sand)	17.1	0.0	18.5	35.6	**3.6**	**99.5**
300~425	(medium sand)	57.0	0.0	1.4	58.4	**5.8**	**95.9**
212~300	(medium sand)	117.8	0.0	0.1	117.9	**11.8**	**90.1**
150~212	(find sand)	129.2	0.6	0.0	129.8	**13.0**	**78.3**
106~150	(find sand)	49.4	8.3	0.0	57.7	**5.8**	**65.3**
75~106	(very find sand)	8.7	32.7	0.0	41.5	**4.1**	**59.5**
50~75	(silt)	0.4	65.5	0.0	65.8	**6.6**	**55.4**
10~50	(silt)	0.0	279.7	0.0	279.7	**28.0**	**48.8**
1~10	(silt)	0.0	208.3	0.0	208.3	**20.8**	**20.8**
SUM		**380.0**	**595.0**	**25.0**	**1000.0**	**100.0**	

Product information source:
1 #dry (65) - http://www.u-s-silica.com/PDS/Pacific/Pac1Dry652000.PDF
SIL-CO-SIL® 106 - http://www.u-s-silica.com/PDS/Ottawa/OttSCS1062000.PDF
20/40 Oil Frac - http://www.u-s-silica.com/PDS/Ottawa/Ott2040OilFrac2000.PDF

The NJCAT target gradation and the tested gradation are illustrated in . The R^2 value (determination of coefficient) and p-value between the two gradations was 0.99 and 0.42, respectively. The granulometric parameters for NJCAT (tested gradation) are summarized and compared with the mean site gradation in rainfall-runoff from Baton Rouge, LA in Table 12. The NJCAT gradation is composed of a significant fraction of silt size particles; 55.4 percent mass of tested NJCAT gradation is finer than 75 μm. It is noted that the 75 μm sizes (#200 sieve) is the differentiation size between silt and sand size designations based on a central tendency (Nybakken, 1998). The Φ_{50} of the NJCAT gradation is 3.9 within the range of 3 to 4. NJCAT gradation is classified as very fine sand according to the Φ_{50} index.

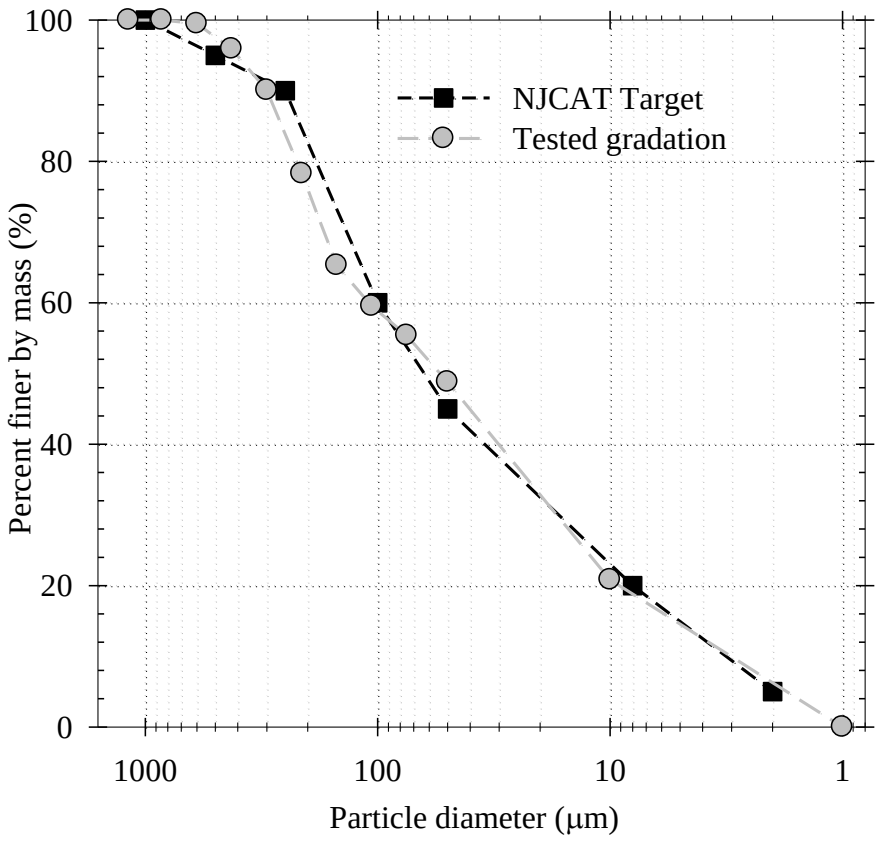

Figure 18
Influent particle gradation based on NJCAT target gradation utilizing 3 different particle gradations

Table 12

Summary of particle size distribution characteristics and granulometric parameters for NJCAT utilized in the presented tests and mean site gradation in rainfall-runoff of Baton Rouge, LA

Granulometric parameter	NJCAT	Mean site gradation in rainfall-runoff of Baton Rouge, LA
d_5	2.0 µm	44.3 µm
d_{16}	6.4 µm	64.2 µm
d_{25}	16.4 µm	80.6 µm
d_{50}	66.7 µm	181.2 µm
d_{75}	175.0 µm	416.0 µm
d_{84}	220.0 µm	585.9 µm
d_{95}	500.0 µm	1860.7 µm
dg	37.5 µm	193.9 µm
Φ_5	9.0	4.5
Φ_{16}	7.3	4.0
Φ_{25}	5.9	3.6
Φ_{50}	3.9	2.5
Φ_{75}	2.5	1.3
Φ_{84}	2.2	0.8
Φ_{95}	1.0	-0.9
σ_g	5.86	3.02
$\boldsymbol{\sigma_I}$	2.48	1.61
S_k	-0.30	0.15
K_G	0.96	0.93
Central tendency (Nybakken 1998)	very fine sand ($3 < \Phi_{50} < 4$)	fine sand ($2 < \Phi_{50} < 3$)
Uniformity	Very poorly sorted ($2 < \sigma_I < 4$)	Poorly sorted ($1 < \sigma_I < 2$)
Skewness (Lee 1998)	coarse skewed (-0.10 to -0.30)	fine skewed (0.10 to 0.30)
Kurtosis	mesokurtic (0.90 – 1.11)	mesokurtic (0.90 – 1.11)

This influent gradation was manually metered into the influent flow. The slurry mixing and feeding system consisting of a slurry tank with a mixing motor, peristaltic/recirculation pump, and slurry discharge/recirculation manifold was constructed on the top of the slurry mixing tower did not function. This slurry mixing system failed to suspend the NJCAT slurry (less than 3percent by mass). Therefore, this entire system was abandoned for these tests and a manual slurry injection was performed. Prepared NJCAT particle mixture was distributed into four of 2-L HDPE bottles evenly on a gravimetric and granulometric basis and was delivered to the field in a dry condition. Slurry condition of NJCAT particles was achieved by adding approximately 1.5 L of tap water into each bottle. The influent NJCAT particle gradation in a slurry form was directly added into a drop box with an evenly distributed manner on a consistent gradation and mass loading basis across the entire duration of each run. The dry mass that became the influent load was measured to the nearest 0.01 g.

Reporting SSC Removal Efficiencies

While there is an expectation that the determination of removal efficiency is straight-forward, the reality is that there is a significant amount of inconsistencies in the literature when claiming and reporting removal efficiencies for stormwater treatment systems. Three measurements are required: influent mass, effluent mass and captured mass, the analog is the same for stormwater treatment systems. However, it continues to be an incredulous revelation how willingly such a basic and universal principle is ignored. Such a universal principle is a minimum requirement for the validity of reported removal efficiency, yet is rarely practiced. In addition, different methods of calculation of removal efficiencies of a constituent in a particular unit operation produce different results and can be potentially misleading for understanding the actual performance of the unit operation. To address these differences, it was recommended (Urbonas, 1995) that the percent removal (PR) for any constituent is calculated and reported for each monitored event using the inflow and outflow loads. The following equation has often been suggested as the basic equation for calculating the removal rate percent of any sampled constituent:

$$PR(\%) = \frac{V_{IN} \times EMC_{IN} - V_{EFF} \times EMC_{EFF}}{V_{in} \times EMC_{IN}} \times 100 \quad (8)$$

However, one caveat associated with this equation that many professionals do not investigate

is the fact that influent or effluent loads are often estimated by integrating concentration of discrete samples with incremental volume or simply multiplying EMC with total flow volume into the investigated treatment system. This indicates that the calculated percent of removal has to involve a certain degree of errors generated from various sources including experimental, instrumental, and sampling errors. Therefore, in the presented report, the following equation was used to calculate SSC removal (%) where the PMSU20_20 Solid Mass is the mass that is actually recovered from PMSU20_20 unit.

$$SSC\ \mathrm{Re}moval\ (\%) = \frac{PMSU\,20\_20\ Solid\ \ Mass}{Influent\ \ Mass\ Load} \times 100 \qquad (9)$$

The only error associated with this equation might be from mass loss during the process of particulate material recovery. Therefore, the likelihood of error associated with the sampling process would be larger than the error with the direct recovery of captured particles from the unit, and 10 percent overall material balance by mass will include both of them as mentioned in the following section of QA/QC.

Quality Assurance/Quality Control (QA/QC)

In addition to the uncertainty associated with the calculated PR (%), the researchers have not identified a single case where a stormwater treatment material balance analysis was conducted as a QA/QC requirement to ensure, at least, the minimum validity of the treatment results. Even the regulatory agencies specifying the requisite performance of a stormwater treatment device do not require a material balance. To ensure this necessary but not sufficient level of QA/QC, a material balance analysis based on mass was also conducted after every event to ensure mass conservation and QA/QC based on the influent, effluent mass load and recovered mass in the screen and volute section of the PMSU_20 20 unit. Mass balance error was required to be within the range of ± 10 by mass and determined by the following equation:

$$\textit{Mass balance error (\%)} = \frac{\textit{[(In Load) - (Eff Load + PMSU20\_20 captured)]}}{\textit{(In Mass Load)}} x\,100 \qquad (10)$$

PMSU20_ 20 load captured = Screen area load captured + Volute area load captured

The QA/QC for the influent gradation was carried out by comparing the target influent gradation to measured (sieved) results. Results of target gradation and the measured gradation are illustrated graphically in Figure 18. Particle density for all size of particles was measured as 2.64 g/cm^3 ± 0.02 (ASTM 1994). Gradation method checks were repeated every 10 runs to ensure the consistency of influent gradation on a mass and gradation basis.

Green Infrastructure Design for the I-10 City Park Lake Bridge

Design Objectives

Elevated transportation infrastructure such as bridges represent sources of nutrients, metals, organics, and PM as direct discharges to water bodies. Management of such discharges at the land-water interface is significantly more challenging than for at-grade transportation systems. The Gulf Coast is traversed by transportation infrastructure, often elevated, with direct discharges to receiving waters. Utilizing this context, design alternatives focused on nutrients and PM management from a typical interstate bridge (the I-10 bridge) discharging to City Park Lake in Baton Rouge are provided. The project design objectives were to develop, design, and analyze water management options for the I-10 bridge. These design options include: (1) a conventional land-side BMP system consisting of clarification and filtration, (2) engineered oxide-admixture cementitious permeable pavement (CPP) as a green infrastructure material alternative to conventional impervious pavement, (3) a network of Buoyant Adsorptive Media (BAM) filters in the lake treating direct discharges from the I-10 bridge, and (4) a combined CPP and a BAM network. The objective functions for the design options included viability to meet existing or promulgated discharge requirements subject to historical continuous simulation data and design storm loadings, maintenance requirements, economics, and context-sensitive integration of the recommended design.

Methodology

The I-10 over City Park Lake consists of two separate approximately 820-ft. long cantilevered concrete bridges. Each bridge consists of a series of structural segments joined by interconnected expansion joints. Because the expansion joints and storm drain inlets hydraulically separate each segment, each segment was modeled hydrologically as a separate subcatchment, and hydrographs from each subcatchment combined through hydraulic routing as required for selected design options. East and west longitudinal slopes are approximately percent slope from the middle of the bridge (4th expansion joint), sloped toward each bridge

abutment. The transverse slope towards the storm drain inlet at each expansion joint is 1.8 percent. Figure 19 displays a plan view of two segments at the eastern bridge abutment. From the center of each bridge, three subcatchments drain to the eastern abutment and three drain to the western abutment. Currently runoff is discharged directly from the expansion joints and storm drains to the lake. Bridge subcatchments that span City Park Lake discharge individually to City Park Lake.

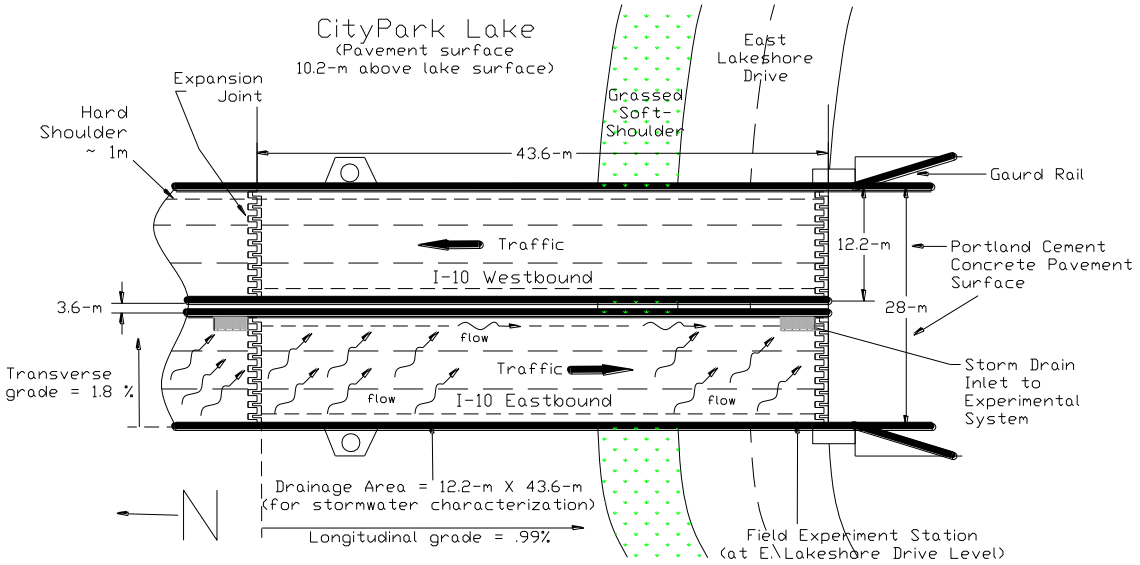

Figure 19
Plan view of two bridge subcatchments at eastern I-10 abutment

Water Chemistry Analysis

In order to examine the existing water chemistry of City Park Lake, samples were taken at mid-depth of the lake for a series of locations in April 2010. Conductivity, pH, redox, alkalinity, temperature, TN, TP, TSS, turbidity and particle size distributions (PSDs) were determined using Standard Method protocols (Greenburg et al., 1995). Rainfall-runoff water chemistry and loads from the bridge were obtained from the peer-reviewed literature utilizing an extensive hydrologic and water chemistry database published for this bridge of the runoff discharges and treatment thereof (Sansalone et al., 2005; Dean et al., 2005; Ying et al., 2008, Ying and Sansalone 2008, Sansalone and Ying 2008, Sheng et al. 2008, Liu et al. 2009, Sansalone et al. 2009, Lin et al. 2009, Liu et al. 2010, Sansalone et al. 2010a, Ma et al. 2010, Ying and Sansalone 2010a, Ying and Sansalone 2010b, and Sansalone et al. 2010b). These data represented the constitutive inputs needed for the treatment and maintenance design.

Modeling, Simulation, and Treatment Analysis

Multiple modeling, simulation and analysis tools were used to evaluate the behavior and maintenance of each design option. A summary of these modeling, simulation and treatment methods follows. USEPA's Stormwater Management Model (SWMM) 5 was chosen for unsteady design storm and continuous modeling providing hydrologic and hydraulic routing. The model is a rigorous unsteady hydrologic model with over four decades of utilization world-wide, having been originally developed at the University of Florida for the USEPA. SWMM is a comprehensive unsteady hydrology and hydraulics model in contrast to classical peak flow models. SWMM allows historical rainfall inputs for continuous simulation, evapo-transpiration, depression storage, and infiltration algorithms that were applied for the conventional treatment system design, the CPP, the BAM network, and the combination of CPP and BAMs. The modeling included infiltration of runoff, surface, and conveyance drainage or nonlinear routing of overland flow. Functionality includes flexible system size constraints and compatibility with existing rainfall data sets obtained from the National Oceanic and Atmospheric Administration's (NOAA) National Climactic Data Center (NCDC). Modeling included elements such as storage/treatment units and flow dividers, applying external flows and pollutant load inputs from surface runoff, and modeling various flow regimes.

The I-10 bridge was modeled as multiple subcatchments comprised of varying hydrologic properties. Subcatchment descriptors were provided for SWMM based on bridge infrastructure geometry and material properties. These descriptors included area, slope, hydraulic transport model, infiltration model (the Green-Ampt model), evaporation model (Penman-Monteith evaporation model) porosity and were determined for the subcatchments and material design properties, for example the CPP or BAMS. One hour rainfall data were obtained from the NCDC since one hour rainfall databases are supported by the NCDC as compared to 15- and 5-minute rainfall data. However shorter time steps were needed to match the catchment time of concentration. The one-hour NCDC data were disaggregated into 15-minute intervals to match the catchment response times. SWMM was validated utilizing published hydrologic datasets from the bridge.

User-defined loading and treatment process components included dry deposition buildup functions, direct contribution by rainfall, washoff (first-flush), fate of load constituents and constituent fractions due to treatment unit operations and processes and changes in loads through treatment by storage or conveyance units as analyzed by deterministic treatment methods; for example surface overflow theory, adsorption models of equilibria and breakthrough, or filtration headloss models such as Ergun. Analytical adsorptive-filtration models (Freundlich equilibria and Thomas breakthrough) for the BAMs and CPP were developed from media and CPP properties. Van Genuchten parameters were used to solve the flow equation and the Freundlich isotherm and kinetics parameters were used to equilibrium phosphorus adsorption by the CPP. Material and fluid flow properties and material-solute interaction properties were obtained from previous material datasets. Adsorption isotherm, kinetics, and breakthrough data were utilized for the CPP and BAM systems (Kuang et al., 2007). Physical modeling data were used to model solute breakthrough for the CPP and for the BAM media separately. The lifetime based on solute (metals) breakthrough was approximately 30 years (Kuang et al., 2007). Physical modeling data from I-75 in Cincinnati were used to demonstrate PM and PSD treatment and breakthrough for the CPP (Teng et al., 2004). The removal efficiency for each particle size was applied across the influent PSD and a subsequent outflow PSD and PM concentration was determined. The CPP as a porous friction course will be replaced every 10 years to maintain structural integrity based on current practice, significantly shorter than the breakthrough lifetime.

A Geographic Information System (GIS), specifically ArcGIS, was used to integrate various road and bridge information acquired primarily from the Florida Department of Transportation and the Louisiana Department of Transportation and Development and information from USEPA's database of impaired water bodies and watersheds. Once spatially integrated, analysis was conducted based on ADT, total bridge deck area and combined with constitutive models of build-up and washoff (Ying et al. 2008, LADOTD, 2010; FDOT, 2010) to provide extensibility for estimating constituent loads on a regional or statewide basis.

Design Year and Storm Selection

A representative year was chosen for continuous simulation of each design option. The parameters for the representative year included no episodic events and total rainfall approximately equal to the average annual rainfall over the last 10 years of 58 in./year. The

year 2008 met these criteria with 58 in. of rainfall and no episodic events. Given the time of concentration for the total bridge watershed was on the order of 15 minutes, a 50-year, 1-hour design storm and the commensurate intensity-duration-frequency (IDF) curve was chosen to simulate the peak flow that is reasonably expected to exceed the majority of storms loading this watershed. Utilizing this dual approach, peak flow from a 50-year storm and separately continuous simulation from an average annual year the behavior of design options was examined.

Unit Cost and Economic Trend Analysis

The cost analysis was primarily based on unit costs of the various design option components. A sensitivity analysis was also performed on the unit costs in which the costs of design components with potentially variable quantities were calculated over a range of possible quantities, leading to an expected range of the expected total cost for each design. Unit costs were obtained from licensed contractors or material/product vendors, comparisons with similar projects, and data found within the latest RSMeans reference manuals (Reed Construction Data, 2009). Costs for maintenance, demolition, and special needs were based on estimates from private companies and prior or current contracts with LADOTD. There were five categories of unit cost for each design option: capital costs, operation and maintenance costs (O&M), disposal costs, an engineering fee, and a contingency fee. The engineering fee for all design options was calculated at 10 percent of the capital cost. Contingency fees for all design options were calculated at 10 percent of the capital cost. The economics of each design option are summarized and compared based on cost per mass treated and removed from rainfall-runoff since all design options are subject to the same annual time series of loadings and separately to the same 50 year design storm. These results are compared to a current database of treatment costs for land-based BMPs (FDEP, 2009).

Presentation of design options

Conventional: Design Option I

The Conventional Option is a land-based option that consists of two separate treatment systems located at each bridge abutment on the east and west shores of the lake but within existing public right-of-way (ROW). Hydrodynamic separators are not utilized as part of a design option because these units cannot provide the design and discharge requirements.

This design option conveys flow from two sets (east and west bound) of subcatchments to a single clarifier followed by two filters in parallel. The process flow diagram is shown in Figure 20.

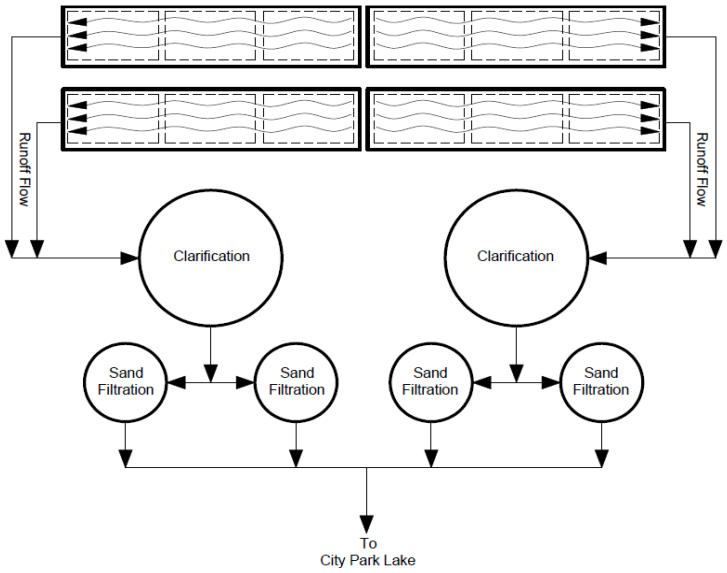

Figure 20
Conventional design option process flow diagram

Buoyant Adsorptive Media (BAM): Design Option II

The BAM option consists of a network of upflow floating radial filters tethered to the bridge piers in order to treat runoff, one BAM per subcatchment. Each filter consists of a screened cartridge located inside a cylindrical outer casing made of polyethylene. Inside the filter cartridge will be an adsorptive mixture of aluminum oxide coated polymeric media (AOPM) and manganese oxide coated polymeric media (MOPM). Radial filters increase the surface area to volume ratio decreasing surface loading rates, distributing flow and filtered PM specific deposits more uniformly than conventional downflow rapid filtration design. This allows for a longer effective lifetime of the filter in regards to head loss. The filter system as a whole will be buoyant in order to reduce loading on the bridge piers. Buoyancy will also ensure the effluent pipe remains above the water surface despite temporal changes in the water elevation of the lake. The BAM filter will be used to reduce clogging and increase filter lifetime. Approximately 25 percent of the PM mass will settle into the sump (Cristina et al., 2002). Head generated from the change in elevation between the bridge deck and BAM through a telescoping pipe drives flow through the filter and out of the top of the

casing for discharge into the lake. A flow process diagram of the BAM filter system is shown in Figure 21. A siphon is inserted in the outflow pipe to remove stored runoff in the filter sump between storm events. The siphoning of stored runoff will prevent the BAM from going anaerobic. The siphon will be made of copper pipe to prevent biological growth which could block the inflow. The BAMs require lower maintenance when compared to other filter systems, consisting of replacing the oxide coated substrate when it has reached breakthrough. Also, the PM collected in the sump area of the filter will need to be vacuumed out once the sump has reached design capacity.

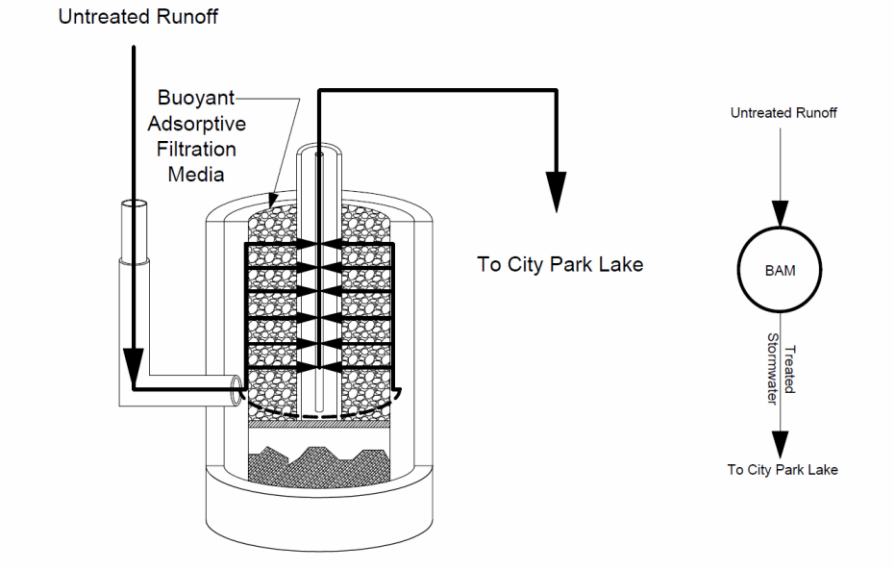

Figure 21
BAM design option process flow diagram

Cementitious Permeable Pavement (CPP): Design Option III

The CPP design option consists of replacing the upper surface of the existing impervious concrete bridge deck through milling with a porous friction course of cementitious permeable pavement (CPP). The mix design parameters were a water/cement ratio (w/c) of 0.25, total porosity (φt) of 0.29 and an adsorptive oxide admixture molarity of 0.5. These parameters provided sufficient hydraulic conductivity and storage while maintaining an unconfined compressive (f'c) strength of 4,000 psi (Kuang et al., 2007). The mix design elements were calculated with the American Concrete Institute (ACI) absolute volume method (Tia, 2008). Granite was used as a coarse aggregate due to its added strength as compared to limestone and resistance to wear (Wu et al., 2001), with the specific gravity

(SG) based on an SG weighted average of the materials (Klein and Hurlbut, 1993). CPP drainage flowed laterally toward the existing expansion joints.

CPP Combined with BAMs: Design Option IV

In this design option, CPP, as a primary treatment, is combined with the network of BAMs as a secondary treatment. At low flow rates, all runoff volume from a subcatchment is first treated by the CPP before routing to the BAM. At high flow rates (i.e., higher than the hydraulic and volumetric capacity of the CPP as is the case for the 50-year, 1-hour design storm), the flow not treated by the CPP is recombined hydraulically with CPP-treated flows and routed to the BAMs for treatment. At these higher flow rates, the recombination of flows of different constituent concentration (for example, the particle size distribution, PSD of PM or TP) requires a weighting by flows for the untreated and CPP-treated runoff to generate the influent flow and concentration to the BAM and the overall treatment behavior of the CPP based on the total inflow.

DISCUSSION OF RESULTS

Transport and Treatability of Particles and Phosphorus in Urban Rainfall-runoff

Hydrologic Indices and Hydrographs Rainfall-runoff

Hydrologic indices of the eight rainfall-runoff events investigated (2004-2005) are presented in Table 13. The first rainfall-runoff event studied particle and phosphorus removal by screened HS; the event on March 14, 2004 has the longest duration (nearly seven hours) and generated 24,076 L of total runoff volume. Peak flow of the event on March 14, 2004 is 6.38 L/s. The second rainfall-runoff event studied particle and P removal by screened HS; the event on April 24, 2004 lasted about three and half hours and generated 7,288 L of total runoff volume. Peak flow of the event on April 24, 2004 is 1.78 L/s. The third rainfall-runoff event studied particle and P removal by screened HS; the event on August 20, 2004 lasted close to one hour and generated 12,307 L of total runoff volume. Peak flow of event on August 20, 2004 is 17.5 L/s, which is the highest one ever studied. The last event studied in 2004 happened on October 14. This event lasted over three hours and produced 1672 L of total runoff volume, which is the smallest one ever studied. Peak flow of the event on October 14, 2004 is 0.58 L/s, which is the lowest one ever studied.

Table 13

Summary of hydrologic and sampling based indices for eight events analyzed for the I-10 experimental catchment site over East Lakeshore Drive

Rainfall Runoff Event	Hydrologic, Rainfall TDP and Sampling based indices								
	PDH[1] (hrs)	Rainfall[2] Duration (min)	Runoff[3] Duration (min)	Total Precip.[4] (mm)	Total Flow[5] (L)	Q_p[6] (L/s)	t_p[7] (min)	Rainfall TP[8] [mg/L]	IPRT[9] (min)
14-Mar-2004	204	413	408	26.2	24076	6.38	295	0.023	8
24-Apr-2004	313	184	215	7.2	7288	1.78	116	0.027	16
20-Aug-2004	26	29	59	17.3	12307	17.5	23	0.025	12
14-Oct-2004	86	179	197	2.6	1672	0.58	60	0.022	48
05-June-2005	117	53	51	7.1	5856	9.35	13	0.021	6
30-June-2005	143	72	71	19.1	15117	13.75	21	0.026	8
21-Aug-2005	94	112	106	51.1	50002	17.32	36	0.024	7
3-Oct-2005	217	9	14	3.81	2615	12.1	5	N/A	2

Notes:

1: PDH: Previous dry hours: Time between current and last event that accumulated at least 0.02 in. of rainfall.

2: Rainfall Duration: The time spanning between the start and stop of effective rainfall for each event.

3: Runoff Duration: The time spanning between the start and stop of runoff for each event.

4: Total Precipitation: The total amount of precipitation recorded on site for each event.

5: Total Flow: The total amount of runoff generated from the experimental section of I-10 for each event.

6: Q_p: The measured peak flow of runoff for each event.

7: t_p: The time spanning between start of effective runoff and the peak flow for each event.

8: Rainfall TP: Rainfall total phosphorus concentration.

9: IPRT: Initial pavement residence time = time between start of effective rainfall and observable runoff.

The event on June 5 was the first event studied in 2005 and has a short duration of nearly one hour and generated 5,856 L of total runoff volume. Peak flow of this event is 9.35 L/s. The event on June 30, 2005 lasted over one hour and generated 15,117 L of total runoff volume. Peak flow of this event is 13.75 L/s. The event on August 21, 2005, lasted close to two hours and generated 50,002 L of total runoff volume. Peak flow of the event on August 20, 2004, is 17.32 L/s, which is the second highest one ever studied. The last rainfall-runoff event studied on particle and P removal by screened HS was the event on October 3, 2005 which had the

shortest duration (about one quarter of an hour) and generated 2,615 L of total runoff volume. The peak flow is 12.1 L/s for this event.

Particle Separation Efficiency (PSE)

Event-based PSE of the screened HS in terms of mass percent removal and EMC reduction for three particle size classes (sediment, settleable, and suspended particle) and total particulate matter for all eight rainfall-runoff events are summarized in Table 14 and Table 15, respectively. Table 14 also presents mass balance error and particle transport distribution based on the definition for mass/flow limited events where the cumulative mass versus cumulative volume curve follows an exponential or a linear pattern **(**Bertrand et al., 1998).

Table 14

Event-based separation performance of the screened HS for sediment, settleable and suspended particle, and total particulate matter transported by eight independent rainfall-runoff events

Rainfall-runoff event	Particle fraction	Sediment particle	Settleable particle	Suspended particle	Total particulate matter	Mass balance error[4]	Particle transport distribution
MAR 14, 04 event	Inf. Mass Load (g)	2325	1424	1201	4949	9.3%	Mass-Limited[2]
	Eff. Mass Load (g)	220	1135	1184	2539		
	ΔParticle (%)[1]	91%	20%	1%	49%		
APR 24, 04 event	Inf. Mass Load (g)	1738	1010	471	3219	-0.8%	Mass-Limited
	Eff. Mass Load (g)	97	475	404	976		
	ΔParticle (%)	94%	53%	14%	70%		
AUG 20, 04 event	Inf. Mass Load (g)	7186	2357	1048	10592	-4.0%	Mass-Limited
	Eff. Mass Load (g)	1501	1858	946	4305		
	ΔParticle (%)	79%	21%	10%	59%		
14 Oct 04 event	Inf. Mass Load (g)	52	125	368	544	2.4%	Mass-Limited
	Eff. Mass Load (g)	3	54	210	267		
	ΔParticle (%)	94%	57%	43%	51%		
JUN 05, 05 event	Inf. Mass Load (g)	3161	1211	386	4758	4.2%	Mass-Limited[2]
	Eff. Mass Load (g)	192	1050	339	1580		
	ΔParticle (%)	94%	13%	11%	67%		
30 Jun 05 event	Inf. Mass Load (g)	1961	1366	717	4044	-3.2%	Mass-Limited
	Inf. Mass Load (g)	470	1321	703	2495		
	ΔParticle (%)	76%	3%	2%	38%		

21 Aug 05 event	Inf. Mass Load (g)	4480	2997	1361	8838	-7.8%	Mass-Limited
	Eff. Mass Load (g)	1003	2586	1296	4884		
	ΔParticle (%)	78%	14%	5%	45%		
03 Oct 05 event	Inf. Mass Load (g)	291	251	197	738	7.5%	Flow-Limited[3]
	Eff. Mass Load (g)	32	181	173	386		
	ΔParticle (%)	89%	28%	12%	48%		
Overall	Inf. Mass Load (g)	21194	10741	5749	37684	-1.3%	-
	Eff. Mass Load (g)	3518	8660	5207	17385		
	ΔParticle (%)	83%	19%	9%	54%		

Note: 1. Calculated by using equation (3).
2. For mass-limited events, mass delivery is skewed towards the initial portion of the event.
3. For flow-limited events, mass delivery tends to follow the hydrograph.
4. Calculated by using equation (4).

Table 15

Summary of event mean concentrations (EMC) of influent and effluent and EMC removal efficiency of particle size fractions and total particulate matter for the rainfall-runoff events treated by the screened HS

Event	Sediment particle (> 75 μm)			Settleable particle (75 μm - 25 μm)			Suspended particle (1.0 μm - 25 μm)			Total particulate matter (> 1.0 μm)		
	Inf. EMC [mg/L]	Eff. EMC [mg/L]	Δ EMC %	Inf. EMC [mg/L]	Eff. EMC [mg/L]	Δ EMC %	Inf. EMC [mg/L]	Eff. EMC [mg/L]	Δ EMC %	Inf. EMC [mg/L]	Eff. EMC [mg/L]	Δ EMC %
14 Mar 2004	96.6 (1.5 to 4052.3)	9.3 (0.8 to 61.5)	90.4	59.1 (4.3 to 1254.4)	48 (4.8 to 284.3)	18.8	49.9 (29.5 to 232.0)	50.1 (39.5 to 138.8)	-0.4	205.6 (50.3 to 5065.3)	107.4 (44.6 to 484.5)	47.8
24 Apr 2004	238.5 (19.9 to 12642.4)	14.4 (1.5 to 33.7)	94.0	138.4 (15.4 to 4389.1)	70.6 (18.1 to 154.4)	49.0	64.6 (40.9 to 493.3)	60.0 (25.9 to 138.6)	7.1	441.7 (99.9 to 17524.8)	144.9 (61.2 to 265.2)	67.2
20 Aug 2004	585.5 (0.8 to 2211.2)	128.3 (0.5 to 322.9)	78.1	192.1 (4.2 to 1044.7)	158.8 (7.6 to 348.5)	17.3	85.4 (49.2 to 176.7)	76.7 (41.7 to 112.5)	10.2	863.4 (71.3 to 2772.1)	363.8 (51.5 to 764.8)	57.9
14 Oct 2004	30.9 (2.7 to 122.7)	3.6 (0.4 to 6.5)	88.3	74.6 (2.3 to 538.1)	58.7 (1.1 to 131.4)	21.3	218.3 (161.8 to 518.6)	229.8 (178.0 to 268.0)	-5.3	323.8 (173.6 to 1072.1)	292.2 (188.2 to 393.2)	9.8

05 Jun 2005	544.0 (52.5 to 2115.2)	36.7 (3.5 to 82.9)	93.3	208.4 (15.1 to 1097.2)	200.9 (13.3 to 709.9)	3.6	65.8 (38.0 to 150.0)	64.8 (36.0 to 132.7)	1.5	830.1 (125.2 to 3362.4)	302.4 (57.6 to 955.5)	63.6
30 Jun 2005	129.8 (17.3 to 3372.6)	32.0 (4.7 to 92.3)	75.3	90.4 (14.2 to 946.9)	89.8 (17.5 to 301.8)	0.7	47.5 (15.0 to 341.0)	47.7 (23.0 to 115.0)	-0.4	267.6 (65.5 to 4617.2)	169.5 (52.0 to 509.1)	36.7
21 Aug 2005	87.9 (27.2 to 503.9)	20.3 (0.7 to 99.2)	76.9	59.5 (9.6 to 472.9)	52.4 (7.4 to 391.1)	11.9	27.2 (11.0 to 176.1)	26.2 (17.9 to 84.2)	3.7	174.7 (59.6 to 1098.8)	98.9 (31.1 to 556.3)	43.4
03 Oct 2005	111.3 (8.7 to 182.3)	15.0 (3.4 to 28.9)	86.5	95.8 (25.3 to 135.7)	86.1 (48.9 to 137.9)	10.1	75.3 (63.4 to 96.1)	82.0 (70.7 to 93.3)	-8.9	282.4 (129.9 to 397.2)	183.1 (125.8 to 258.7)	35.2
Mean	228.1	32.5	85.8	114.8	95.7	16.7	79.3	79.7	-0.5	423.7	207.8	51.0
Median	120.6	17.7	87.4	93.1	78.4	14.6	65.2	62.4	0.6	303.1	176.3	45.6
SD	216.1	40.3	7.5	58.6	55.2	14.9	59.0	63.2	6.2	273.3	98.8	18.6
Range	30.9 to 585.8	3.6 to 128.3	75.3 to 94.0	59.1 to 208.4	48.0 to 200.9	0.7 to 49.0	27.9 to 218.3	26.2 to 229.8	-8.9 to 33.7	179.2 to 863.4	98.9 to 343.6	9.8 to 67.2

Loaded by variable hydraulic (flow rate) and hydrologic (duration and intensity) event characteristics, the screened HS separation capability for the coarser sediment fraction of particulate matter for all eight monitored events in the range of from 76% (Jun 30, 2005) to 94% (April 24, 2004 and October 14, 2004) as presented in Table 14. While the screened HS exhibited relatively consistent and efficient separation performance for coarser sediment fraction particles, the clarification response of the screened HS to settleable and suspended particles was poor and variable, anywhere from 3 to 57 percent and 1 to 43 percent respectively. Table 14 also indicates that separation performances of the screened HS for those two particle size fractions are more influenced by hydraulic loading than that for sediment particles. High percent mass reductions (53 and 57 percent in Table 14) and event mean concentration (49 and 21 percent in Table 15) reductions of settleable fraction particles are observed in the April 24, 2004 and October 14, 2004 events which generated considerably lower peak flow rate (1.78 L/s and 0.58 L/s) compared to all other events examined in this study.

As described previously, total particulate matter is separated into three particle classes by size. Thus, overall particle separation performance of the screened HS is determined by PSE of each individual particle fraction and their mass ratio in influent flow. Since a higher level

of separation efficiency was observed for coarser sediment fractions, overall PSE for the screened HS was greatly influenced by the relative contribution of coarser sediment fraction to influent load of particulate matter. This point is well demonstrated in Table 14. Influent mass load transported by the August 20, 2004 and June 05, 2005 events contain 68 percent and 66 percent of sediment fraction producing 59 percent and 67 percent separation of particulate matter, respectively. In contrast, 68 percent of influent particulate matter in the October 14, 2004 event is suspended particles while sediment fraction constitutes only 10 percent of influent load. In spite of the advantage of the lowest hydraulic loading (Q_{ave} = 0.14 L/s) among all eight events monitored, the screened HS could separate only 51 percent of influent particulate matter.

Granulometric Analysis for Influent, Screened HS, and Effluent Particles

Table 16 summarizes granulometric indices and statistics for particulate matter transported by each event (influent) and treated by the screened HS (effluent). The screened HS is physically divided into two compartments: screened and volute areas. The internal configuration of the screened HS is designed in such a way that influent flow has to go through the screened area first before entering the volute area. Thus, overall particle separation is accomplished by the combination of sequential separation performances from these two annular volumes. Granulometric characteristics and statistics for particulate matter captured by screened and volute area in the HS for each event are summarized in Table 17. Figure 6 graphically illustrates PSDs of influent particulate matter transported by the eight runoff events and describes changes of influent PSDs as it flow through the screened and volute area of the HS unit.

Table 16

Summary of statistical characteristics of particle size distribution for the influent and effluent particulate mass load of the screened HS unit at Baton Rouge

Rainfall Runoff Event	d_{50} (µm)	Φ_{50}	d_g (µm)	σ_g	σ_I	S_k	K_G	Central Tendency	Mass load (g)
INFLUENT particle size distribution									
14-Mar-04	43	4.53	54	5.10	2.36	0.17	0.95	silt	4949
24-Apr-04	233	2.10	269	8.36	2.97	0.02	0.91	Fine sand	3219
20-Aug-04	300	1.74	440	12.15	3.35	0.11	0.79	Medium sand	10591
14-Oct-04	45	4.48	54	6.11	2.37	0.1	0.73	Silt	544
5-Jun-05	247	2.02	418	11.22	3.16	0.16	0.71	Fine sand	4758

30-Jun-05	69	3.85	103	5.11	2.61	0.25	1.27	very fine sand	4044
21-Aug-05	106	3.23	162	7.25	2.99	0.21	1.23	very fine sand	8733
3-Oct-05	58	4.1	79	6.51	2.86	0.21	1.21	Silt	739
Mean	**127**	**3.34**	**186**	**7.63**	**2.82**	**0.16**	**0.99**	**very fine sand**	**4697**
Std. dev.	**98**	**1.08**	**157**	**2.67**	**0.36**	**0.06**	**0.23**		**3518**
EFFLUENT particle size distribution									
14-Mar-04	20	5.65	18	2.61	1.41	-0.04	1.02	silt	2539
24-Apr-04	31	5.03	26	3.24	1.64	-0.15	0.93	silt	973
20-Aug-04	52	4.25	45	3.35	1.7	-0.13	0.97	silt	4124
14-Oct-04	13	6.29	14	2.29	1.19	0.13	1.02	silt	270
5-Jun-05	42	4.56	39	2.63	1.45	-0.09	1.13	silt	1585
30-Jun-05	39	4.68	32	2.86	1.54	-0.19	1.15	silt	2495
21-Aug-05	42	4.59	36	3.44	1.76	-0.12	1.03	silt	4884
3-Oct-05	26	5.25	22	3.14	1.58	-0.15	0.88	silt	386
Mean	**33**	**5.04**	**29**	**2.95**	**1.53**	**-0.09**	**1.02**	**silt**	**2157**
Std. dev.	**13**	**0.67**	**11**	**0.41**	**0.18**	**0.1**	**0.09**		**1690**

Table 17

Summary of statistical characteristics of particle size distribution for the screened and volute particles of the screened HS unit at Baton Rouge

Rainfall Runoff Event	d_{50} (μm)	Φ_{50}	d_g (μm)	σ_g	σ_I	S_k	K_G	Central Tendency	Mass load (g)
SCREENED particle size distribution									
14-Mar-04	388	1.4	546	4.27	2.11	0.19	0.98	medium sand	770
24-Apr-04	599	0.7	806	4.67	2.13	0.13	0.86	coarse sand	2004
20-Aug-04	2202	-1.1	1757	5.19	1.83	-0.44	0.47	gravel	5315
14-Oct-04	270	1.9	219	3.29	1.90	-0.17	1.26	medium sand	118
5-Jun-05	2179	-1.1	1465	5.21	2.07	-0.32	0.63	gravel	2336
30-Jun-05	731	0.5	1043	5.11	2.21	0.15	0.80	coarse sand	1029
21-Aug-05	861	0.2	1293	5.84	2.16	0.04	0.62	coarse sand	3092
3-Oct-05	445	1.2	784	5.88	2.35	0.25	0.74	medium sand	204
Mean	**953**	**0.5**	**975**	**4.87**	**2.08**	**-0.02**	**0.80**	**coarse sand**	**1771**
Std. dev.	**786**	**1.1**	**511**	**0.89**	**0.17**	**0.25**	**0.25**		**1756**
VOLUTE particle size distribution									
14-Mar-04	145.5	2.8	125	2.34	1.20	-0.15	0.91	find sand	1181
24-Apr-04	103.2	3.3	145	2.67	1.34	0.38	0.87	very find sand	265
20-Aug-04	140.4	2.8	117	2.47	1.27	-0.15	0.90	find sand	749
14-Oct-04	137.7	2.9	150	2.66	1.29	0.09	0.70	find sand	146
5-Jun-05	171.3	2.5	156	2.37	1.28	-0.10	1.12	find sand	643
30-Jun-05	171.5	2.5	157	2.64	1.41	0.00	0.96	find sand	616
21-Aug-05	157.4	2.7	142	2.45	1.27	-0.09	0.89	find sand	1157
3-Oct-05	96.2	3.4	148	2.79	1.54	0.41	1.03	very find sand	93
Mean	**140**	**2.9**	**142**	**2.55**	**1.33**	**0.05**	**0.92**	**find sand**	**606**
Std. dev.	**28**	**0.3**	**14**	**0.16**	**0.11**	**0.23**	**0.12**		**422**

The coarser the influent PSD, the greater shift in the distribution was observed between influent and effluent. The wide variation of event-based influent PSD was observed among eight events treated by the screened HS. Three events (April 24, 2004, August 20, 2004, and June, 05, 2005) transported particulate matter, size distributions of which are coarser than other events as illustrated in Figure 2. PSDs of the event of March 14, 2004 (d_{50m} of 43 μm) and October 14, 2004 (d_{50m} of 45 μm) indicate the screened HS was loaded by relatively fine sizes of particles throughout the duration of the events. 25 - 35% of overall influent particulate matter by mass in those three events (April 24, 2004, August 20, 2004 and June,

05, 2005) was coarser than 1000 μm, while only 7% was found in influent PSDs transported by the March 14, 2004 and October 14, 2004 events. PSD results in this study are similar to source area results by Sansalone et al. (1998) for urban pavement rainfall-runoff which indicated 30 percent was from 1000 to 10,000 μm.

Particle Separation Mechanisms

The particle removal mechanisms by a screened hydrodynamic separator are a combination of size exclusion for gravel-size material and mainly discrete settling. Removal efficiencies of particles are pronouncedly dependent of size of particulate matter and distribution of particulate mass and hydrological parameters of the specific events.

Transport and Treatability of Particle Fractions

Figure 22, Figure 23, and Figure 24 show the cumulative mass delivery of particulate matter (the suspended, settleable, and sediment size fractions) as a function of the cumulative runoff volume generated throughout each event. Corresponding effluent cumulative mass describe simultaneous clarification response of the screened HS to each particle fraction. The results indicate the mass delivery pattern and actual cumulative mass of three size classes of particulate (the suspended, settleable, and sediment size fractions) matter to the associated runoff volume. Vertical distance between lines of influent and effluent particle fractions illustrates the degree of particle separation performance of the screened HS.

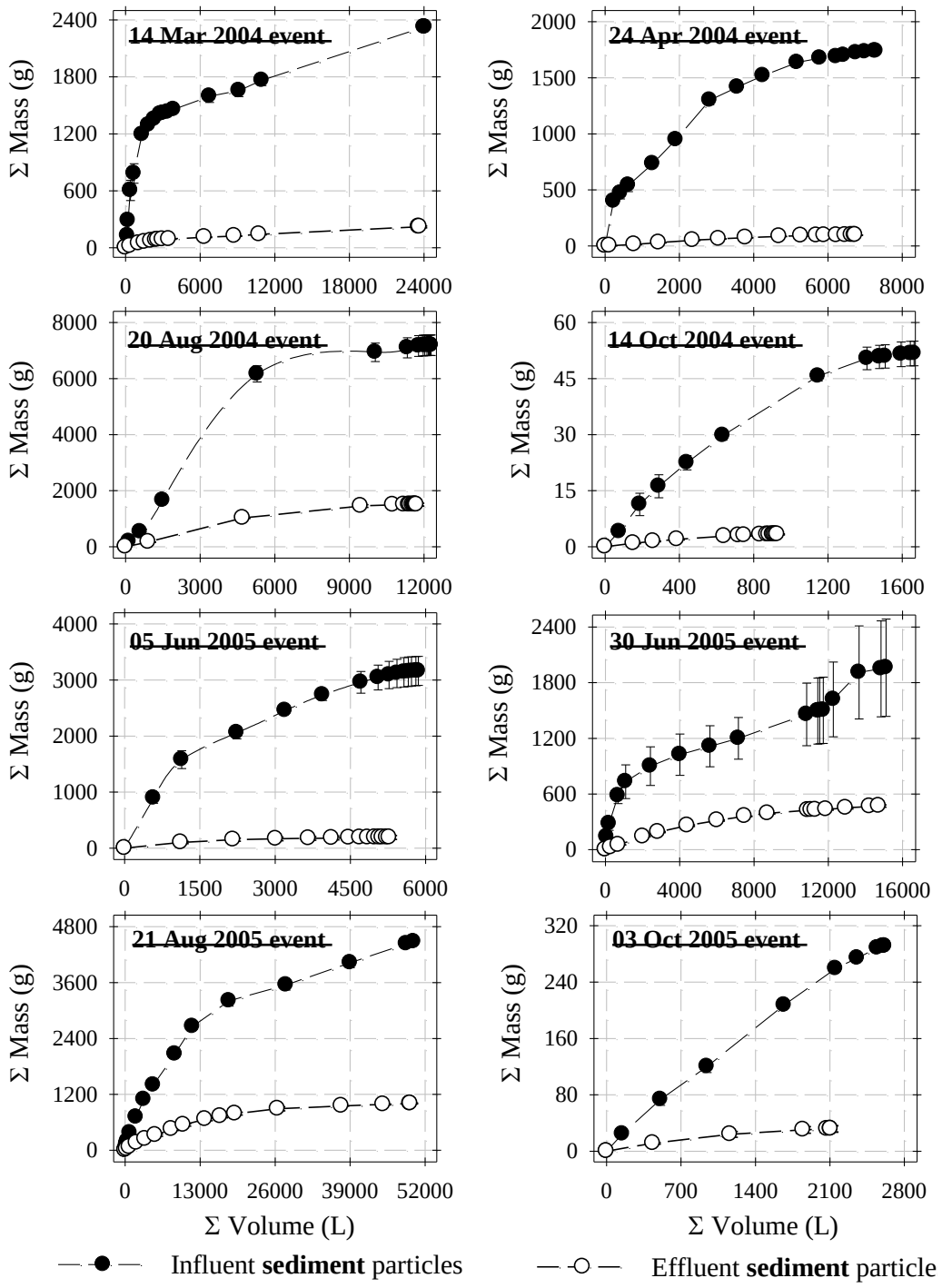

Figure 22

Mass delivery of sediment fraction (> 75 µms) particulate matter in influent and effluent runoff volume for eight urban rainfall-runoff events treated by the screened HS unit

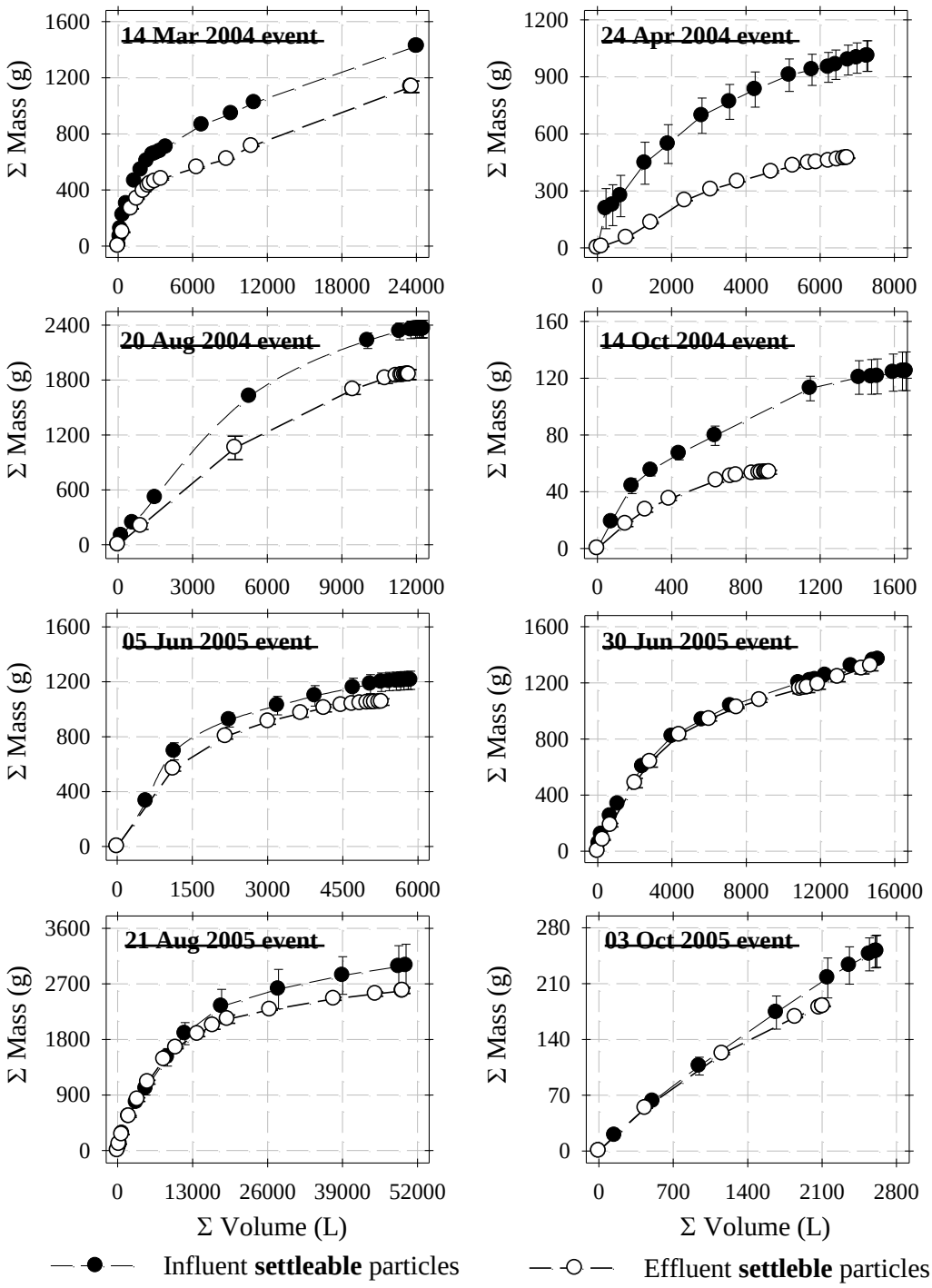

Figure 23
Mass delivery of settleable fraction (25-75 µms) particulate matter in influent and effluent runof volume for the eight urban rainfall-runoff of events treated by the screened HS unit

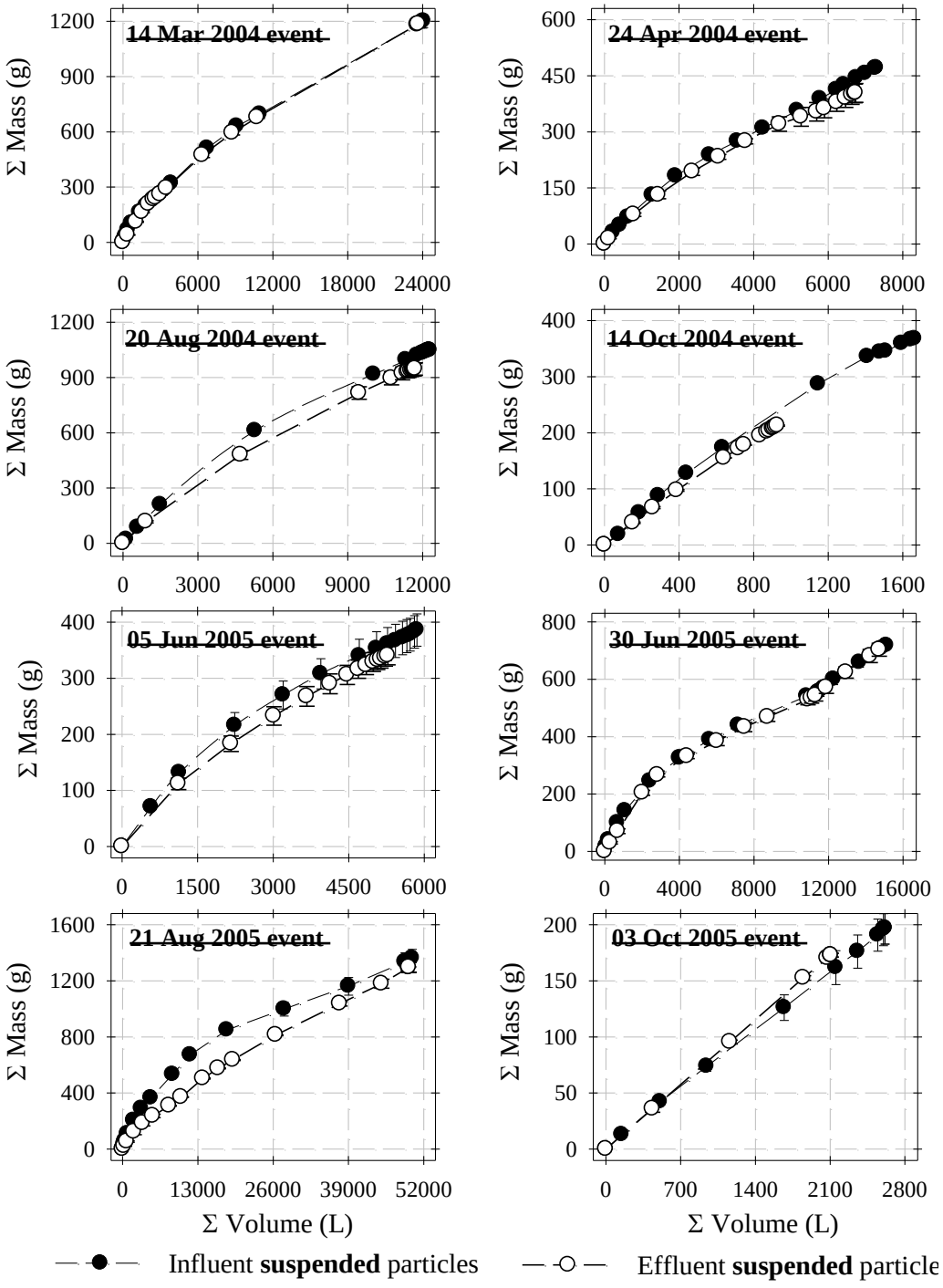

Figure 24

Mass delivery of suspended fraction (1-25 µms) particulate matter in influent and effluent runoff volume for the eight urban rainfall-runoff events treated by the screened HS unit

Comparison of observed curves for inflow and outflow suggests a significant removal of sediment particles throughout the runoff hydrographs while mass delivery curves for influent and effluent of suspended particles nearly overlap each other, illustrating poor particle separation performance for the suspended fraction. It is important to recognize that 43 percent of the mass removal for suspended particles was achieved by the screened HS while the effluent EMC was higher than influent EMC in the October 14, 2004 event. This indicates most of suspended particle mass removal is attributable to volumetric confinement of particles rather than actual particle separation performance in the unit.

Among the eight runoff events examined in this study, the Oct 30, 2005 event was the only event that exhibited the cumulative mass versus the cumulative volume curve following a linear pattern, indicating it is flow-limited. This linear mass delivery pattern in the October 30, 2005 event was observed consistently for all three particle size fractions. Examination of Figure 22, Figure 23, and Figure 24 reveals that a mass delivery pattern within a single event was influenced by transported particle size. While clear disproportionate deliveries of sediment and settleable fractions of particulate matter were observed for mass-limited events, mass delivery of suspended particles was more proportionally distributed to cumulative runoff volume.

Impact of Hydrologic Loading and Influent PSD on Screened Hydrodynamic Separator Performance

Event-based statistics for hydrology and representative influent PSD of particulate matter transported by each event were compared in Figure 25. It shows distribution of runoff flow rate and mass-based size distribution of influent particulate matter. To further investigate relative contribution of these hydrologic and granulometric characteristics of rainfall-runoff event to overall separation performance of the screened HS and particulate matter concentration in runoff, additional bar plots were generated showing results of separation efficiency of the screened HS for total particulate matter and influent event mean concentration (EMC) from an individual event.

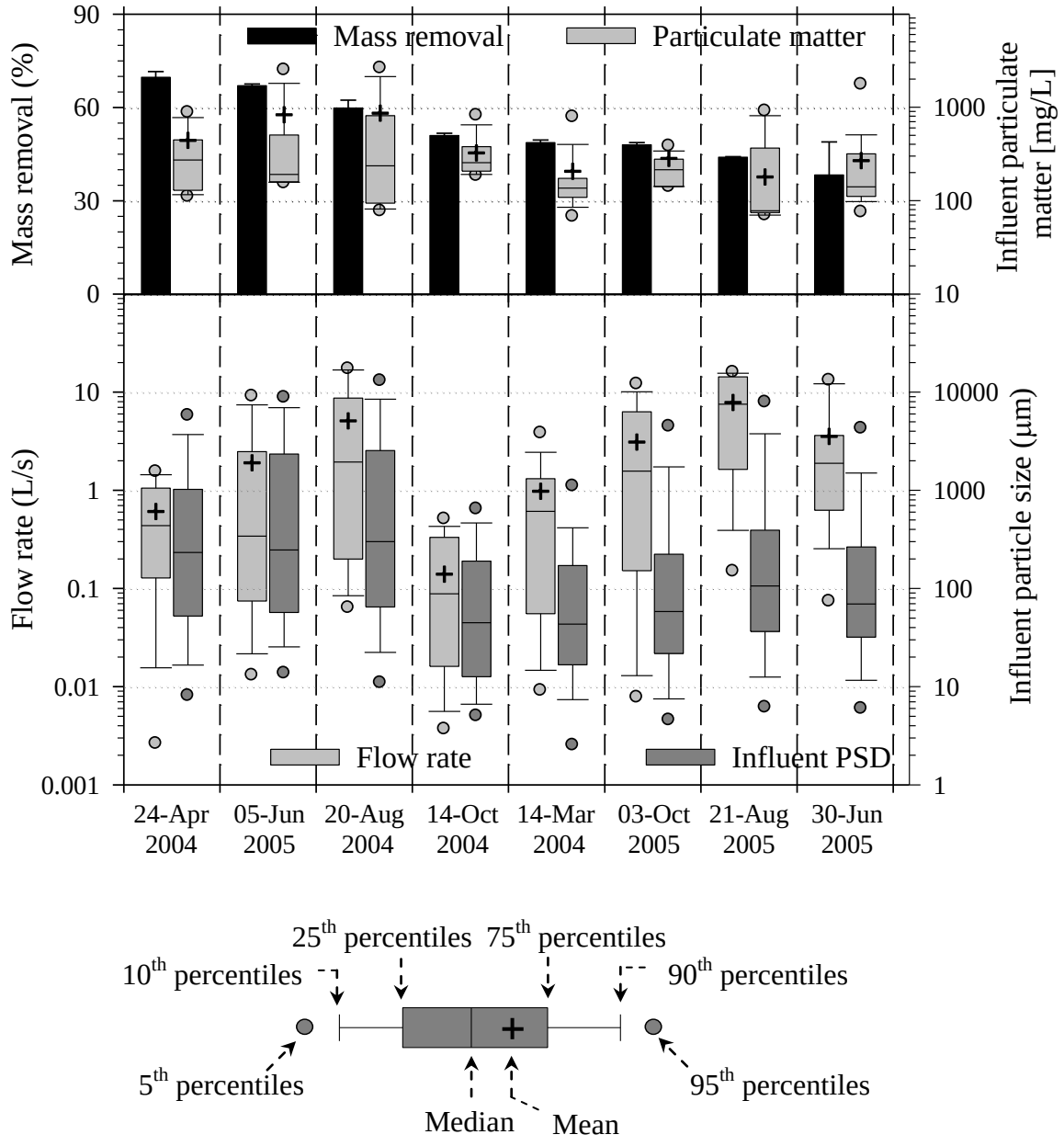

Figure 25
Event-based particle separation performance of the screened HS

While in general both runoff flow rate and influent PSD affected the particle separation performance of the screened HS, influent PSD appears to have a major impact on the percent removal of particulate matter. For example, both the August 20, 2004 and June 30, 2005 events generated reasonably similar hydrologic characteristics (i.e., Q_{median}, Q_{mean}, and Q_{peak})

as presented in Table 13 and Figure 25. However, particulate matter transported by both events exhibited drastically different PSD. Coarser PSD of the August 20, 2004 event was a major contribution to the substantial improvement of particle separation efficiency by 22 percent compared to June 30, 2005 event. On the other hand, while the March 2004 and October 2004 events transported particulate matters with similar PSDs (d_{50m}= 43 μm and 45 μm, respectively as summarized in Table 16), the March 2004 event yielded 0.98 L/s (mean) and 6.38 L/s (peak) of runoff flow rate, which were about 10 times higher than 0.14 L/s (mean) and 0.58 L/s (peak) for the October 2004 event. While an order of magnitude, higher hydraulic loading caused only marginal decrease (-2%) of PSE of the screened HS with similar influent PSD; the finer influent PSD of the June 30, 2005 event caused significantly deteriorated particle separation performance compared to the August 20, 2004 event, which generated a similar level of flow rate. The marked influence of PSD on particle separation efficiency of the screened HS is also reflected by 0.80 of the Pearson product-moment correlation coefficient (*r*) between PSD and mass removal (%) while *r* between Q_{mean} and mass removal (%) was -0.39. A value of 1 or -1 for correlation coefficient indicates the perfect positive or negative association between two variables, respectively (Hayter, 2002).

In addition, EMC and influent PSD in Figure 25 reconfirms the positive relationship between particulate matter concentration and particle size distribution in runoff flow. This positive relationship between EMC and PSD is quantitatively described by 0.88 of the Pearson's coefficient for eight runoff events. For example, the August 20, 2004 and June 05, 2004 events yielding high EMCs of total particulate matter transported coarser influent PSDs than the rest of events.

TP Removal Efficiency

Screened HS total phosphorus mass separation results are summarized graphically in Figure 26, Figure 27, Figure 28, Figure 29, Figure 30, Figure 31, and Figure 32 in the categories of sediment bound fraction, settleable bound fraction, suspended bound fraction and dissolved fraction. As the first stormwater runoff event studied for total phosphorus, the March 14, 2004 event was presented as a particulate and dissolved fraction. The corresponding separation efficiency results are summarized in a tabular fashion in Table 18.

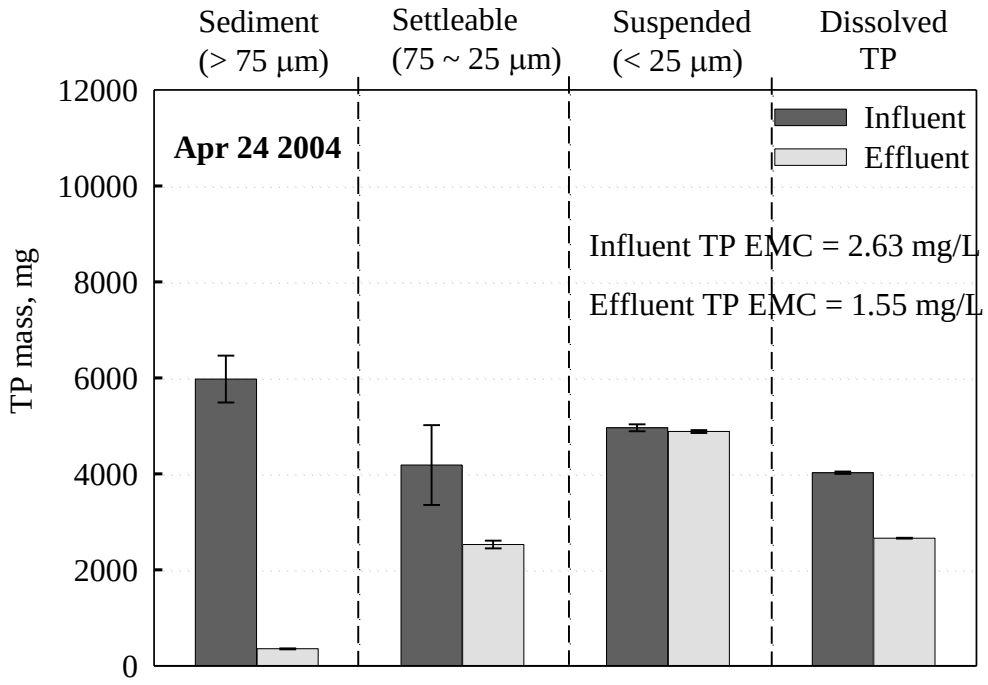

Figure 26
TP removal by screened HS for event April 24, 2004

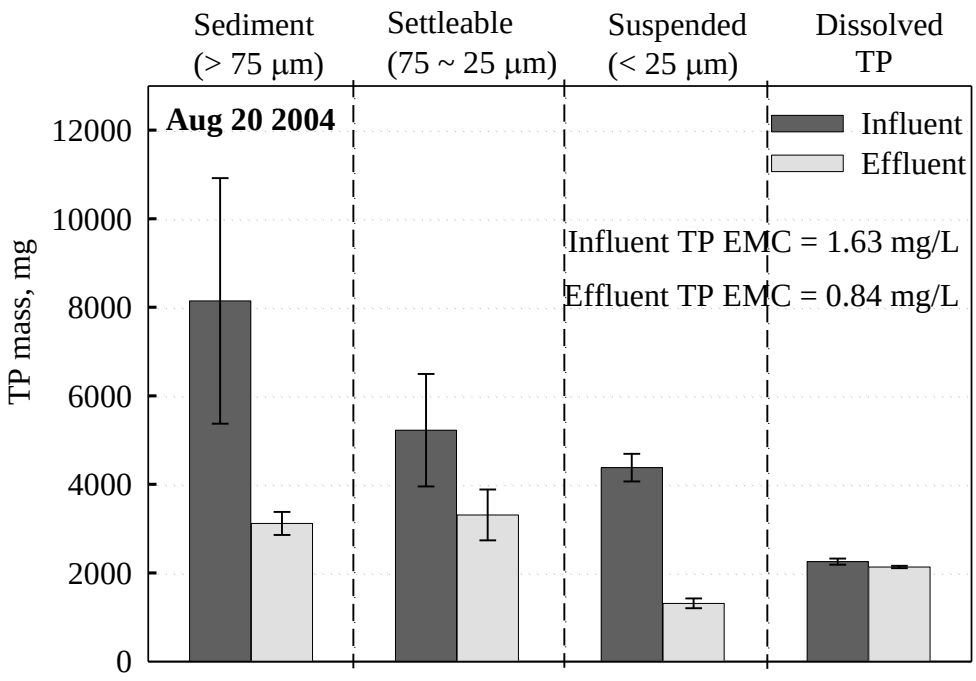

Figure 27

TP removal by screened HS for event August 20, 2004

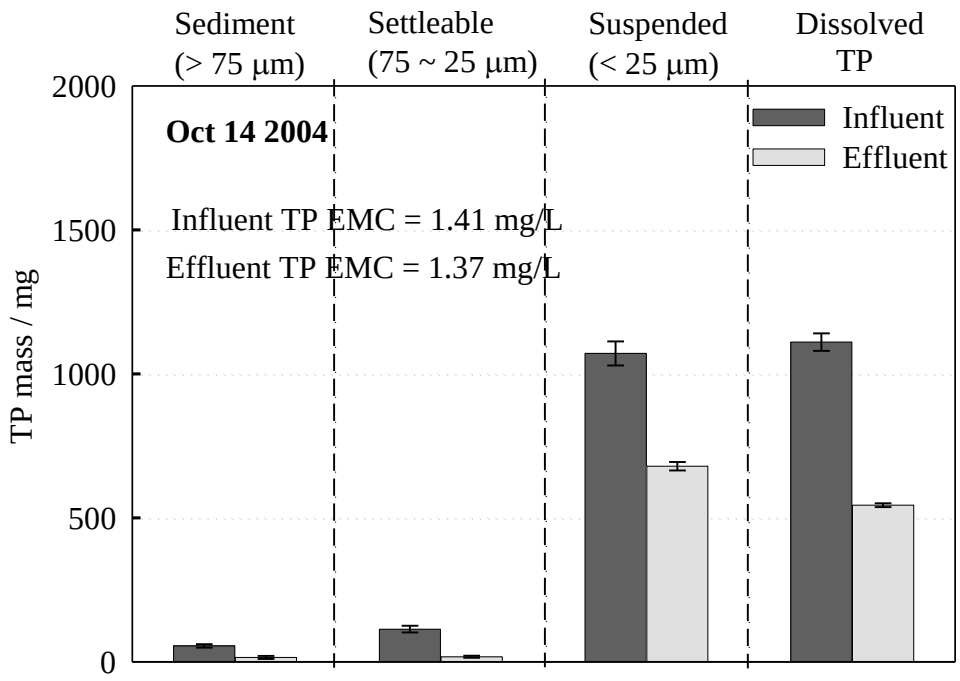

Figure 28
TP removal by screened HS for the October 14, 2004 event

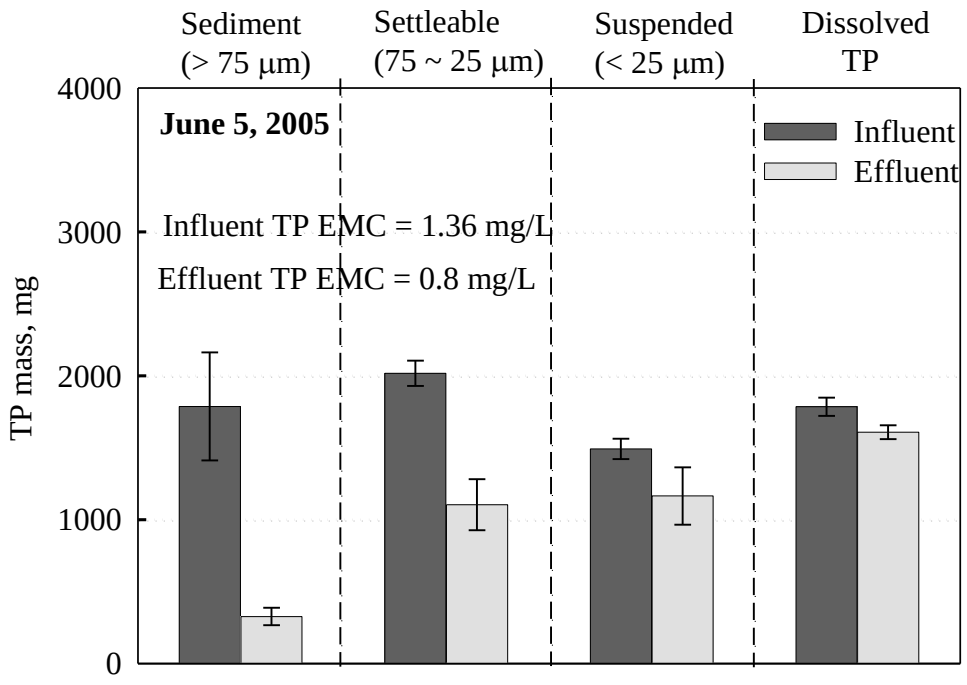

Figure 29

TP removal by screened HS for event June 5, 2005

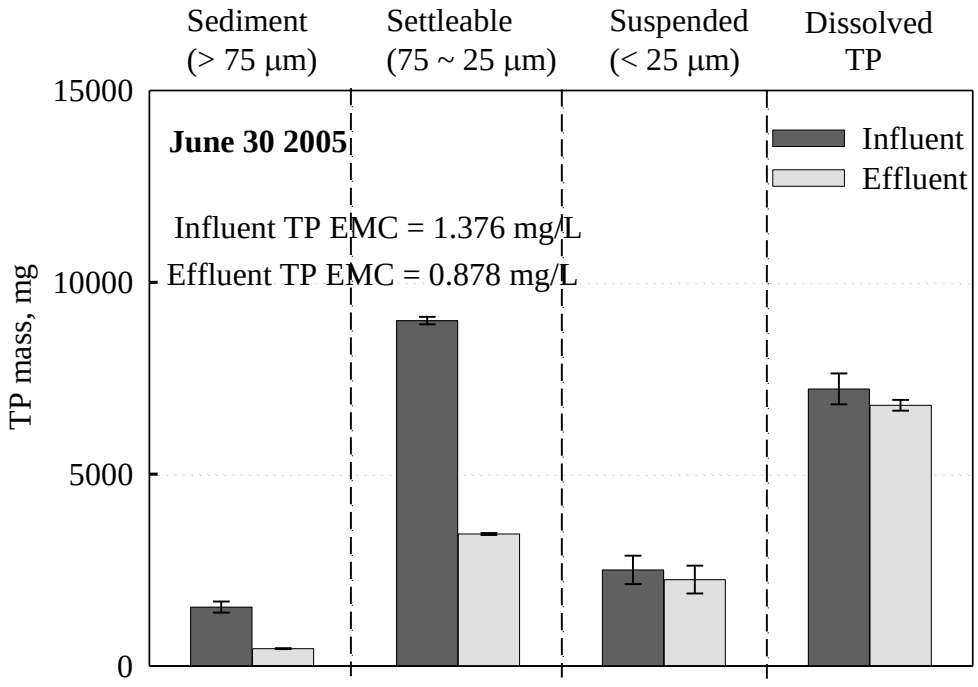

Figure 30

TP removal by screened HS for event June 30, 2005

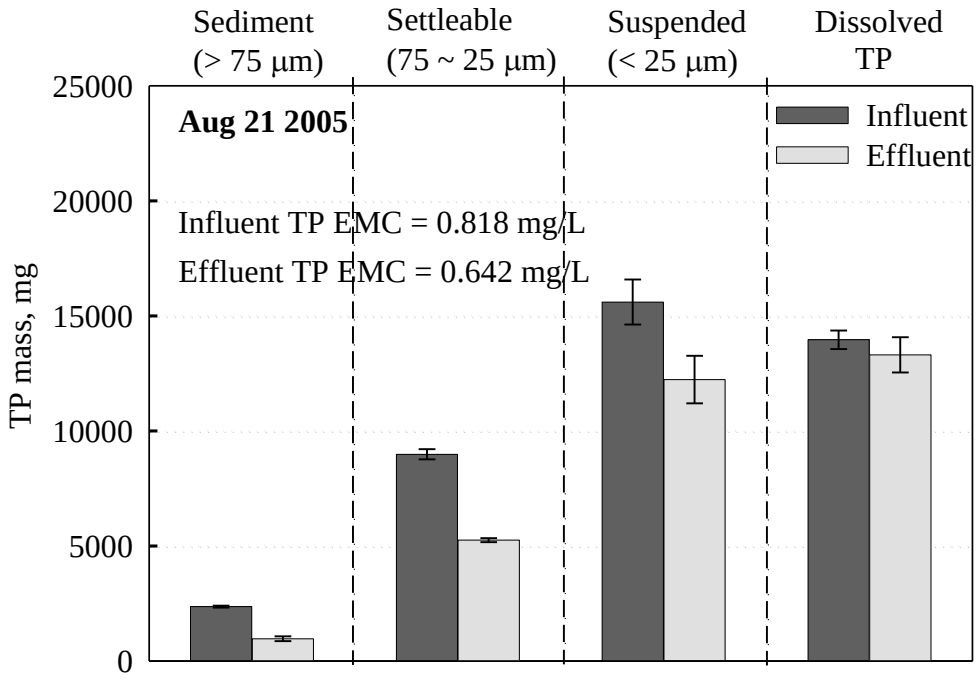

Figure 31

TP removal by screened HS for the August 21, 2005 event

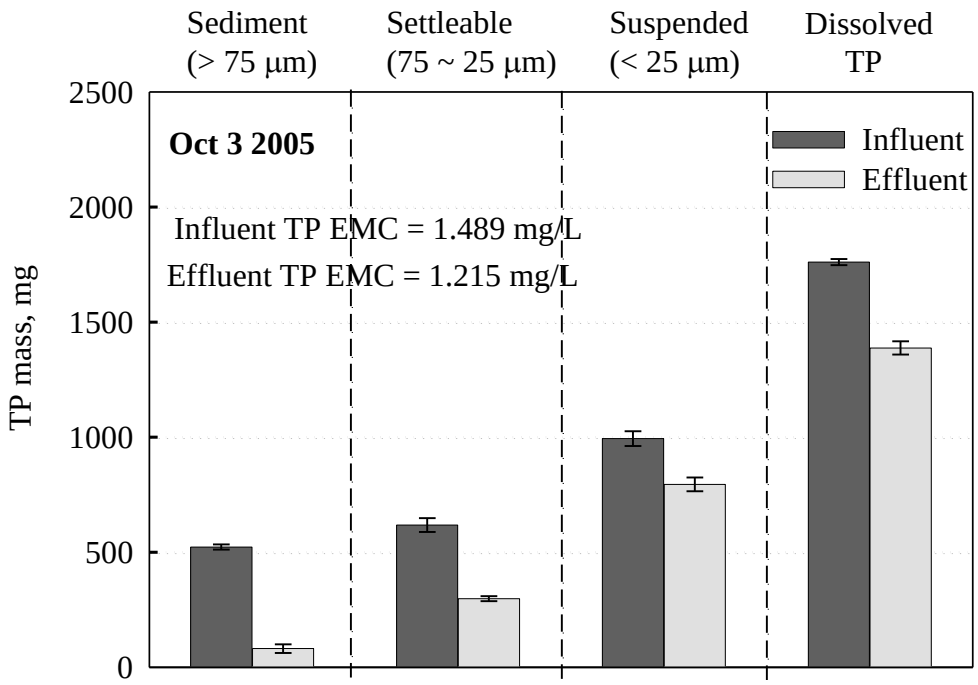

Figure 32
TP removal by screened HS for the October 3, 2005 event

Table 18
Summary of TP removal efficiency by screened HS

Event	TP Removal efficiency by Screened HS				
	Sediment bound	Settleable bound	Suspended bound	Dissolved	Overall
Mar 14, 2004	12.6%			-2.0%	7.7%
Apr 24, 2004	93.6%	34.7%	1.0%	10.6%	40.8%
Oct 3, 2005	80.7%	40.1%	0.8%	2.2%	18.4%
Aug 20, 2004	59.9%	33.6%	71.3%	0.8%	48.8%
Oct 14, 2004	68.4%	84.8%	1.3%	10.6%	12.7%
June 5, 2005	81.7%	45.3%	21.9%	9.9%	40.6%
June 30, 2005	70.7%	61.8%	10.2%	5.9%	36.2%
Aug 21, 2005	58.6%	40.9%	20.7%	3.6%	21.5%

Results indicated that both concentrations of dissolved and particulate-bound fractions of phosphorus measured by discrete manual samples in urban rainfall-runoff commonly exceed water quality criteria of 0.1 mg/L recommended by USEPA 1986 on a rainfall-runoff event basis. In addition, particulate matter is designated to three categories: sediments, settleables, and suspended according to their ease of treatability and difference of physical properties. Therefore the in-situ rainfall-runoff treatments have to address sediments bound, settleables bound, and suspended bound and dissolved phosphorus. The overall TP removal efficiencies were in range of 10-50 percent for all the rainfall runoff events studied. Sediment bound TP removal efficiencies varied from about 60 to 94 percent; majorities of settleable bound TP removal efficiencies differed 30 to 60 percent, and suspended bound TP removal efficiencies were generally smaller than 20 percent with the exception of the value of 71.3 percent for the August 20, 2004 event, which was a pronounced mass limited event with high intensity, short duration, and a single hydrograph peak. Typical dissolved P removal efficiencies fell into less than 10 percent. In brief, the results indicated that removal percent of sediment-bound phosphorus is highest, settleable-bound phosphorus moderate, and suspended-bound phosphorus and dissolved phosphorus to a varying lower extent. Such an overall performance is not surprising because removal mechanisms of hydrodynamic separation include hydrodynamic screening and vortex settling, both of which primarily depend on particle size. The coarser of particulate matter, the more pronounced of effect of screening and settling. Rainfall-runoff flow rate caused by rainfall intensity and hydraulic difference could be another factor which influences particulate bound TP removal efficiency by screened HS. However it would be too early to argue about how flow rate affected particulate bound TP removal efficiency by screened HS due to the limited number of rainfall runoff events studied. Even considering that, the differences of the sediment bound, settleable bound, suspended bound, and dissolved TP removal efficiencies are evidently significant. Therefore hydrodynamic separation can be utilized only as in-situ pre-treatment dealing with coarse particles and particulate-bound phosphorus, especially for sediment and settleable fractions but with frequent maintenance. With respect to adsorptive filtration applied downstream of an HS to achieve higher P removal efficiency if required, amorphous oxide coated media filter could be applied following an HS because of the media's good adsorption capacity and high hydraulic conductivity. Such a combination of operations by the media would ensure that concentrations of effluent P is low enough for discharge to surrounding surface waters as will be shown subsequently in the green infrastructure section.

Influence of Hydrology on Rainfall-runoff Metal Element Speciation

Storm Event Characterization

Water quality concentrations measured at the I-10 experimental site were compared to various storm characterization studies in other urban areas to determine if the results were comparable. Runoff from the Baton Rouge site yielded aqueous metal EMCs ranging from 2.7-31.6 μg/L for Cd, 12.1-206.3 μg/L for Cu, 1.5-58.0 μg/L for Pb, and 44.1-985.6 μg/L for Zn. Mean SSC values for the four targeted storms analyzed at the Baton Rouge site ranged from l79.2-526.4 mg/L. A study done in Austin, Texas by Barrett et al. found two separate ranges of median TSS values bound between 45-798 mg/L for one study (Barrett et al. 1993) and 19-131 mg/L for a latter study (Barrett et al. 1995). Studies by Ellis et al. (1987) on runoff from a watershed in northwest London revealed average aqueous metal concentrations of 2.0, 61.0, and 298 μg/L for Cd, Cu, and Zn, respectively. A study by Sansalone and Buchberger (1997) on a small urban catchment in Cincinnati, Ohio revealed similar concentrations of dissolved metals ranging between 2.0-4.0 μg/L for Cd, 13-279 μg/L for Cu and 13-21 μg/L for Pb. Comparisons to other data from around the US revealed that TSS/SSC and Cu values for the April 11, 2002 and May 13, 2002 events were higher for the Baton Rouge site than other similar sites.

In order to assess the speciation of the four targeted divalent heavy metals, results from the extensive water quality analyses were utilized to perform a charge balance to account for the majority of the ionic constituents. All ionic and water quality components were normalized to their respective maximum concentrations to compare the profiles of the pollutographs with profiles of the hydrographs. This aided in investigating the influences of hydrology impacted water quality concentrations on metal speciation. Pertinent event information including hydrologic data is presented in Table 19. Event mean concentrations and associated concentration ranges are presented on an event basis in Table 20.

Table 19

Summary of hydrologic, traffic, and sampling based indices for four events analyzed for the I-10 experimental catchment site over East Lakeshore Drive

Rainfall Runoff Event	Hydrologic, Traffic, and Sampling Based Indices										
	PDH[1] (hrs)	VDS[2] (vehicles)	Rainfall[3] Duration (min)	Runoff[4] Duration (min)	Total Precip.[5] (in)	Total Flow[6] (L)	Q_p[7] (L/min)	t_p[8] (min)	VPV[9] (#/L)	n[10]	IPRT[11] (min)
Mass-limited, High Runoff Volume Events[12]											
13-May-2002	758	2457	30	33	0.31	1964	150	25	1.3	15	2
30-May-2002	306	8952	136	137	1.63	7336.8	300	87	1.2	15	4
Flow-limited, Low Runoff Volume Events[13]											
11-Apr-2002	68	2353	14	20	0.05	53.6	5.4	11	43.9	13	9
16-Jun-2002	188	2106	34	27	0.04	50.7	3.3	8	41.5	15	7
Statistics for the Rainfall-Runoff Events											
Median[14]	247.0	2405.0	32.0	30.0	0.2	1008.8	77.7	18.0	21.4	15.0	5.5
Mean[15]	330.0	3967.0	53.5	54.3	0.5	2351.3	114.7	32.8	22.0	14.5	5.5
SD[16]	301.4	3326.6	55.7	55.4	0.8	3443.7	141.3	36.9	24.0	1.0	3.1
RPD[17] (%)	91.3	83.9	104.1	102.2	149.5	146.5	123.3	112.7	109.0	6.9	56.5

Notes:

1. PDH: Previous dry hours: Time spanning between the current event and the last event that accumulated at least 0.02 in. of rainfall.
2. VDS: Vehicles during storm = The total number of vehicles passing the eastbound lanes of I-10 during an event (Chin et al. 1980).
3. Rainfall Duration: The time spanning between the start and stop of effective rainfall for each event.
4. Runoff Duration: The time spanning between the start and stop of runoff for each event.
5. Total Precipitation: The total amount of precipitation recorded on site for each event.
6. Total Flow: The total amount of runoff generated from the experimental section of I-10 for each event.
7. Q_p: The measured peak flow of runoff for each event.
8. t_p: The time spanning between start of effective runoff and the peak flow for each event.
9. VPV: Vehicles per volume (vehicles/ L): Determined by dividing total traffic counts by total flows.
10. n: Number of samples collected for each event.
11. IPRT: Initial pavement residence time = time between start of effective rainfall and observable runoff.
12. Mass-limited, high runoff volume event.
13. Flow-limited, low runoff volume event.
14. Median: Median parameter of all 4 events.
15. Mean: Arithmetic Mean of all 4 event parameters
16. SD: Standard Deviation of all 4 event parameters.
17. RSD (%): Relative Standard Deviation of all 4 event parameters- expressed as a percent.

Table 20

Summary of aggregate water quality and metal constituent concentrations for four events analyzed for the I-10 experimental catchment site over East Lakeshore Drive expressed as Event Mean Concentrations (Range)

Constituent	*11-Apr-02*	*13-May-02*	*30-May-02*	*16-Jun-02*
SSC [mg/L]	251.7 (100.7 - 486.0)[1]	526.4 (156.7 - 7598.7)	228.0 (16.0 - 2.1e3)	179.2 (82.2 - 553.3)
TDS [mg/L]	301.1 (268.0 - 412.0[2])	150.9 (49.0 - 802.5)	39.9 (14.0 - 671.5)	513.9 (426.0 - 701.5)
Alkalinity [mg/L $CaCO_3$]	63.5 (48.0 - 83.0)	44.5 (30.5 - 121.0)	14.0 (5.5 - 88.0)	61.7 (55.0 - 82.5)
pH	7.4 (7.3 - 7.5)	7.4 (6.5 - 7.6)	6.8 (6.5 - 7.4)	7.0 (6.8 - 7.3)
PO_4^{-3} [mg/L]	0.3 (0.11 - 0.69)	1.6 (0.72 - 4.11)	0.3 (0.15 - 1.77)	1.4 (0.89 - 2.49)
NO_3^- [mg/L]	5.5 (4.53 - 8.02)	1.2 (0.0 - 7.5)	0.7 (0.0 - 21.8)	11.1 (9.06 - 14.66)
SO_4^{-2} [mg/L]	197.2 (167.8 - 290.3)	87.7 (19.5 - 361.5)	14.5 (1.83 - 500.3)	412.9 (306.0 - 608.9)
Cl^- [mg/L]	23.9 (22.5 - 28.3)	19.6 (7.8 - 46.2)	2.6 (0.0 - 85.5)	37.6 (27.8 - 51.2)
DOC [mg/L]	92.7 (80.0 - 137.5)	34.3 (14.0 - 139.5)	71.2 (4.13 - 202.3)	172.1 (141.2 - 235.3)
Cu [μg/L]	123.6 (101.9 - 185.0)	68.9 (43.6 - 235.4)	12.1 (6.3 - 129.1)	206.3 (172.8 - 274.2)
Zn [μg/L]	193.6 (25.6 - 569.6)	274.8 (80.4 - 1537.4)	44.1 (25.6 - 569.6)	985.6 (740.9 - 1.9e3)
Cd [μg/L]	31.6 (24.6 - 89.9)	2.7 (1.1 - 8.8)	0.4 (0.3 - 3.7)	25.7 (18.8 - 39.3)
Pb [μg/L]	32.0 (24.7 - 38.1)	10.1 (3.5 - 36.0)	1.5 (1.3 - 5.7)	58.0 (33.3 - 101.6)
Mg[μg/L]	1.4e4 (1.2e4 - 2.1e4)	1.5e3 (538 - 1.3e4)	420.7 (115 - 9.4e3)	7.6e3 (6.2e3 - 1.1e4)
Ca [μg/L]	3.4e5 (2.8e5 - 4.4e5)	2.6e4 (8.4e3 - 1.3e5	8.0e3 (2.6e3 - 1.5e5)	1.3e5 (1.2e5 - 1.4e5)
Notes:				
1. Data is presented as: Event Mean Concentration (Range).				
2. Upper range values indicate maximum concentrations.				

Low Intensity Events

Low intensity events generally produce low runoff volumes and exhibit a pollutant mass delivery proportional to the hydrograph. Such trends have been observed for the advective transport of aggregate constituents (SSC, TDS, COD, and alkalinity) as well as heavy metals (Sansalone and Buchberger, 1997; Sansalone et al., 1998) and are often referred to as flow-limited events. Of the four hydrologic events analyzed in this research, two events exhibited flow-limited behavior. The first storm analyzed was a low intensity event that occurred on April 11, 2002. It lasted 14 min. and produced 53.6 L of flow. The second flow-limited, low

intensity event was characterized on June 16, 2002, lasted 14 minutes, and produced a total runoff volume of 50.7 L.

As exhibited in Figure 33, the dissolved fraction of Cu, Pb and Zn for the April 11, 2002 event stayed below 0.5 for approximately 70 percent of the storm, while f_d values of Cd dropped below 0.5 after the initial 45 percent of the event. These relatively low f_d values indicated that the four targeted metals were predominately in the particulate phase for the majority of the flow-limited events. However, there was a slight general increase in f_d values at the lower flows associated with the latter portion of the storm, enhancing aqueous levels of Cd and Cu. Dissolved fraction values of Zn slightly increased at the declining limb of the hydrograph for the high intensity events (May 13, 2002 and May 30, 2002) but remained relatively stable at this point for the low intensity events (April 11, 2002 and June 16, 2002). When examining the June 16, 2002 event, f_d values for Zn and Cu were generally higher than the April event. With the exception of the May 13, 2002 event, f_d values for Pb remained relatively stable.

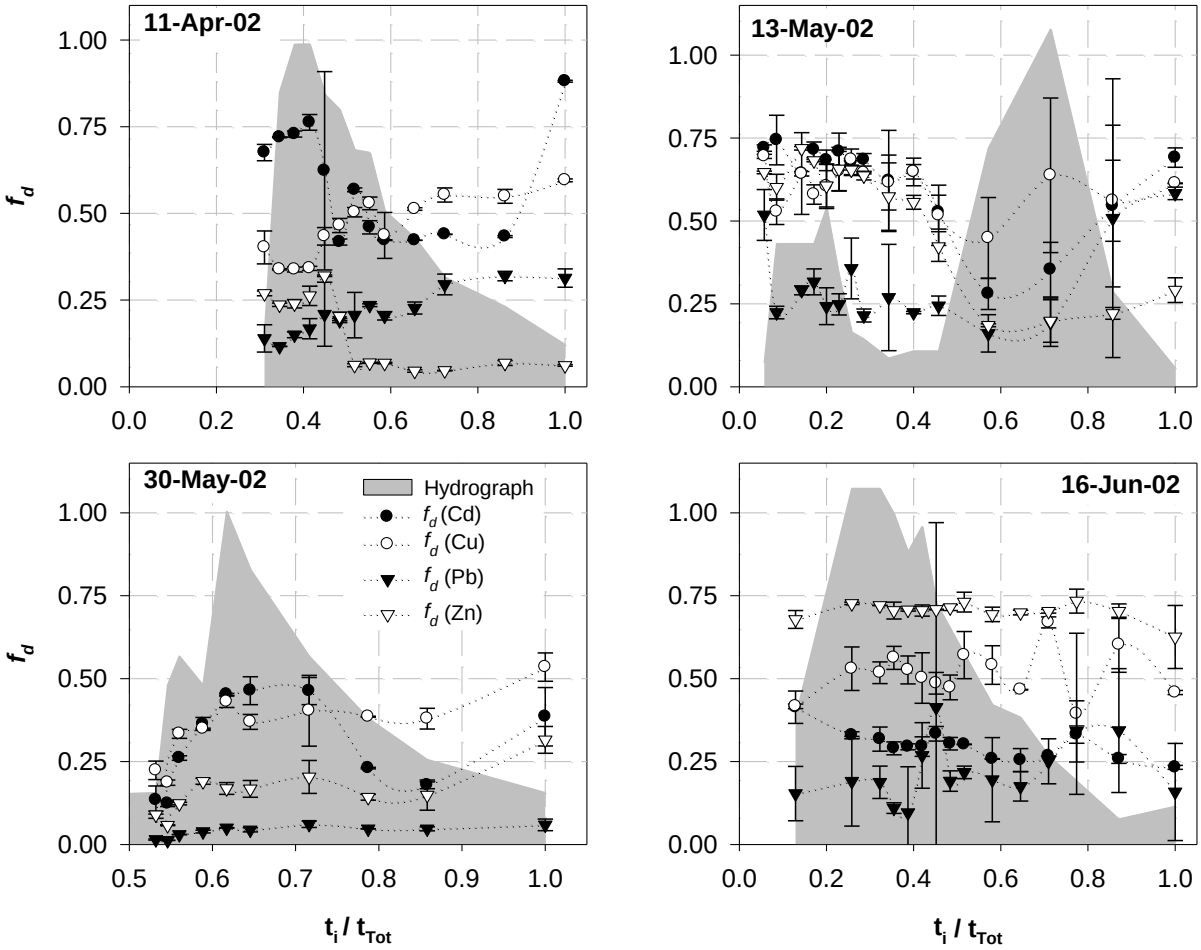

Figure 33

Metal phase partitioning as a function of flow rate for each of the four storm events

When comparing the aggregate water quality pollutographs (temporal concentration profiles) in Figure 34 and Figure 35 to the associated hydrographs for flow-limited events, a consistent trend is apparent. The highest concentrations of SSC, TDS, and alkalinity were observed in the early part of the runoff hydrograph. As the hydrologic event progressed, there was an exponential-type decrease in concentration. Aqueous phases of the ionic constituents analyzed generally followed the same trend, closely mimicking the behavior of TDS. Exceptions to this trend were observed in the behavior of Al and Fe that exhibited behavior identical to one another and were apparently uninfluenced by hydrology. The pH of the runoff increased slightly with increasing flow rates. Due to the relatively low maximum flow rates of the two events, the cementitious pavement was able to effectively buffer the rainfall and maintain higher pH conditions (pH > 7.4) at elevated flows.

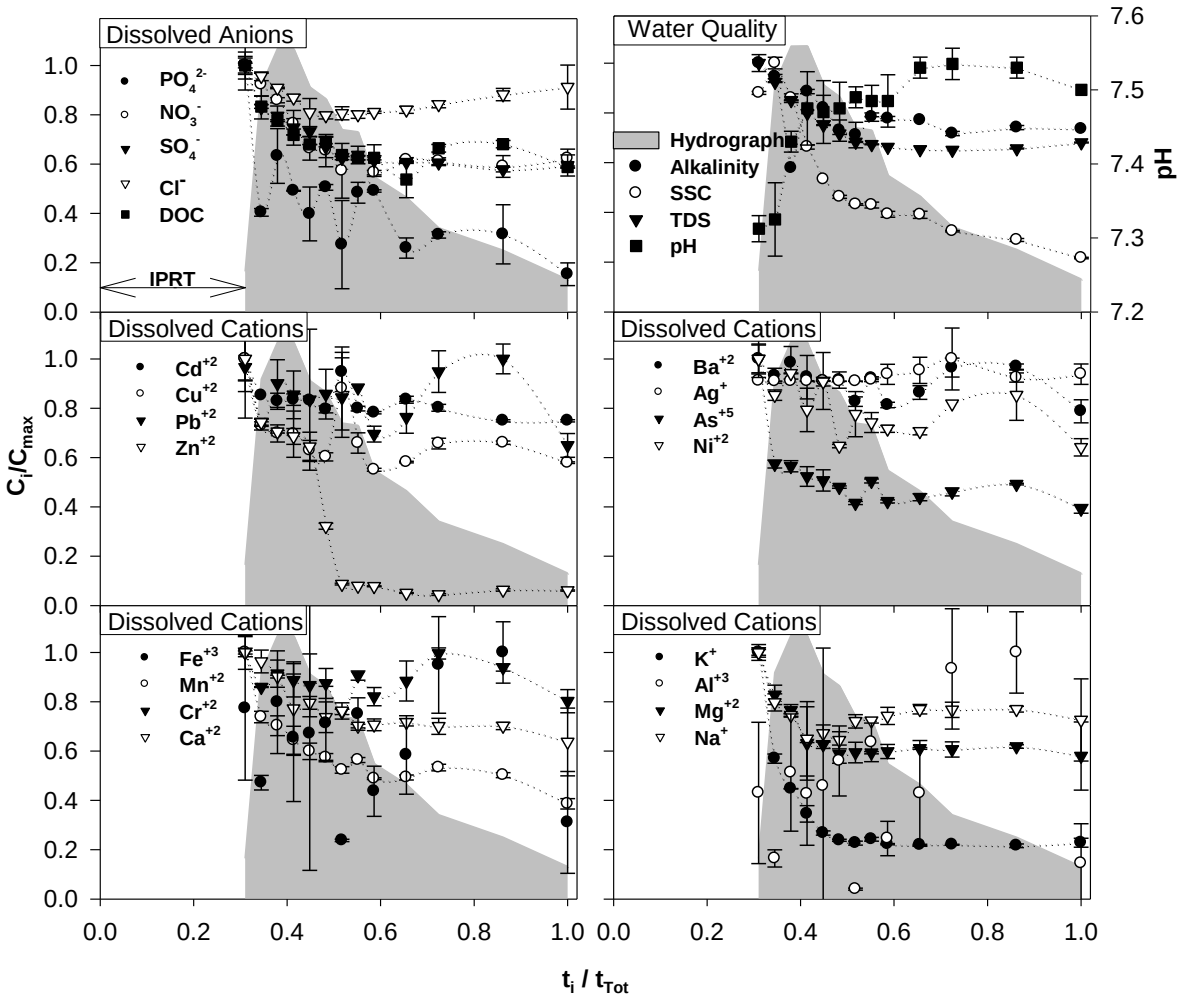

Figure 34

Transport of water quality and ionic constituent at the upper end of an urban watershed (concrete pavement) for the April 11, 2002, flow-limited-rainfall-runoff event

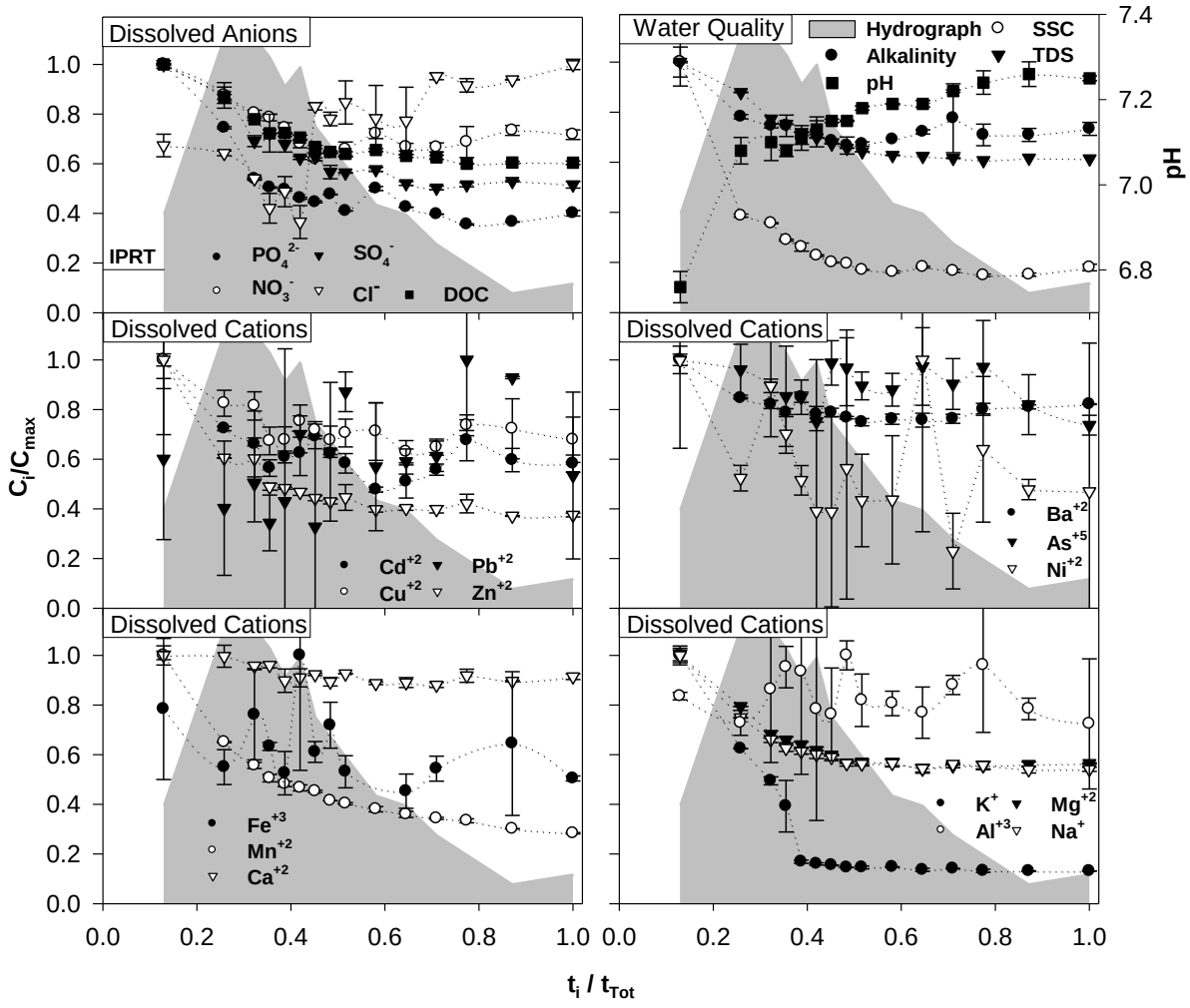

Figure 35

Transport of water quality and ionic constituent at the upper end of an urban watershed (concrete pavement) for the June 16, 2002, flow-limited-rainfall-runoff event

MINTEQ revealed similar results for both of the flow-limited storm events (Figure 36 and Figure 37). Modeling results demonstrated that the dominant species of Cd across each of the event hydrographs was Cd^{+2}. Concentrations of Cd^{+2} were approximately five times higher than the next dominant species ($CdSO_4$) and remained relatively constant across the event. These results were similar to those found by (Revitt and Morrison, 1987) as well as (Flores-Rodriguez et al., 1994). Due to the relatively constant pH of the runoff, pH was not a major factor for this event. Carbonate species made up a larger percent of the total metal concentrations in the flow-limited events than in the higher intensity events, while ionic

species were slightly lower. Ionic species of Cd encompassed between 70 and 78.5 percent of the total dissolved Cd concentration. The varying trends in f_d values had little impact on Cd speciation.

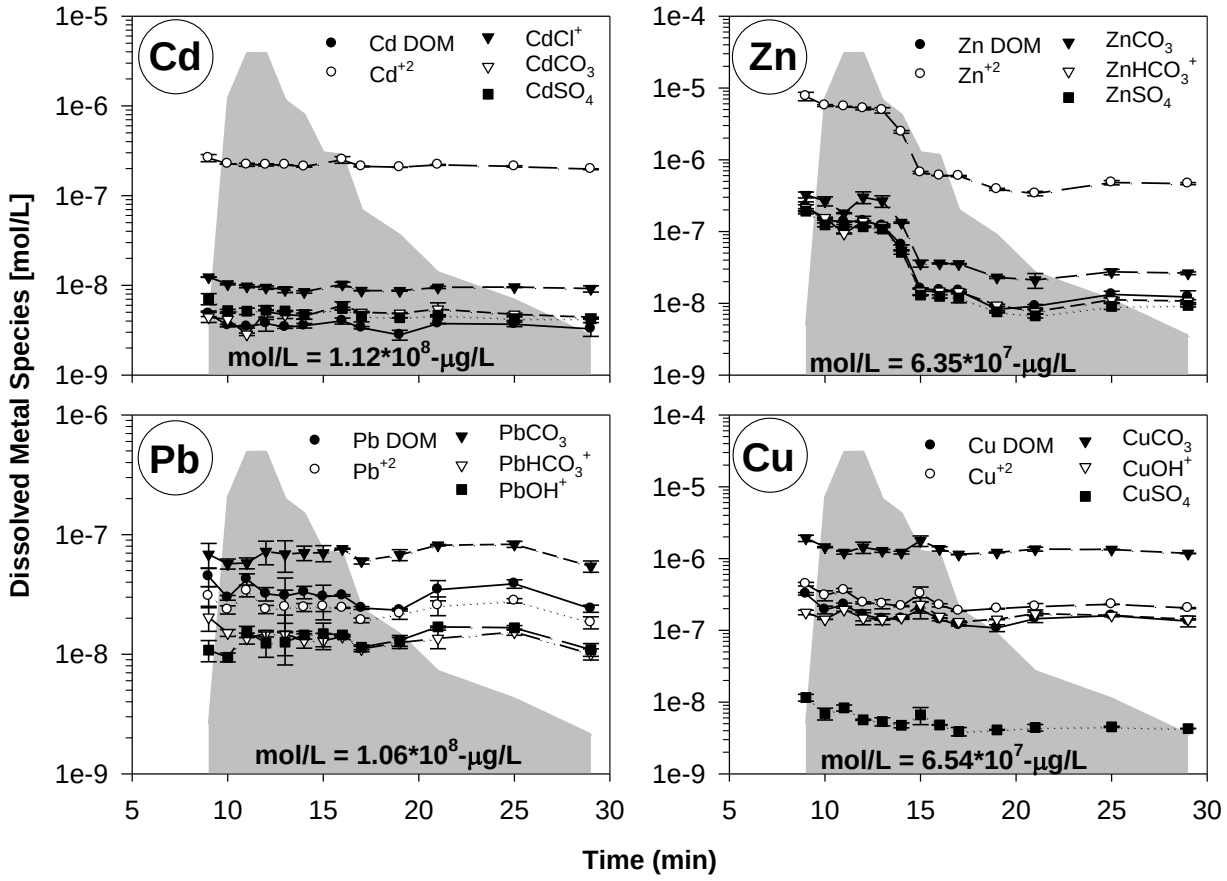

Figure 36

MINTEQ-calculated dissolved metal species as a function of the hydrograph for the April 11, 2002, flow-limited-rainfall-runoff event

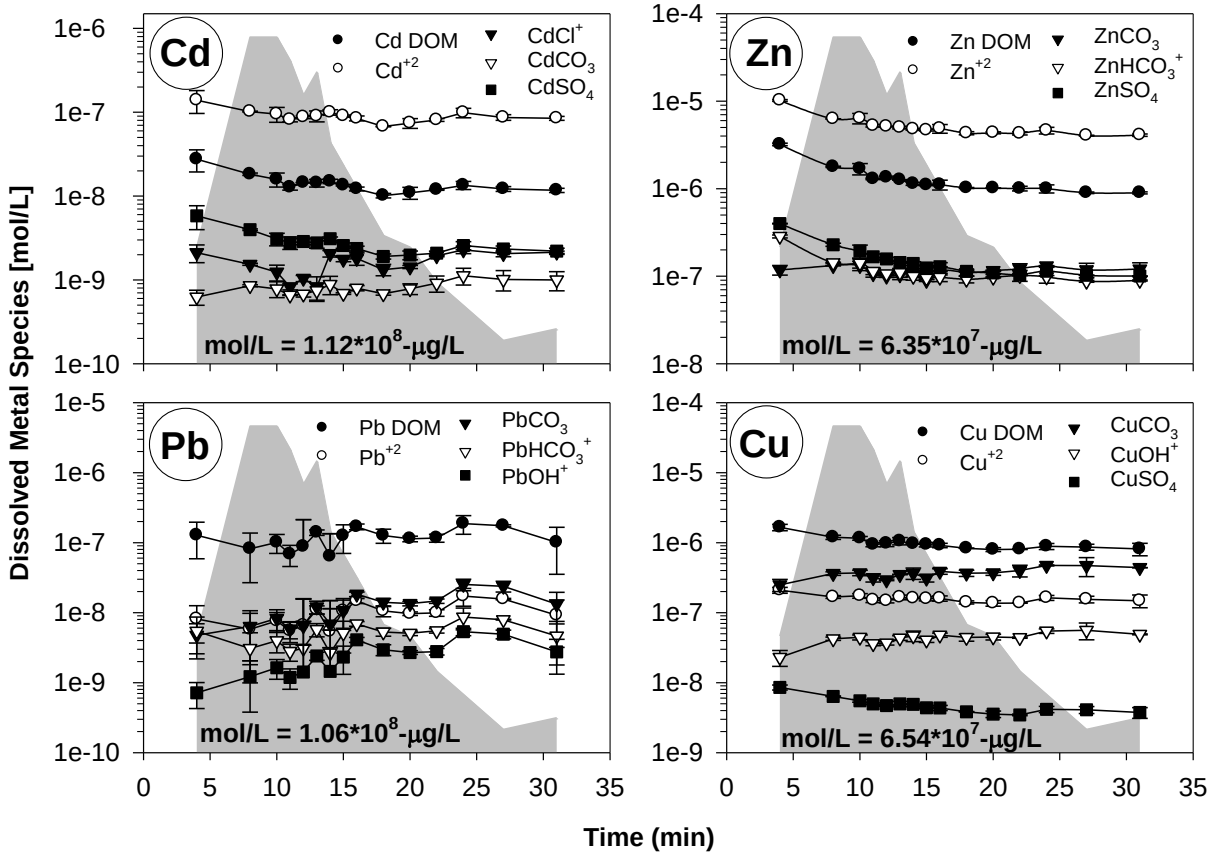

Figure 37

MINTEQ-calculated dissolved metal species as a function of the hydrograph for the June 16, 2002 flow-limited-rainfall-runoff event

The model predicted that the behavior of Zn mimicked that of Cd, which was dominated by the ionic species. Partitioning of Zn remained relatively constant during the event despite the variable hydrology. As with Cd, concentrations of Zn^{+2} remained at least five times higher than the next dominant species ($ZnSO_4$), representing between 71.5 and 75.3 percent of the total dissolved Zn concentration. Influences of the hydrograph were insignificant on the speciation of Zn even during the peak flow rates. Similar results for Zn speciation were also seen in studies by (Revitt and Morrison, 1987; Flores-Rodriguez et al., 1994).

The speciation of Pb was slightly less uniform over the course of the event than that of Cd and Zn. However, the dominant species remained as PbDOM throughout the April 11, 2002, and June 16, 2002, events. The extent of dominance for the PbDOM species appeared to be

relatively uninfluenced by flow-limited hydrology. Concentrations of PbDOM were closely followed by concentrations of $PbCO_3$. Toxic species of Pb (ionic forms) were less of a threat than with Cd and Zn. The total concentration of PbDOM represented between 30 and 70 percent of the aqueous concentration of Pb. The predominance of the strongly bound, less available species was also reported in previous studies (Flores-Rodriguez et al., 1994).

As with Cd, Zn, and Pb, Cu maintained a single dominant species throughout the low intensity events, predominating as $CuCO_3$. The composition percentages remained relatively constant throughout the event due to the low flow rates, indicating that the hydrograph had little influence on the speciation. $CuCO_3$ concentrations fluctuated between 48 and 65 percent of the total dissolved Cu concentrations. These results are contrary to previous studies on Cu speciation (Reemtsma et al., 2000) that identified CuDOM as a primary species. In this study, CuDOM accounted for 27 percent of the total dissolved Cu concentration.

Examinations of the concentration profiles for aggregate water quality constituents (SSC, TDS, and alkalinity) revealed that these water quality aggregate parameters did not significantly influence the speciation of metal complexes for the low intensity events. The low flow rates of flow-limited events generally exhibit a stable distribution of the various species of Cd, Zn, Cu, and Pb as a result of the proportionate delivery of pollutants to the hydrograph. Partitioning (represented by the trend in f_d values) appeared to have little influence on the distribution of the various dominant species because aqueous speciation is a phenomenon relative to the dissolved portion.

High Intensity Events

High intensity events typically produce high runoff volumes and exhibit a disproportionate delivery of constituents. Disproportionate delivery refers to metal mass transport profiles that do not follow the hydrograph profiles and typically exhibit a surface exhaustion of metal constituents early in the event. These events are labeled as mass-limited events and often display a disproportionate "first flush" of constituent mass and concentration during the early portion of the event. Of the four hydrologic events analyzed in this research, two exhibited mass-limited behavior. These included a 30-min. event occurring on May 13, 2002 and a 136-min. event occurring on May 30, 2002. A total of 1974.4 L and 7336.8 L of runoff were collected from the May 13, 2002, and May 30, 2002, events, respectively.

Investigation into the partitioning of Cd, Zn, Cu, and Pb revealed contrasting results for the two events. The May 13, 2002 event exhibited a separate hydrograph early in the event. As shown in Figure 33, the f_d values at this point were relatively high, indicating that the metals were predominately dissolved with the exception of Pb that remains particulate-bound, regardless of flow. Once the second hydrograph was reached, the predominance of metals shifted to the particulate-bound phase with the exception of Cu. For the May 30, 2002 event, the total metal concentrations remained predominately particulate-bound. A slight increase in f_d values was observed at the decreasing limb of the hydrograph for both events. As in the flow-limited events, the highest SSC, TDS and alkalinity concentrations were associated with the first samples of the events and decreased rapidly with flow (Figure 38 and Figure 39). The May 13, 2002 event exhibited a stabilization of TDS and alkalinity at the peak of the first hydrograph, and these parameters remained relatively constant until the rising limb of the second hydrograph. Concentrations of SSC remained relatively low throughout the remainder of the event, indicating an exhaustion of surface particulates. The behavior of TDS and alkalinity at the second hydrograph mimicked that of the SSC, TDS, and alkalinity for the May 30, 2002 event. Aggregate pollutant concentrations inversely followed the behavior of the hydrographs indicating a diluting effect on the concentrations. The trends in anion concentrations typically followed that of TDS. However, cation concentrations followed less discernable trends with the exception of a few metals that tended to follow similar trends as TDS. As with f_d values, the behavior of pH varied between the two events. For the May 13, 2002 event, there was no diluting effect on the buffering capacity of pavement. The May 13, 2002 event exhibited pH trends that inversely followed the hydrograph, indicating that the acidic rainwater was unable to be neutralized by alkaline constituents leached from the pavement. As the flow rate increased and the alkalinity decreased, the pH became more acidic. In each case, the range of pH was relatively tight, bound by 6.5 and 7.

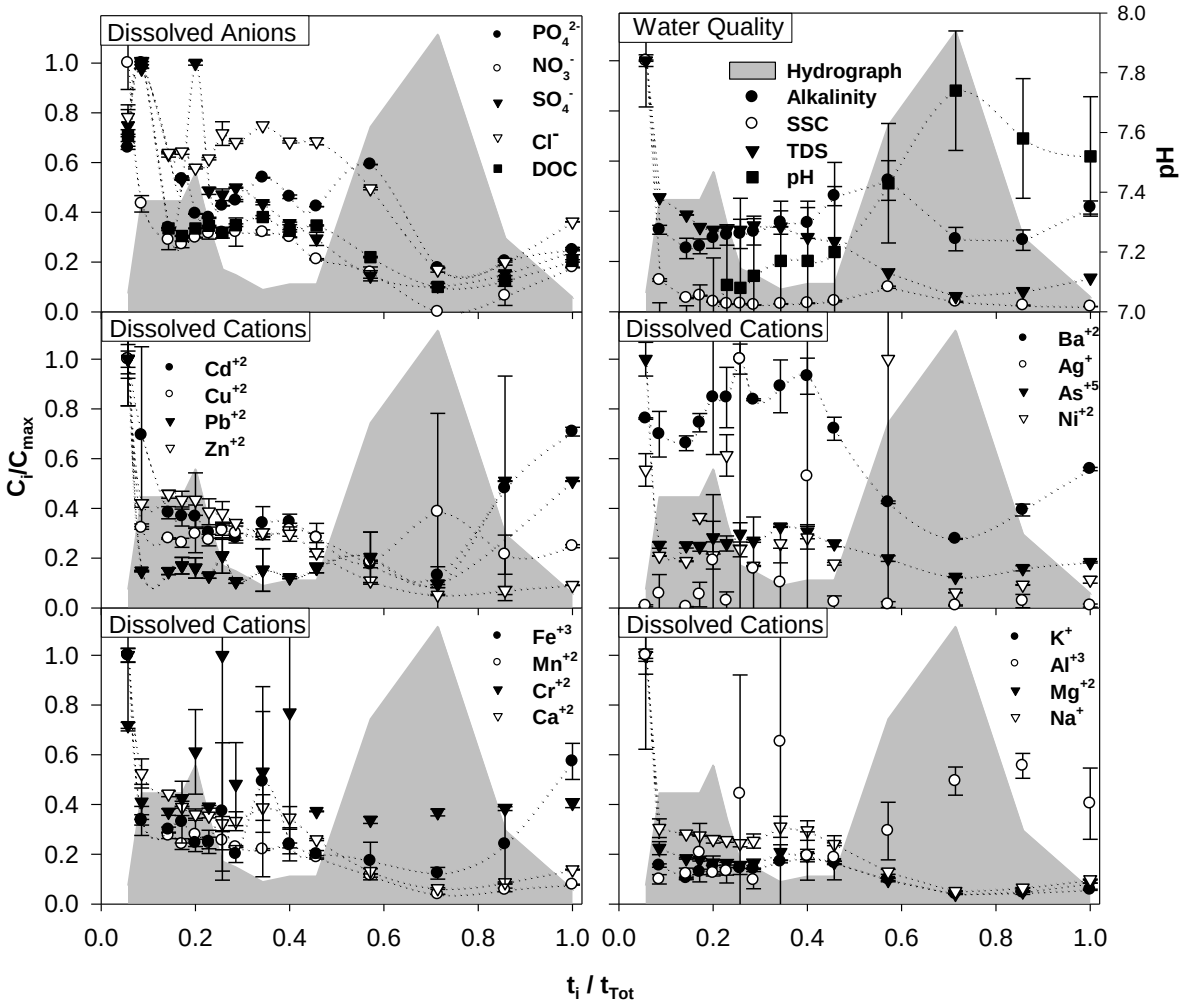

Figure 38

Transport of water quality and ionic constituent at the upper end of an urban watershed (concrete pavement) for the May 13, 2002, mass-limited-rainfall-runoff event

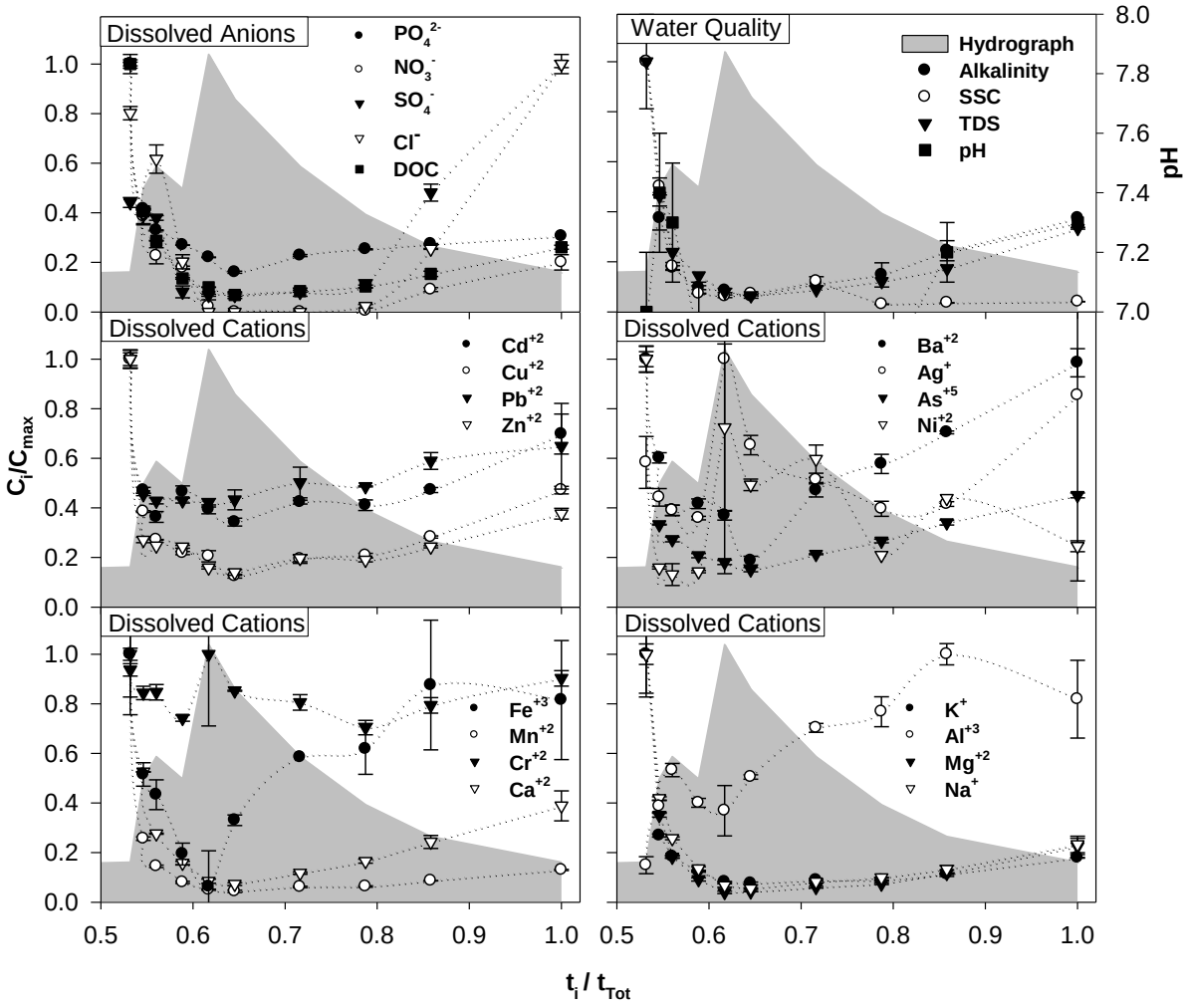

Figure 39

Transport of water quality and ionic constituent at the upper end of an urban watershed (concrete pavement) for the May 30, 2002, mass-limited-rainfall-runoff event

Results from MINTEQ revealed similar dominate species as observed in the flow-limited events (Figure 40 and Figure 41). However, there was a pronounced influence of hydrology on the overall speciation of the metals. The dominant species of Cd was Cd^{+2} throughout the entire event. However, the magnitude of the concentration differences between ionic forms of Cd and the remaining species was maximal at the peak of the hydrographs when alkalinity was minimal. At hydrograph peaks, carbonate and bicarbonate species were not as pronounced as organic and ionic species of Cd. Ionic species of Cd encompassed between 63.0 and 96.6 percent of the total dissolved Cd concentration. As with Cd^{+2}, Zn^{+2}

predominated throughout the entire event for all four storms. Influences of the hydrograph were more evident when examining the fluctuation of Zn throughout the event. Ionic forms of Zn made their highest contribution to the total dissolved Zn concentrations during the peaks of the hydrographs. Ionic forms of Zn represented between 65.6 and 94.2 percent of the total dissolved Zn concentration.

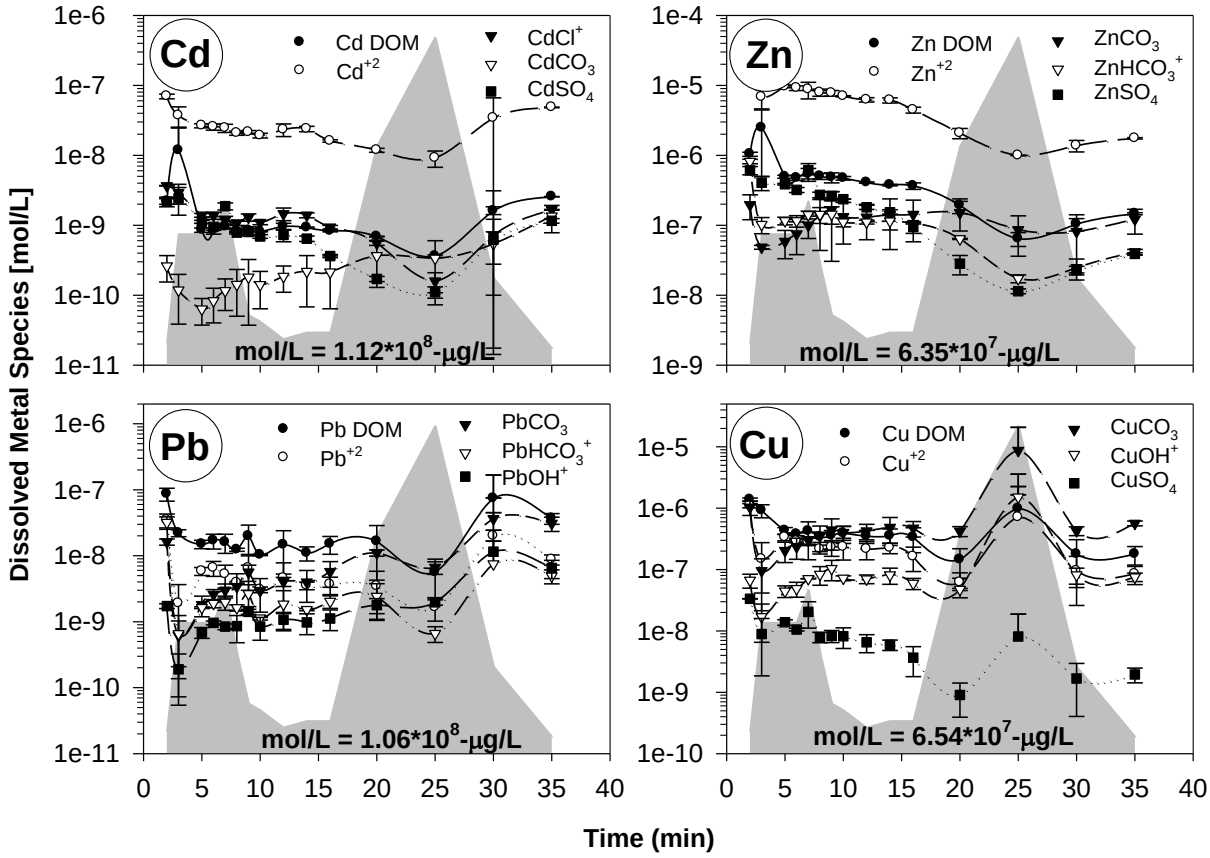

Figure 40

MINTEQ-calculated dissolved metal species as a function of the hydrograph for the May 13, 2002, mass-limited rainfall-runoff event

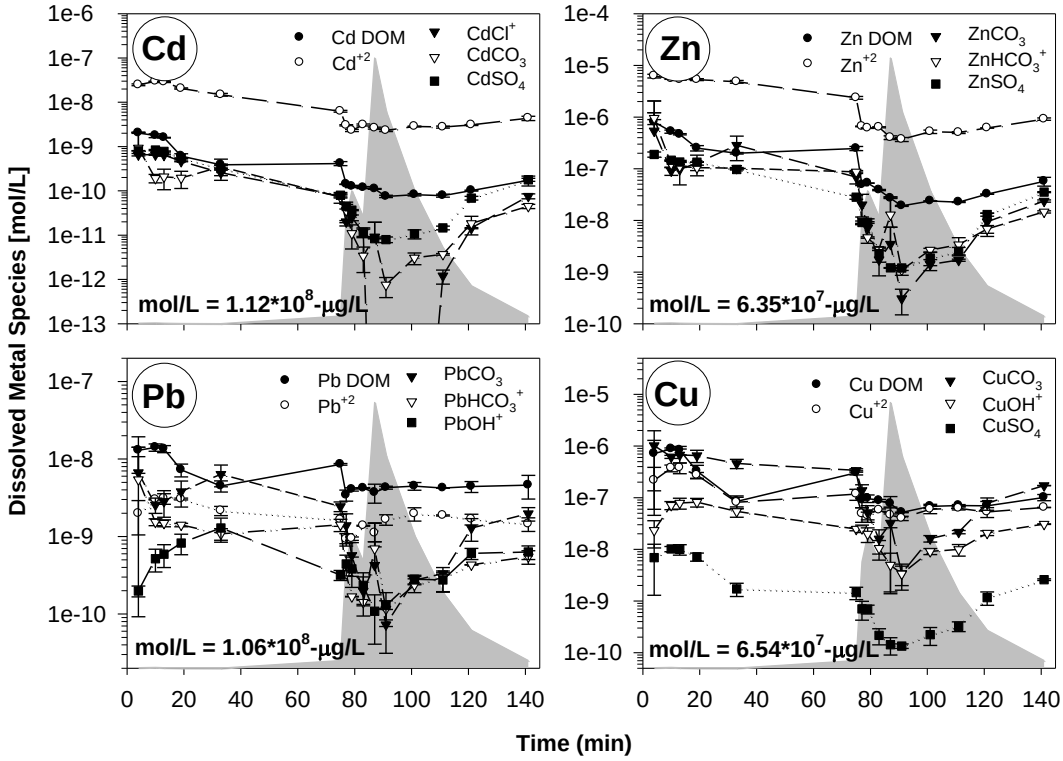

Figure 41

MINTEQ-calculated dissolved metal species as a function of the hydrograph for the May 30, 2002, mass-limited rainfall-runoff event

The dominant species of Pb was PbDOM throughout the study. Influences of the hydrograph were evident during peak flows of the Mar 13, 2002 event when concentrations of PbDOM and $PbCO_3$ approximately equal. This phenomenon was mimicked at the positive slope of the hydrograph occurring on May 30, 2002, but diminished before the peak was reached. Hydrograph influences were evident in the May 30, 2002 event when carbonate, bicarbonate and hydroxide bound species of Pb significantly decreased as a result of amplified flows. As indicated by the water quality plots, sources of alkalinity were exhausted at this point, possibly causing the less significant contributions of carbonate and hydroxide species. Toxic species of Pb (ionic forms) were more of a threat during periods of intense flows due to a more acidic runoff pH. The total concentration of PbDOM represented between 31.5 and 75.8 percent of the aqueous concentration of Pb. Due to major influences of the hydrograph on the speciation of Pb, $PbCO_3$ represented between 1.1 and 37.4 percent of the total Pb composition. Ionic species of Pb represented 9.3 to 26.5 percent of the total dissolved Pb concentration for both high intensity events.

The event occurring on May 13, 2002 was a high intensity event producing a flow rate that appeared to significantly influence the speciation of Cu. At periods of low flow (between the two peaks of the hydrograph), the concentration profiles for the various species were similar, indicating a more uniform distribution of species (temporal species concentrations were comparable). During the peak of the hydrograph, the distribution became more disperse with $CuCO_3$ dominant. At this point in the event, CuOH concentrations exceeded ionic forms of copper. Analysis of the May 30, 2002 event revealed results similar to that of Pb. $CuCO_3$ was the dominant species until the positive slope of the hydrograph peak was reached, representing between 3.22 and 62.5 percent of the total dissolved Cu concentration. At that point, CuDOM became the most common species closely followed by ionic copper. As the pavement became depleted of alkaline sources, the carbonate and hydroxide species became less significant. CuDOM and Cu^{+2}concentrations ranged from 15.7 to 57.8 percent and 8.2 to 40.3 percent of the total dissolved Cu concentration, respectively.

Toxicity of Particulates in Urban Rainfall-runoff

Runoff Event Hydrology and Sampling Point

The April 06, 2004, and April 24, 2004, storms were grouped and compared as high intensity, high runoff volume events. The October 24, 2004, and April 22, 2005, storms were grouped and compared as low intensity, low runoff volume events. First-flush, middle event flush and end event flush were captured and the role of hydrologic transport on total suspended solid and turbidity examined across each event. TSS and turbidity are of interest in this study because fine particles can suspend longer in water column and contribute more to the toxicity of runoff particles. Figure 42 and Figure 43 show a good concurrent relationship between TSS and turbidity. For the high intensity events, TSS exhibits a strong first flush and shows a low and relative constant concentration after that. The results in Figure 43 indicate that the October 24, 2004, event is a TSS and turbidity concentration limit event. As a result of the low but relatively uniform intensity in storm event April 22, 2005, TSS and turbidity gradually decreased in general. First flush present the peak value of TSS and turbidity for all events except the October 24, 2004, event. There is no significant difference between the middle event and end event flush on TSS and turbidity, which can be representative of the average values for runoff after first flush.

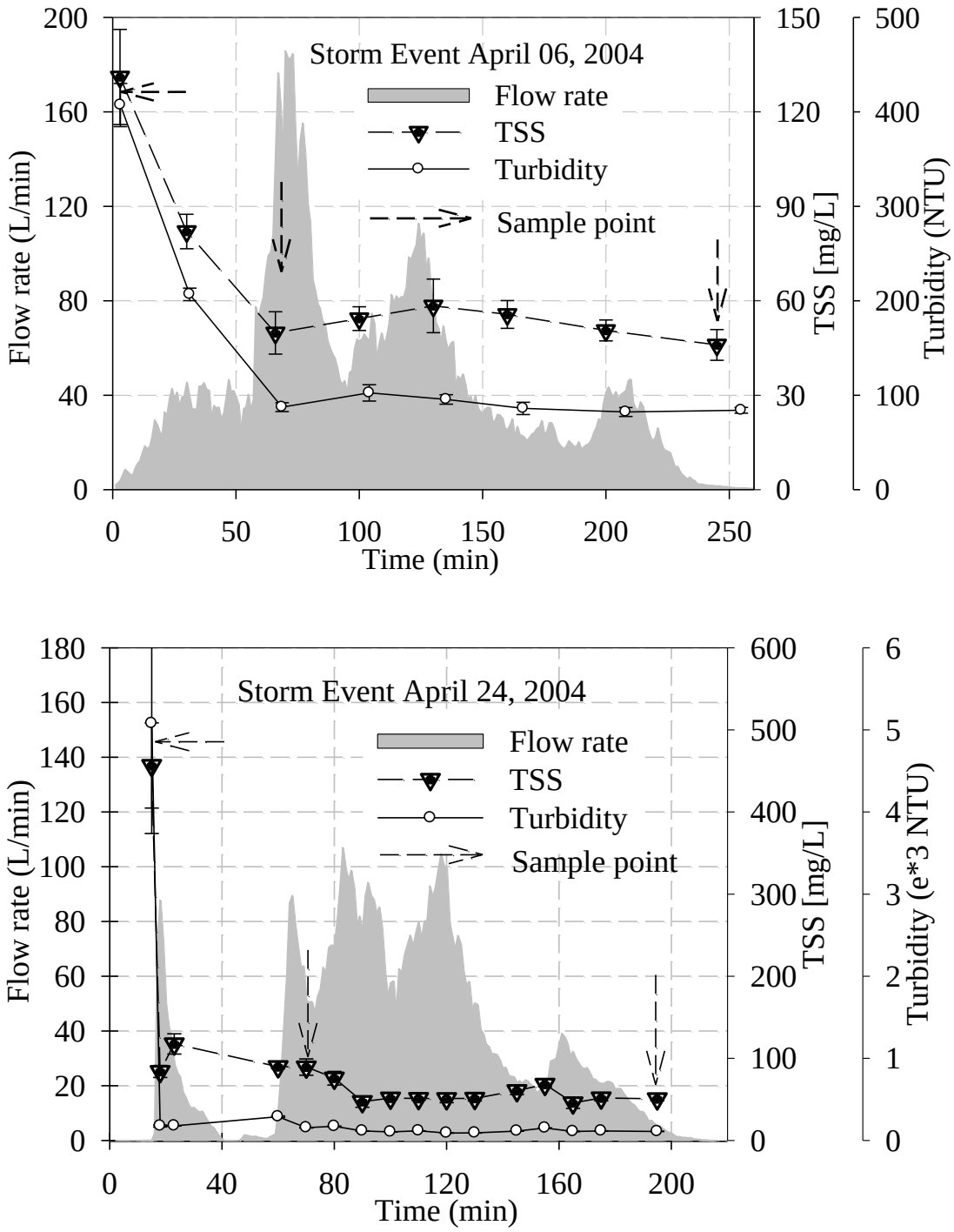

Figure 42

Total suspended solid (TSS), turbidity and rainfall-runoff flow rate change with elapsing time for two longer rainfall-runoff event

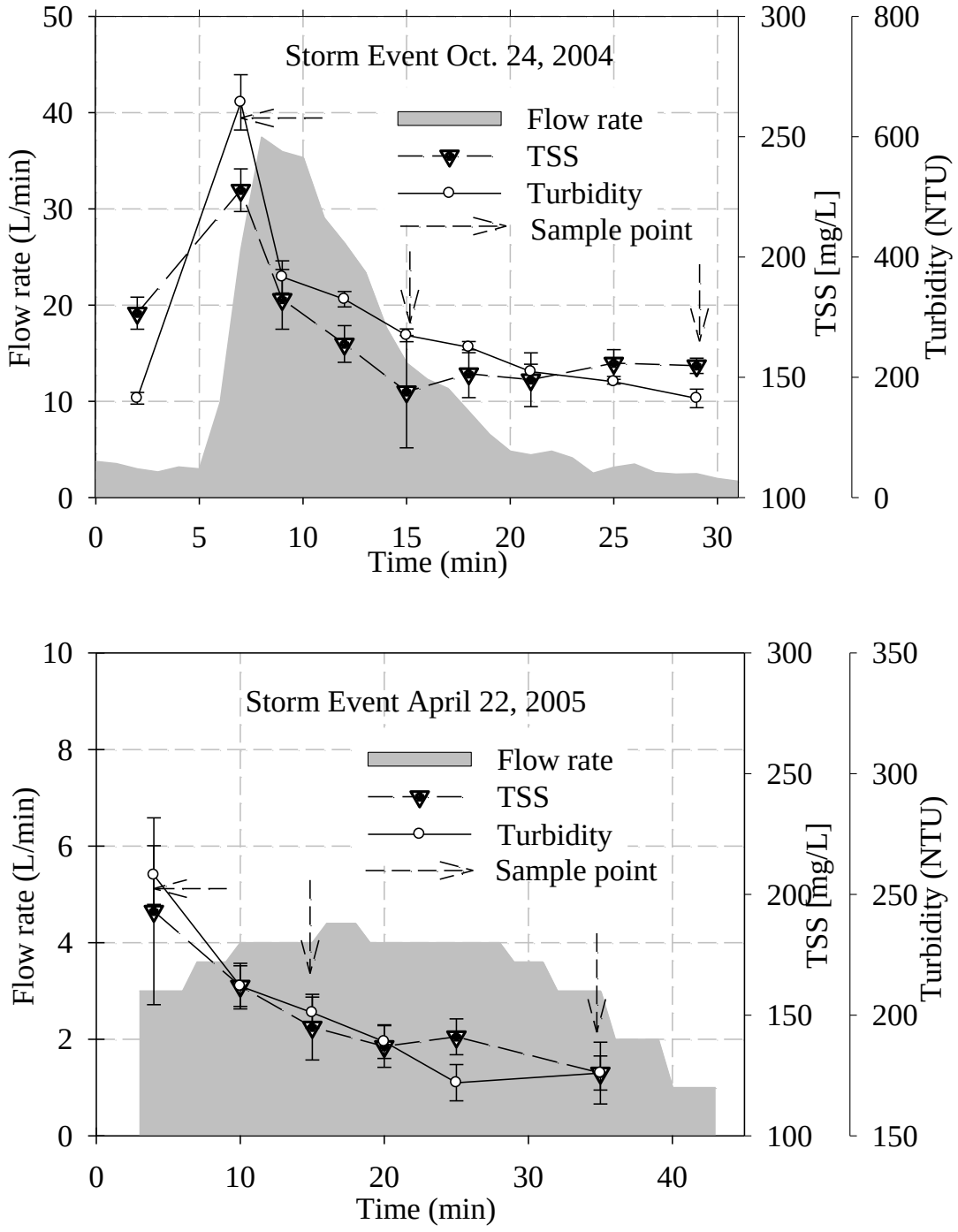

Figure 43

Total suspended solid (TSS), turbidity and rainfall-runoff flow rate change with elapsing time for two shorter rainfall-runoff events

Generally, the pH, dissolved oxygen (DO), toxic ammonia (NH_3-N) and temperature were maintained in an acceptable range throughout the tests (Table 21). The pH ranged from 7.0 to 8.5 and ambient temperature changed from 19 ˚C-22 ˚C. Toxic ammonia level and nitrite level was below 0.05 mg/L and 0.4 mg/L in most tests, respectively. Dissolved oxygen concentrations are all above 5 mg/L, which was essential to provide a healthy exposure condition.

Table 21

Exposure condition and water quality analysis results during 96 hours for four storm events

Exposure condition/ Water quality						
Event	Exposure time (hr)	Temp. (^oC)	pH	NH_3-N [mg/L]	NO^-_2-N [mg/L]	DO [mg/L]
April 06, 2004	0	20.7 ± 0.50	7.90 ± 0.35	0	0	6.90 ± 0.40
	24	22.2 ± 0.37	7.28 ± 0.44	0.010± 0.010	0.2 ± 0.05	6.63 ± 0.97
	48	21.1 ± 0.17	7.53 ± 0.21	0.022± 0.015	0.33 ± 0.06	7.00 ± 1.05
	72	22.8 ± 0.14	7.48 ± 0.13	0.035± 0.006	0.33 ± 0.06	6.97 ± 0.40
	96	22.5 ± 0.20	7.48 ± 0.12	0.037± 0.006	0.33 ± 0.06	7.17 ± 0.76
April 24, 2004	0	21.3 ± 0.58	7.90 ± 0.35	0	0	7.47 ± 0.67
	24	21.3 ± 0.58	7.28 ± 0.44	0.027±0.015	0.5 ± 0.06	6.53 ± 0.75
	48	21.0 ± 0.00	7.53± 0.21	0.037±0.015	0.46 ± 0.05	7.13 ± 0.71
	72	22.7 ± 0.58	7.48 ± 0.13	0.040±0.017	0.43 ± 0.11	7.07 ± 0.42
	96	22.3 ± 0.58	7.48 ± 0.12	0.050±0.000	0.46 ± 0.15	7.60 ± 0.46
October 24, 2004	0	21.3 ± 0.10	6.71 ± 0.04	0	0	7.03 ± 0.55
	24	20.3 ± 0.05	6.80 ± 0.11	0.020±0.010	0.33 ± 0.15	6.87 ± 0.25
	48	20.3 ± 0.10	7.05 ± 0.03	0.040±0.010	0.36 ± 0.05	6.80 ± 1.14
	72	22.2 ± 0.13	7.07 ± 0.02	0.047±0.006	0.36 ± 0.06	6.63 ± 0.47
	96	20.1 ± 0.14	7.02 ± 0.02	0.053±0.006	0.36 ± 0.06	7.033 ± 0.31
April 22, 2005	0	20.1 ± 0.10	7.01 ± 0.01	0	0	7.30 ± 0.46
	24	20.8 ± 0.08	6.92 ± 0.01	0.023±0.006	0.43 ± 0.11	6.63 ± 0.60
	48	21.0 ± 0.13	6.90 ± 0.04	0.037±0.015	0.36 ± 0.06	6.43 ± 0.57
	72	21.2 ± 0.10	6.86 ± 0.04	0.040±0.000	0.36 ± 0.05	7.63 ± 0.45
	96	20.5 ± 0.18	6.94 ± 0.12	0.057±0.010	0.33 ± 0.06	7.43 ± 0.59
Notes:						
Data is presented as: Mean Concentration ± 95% confidence interval						

Turbidity values in Figure 44 and Figure 45 dramatically decreased in 24 hours and below 100 NTU in most cases. This trend showed that the flocculation and settling process could happen during the exposure and particle concentration and distribution change with exposure time. Actually test organisms were exposed to the highest concentration of particles

including colloidal, suspended, settleable, and sediment particles in the initial period of test and gradually decreased until only fine particles including colloidal materials remain in the exposure solution after 48 hours. In this case, part of settleable solids, especially sediment solids are considered as no or very low impact on test organisms since the short exposure time.

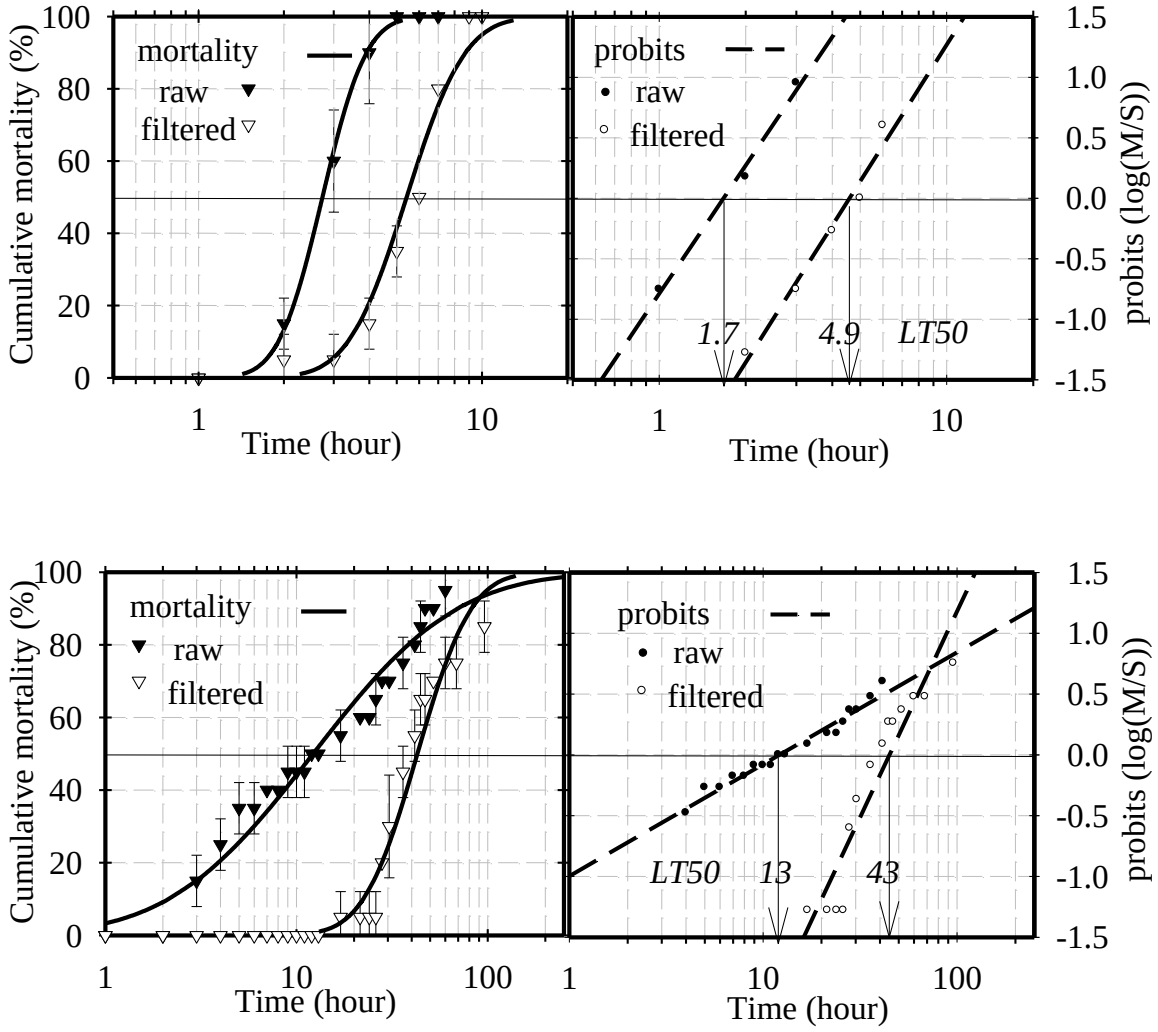

Figure 44

Response curve for cumulative mortality of channel catfish post larva as a function of exposure time (left side) and the trend based on probit values (right side) for storm event April 6, 2004

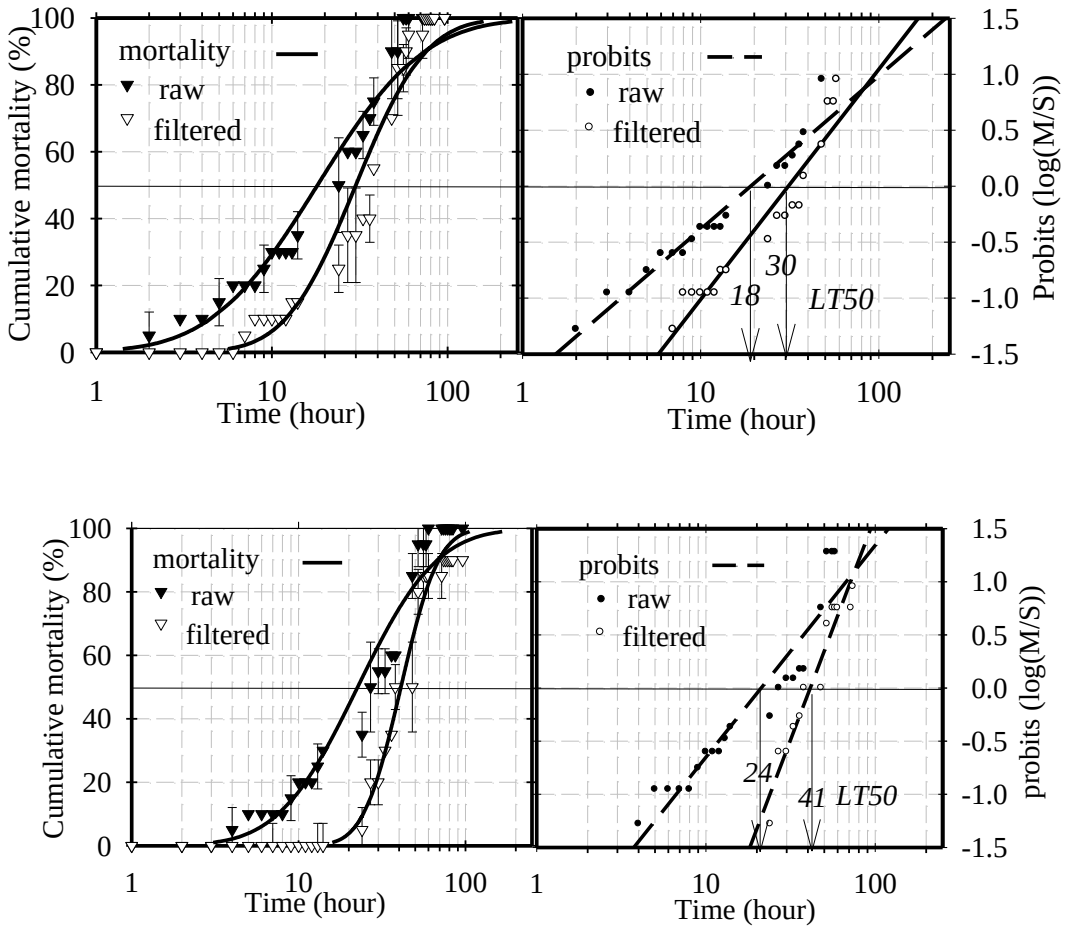

Figure 45

Response curve for cumulative mortality of channel catfish larva as a function of exposure time (left side) and the trend based on probit values (right side) for storm event April 6, 2004

From Figure 45 we can see that all particulate bound metals concentrations had no significant change as the turbidity values change throughout the test. It is possible that all these metals are mostly associated with fine particles because of the larger specific surface area. And all these particulate metals may cause adverse effects on test organisms as well as dissolved metals while they are in the suspension.

Figure 44 shows a different picture. All particulate bounded metals concentrations except Cd decreased greatly in 24 hours and less from 24 to 48 hours or more. It suggests that catfish postlarvae might ingest some fine or colloidal particles in a proper range of size. This

phenomena indicates that a more toxic exposure of particulate metals could happen for this lifestage organisms. The exception for Cd may due to the cadmium bounding particles are not in the proper range of size for test organisms even they still remain in the water column. This trend is not significant in Figure 45 because the test for the October 24, 2004 event was on juvenile fathead minnows which won't feed on these tiny particles instead of feeding on the larger size materials on the bottom.

As shown in Figure 44 and 45, the concentration of dissolved metals had no significant change in general except for Mn. The dissolved fraction of lead was very low (< 1 ug/L) compared to the particulate fraction (20-200 ug/L). For cadmium, these two fractions were very close. The decrease of dissolved Mn and big change during exposure time suggest that Mn may have a significant accumulation and bioconcentration for both catfish postlarvae and juvenile fathead minnows. From both figures, researchers can also find that particulate metals concentrations have a significant or slight decrease from first flush to end flush. The same trend happened for dissolved metals also. This may suggest that first flush including dissolved and particulate fractions could be more toxic than the other two from the metals point of view.

Acute Lethal Toxicity Test

Channel Catfish Post. Larvae time-response curves in Figure 46 and Figure 47 show the cumulative mortality and probit values of mortality of channel catfish postlarvae change with exposure time. The figures show that the cumulative mortality reached 100 percent in 10 hours for first flush (Figure 46, upper-left) and more than 100 hours for middle event flush (Figure 47, upper-left), end event flush (Figure 46, bottom-left), and the composite samples from Little Rock (Figure 47, bottom-left). The raw flush has higher accumulative mortalities than filtered flush during exposure in general, which indicate that raw flush with particles could be more toxic. From Figure 47, it is obvious that the time-response curves are similar among middle event flush, end event flush, and the Little Rock composite samples. This also indicates that middle event flush or end event flush may act as the representative of the average based on samples taken. In addition, the sudden increase of accumulative mortalities after 10 hours exposure with 0 percent mortality are found in end event flush and Little Rock composite sample, which may indicate a delay of the toxic effect.

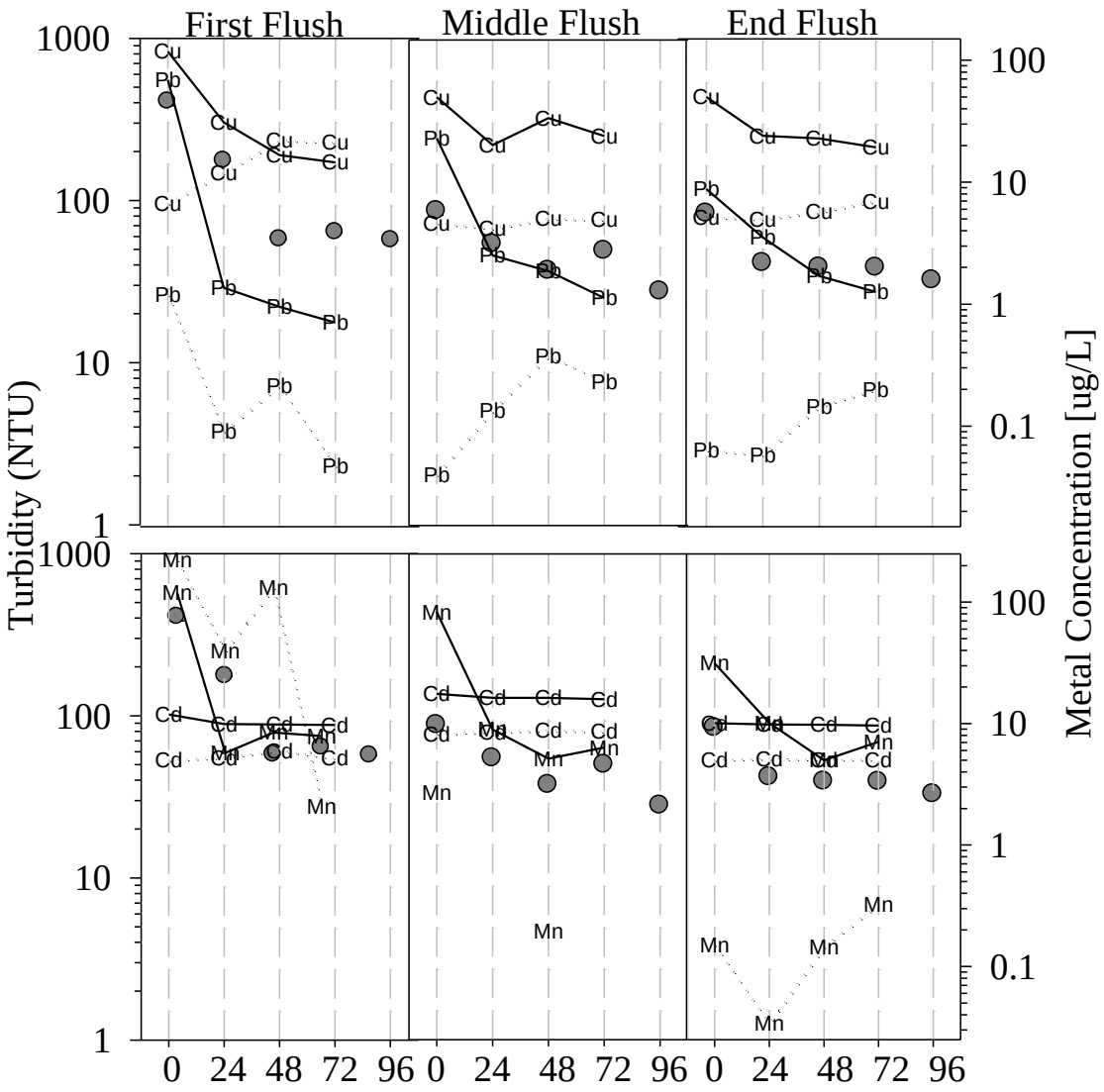

Figure 46

Turbidity values and four major metal species Cu, Pb, Cd, and Mn change with exposure time during 96-hour non-renewal static exposure for storm event April 6, 2004

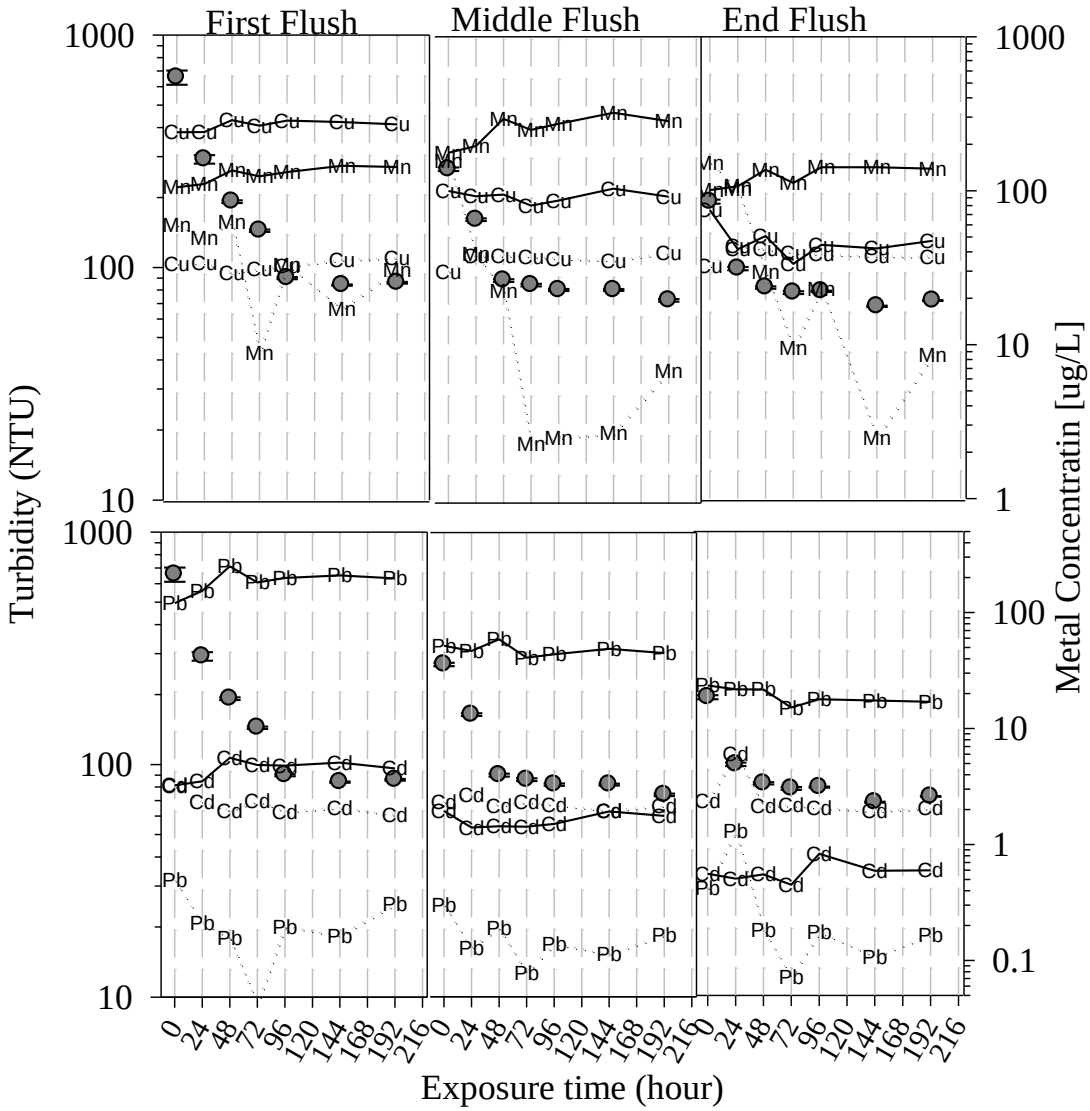

Figure 47

Turbidity values and four major metal species Cu, Pb, Cd, and Mn change with exposure time during 96-hour non-renewal static exposure for storm event October 24, 2004

From Figure 46 and Figure 47, the probit values of cumulative mortalities are calculated based on log scale and the zero values are corresponded with the 50% cumulative mortalities. The median lethal exposure time (LT50) values are 1.7 hours and 4.9 hours for raw and filtered first flush, 18 hours and 30 hours for raw and filtered middle event flush, 24 hours and 41 hours for raw and end event flush, and 13 hours and 38 hours for raw and

filtered Little Rock composite samples. Generally, the LT50 values are the smallest for first flush and increase from first flush to end event flush, which indicates that first flush is most toxic and the toxicity decreases along the event. When examining the data from Little Rock composite samples, it was noted that moderate toxicity responses were observed and the LT50 values are among the values for three flush samples collected from the Baton Rouge site, which indicates the possible average toxicity. All the raw sample LT50 values are smaller than those for filtered samples, which indicates that raw samples are more toxic.

Juvenile Fathead Minnow. The data in Figure 48, Figure 49, and Figure 50 indicate large variations in toxic responses among the various events studied. The detection of toxic responses may be affected by the type of events sampled and the timing of sample collection during individual events. There exists high variations in event mean concentrations (EMCs) of TSS and metals between events, typically two orders of magnitude for heavy metals (Marsalek et al., 1997). Events with high EMCs would most likely produce toxic responses. For all events, the accumulative mortalities in 96 hours are less than 50 percent and 96-hr LT50 cannot be reached. The survival rate, probit values, and No Observed Effect Time (NOET) results are summarized in Figure 48, Figure 49, and Figure 50.

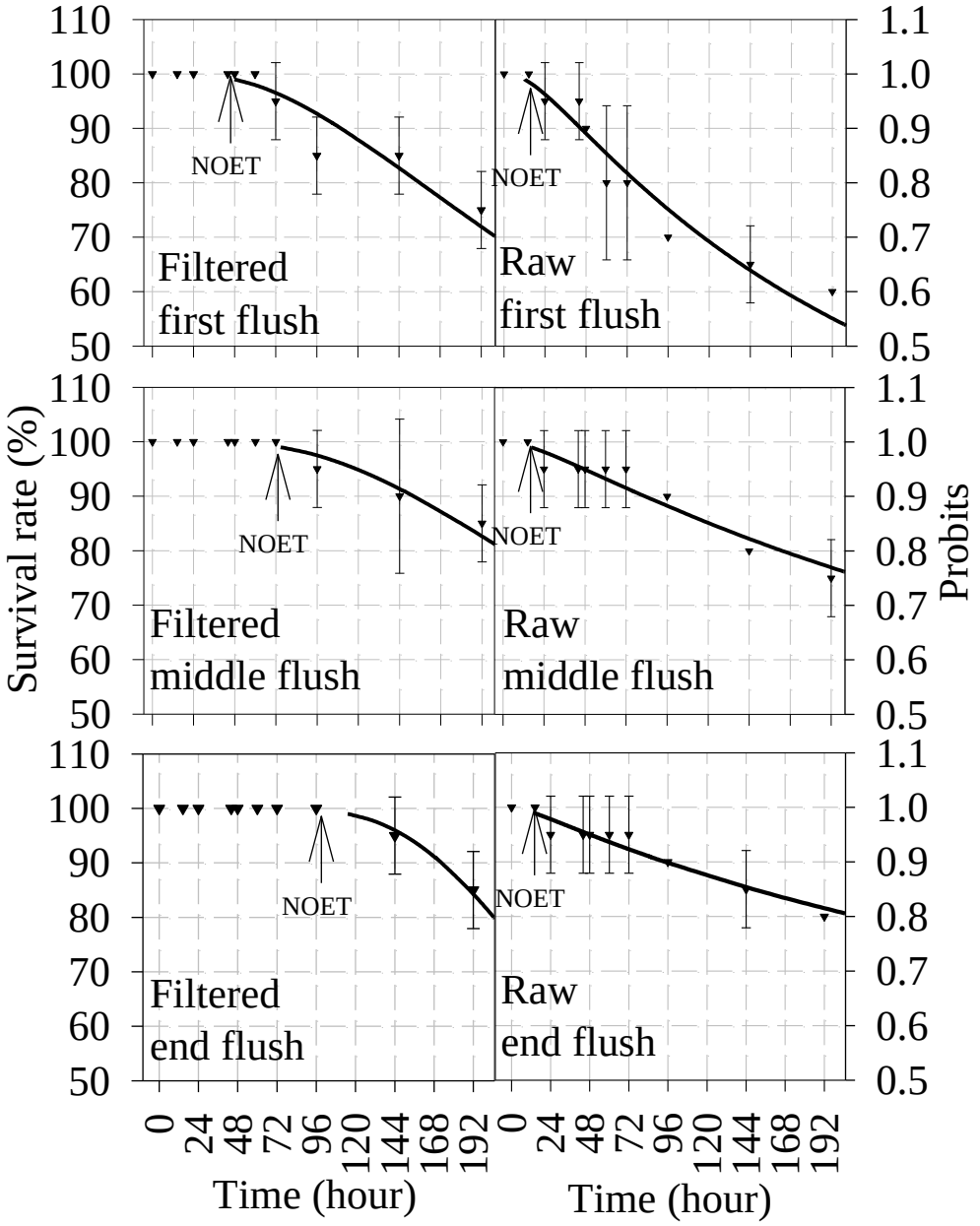

Figure 48

Response curve for cumulative survival rate of juvenile fathead minnow as a function of exposure time (triangular dot) and the trend based on probit values (spine curve) for storm event October 24, 2004 (NOET is No Observed Effect Time)

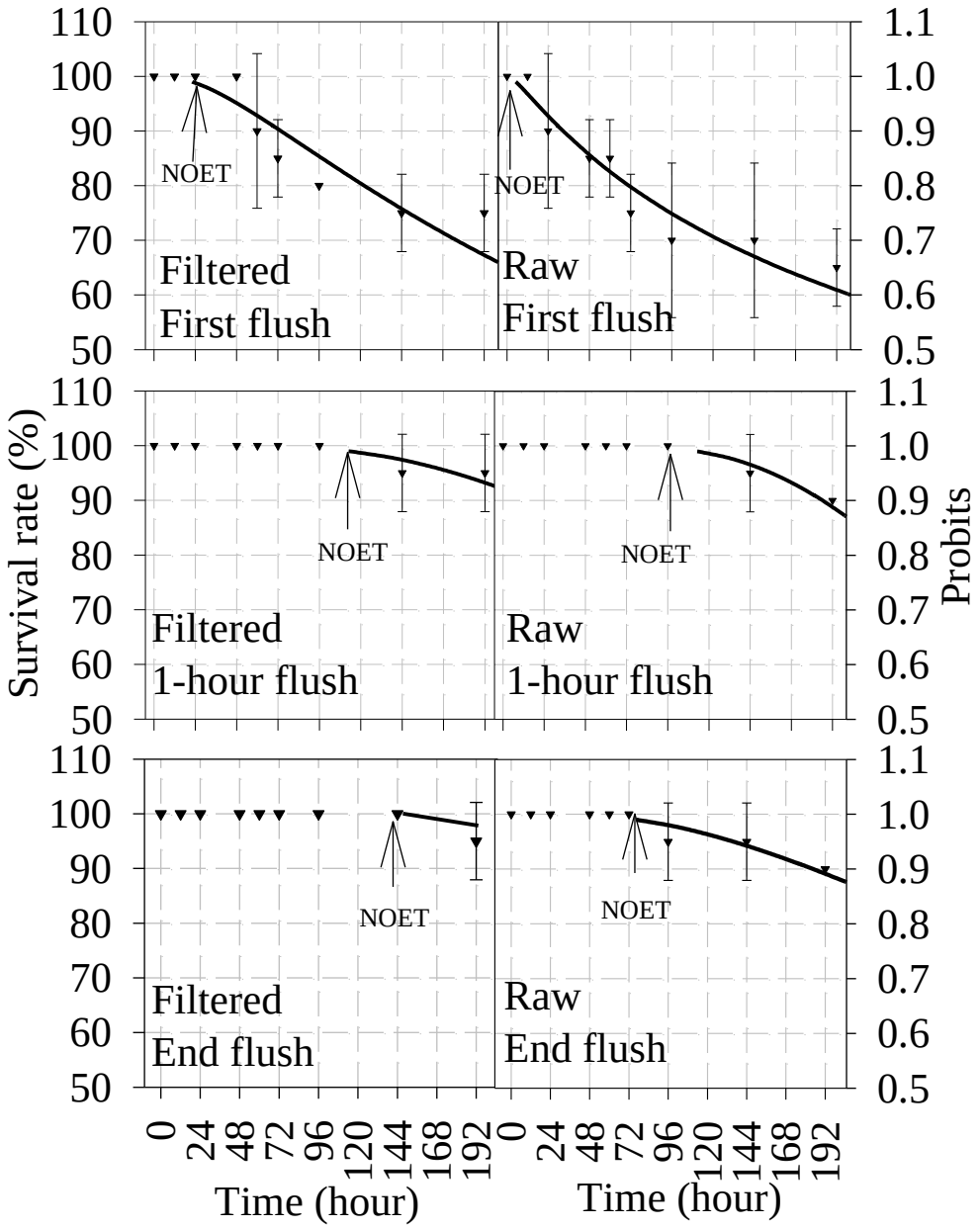

Figure 49

Response curve for cumulative survival rate of juvenile fathead minnow as a function of exposure time (triangular dot) and the trend based on probit values (spine curve) for storm event April 22, 2004 (NOET is No Observed Effect Time)

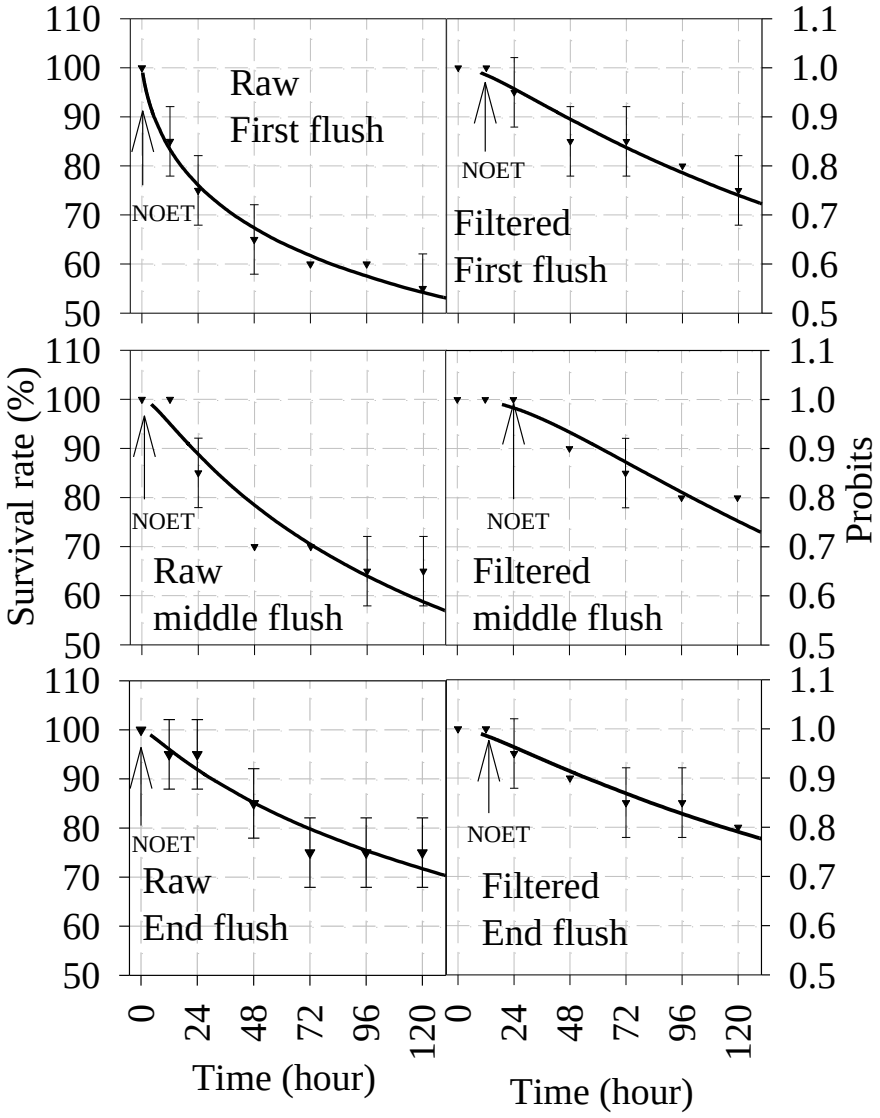

Figure 50

Response curve for cumulative survival rate of juvenile fathead minnow as a function of exposure time (triangular dot) and the trend based on probit values (spine curve) for storm event April 22, 2005 (NOET is No Observed Effect Time)

A quick perusal of the survival curve indicates that the most toxic responses were found for the first flush for three events (April 22, 2004; October 24, 2004; and April 22, 2005) with average NOET values of 12.05, 5.18, and 5.18 for raw flush and 48, 48, and 22.28 for filtered flush, respectively. It was further noted that raw samples were likely to be more toxic than filtered samples for all events as indicated by both the survival curves and NOET values.

From Figure 48, the NOETs for filtered samples were greater than 48 hours, while those for raw samples were less than 12 hours in the storm event October 24, 2004. Similar phenomena were found in other two storm events. From Figure 49, significant reductions in toxic responses were observed for the April 22, 2004 event during the first hour of the event, but hardly any changes were observed between one hour flush and end flush according to the survival data. The survival rate was around 100 percent at 96-hour and over 85 percent in 7 days for both 1-hour flush and end flush, while it was less than 90 percent in 96 hours and 70 percent in 7 days for first flush. For the other two events (October 24, 2004 and April 22, 2005) in Figure 48 and Figure 50, these data indicated some toxicity reduction, but these reductions are relatively small.

PSD for Fish Gill Function

Figure 51 shows the particle size distribution (PSD) and incremental particle number distribution (PND) across range from 1 to 250 μm for runoff samples before 60 minutes quiescent settling. At the beginning of test, there is no significant difference of PSD and PND between samples with fish loading and without fish loading. After 3 hours, the total volume concentrations (TVC) of particles were lower for fish exposed treatment than the values for control without fish. The TVC values were generally increased 6 hours after initiation of the test. After 12 hours, the difference was more significant, especially for the fine particles ranging from 5 to 30 μm. But the PND values showed that a significant difference was found for particles less than 10 μm. Figure 52 and Figure 53 present the PSD and PND change for samples after 60 minutes quiescent settling. There is a slight difference between the treatment with fish loading and control without fish loading according to the PSD results. The PND results showed the only significant difference exists at very fine particles with size range less than 5 μm after 6 hours of initiation of test.

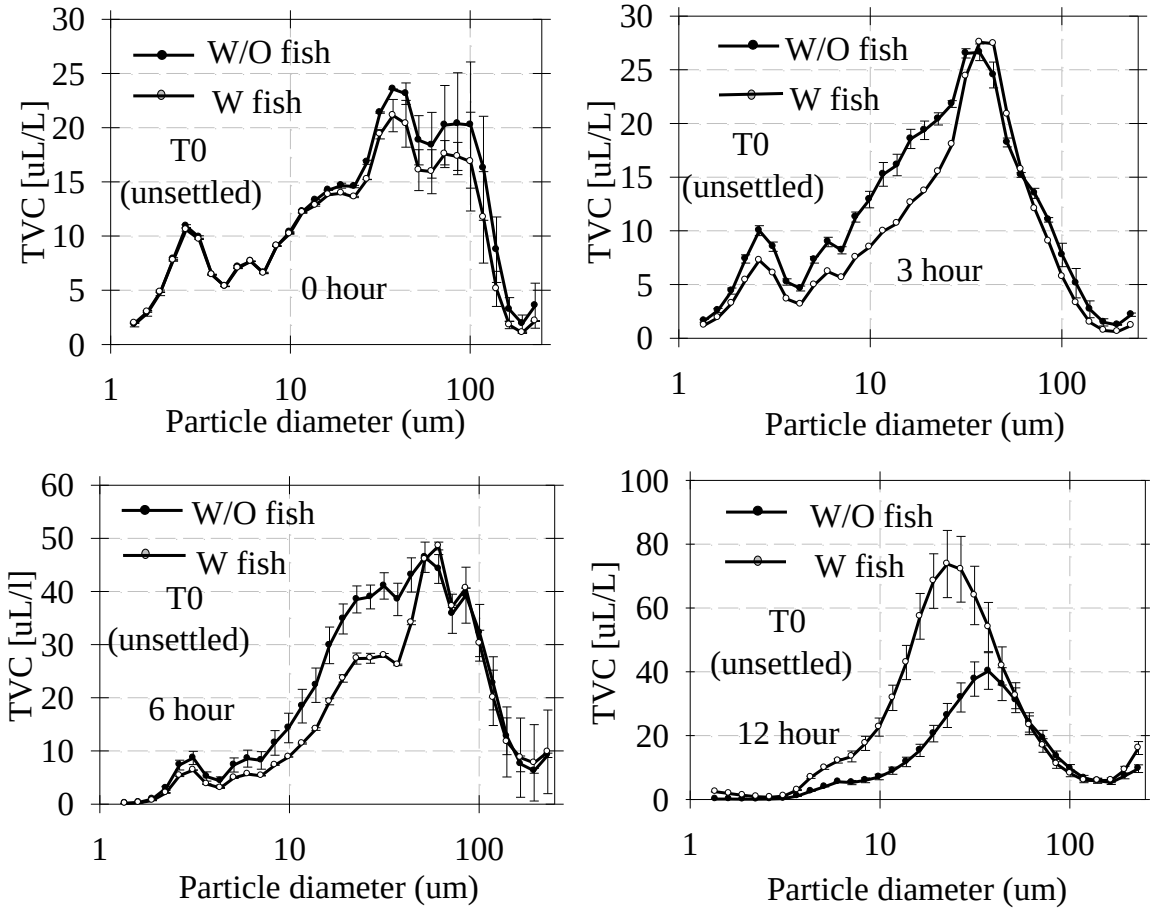

Figure 51

Total volume concentration of particles across the size gradation from 1-250 µms for stormwater runoff before 60 minute quiescent settling

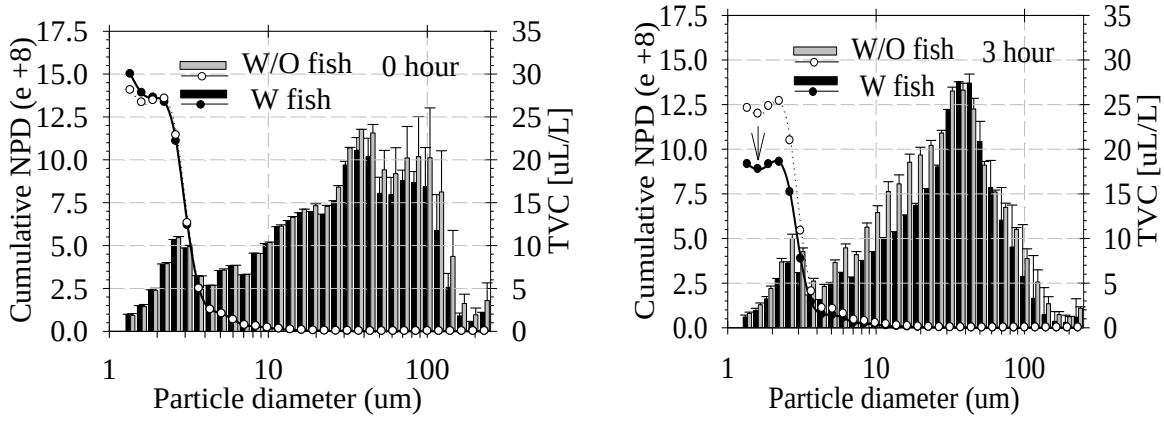

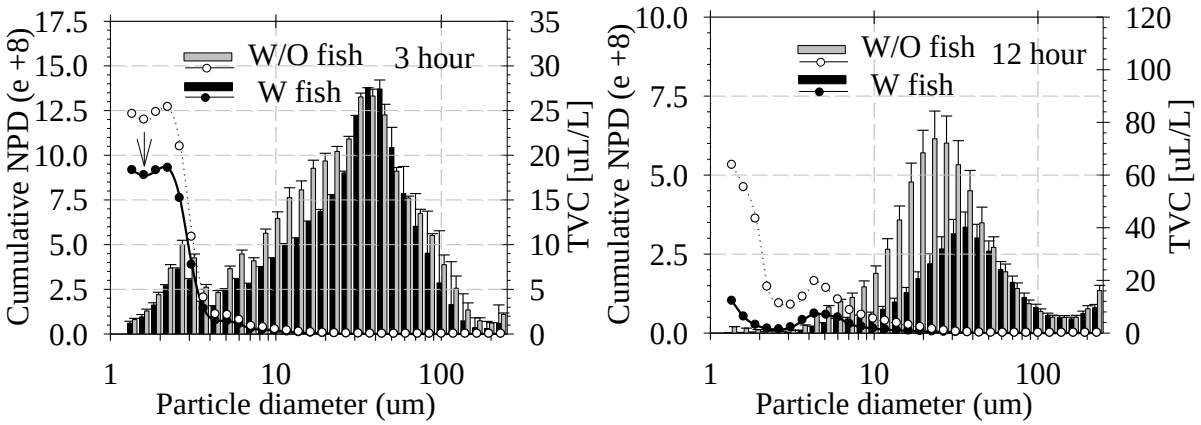

Figure 52

Total volume concentration and cumulative number distribution of particles across the size gradation from 1-250 µms for storm runoff before 60 minutes quiescent settling

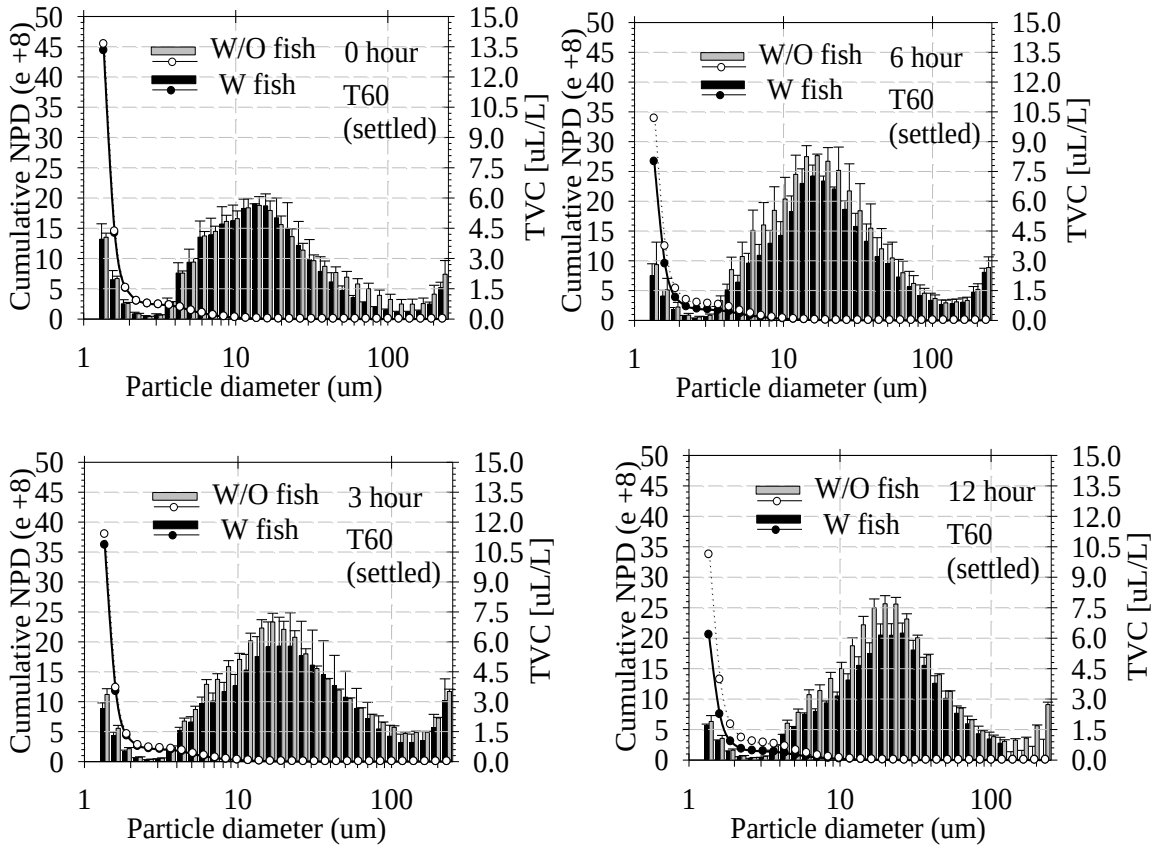

Figure 53

Total volume concentration of particles across the size gradation from 1-250 µms for stormwater runoff after 60 minutes quiescent settling

Oxygen Consumption

Comparison of total weight with corresponding total length of fish provided a good curve-fitting routine in the exponential relationship. In addition to that, a significant correlation was established between fish oxygen consumption rate and total weight of fish of difference sizes under laboratory conditions (dark/light: 12/12, 19-21°C). These results are summarized in Figure 54. Twelve fish with weight range from 0.3 to 0.7 gram were used in this test, and it indicated that smaller fish have the higher oxygen consumption rate (V_{O2}), and all V_{O2} values were from 0.3 to 0.4 $mghr^{-1}g^{-1}$ based on the unit weight of test fish.

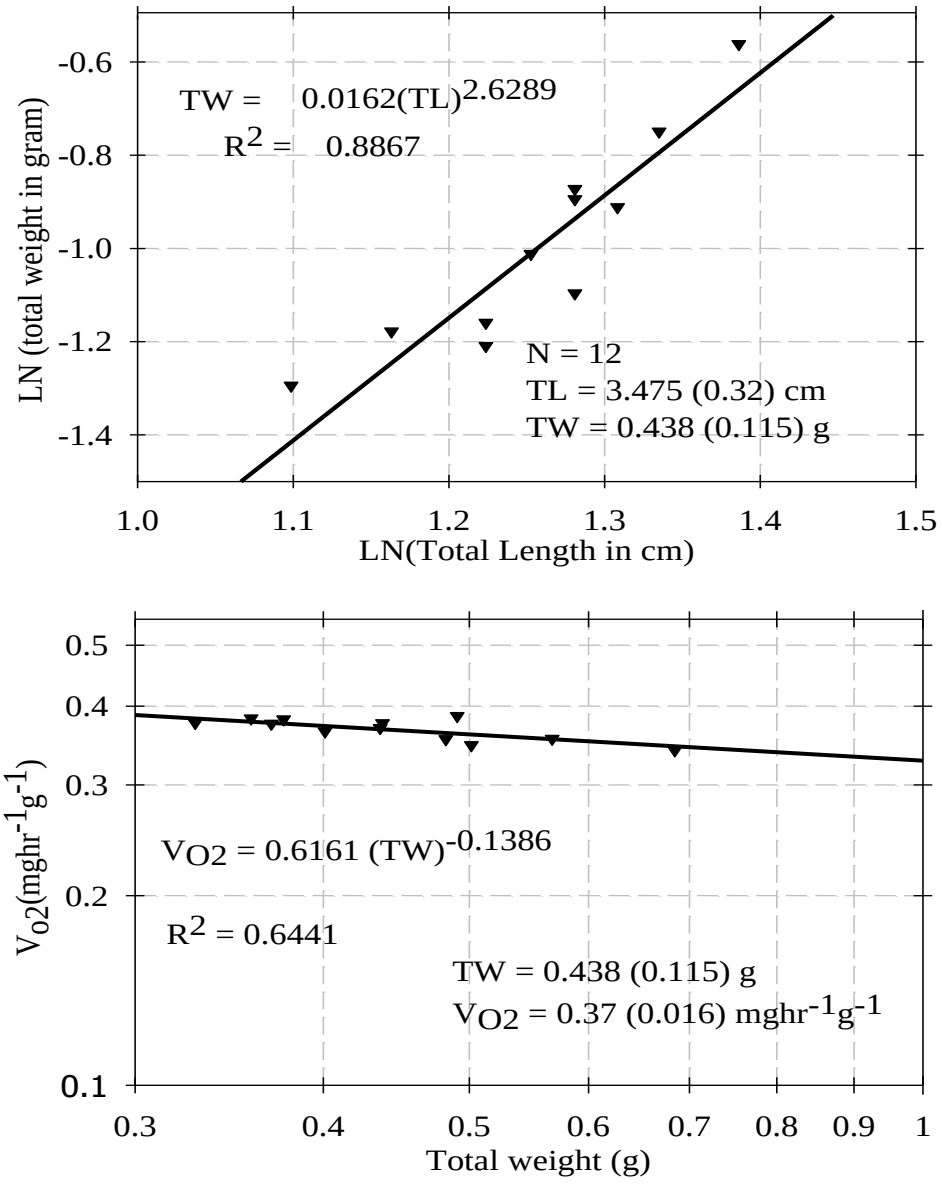

Figure 54

The log linear relationship between the total length and total weight of juvenile fathead minnow (upper plot) and the log linear relationship between oxygen consumption rate based on unit weight of fish exposed and total weight of fish (lower plot)

Figure 55 showed the DO concentration change with time after 24 hours exposure for test solution containing solid (TS = 500 mg/L) with size range less than 25 μm, 53-63 μm, and 75-106 μm, which act as representatives of suspended, settleable, and sediment particles. It is

obvious that the slope for the suspended solids is significantly larger than other two treatments and control. There is no significant difference between sediment solid treatment and control which suggest that larger particles have no sufficiently toxic effect on the gill function. The lethal points in the figure are considered as the lethal DO concentration and bacteria was considered the only oxygen consumer below this point. The higher lethal point suggests the histological change and the increase of energy demand (Grobler et al., 1989).

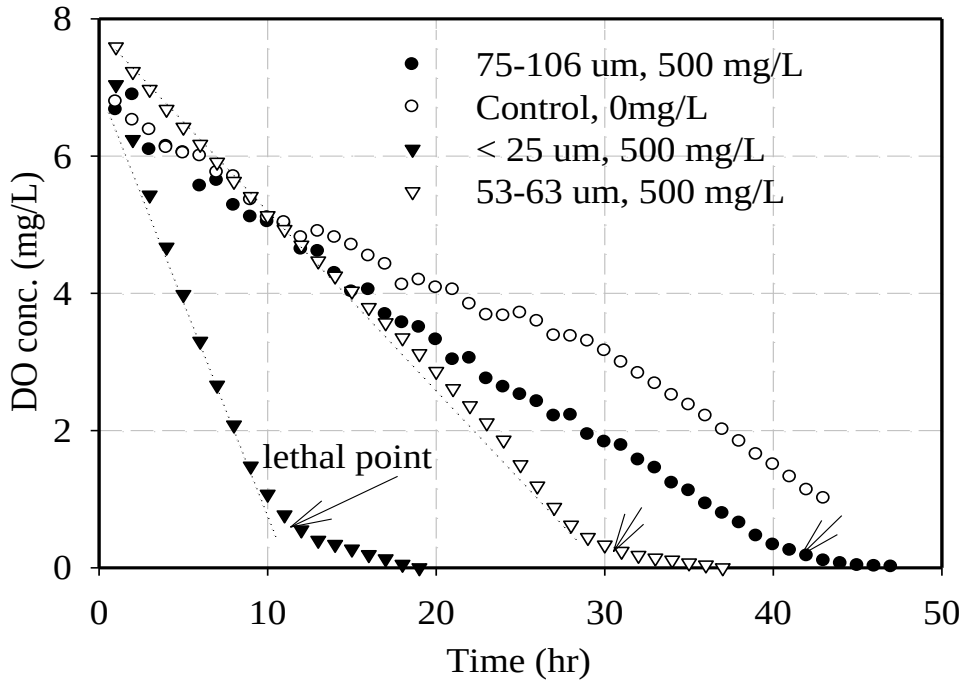

Figure 55
The dissolved oxygen concentration change with time for juvenile fathead minnows exposed in solution with solid concentration at 500mg/L for 24 hours

The oxygen consumption rate based on unit weight test fish could be compared by using the *b* values (slope) in Figure 56 and Figure 57. All the R-square values indicate a goodness of fit for the linear relationship between oxygen consumption and time. From Figure 56, the results show that *b* values are less than 0.4 $mgg^{-1}hr^{-1}$ in 2 hours and they increase in 6 hours. After 6 hours, the recover test *b* values showed there was no significant difference between the test before recover and after recover. From Figure 57, the *b* values show that both unsettled and settled treatments have the higher oxygen consumption rate than control. The ANOVA SAS

output also showed the significant difference ($p < 0.001$), but there is no significant difference between settled and unsettled treatments ($p > 0.05$).

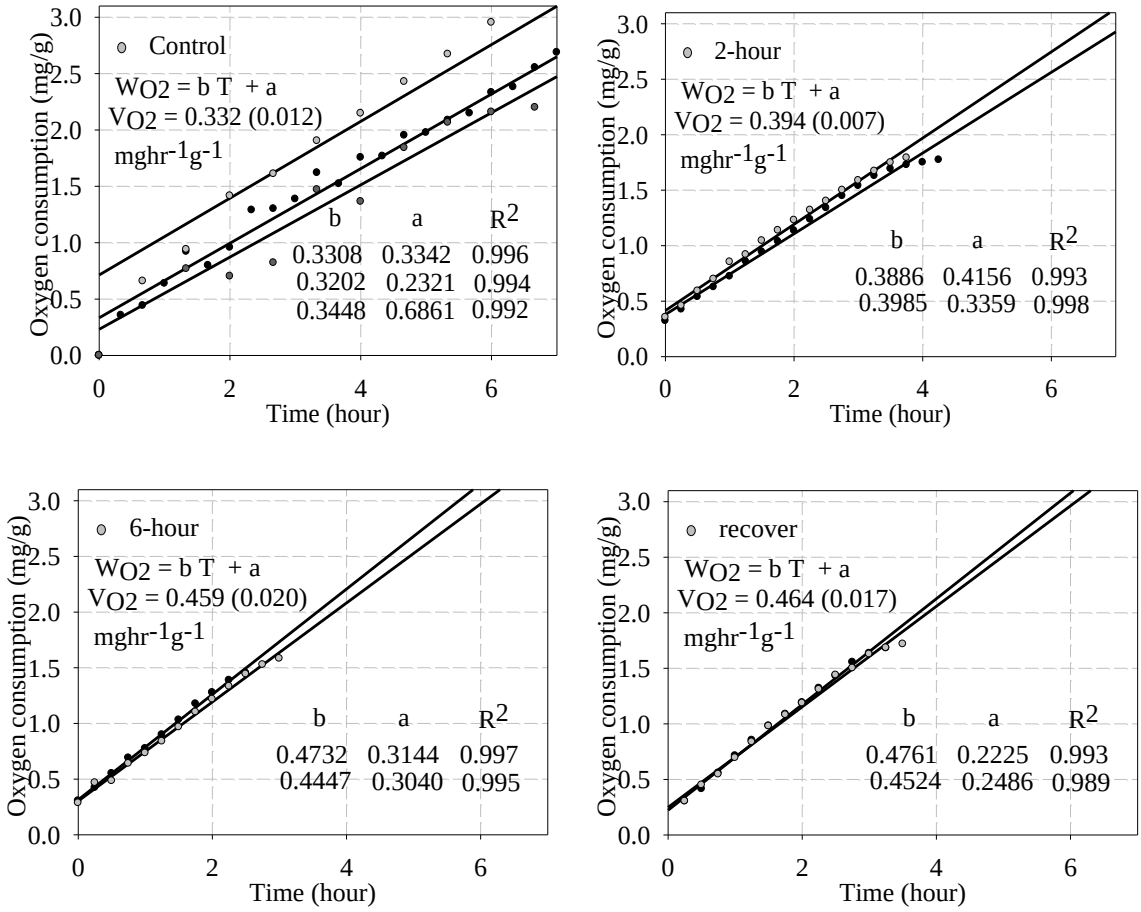

Figure 56

Amount of oxygen consumed based on unit weight of fish change with time after 0, 3, and 6 hours exposure to the composite stormwater runoff samples for October 24, 2004, event

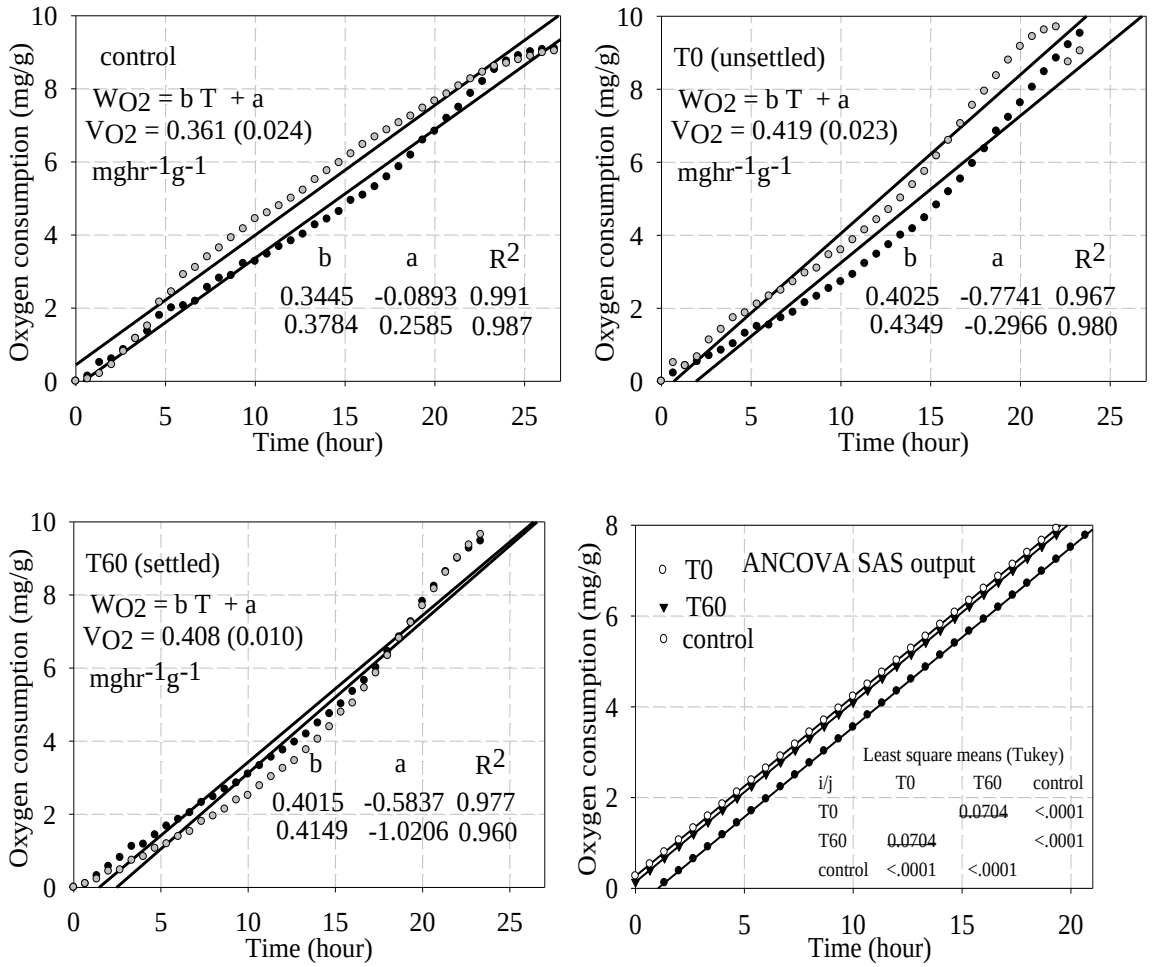

Figure 57

Amount of oxygen consumption based on unit weight of fish change with time after 6 hours exposure to settled and unsettled stormwater runoff samples for October 24, 2004, event

Testing of the Hydrodynamic Separator (HS) "L-Unit"

SSC Removal Efficiency

"L-Unit" SSC removal efficiency results are illustrated graphically in the upper plot of Figure 58 and the same results are summarized in a tabular fashion in Table 22, along with addition mass and turbidity results. "L-Unit" results indicate that SSC removal efficiency decreases with increasing operating flow rate, from 44.7 to 22.3 percent although the decrease is

gradual for a fixed concentration given the wide range of operating flow rates (from 10 to 125 percent of 150 gallons/minute). These results are not unexpected.

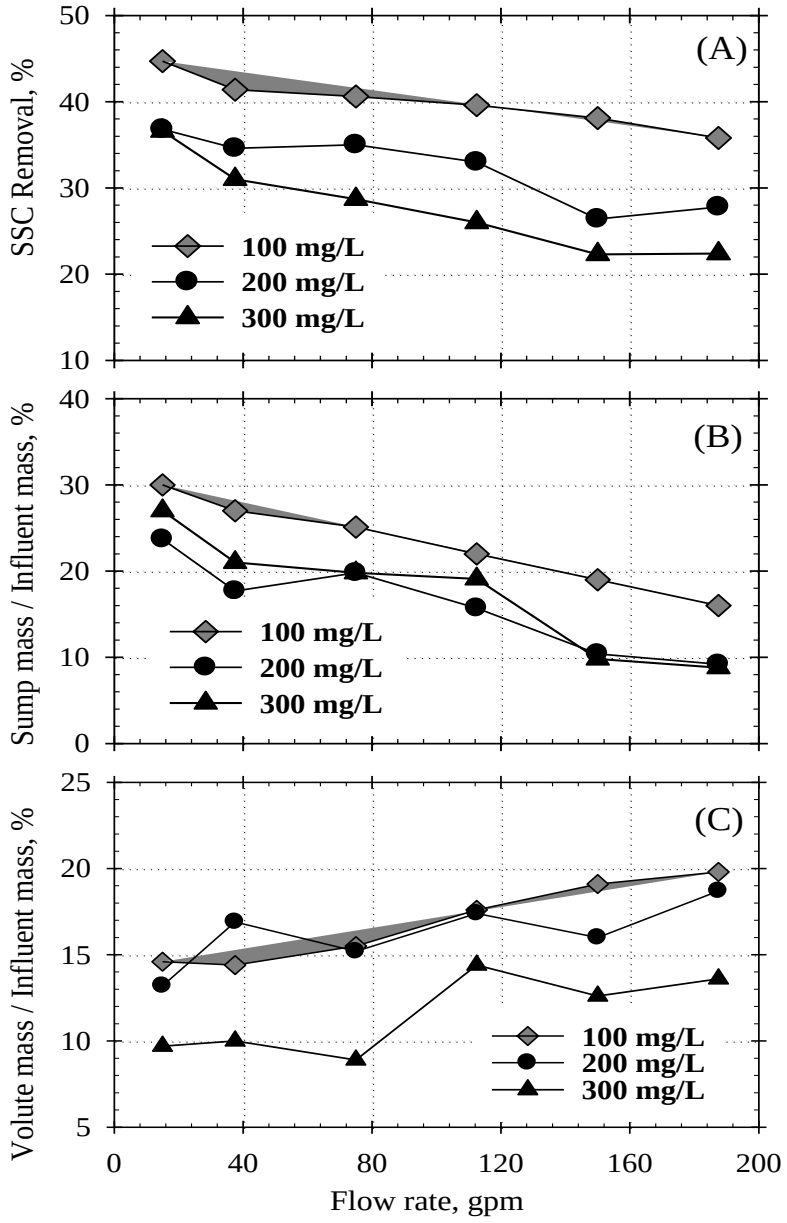

Figure 58

Plots of "L-unit" treatment performance with a 2400 µm screen at a constant flow rate of 25, 50, 75, 100, and 125 percent of the maximum hydraulic operating rate (150-gpm)

Table 22

Summary of treatment run results for HS "L-Unit" with a 2400 µm screen aperture loaded by NJCAT gradation under different SSC and operating flow rates

Run	Influent SSC	Flow rate	Influent mass	Volute mass captured	Volute/ Influent	Sump mass captured	Sump/ Influent	SSC Removal efficiency	Mass balance check	Turbidity Removal
	[mg/L]	[gpm]	[g]	[g]	[%]	[g]	[%]	[%]	[%]	[%]
2	**300**	**75**	1405.7	124.7	8.9	278.8	19.8	28.7	6.3	7.6
3	**200**	**75**	786	119.3	15.2	155.8	19.8	35	10.2	8.9
4	**300**	**37.5**	894.5	89.4	10.0	188.1	21.0	31	10.7	13.6
5	**300**	**112.5**	1037	120.4	11.6	168.3	16.2	27.8	9.1	16.6
6	**200**	**112.5**	801.9	139.2	17.4	125.6	15.7	33	9.6	16.3
7	**200**	**37.5**	818.6	138	16.9	145.2	17.7	34.6	11.5	17.7
8	**100**	**75**	401.7	62.4	15.5	100.7	25.1	40.6	8.7	10.7
9	**300**	**150**	1190	149.6	12.6	116.1	9.8	22.3	7.7	15
10	**200**	**150**	747.1	119.4	16.0	78	10.4	26.4	7.3	13.4
11	**300**	**187.5**	1157.7	157.1	13.6	102.1	8.8	22.4	8.3	13
12	**200**	**187.5**	732.4	136.7	18.7	67.3	9.2	27.8	7.8	12.3
13	**100**	**150**	373.7	71.3	19.1	71	19.0	38.1	10	9.9
14	**100**	**187.5**	388.7	77.1	19.8	62.2	16.0	35.8	9.4	13.9
15	**200**	**15**	597.6	78.6	13.2	141.4	23.7	36.8	7.1	17.5
16	**300**	**15**	1120.9	108.2	9.7	302.1	27.0	36.6	7.1	11.4
17	**100**	**15**	371.1	54.2	14.6	111.5	30.0	44.7	5.3	17.1
35	**100**	**37.5**	447.1	64.4	14.4	120.8	27.0	41.4	10.9	17.7
36	**100**	**112.5**	520.5	91.5	17.6	114.5	22.0	39.6	8.2	11.1
Runs at SSC = 100 mg/L										
17	100	**15**	371.1	54.2	14.6	111.5	30	44.7	5.3	17.1
35	100	**37.5**	447.1	64.4	14.4	120.8	27	41.4	10.9	17.7
8	100	**75**	401.7	62.4	15.5	100.7	25.1	40.6	8.7	10.7
36	100	**112.5**	520.5	91.5	17.6	114.5	22	39.6	8.2	11.1
13	100	**150**	373.7	71.3	19.1	71	19	38.1	10	9.9
14	100	**187.5**	388.7	77.1	19.8	62.2	16	35.8	9.4	13.9
Runs at SSC = 200 mg/L										
15	200	**15**	597.6	78.6	13.2	141.4	23.7	36.8	7.1	17.5
7	200	**37.5**	818.6	138	16.9	145.2	17.7	34.6	11.5	17.7
3	200	**75**	786	119.3	15.2	155.8	19.8	35	10.2	8.9
6	200	**112.5**	801.9	139.2	17.4	125.6	15.7	33	9.6	16.3
10	200	**150**	747.1	119.4	16	78	10.4	26.4	7.3	13.4

(continued)

12	200	**187.5**	732.4	136.7	18.7	67.3	9.2	27.8	7.8	12.3
Runs at SSC = 300 mg/L										
16	300	**15**	1120.9	108.2	9.7	302.1	27	36.6	7.1	11.4
4	300	**37.5**	894.5	89.4	10	188.1	21	31	10.7	13.6
2	300	**75**	1405.7	124.7	8.9	278.8	19.8	28.7	6.3	7.6
5	300	**112.5**	1037	120.4	11.6	168.3	16.2	27.8	9.1	16.6
9	300	**150**	1190	149.6	12.6	116.1	9.8	22.3	7.7	15
11	300	**187.5**	1157.7	157.1	13.6	102.1	8.8	22.4	8.3	13

Results also demonstrated that there was a consistent increase in removal efficiency with decreasing loading concentrations (from 100 to 300 mg/L as SSC). These results were generally consistent for a given operating flow rate. The trend of increasing removal efficiency with decreasing concentration is likely due to cleaning the unit after every run to ensure that no scour occurred. If the unit was not cleaned after each event, scour would result in deteriorating effluent conditions. Selected testing of a 1200-μm screen in the "L-Unit" for these three loading concentrations suggest similar trends may be realized for a 1200-μm screen. However, it remains to be seen whether a similar trend would occur for different combinations of granulometry, loadings and system parameters, and geometrics.

As summarized in the lower two plots of Figure 58, the relative mass of particles (with respect to the influent) captured in the sump decreased with increasing operating flow rate, while the relative mass of particles (with respect to the influent) captured by the volute chamber increased with increasing flow rate. However the increasing trap efficiency exhibited by the volute section did not offset the decreasing trap efficiency exhibited by the sump section. While trends exhibited some variability, results were consistent for each of the concentration levels.

Particle Size Gradations

Figure 59 to Figure 77 illustrate particle size distributions PSDs or gradations (and mass) for influent, effluent, and captured volute and sump particles. Influent PSDs were kept constant for each run. While there is some variability in the captured PSDs trends, it is instructive to compare the sump and volute PSDs of the 10 percent operating flow rate to those of the 125 percent operating flow rate. The PSDs of the 10 percent operating flow rate were significantly finer than those of the 125 percent operating flow rate. PSD results as a

function of operating flow rate were generally consistent at each concentration level. Volute PSDs were consistently finer than sump PSDs at a given operating flow rate. These PSD results were also consistent at each concentration level.

Washout Tests

Finally, the potential for re-suspension and washout of trapped particles is a major weakness for screened HS units and this was examined at the maximum operating flow rate. The trapped solids levels were at a 50 percent and 100 percent of the "L-Unit" sump capacity. For the 100 percent trapped solids level, results indicate that with a SSC influent level of approximately 0 (clean tap water) the washout run resulted in an effluent SSC level of 540-mg/L with a standard deviation of 21-mg/L. The 50 percent trapped solids level results indicated that with a SSC influent level of approximately 0 (clean tap water) the washout run resulted in an effluent SSC level of 376-mg/L with a standard deviation of 11-mg/L. Results suggest frequent clean-out schedules and procedures as well as captured solids sump design (shear/baffle plates and geometry) and capacity can be critical factors to ensure that solids trapped are not washed from the system.

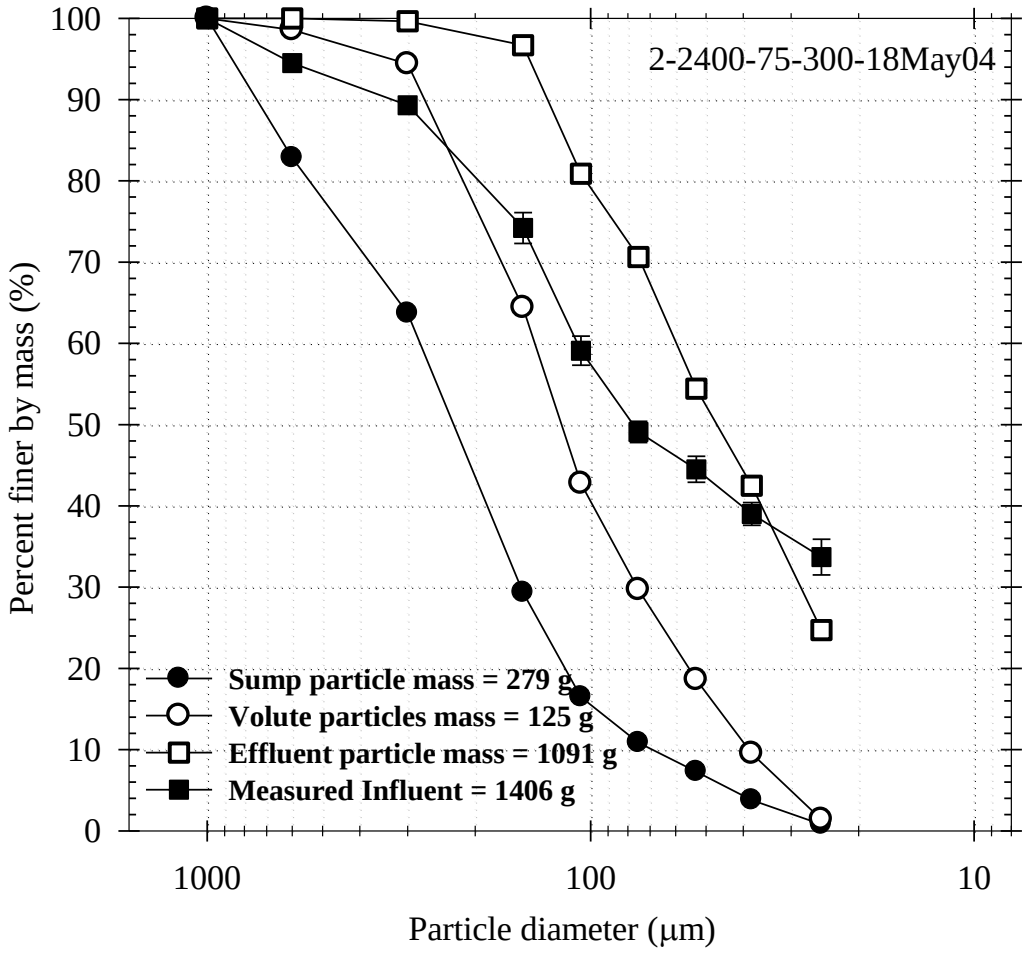

Figure 59

Influent and effluent particle gradations for run 2 (May 18, 2004) with a 2400 μm screen at 75-gpm flow (50% of "L-unit" capacity) for an influent concentration of 300 mg/L

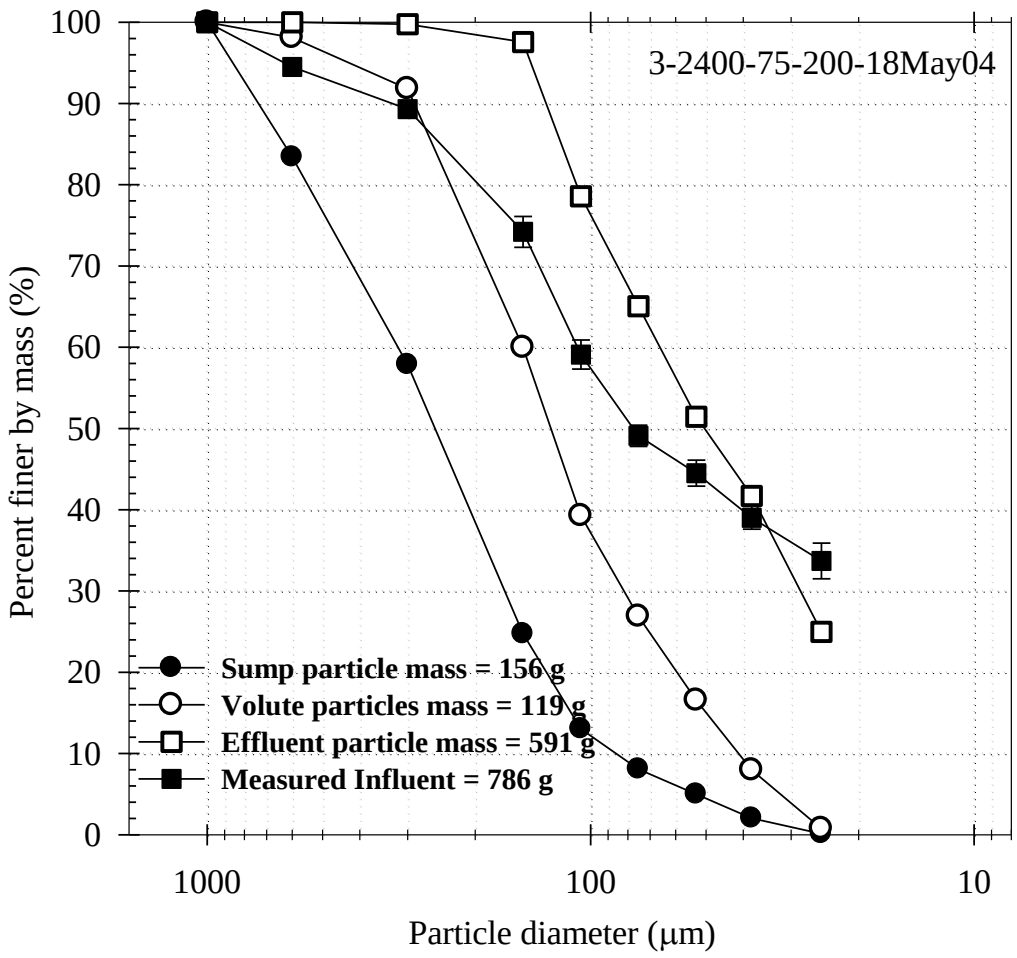

Figure 60

Influent and effluent particle gradations for run 3 (May 18, 2004) with a 2400 μm screen at 75-gpm flow (50% of "L-unit" capacity) for an influent concentration of 200 mg/L

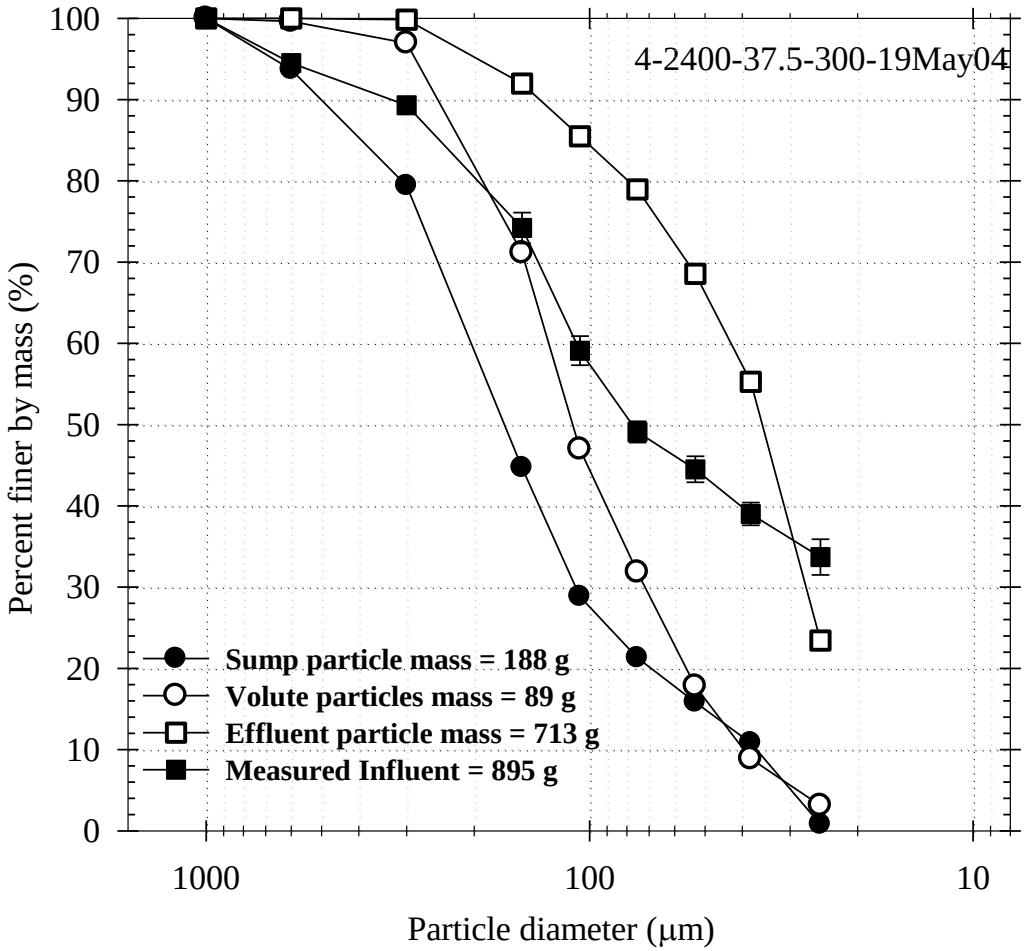

Figure 61
Influent and effluent particle gradations for run 4 (May 19, 2004) with a 2400 μm screen at 37.5-gpm flow (25% of "L-unit" capacity) for an influent concentration of 300 mg/L

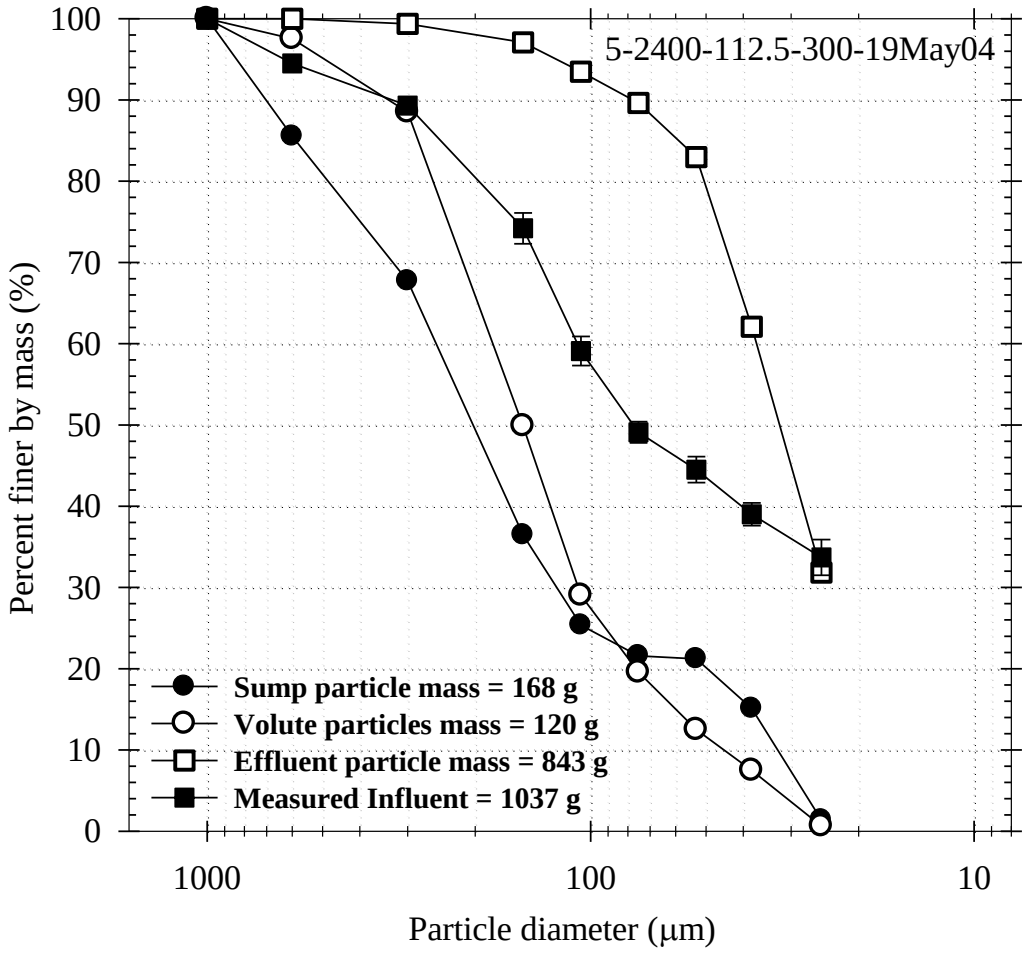

Figure 62

Influent and effluent particle gradations for run 5 (May 19, 2004) with a 2400 μm screen at 112.5-gpm flow (75% of "L-unit" capacity) for an influent concentration of 300mg/L

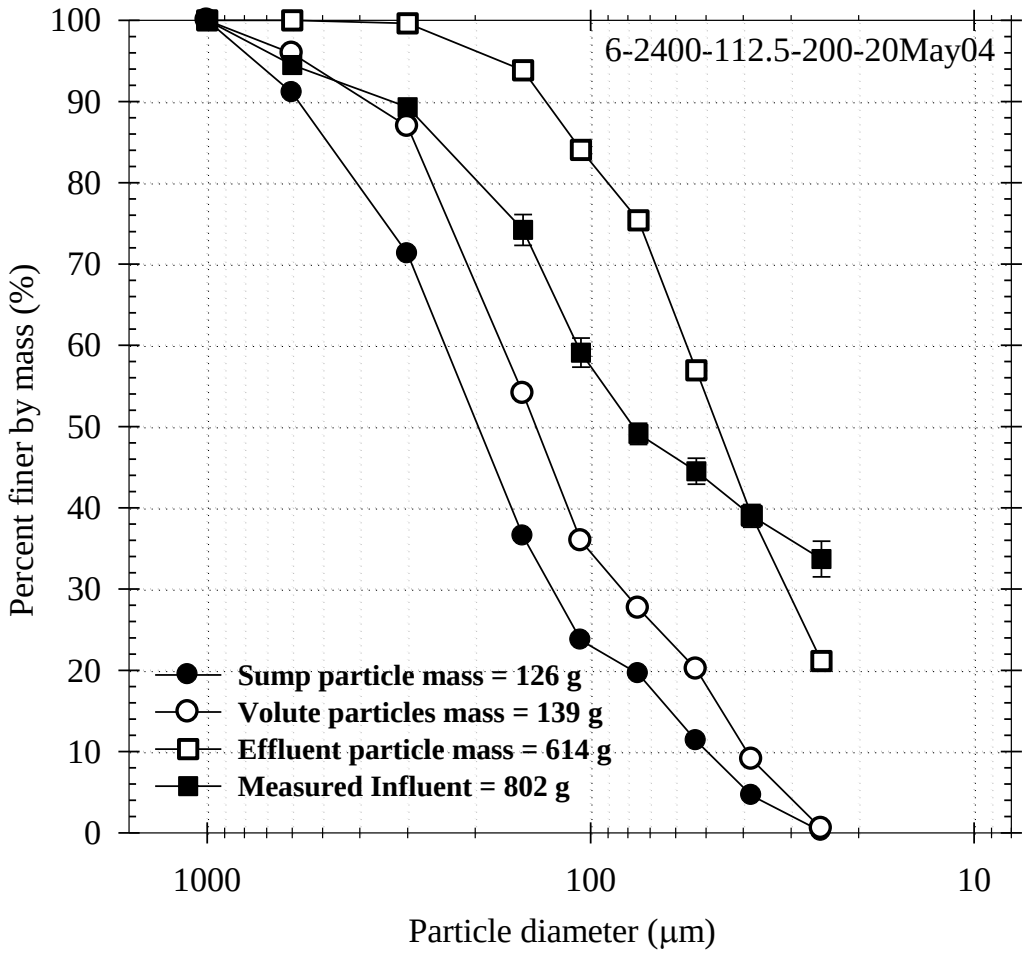

Figure 63

Influent and effluent particle gradations for run 6 (May 20, 2004) with a 2400 μm screen at 112.5-gpm flow (75% of "L-unit" capacity) for an influent concentration of 200 mg/L

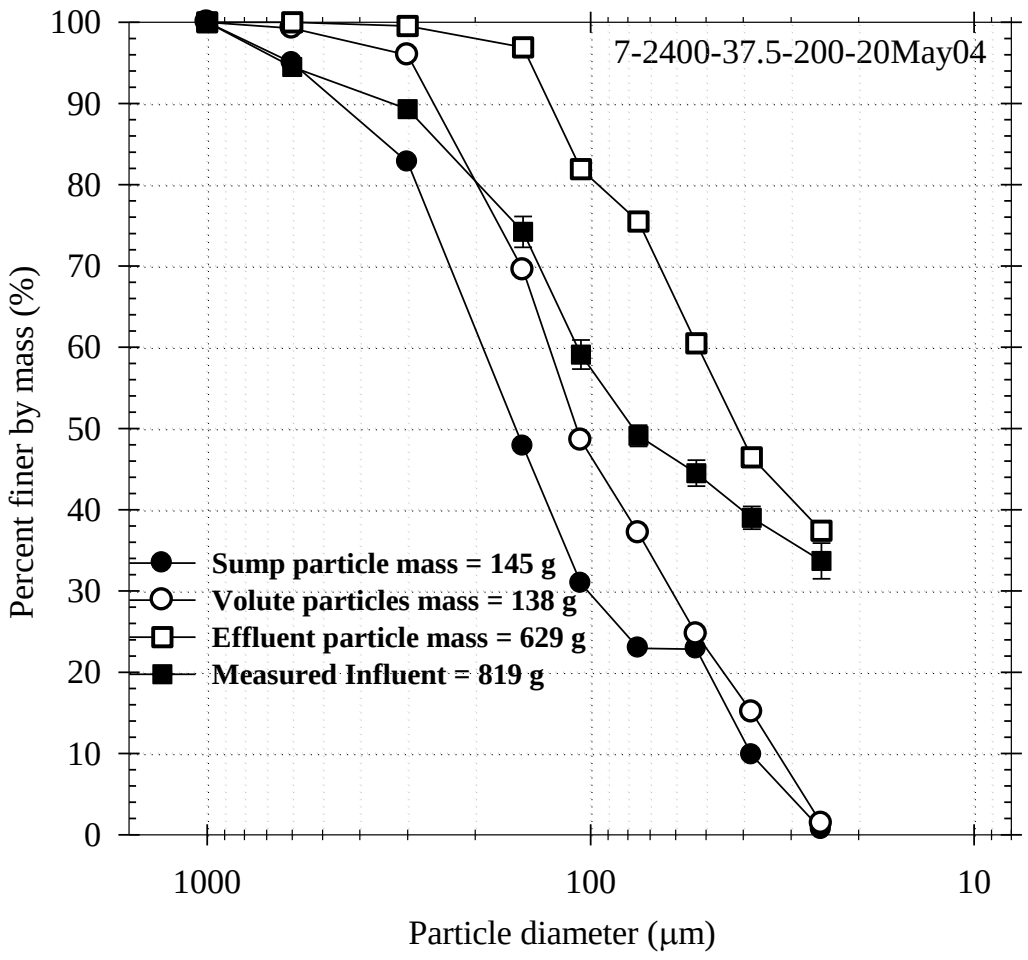

Figure 64

Influent and effluent particle gradations for run 7 (May 20, 2004) with a 2400 μm screen at 37.5-gpm flow (25% of "L-unit" capacity) for an influent concentration of 200 mg/L

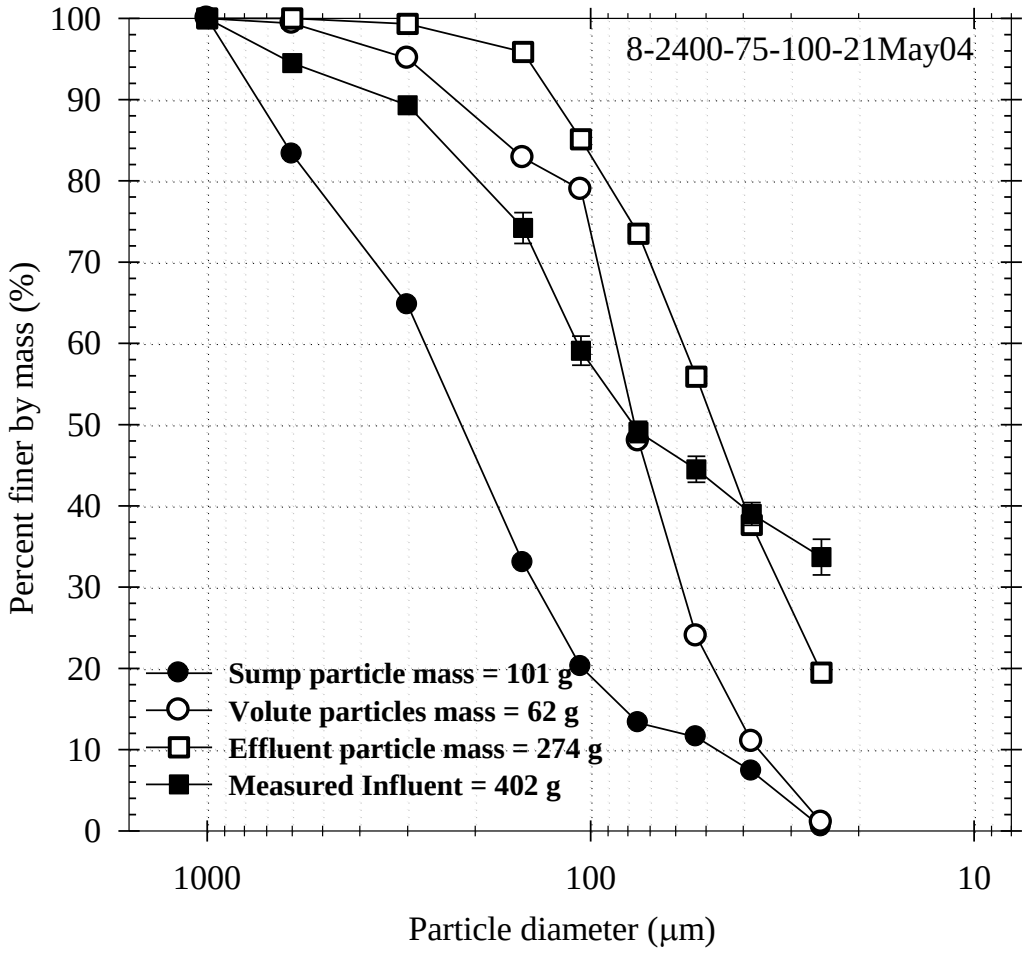

Figure 65

Influent and effluent particle gradations for run 8 (May 21, 2004) with a 2400 μm screen at 75-gpm (50% of "L-unit" capacity) for an influent concentration of 100 mg/L

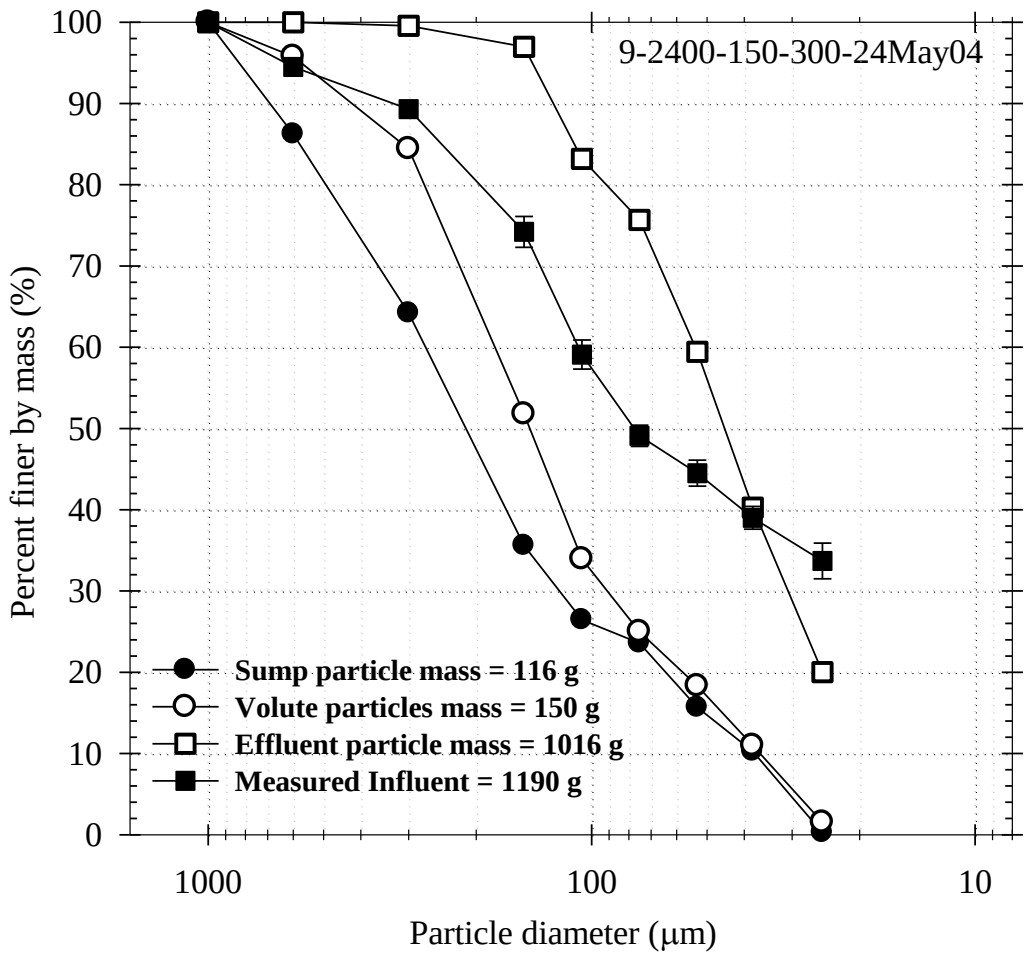

Figure 66

Influent and effluent particle gradations for run 9 (May 24, 2004) with a 2400 μm screen at 150-gpm flow (100% of "L-unit" capacity) for an influent concentration of 300 mg/L

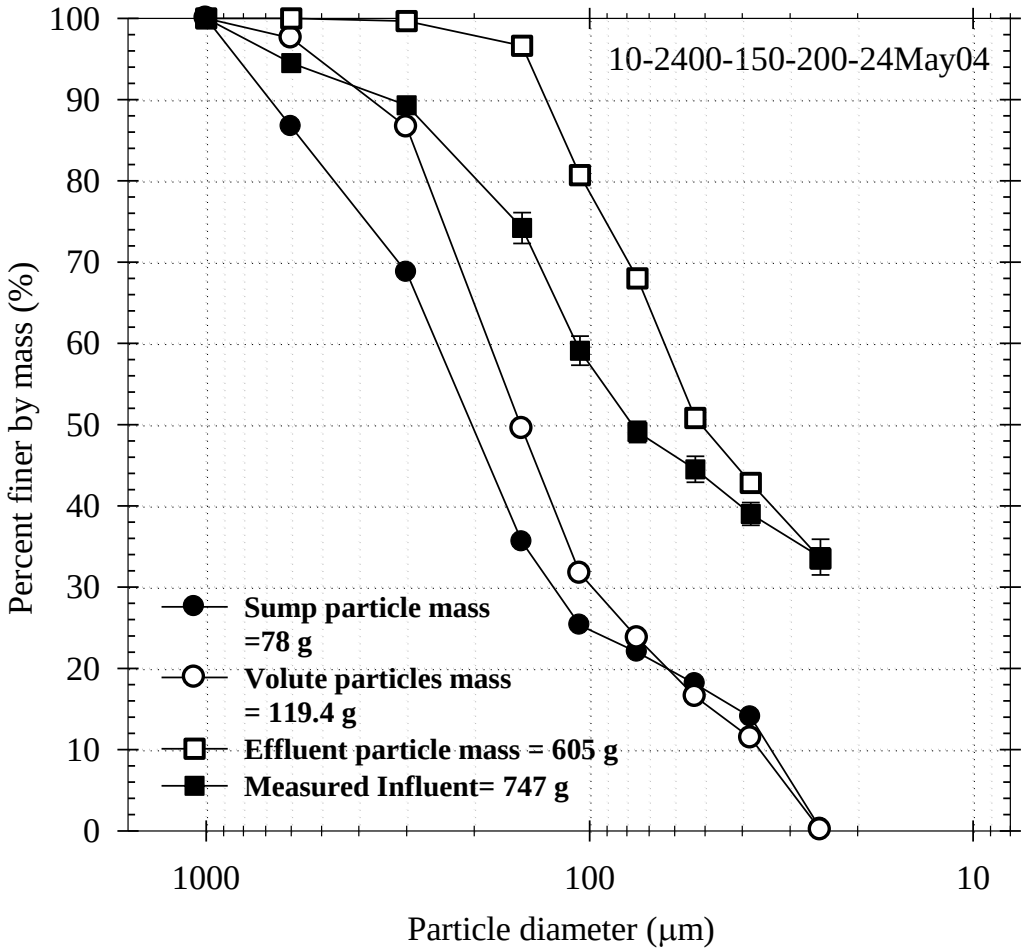

Figure 67

Influent and effluent particle gradations for run 10 (May 24, 2004) with a 2400 μm screen at 150-gpm flow (100% of "L-unit" capacity) for an influent concentration of 200 mg/L

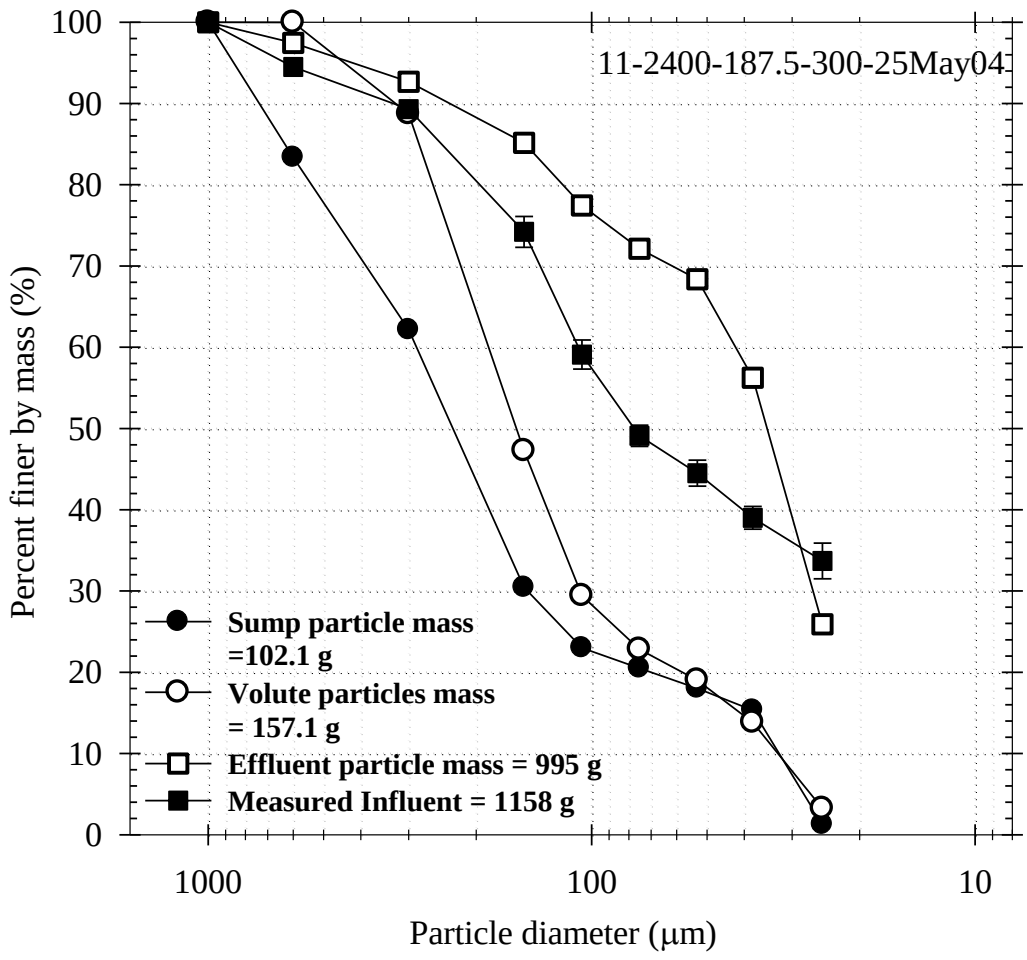

Figure 68

Influent and effluent particle gradations for run 11 (May 25, 2004) with a 2400 μm screen at 187.5-gpm flow (125% of "L-unit" capacity) for an influent concentration of 300 mg/L

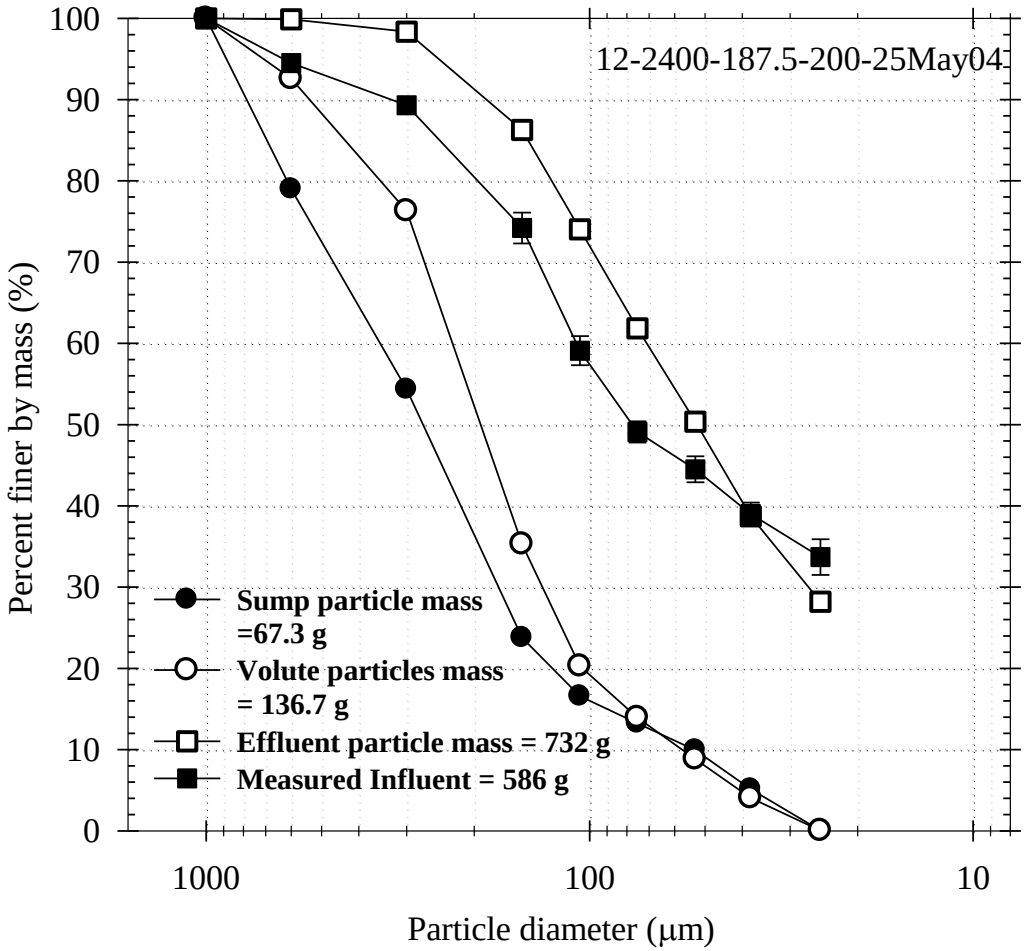

Figure 69

Influent and effluent particle gradations for run 12 (May 25, 2004) with a 2400 μm screen, at 187.5-gpm flow (125% of "L-unit" capacity) for an influent concentration of 200 mg/L

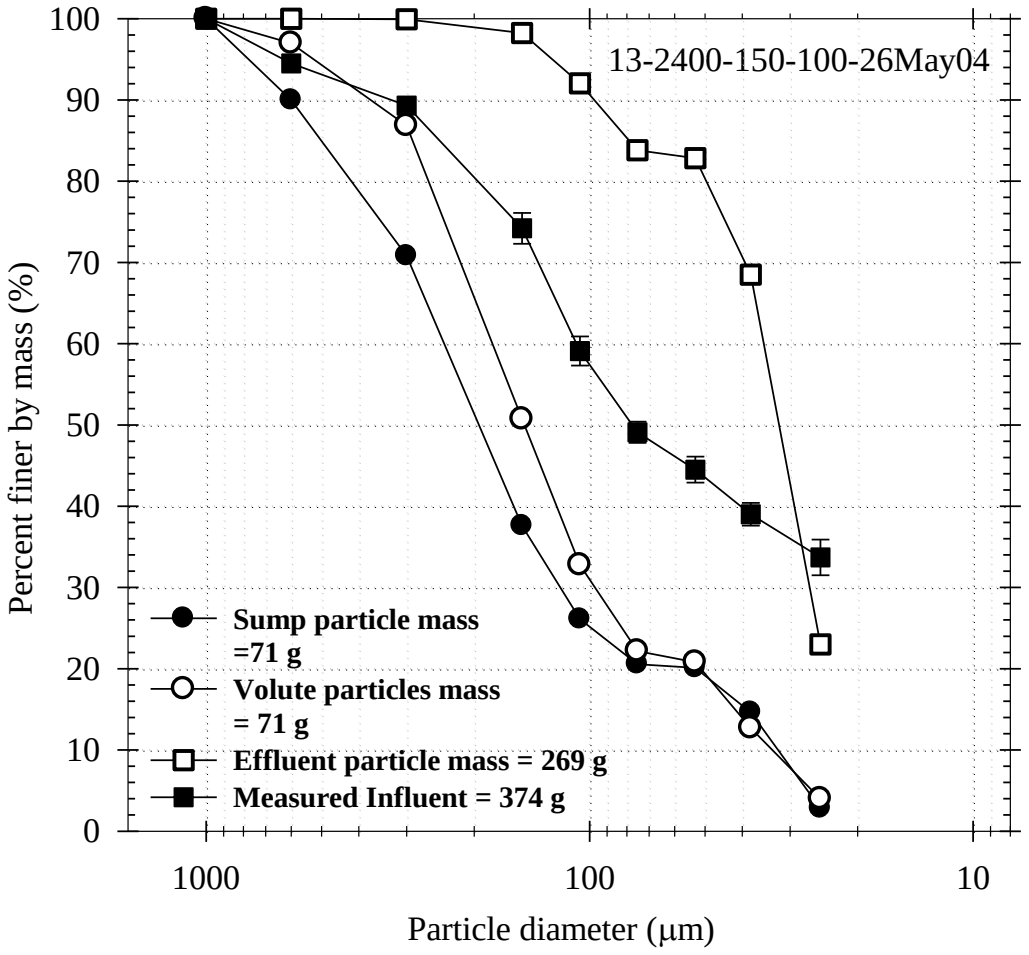

Figure 70

Influent and effluent particle gradations for run (May 26, 2004) with a 2400 μm screen at 150-gpm flow (100% of "L-unit" capacity) for an influent concentration of 100 mg/L

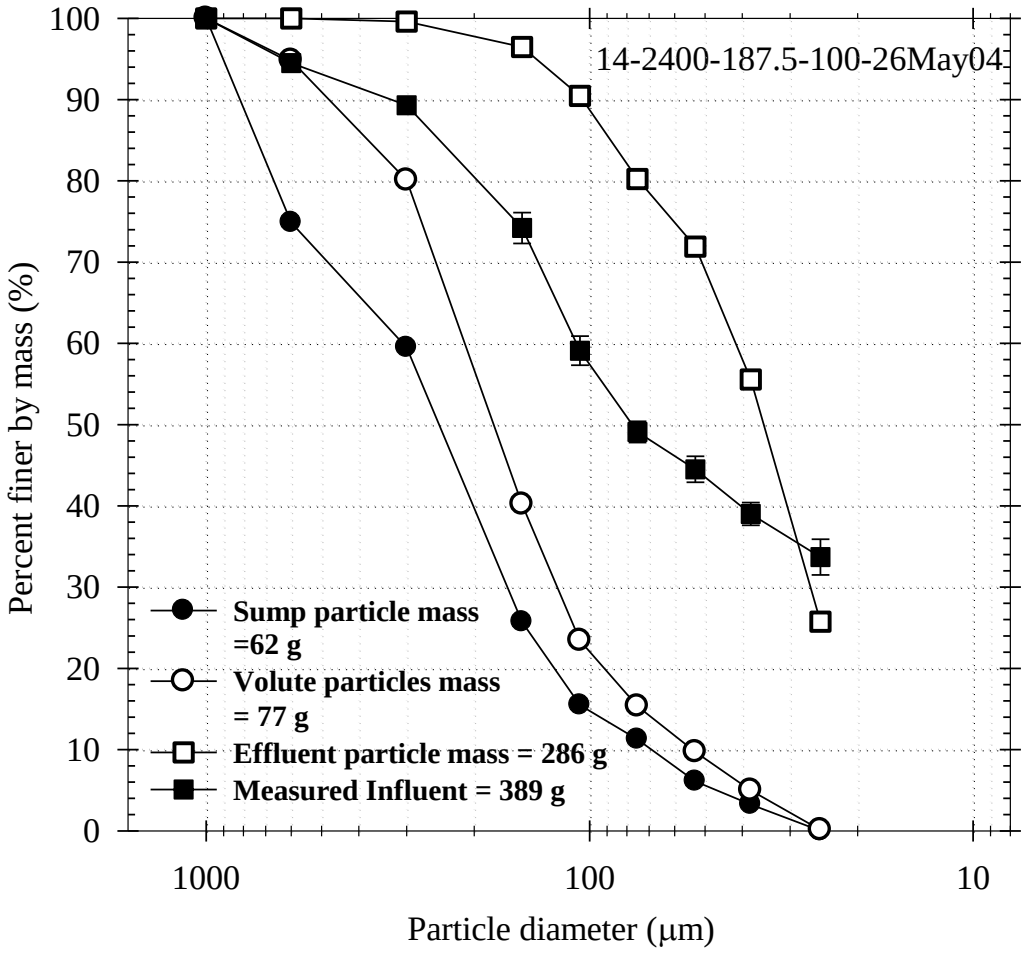

Figure 71

Influent and effluent particle gradations for run 14 (May 26, 2004) with a 2400 μm screen at 187.5-gpm flow (125% of "L-unit" capacity) for an influent concentration of 100 mg/L

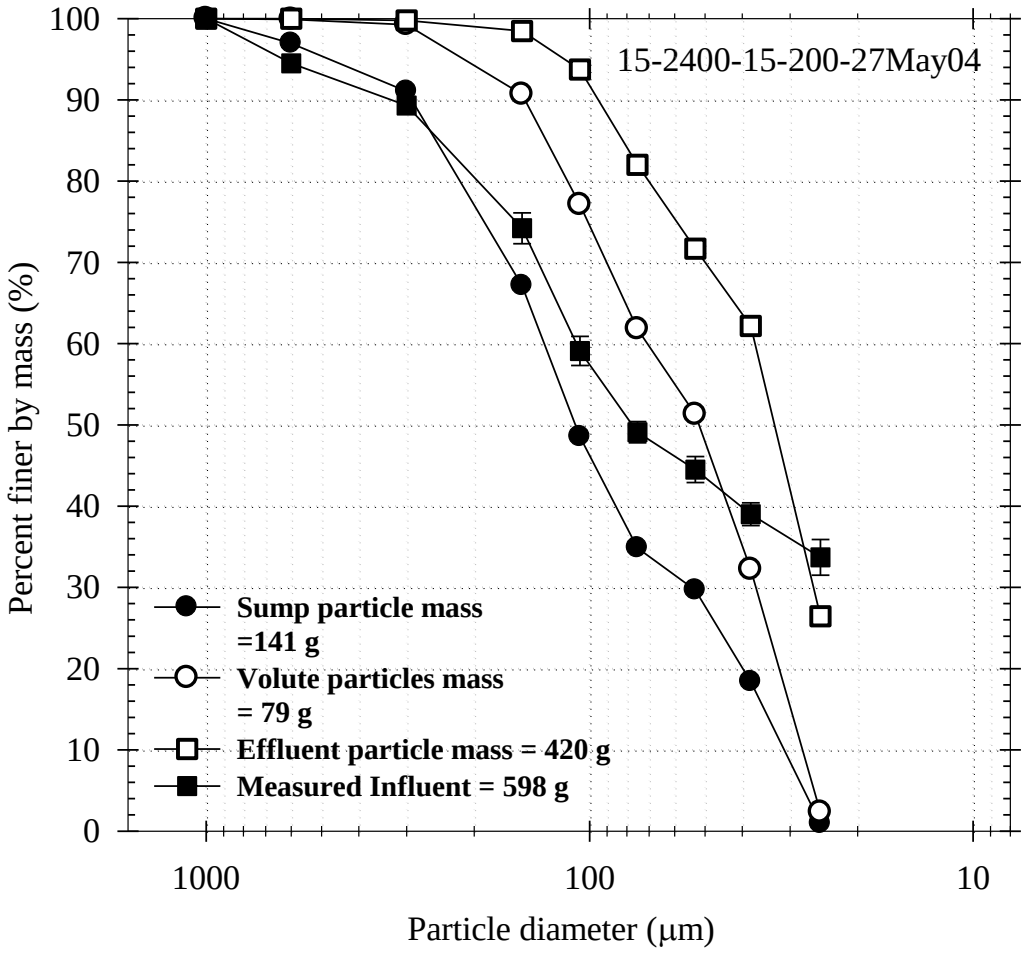

Figure 72

Influent and effluent particle gradations run 15 (May 27, 2004) with a 2400 μm screen at 15-gpm flow (10% of "L-unit" capacity) for an influent concentration of 200 mg/L

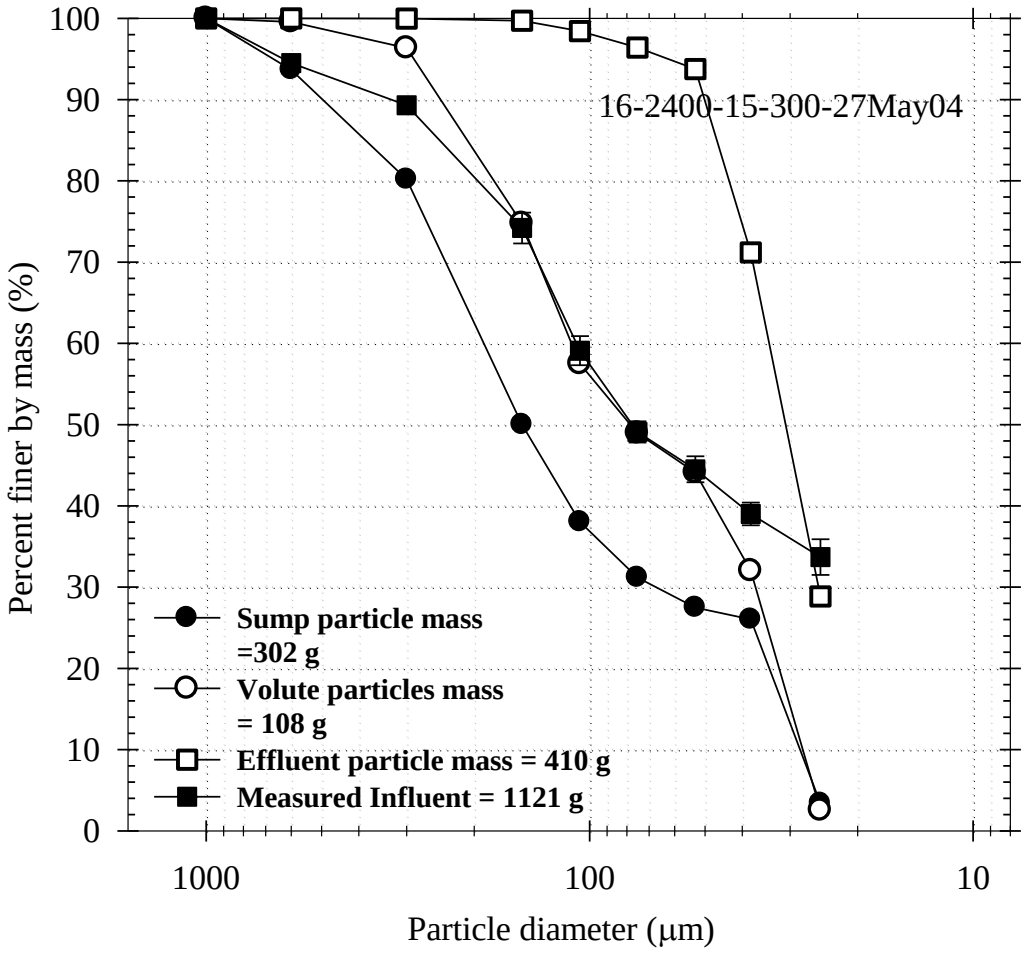

Figure 73

Influent and effluent particle gradations run 16 (May 27, 2004) with a 2400 μm screen at 15-gpm (10% of "L-unit" capacity) for an influent concentration of 300 mg/L

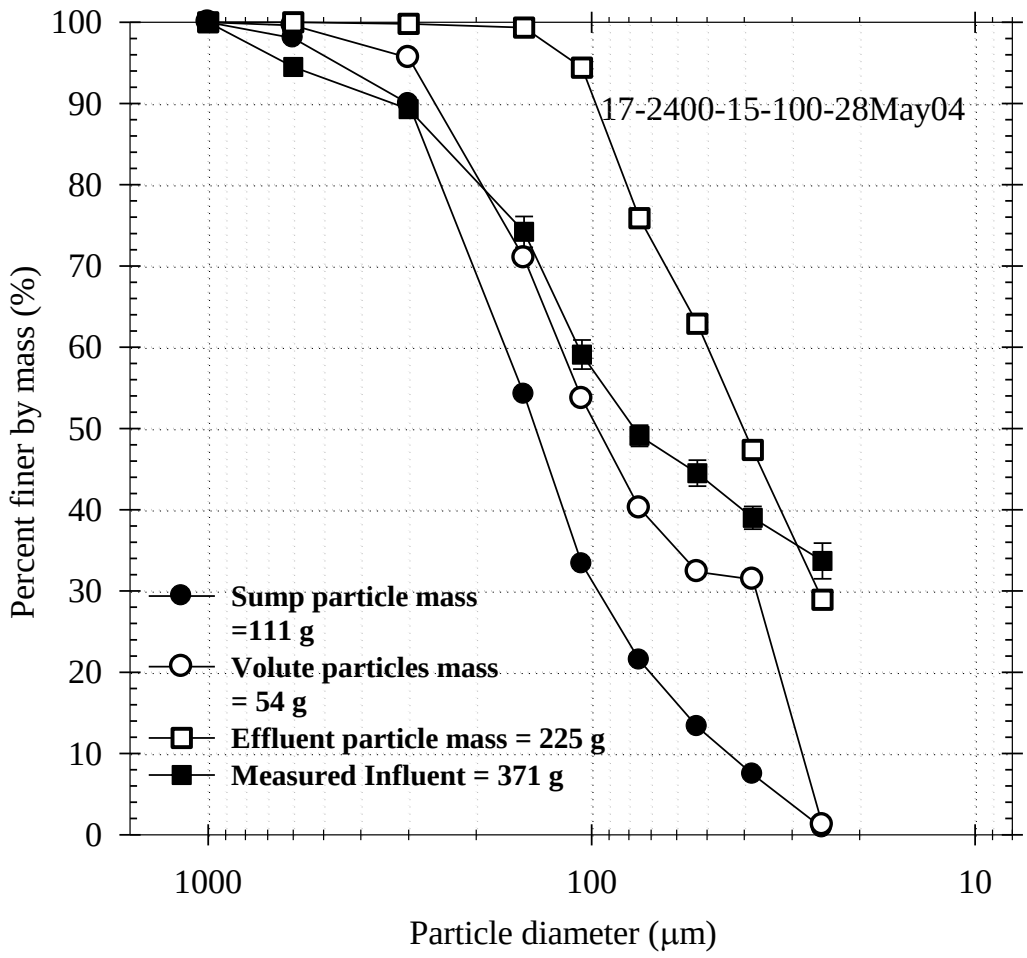

Figure 74

Influent and effluent particle gradations for run 17 (May 27, 2004) with a 2400 μm screen at 15-gpm flow (10% of "L-unit" capacity) for an influent concentration of 100 mg/L

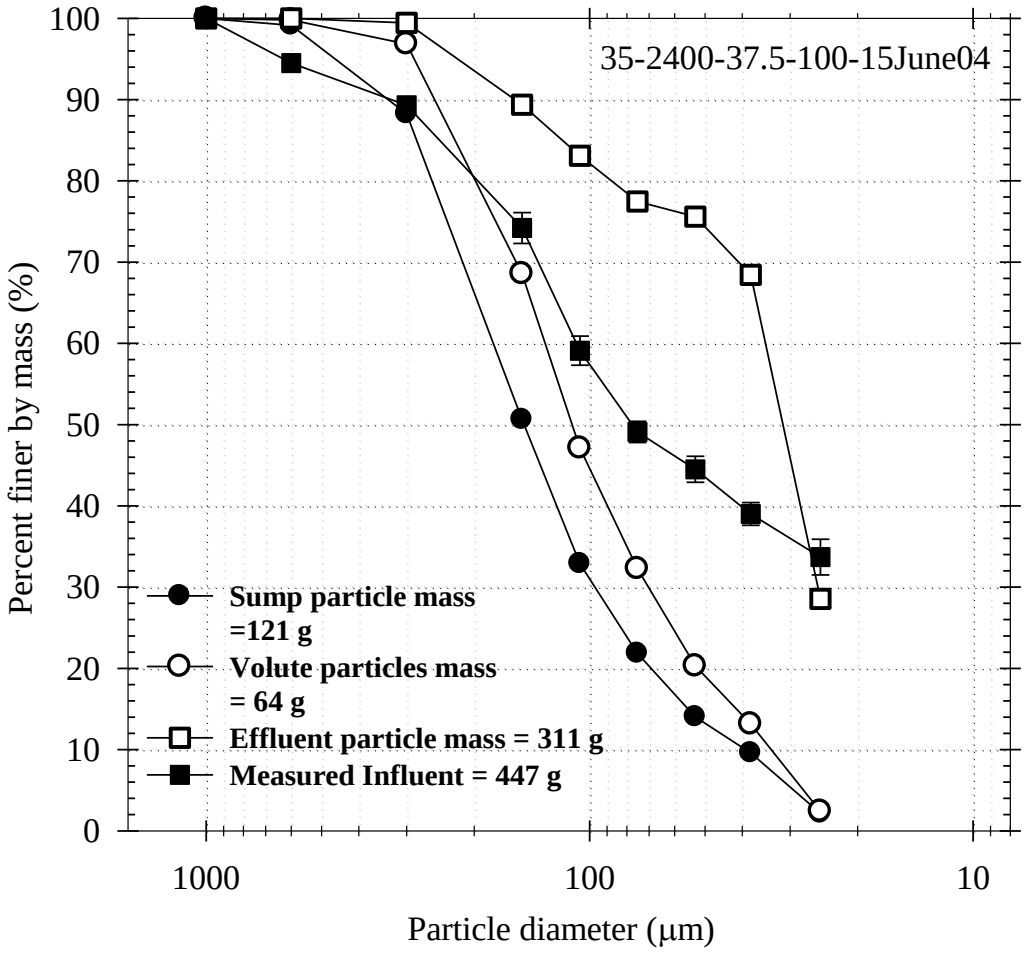

Figure 75

Influent and effluent particle gradations for run 35 (June 15, 2004) with a 2400 μm screen at 37.5-gpm flow (25% of "L-unit" capacity) for an influent concentration of 100 mg/L

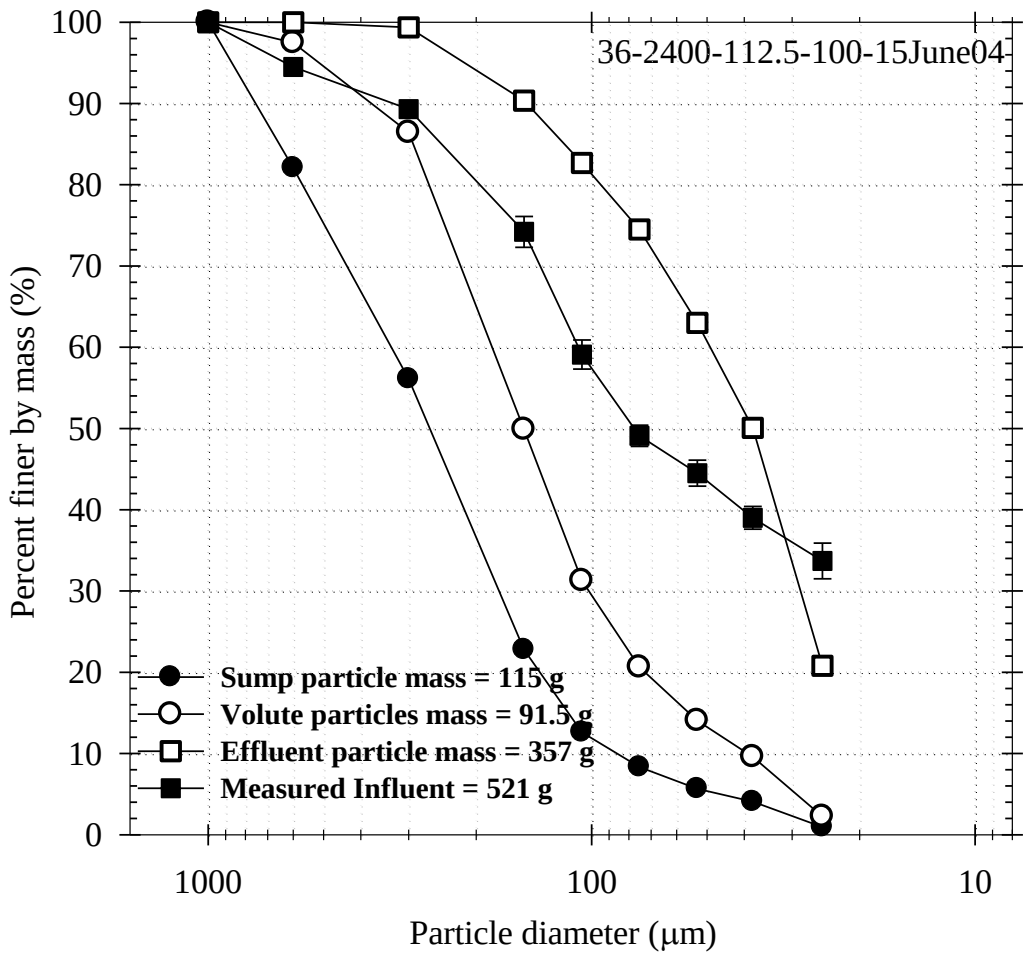

Figure 76

Influent and effluent particle gradations for run 36 (June 15, 2004) with a 2400 μm screen at 112.5-gpm flow (75% of "L-unit" capacity) for an influent concentration of 100 mg/L

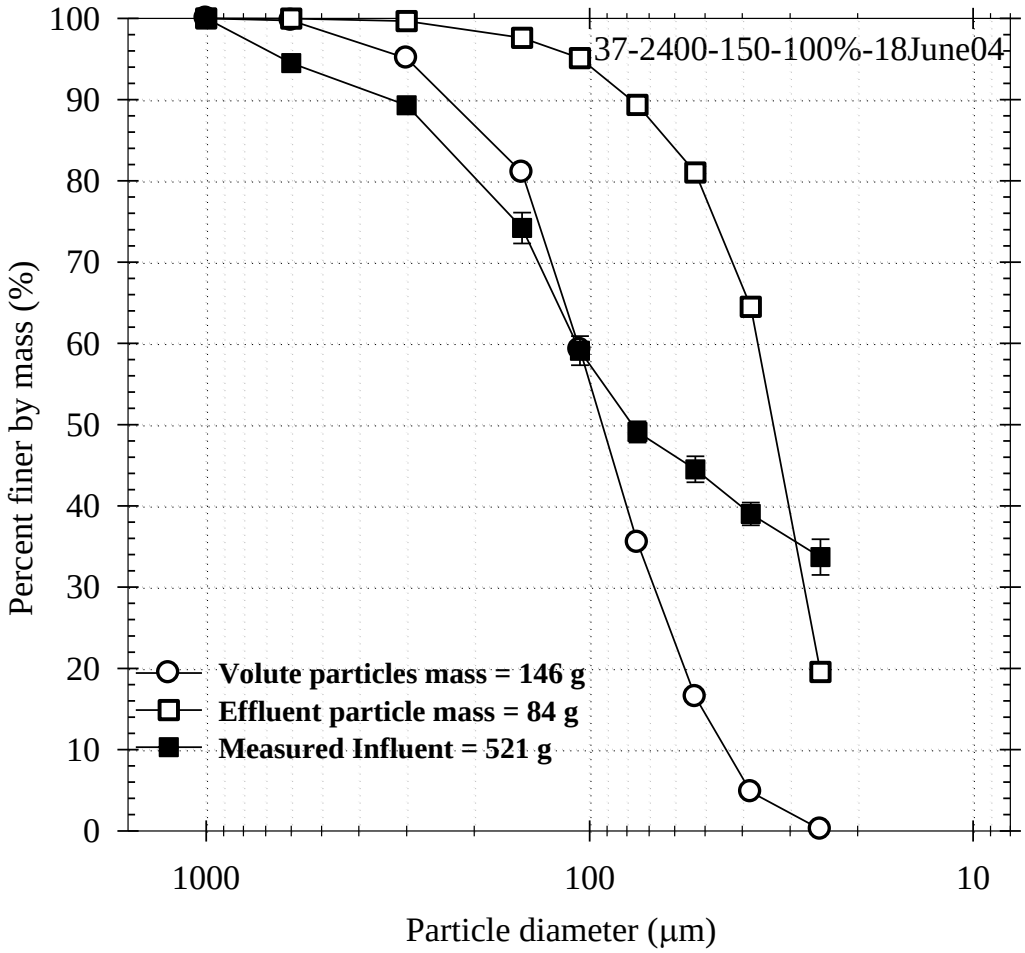

Figure 77

Washout run. Influent and effluent particle gradations for run 37 (June 18, 2004) with a 2400 μm screen at 150-gpm flow (100% of "L-unit" flow capacity) for an initial sediment loading at 100% of unit's solids capture capacity

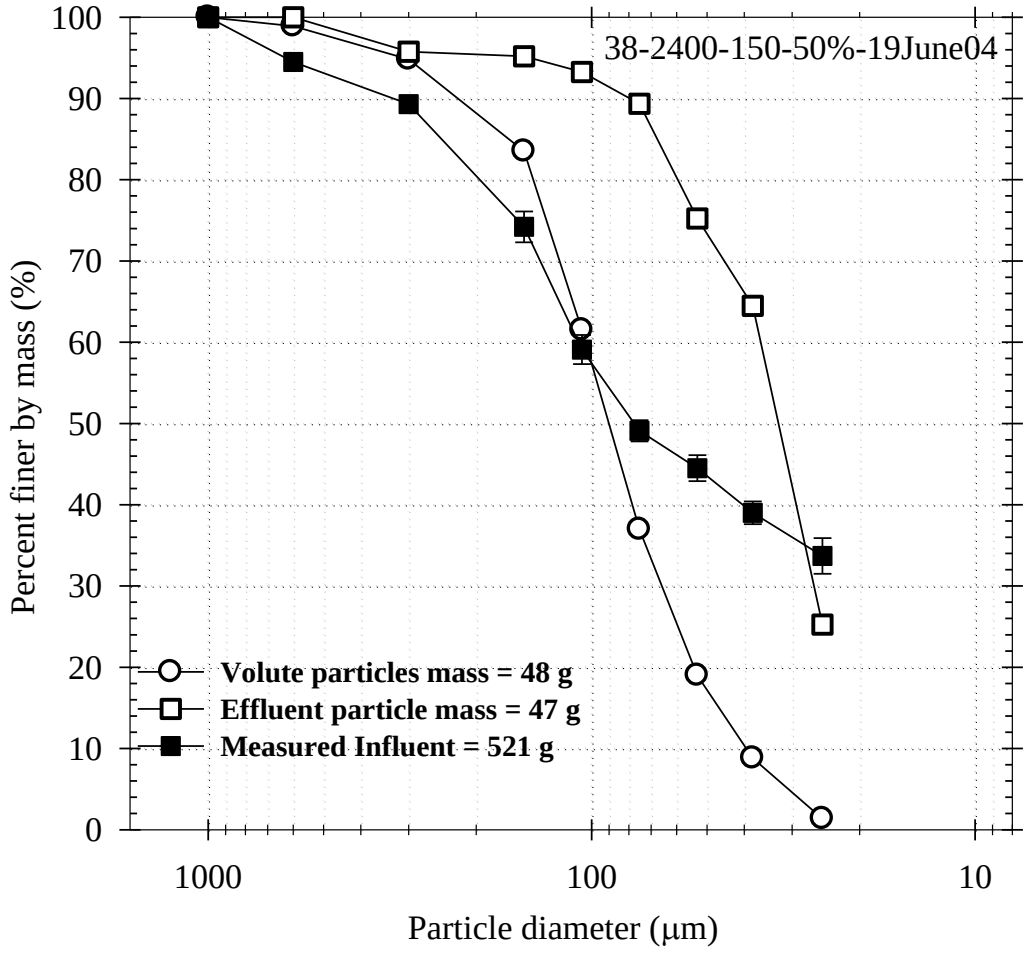

Figure 78

Washout run. Influent and effluent particle gradations for run 38 (June 19, 2004) with a 2400 μm screen at 150-gpm flow (100% of "L-unit" flow rate capacity) for an initial sediment loading at 50% of unit's solid capture capacity

Testing of the Hydrodynamic Separator (HS) PMSU20_20

SSC Removal Efficiency

A series of performance tests for a PMSU20_20 loaded by an NJCAT gradation over a range of flow rates were conducted at the Baton Rouge testing facility. The unit was cleaned after every run to eliminate the problem of scour from the unit. Experimental design parameters for the non-cohesive sandy-silt gradation of particles included influent particle concentration (100 mg/L, 200 mg/L, and 300 mg/L), ranges of flow rates (from 25 gpm to 617 gpm), screen

aperture size (2400 μm and 4700 μm), and diameters of volute separation chamber (5 ft., 6 ft. and 7 ft.). Results for particle separation efficiency (measured as SSC separation efficiency) for the PMSU20_20 with three different volute diameter areas are summarized graphically in Figure 79 to Figure 82. The same results are summarized in a tabular fashion in Table 7, Table 8, Table 9, and Table 10, along with influent, screen area and volute area captured particle mass, and corresponding operating flow rates. Results indicated that as the flow rate increased, particle separation efficiency for the tested NJCAT gradation showed a decreasing trend, from 67 to 35 percent, 68 to 38 percent and 70 percent to 43 percent for the unit diameter of 5 ft., 6 ft. and 7 ft. diameter, respectively, under the specified operating range of flow rate and loading conditions.

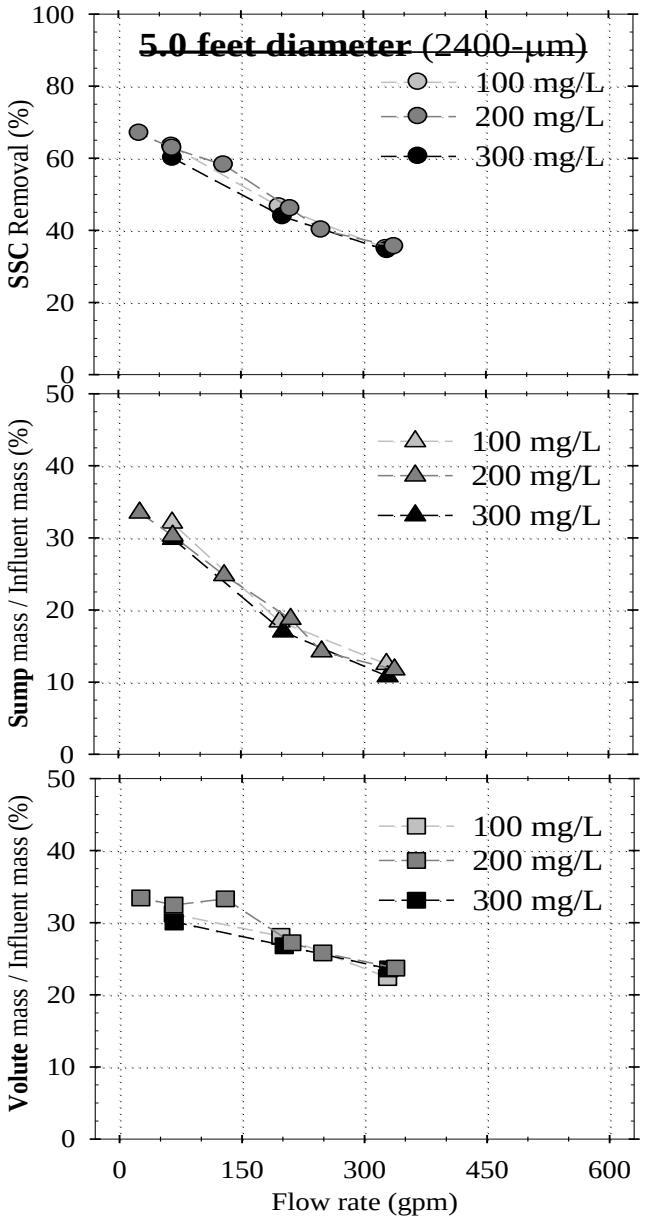

Figure 79

Plots of 5.0-ft. diameter PMSU20_20 treatment performance with a 2400 µm screen at 100, 200, and 300 mg/L and various operating flow rates for SSC (suspended sediment concentration) separation

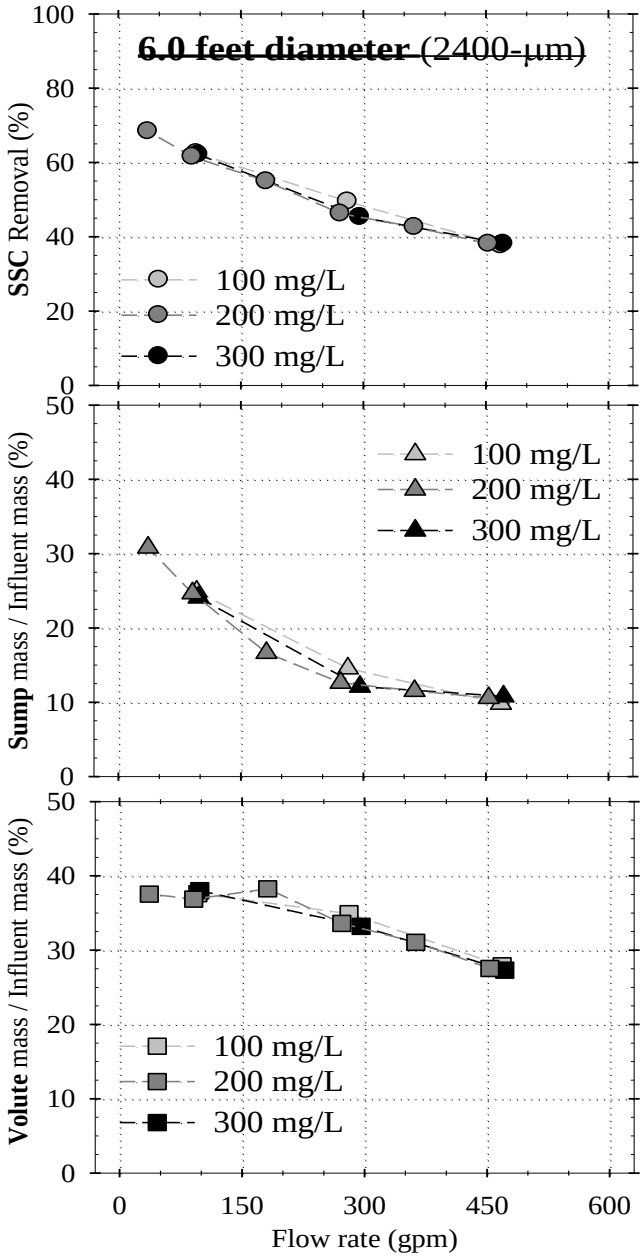

Figure 80

Plots of 6.0-ft. diameter PMSU20_20 treatment performance with a 2400 µm screen at 100, 200, and 300 mg/L and various operating flow rates for SSC (suspended sediment concentration) separation

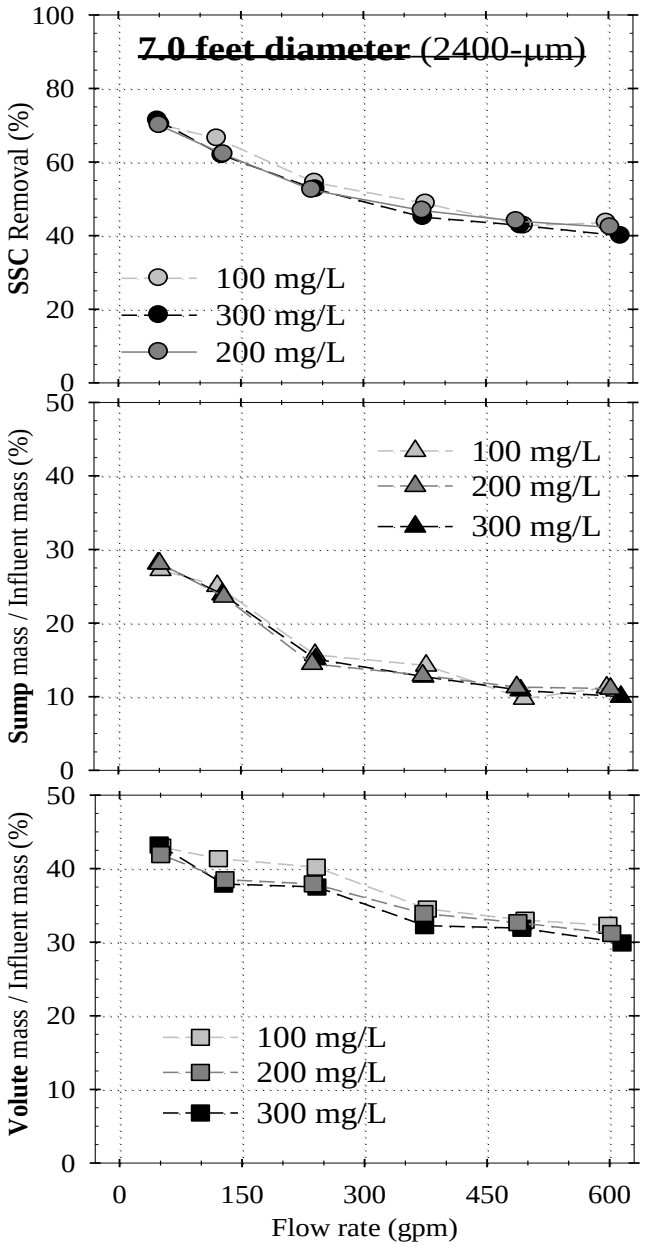

Figure 81

Plots of 7.0-ft. diameter PMSU20_20 treatment performance with a 2400 µm screen at 100, 200, and 300 mg/L and various operating flow rates for SSC (suspended sediment concentration) separation

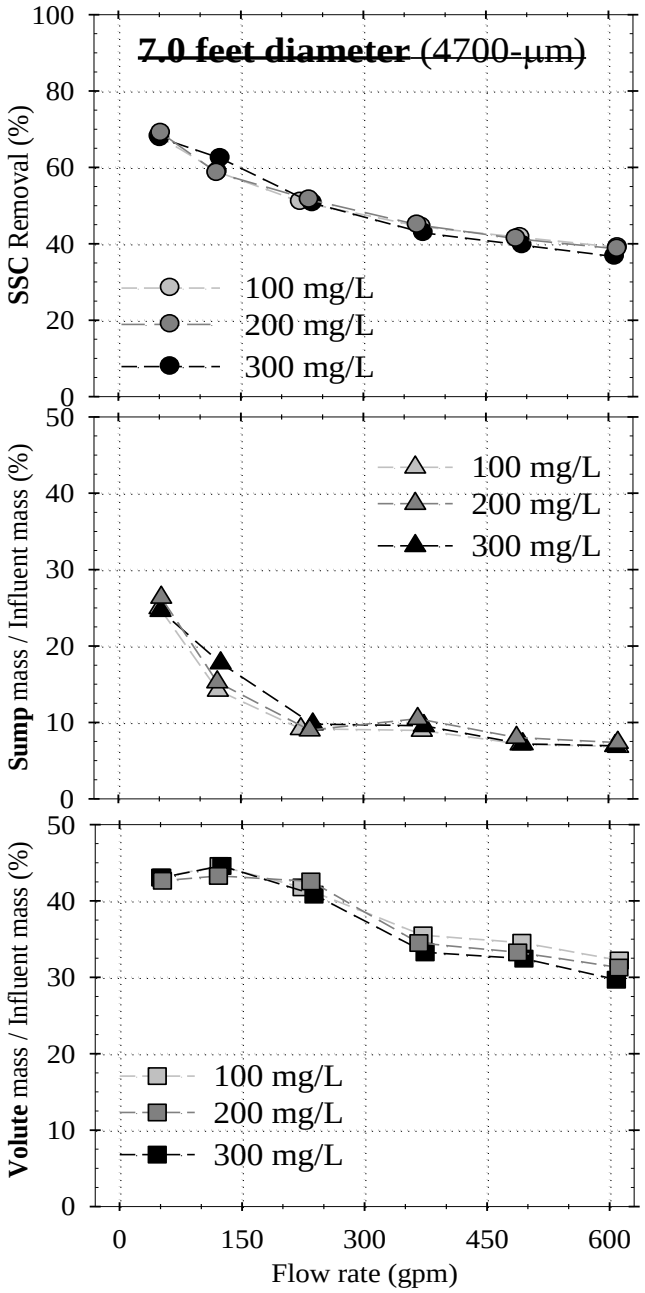

Figure 82

Plots of 7.0-ft. diameter PMSU20_20 treatment performance with a 4700 µm screen at 100, 200, and 300 mg/L and various operating flow rates for SSC (suspended sediment concentration) separation

As hypothesized, results indicated that larger volute area diameters with respect to the screen area provided a higher SSC removal subject to the same operating flow rate. Figure 76, Figure 77, and Figure 78 illustrate that 50 percent of the overall SSC removal occurred at higher flow rates as unit diameter increased from 5 to 7 ft.

As depicted in the plot (B) of Figure 79, Figure 80, and Figure 81, the relative mass of particles (with respect to the influent) captured in the screen area (inside the 2400 μm screen) decreased almost linearly (from 33.5 percent to 23.9 percent) as operating flow rate increased up to approximately 240 gpm and then it gradually decreased from that point toward an asymptotic level of 10 percent at increasingly higher flow rates.

It is important to recognize that particle separation performance by the screen area is independent of the volute diameter, as illustrated in Figure 83. Regardless of the volute diameter, particle separation performance of the screen area is predominantly a function of operating flow rates as long as the screen geometrics (screen diameter, screen height, and screen aperture diameter) remain the same and the unit is loaded by the consistent influent particle gradation and particle density. In this figure, S/I is the ratio of the mass of particles captured in the screen area (S) with respect to the influent particle mass (I).

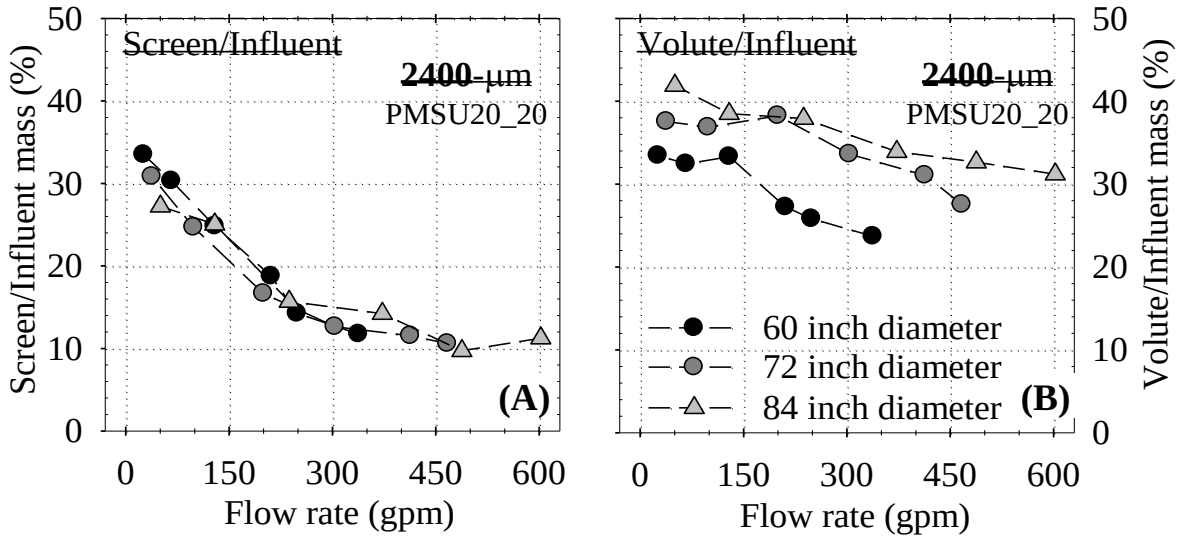

Figure 83
Particle separation performance by screen and volute area of 5.0-ft., 6.0-ft., and 7.0-ft. diameter PMSU20_20

25.5 in. and 24.5 in. in height for the PMSU20_20 ranged from 10 percent to 34 percent with respect to influent mass across the range of operating flow rates of 25 gpm to 605 gpm for the

The particle separation efficiency exhibited by the screen section with the dimensions of 25.5-in. and 24.5-in. in height for the PMSU20_20 ranged from 10 percent to 34 percent with respect to influent mass across the range of operating flow rates of 25 gpm to 605 gpm for the specified NJCAT gradation and particle concentration range of 100 to 300 mg/L.

The particle separation efficiency exhibited by the 5.0 ft. diameter volute section ranged from 50 percent to 67 percent with respect to total captured mass across the range of operating flow rates, from 25 gpm to 315 gpm. This contribution of volute area to the overall captured mass increases as the diameter of the unit increases although there was no significant difference between the performance of the 6.0- and 7.0 ft.- diameter configurations as illustrated in Figure 84. When the 2400 μm screen was replaced with the 4700 μm, the volute area played a significantly increased role in SSC removal relative to the total removal of mass, trapping 62 percent to 83 percent of captured particle mass. Conversely, particle separation contribution from the screen area was relatively less significant for this configuration and loading condition. These results infer that a 2400 μm size of screen aperture outperforms the 4700 μm screen aperture and will enhance the performance of screen area and reduce the dependence on volute area for overall SSC removal. Referring to previous reports regarding the L-unit with NJCAT loadings, this result also provides insight as to why there was only a marginal improvement for the 1200 μm screen as compared to the 2400 μm screen. However, using 2400 μm does not immediately ensure a higher overall performance of particle separation because overall SSC removal is achieved by not only in the screen area but as a combined interaction between these two sections (screen area and volute area). Particle separation by the volute area was dominant based on the tested unit configuration (e.g., outer diameter) and loading conditions. If the unit diameter becomes smaller while screen size is kept constant, the importance of separation performance by screen will increase. It is noted that the potential for scour from the volute has led to questions regarding the inclusion of the volute in performance results. However, it should be recognized that there is only a relative improvement between unit compartments and does not necessarily represent a treatment performance improvement with respect to the entire unit (e.g., clarified effluent).

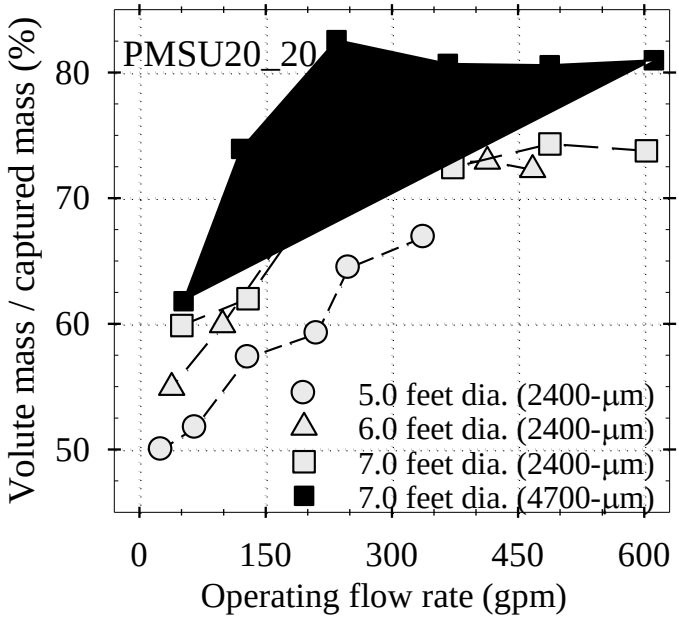

Figure 84

Contribution of volute mass capture to the overall captured mass by PMSU20_20 with three different unit diameters (5.0, 6.0, and 7.0 ft.) and screen set-ups (2400 µm or 4700 µm) across the range of operating flow rates

It can be observed that particle separation curves for the volute area are composed of two phases as illustrated in plot (B) of Figure 85 and Figure 86, a constant and relatively horizontal phase followed by a roughly linear decreasing phase at higher flow rates. During the constant and horizontal phase, relative particle capture by volute area as measured by volute mass/influent mass (%) and expressed as the ratio (V/I) did not vary significantly as flow rates increased. However, at flow rates exceeding those in this constant and horizontal phase, V/I started exhibiting a clear decreasing trend as a function of flow rate. As the unit diameter decreased, the two phases were more distinct, and the change from the first phase to the second declining phase occurred at a lower flow rate.

In order to describe this phenomenon, the fundamental separation mechanisms utilized by PMSU20_20 need to be identified. The internal hydraulic geometry of the PMSU20_20 is designed in such a way that the entire influent flow enters the screen area first and then enters the volute area by passing through the screen. Therefore, the overall particle separation in a PMSU20_20 is accomplished by two serial UOPs. This conceptual process

flow model also requires that the particle gradation entering the volute area is directly influenced by the separation performance in the screen area.

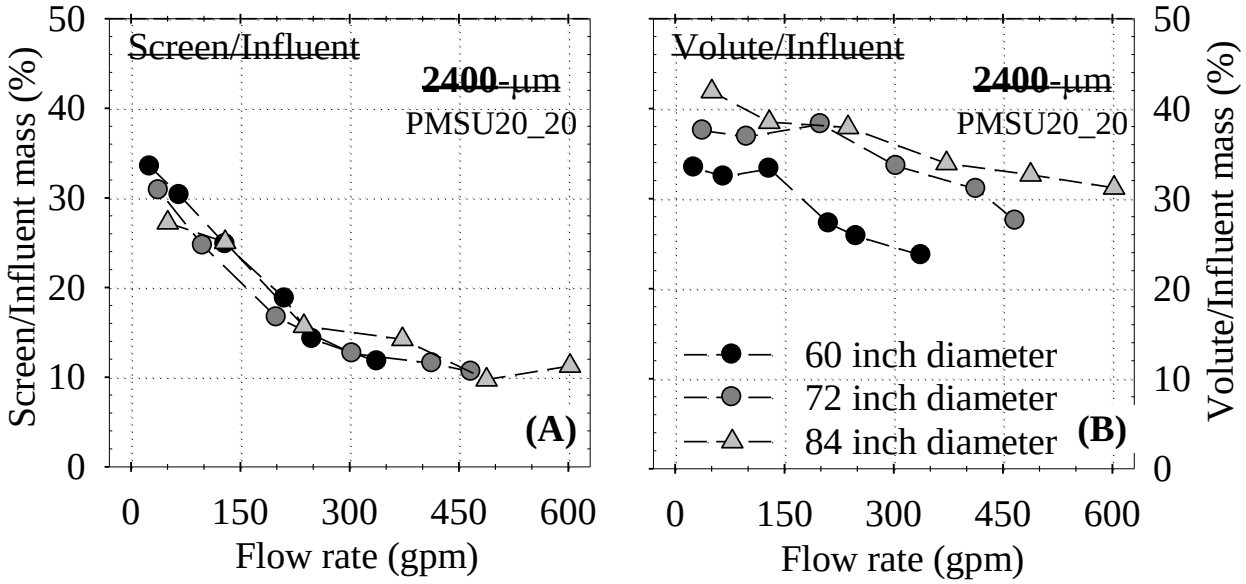

Figure 85
Particle separation performance by screen and volute area of 5.0-ft., 6.0-ft., and 7.0 ft. diameter PMSU20_20

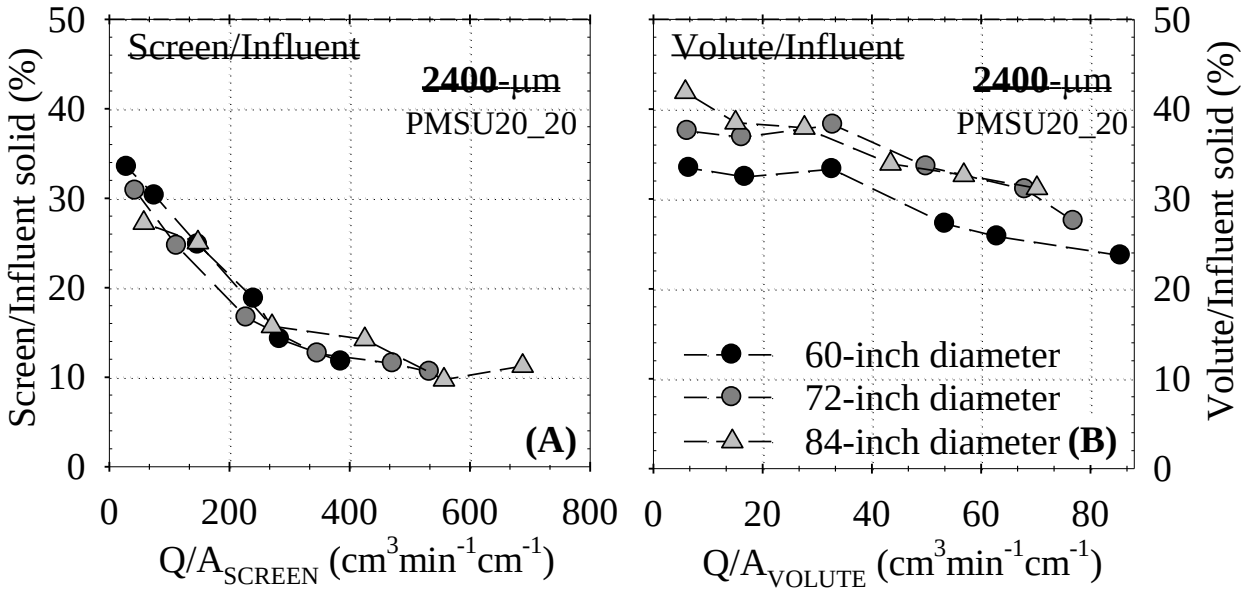

Figure 86
Particle separation performances by screen and volute area of 5.0-ft., 6.0-ft., and 7.0-ft. diameter PMSU20_20 as a function of surface loading rate with respect to A_{screen} and A_{volute} respectively

SSC Removal as a Function of Surface Loading Rate (SLR)

Particle separation performance by the screen area and volute area was also studied as a function of SLR (surface overflow rate). The SLR for the screen area was calculated as Q/A_{screen} where A_{screen} was calculated based on the measured diameter of the screen. In contrast with changes in surface area corresponding to changes in outer diameter for the volute area, the horizontal area associated with the sump remained the same. Therefore, the plots describing particle removal performance for the screen area as a function of surface loading rate and as a function of influent flow rate do not differ from each other as is seen in plot (A) of Figure 85 and plot (A) of Figure 86, respectively. This observation reinforces the hypothesis that the behavior of the screen area is independent of the diameter of the volute area.

On the contrary, particle separation performance by the volute area varied significantly as a function of the diameter of the section being used. A 60-in. diameter unit exhibited significantly lower particle removal than a 72-in. diameter unit which was lower than an 84-in. diameter unit at the same SLR (Q/A_{volute}). At this point, it was emphasized that in order to maintain the SLR in the volute area (Q/A_{volute}) constant across the three different volute areas, it was required that the influent flow rates be increased correspondingly. While this increase in flow rate maintained the SLR constant in the volute area, it increased the SLR for the screen area. As discussed previously, the particle separation performance of the screen area is largely dependent on the influent flow rate and that the screen area captures only coarser particles with an increasing flow rate.

At the same SLR for volute areas, the influent flow rate to the 60-in. diameter unit was lower than that with the 72-in. and still lower for the 84-in. diameter unit. There appears to be a threshold flow rate, approximately around 300 gpm, beyond which the screen area reaches a asymptotic limit for separation of the influent particulate gradation. This results in an altered effluent gradation leaving the screen area and entering the volute area as a function of influent flow rate and screen area.

A larger fraction of coarse particles were separated in the screen area with a 60-in. diameter unit, in contrast with the 72-in. and 84-in. diameter units. Therefore, the particle gradation passing into the volute area through the screen in the 72-in. and 84-in. units was coarser that that with the 60- in. diameter unit. This explains the higher particle removal in the volute area with the two larger diameters as a result of a larger number of coarse particles being captured in the volute area. However, it was noticed that there was no significant difference in the particle removal performance of a 72-in. diameter unit compared with a 84-in. diameter unit. This is due to the fact that the influent flow rates for these two diameters were predominantly above the defined threshold flow rate (~300 pm).

Effect of Screen Aperture Size on Particle Removal Efficiency

A comparison was made between the performance of the PMSU20_20 with a 2400 μm screen and a 4700 μm screen to evaluate the impact of changing screen aperture size on overall SSC removal and particle separation performance by the screen area. Plot (B) in Figure 82 shows 7.0-ft. diameter PMSU20_20 treatment performance with a 4700 μm screen at various influent solid concentrations and flow rates. By comparison with Plot (B) in Figure 81, it was shown that using a 2400 μm screen provided 2 to 8 percent of increase in relative

particle capture by screen area as measured by "screen mass/influent mass (%)" across the entire flow rate range. Statistical analysis (paired t-test) indicated that improvement (2 to 8 percent increase) of particle separation efficiency by using 2400 μm screen area measured as "screen mass/influent mass (%)" was statistically significant across the entire flow rate range ($p = 0.0092, 0.0046, 0.0005$ for 100 mg/L, 200 mg/L, and 300 mg/L, respectively).

However, the particle separation performance by screen area with the 2400 μm screen did not immediately ensure the improvement of overall SSC removal by PMSU20_20. While overall unit particle separation efficiency of the 7.0-ft. diameter PMSU20_20 with the 2400 μm screen was higher than that of the unit with 4700 μm screen, the difference was not statistically significant ($p = 0.0091, 0.0064$, and 0.0141 for 100 mg/L, 200 mg/L, and 300 mg/L, respectively). This was due to the reason that any particles that managed to escape through the larger aperture size screen (4700 μm) were still captured in the volute area at the lower range of operating flow rates (50 to 250 gpm). Plot (C) in Figure 82 illustrates this point that the relative mass of particles (with respect to the influent) captured in the volute area of 7.0-ft. diameter PMSU20_20 with 4700 μm screen was higher ($p < 0.05$) than the unit with a 2400 μm screen. As flow rates exceeded 350 gpm, no statistically significant difference ($p > 0.05$) could be found between separation efficiencies by the volute area of the PMSU20_20 with a 2400 μm screen and a 4700 μm screen. Overall, a statistically significant improvement ($p < 0.05$) was demonstrated using a 2400 μm screen for all three loading concentrations given the wide range of operating flow rates, from 49 gpm to 617 gpm.

Treatment Runs for PMSU20_20 without Screen

In order to identify the relative contribution of the separation screen to overall particle separation capability of the unit, 7.0-ft. diameter PMSU20_20 without any screen was selected as a control set-up and tested in parallel with a 2400 μm screen at 100 mg/L concentration. Particle separation efficiencies under control set-up could be attributed to mostly gravitational sedimentation effect due to the volume of PMSU20_20. Therefore, the true benefit of using screen in particle separation was visualized by the difference in SSC removal of between PMSU20_20 with control and screen**.**

As presented in Figure 87 and summarized in

Table **23**, the results from selected testing of 7.0-ft. diameter PMSU20_20 with a control set-up (without screen) at 100 mg/L of NJCAT influent particle concentration indicates that SSC removal efficiencies were in the range from 60.7 percent to 17.6 percent as flow rate increased from 10 percent to 125 percent of 1.1 cfs. SSC removal with control set-up decreased more rapidly than for a 2400 µm screen (and from previous testing, much more rapidly than a 1200 µm screen) as flow rate increased up to 100 percent of 1.1 cfs, after which the decrease of SSC removal (%) reached a plateau. The inference is that the benefit of the screen in particle separation of PMSU20_20 tends to be more significant as flow rate increases. Improvement of particle capture efficiency as a result of screen was in the range of 9 to 26 percent for 2400 µm and 5 to 25 percent for 4700 µm, respectively, and tends to be maximized at high range of flow rate (100 percent ~ 125 percent of 1.1 cfs).

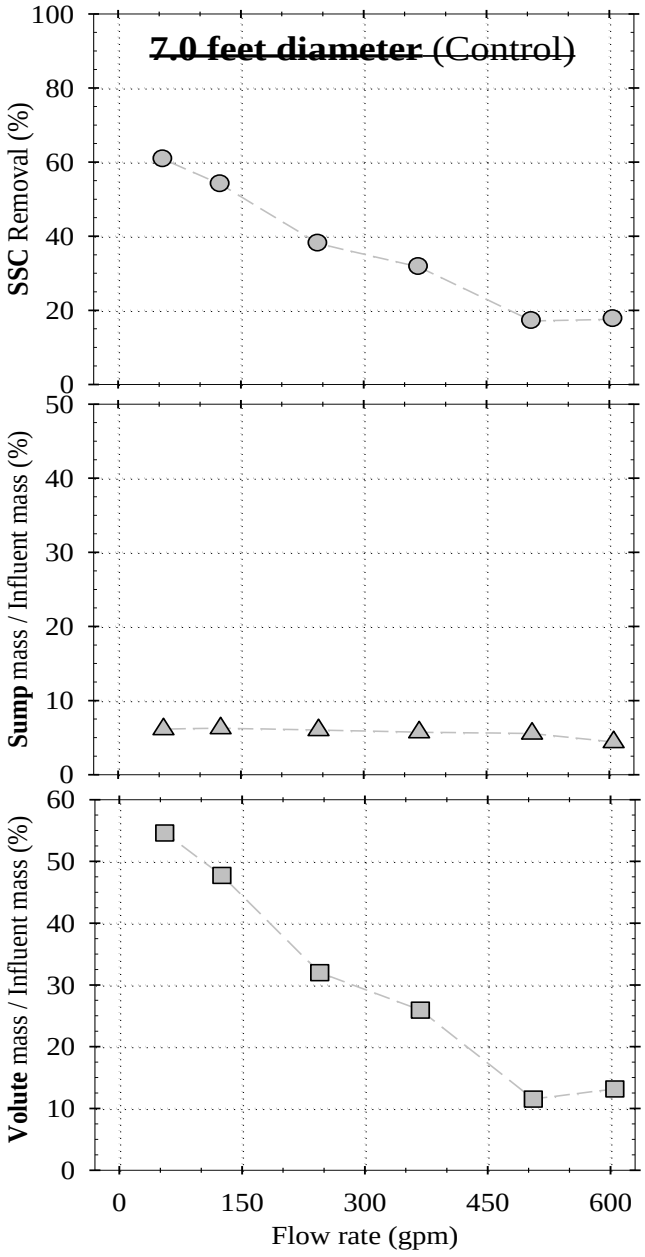

Figure 87

Plots of 7.0-ft. diameter PMSU20_20 treatment performance with control setup (without a screen) at 100 mg/L and various operating flow rates for SSC separation

Table 23

Summary of treatment run results for 7.0 ft. diameter PMSU20_20 without a screen as a control setup loaded by NJCAT gradation under 100 mg/L and various operating flow rates

Run	Flow rate	Influent conc.	Influent mass	Volute mass captured	Volute/ Influent	Sump mass captured	Sump/ Influent	SSC Removal efficiency	Mass balance check	Turbidity Removal
	[gpm]	[mg/L]	[g]	[g]	[%]	[g]	[%]	[%]	[%]	[%]
45	605.3	100	2800	368.7	13.2	123.2	4.4	17.6	-6.6	16.7
44	505.7	100	2800	322.6	11.5	155.6	5.6	17.1	-4.4	24.9
43	367.8	100	2800	725.8	25.9	160.3	5.7	31.6	-4.2	14.3
42	244.7	100	2800	895.2	32.0	168.3	6.0	38.0	-3.2	16.9
46	125.3	100	2800	1336.4	47.7	175.2	6.3	54.0	-4.2	31.0
47	55.4	100	2800	1528.9	54.6	171.8	6.1	60.7	-2.1	28.6

Effect of Influent Concentration on Particle Removal Efficiency

It is commonly accepted in the stormwater treatment industry that higher loading concentrations promote higher removal efficiencies (Barrett, 2005). There is also evidence (Grizzard et al., 1986) that TSS and other constituent removal efficiencies can be significantly affected by the initial concentrations of the constituent. For example, Grizzard et al. found that it is easy to remove 80-90 percent of TSS when its initial concentration is high (e.g., > 400 mg/L) and difficult to remove TSS when its initial concentrations are low (e.g., < 20 mg/L). This implies the critical role of the properties of the influent particle size distribution. Because no particle size distribution for particles in the influent flow was analyzed during his study, there is not sufficient information to determine how influent concentration affected removal efficiency. It was also shown by previous study that the removal efficiency of discrete particles in continuous flow sedimentation tanks (Thompson, 1969) and conventional hydrodynamic separators (Fenner and Tyack, 1997) were independent of the concentration of solids in the influent flow.

These contradictory results imply that types of UOPs investigated, influent particle gradation, method of sampling and analyses, and range of particle concentration that in turn affects particle-particle interactions need to be carefully examined before we accept any conclusion of previous studies with regards to the relationship between removal efficiencies of any UOPs and initial concentration.

PMSU20_20 results with the specified NJCAT gradation demonstrated that there was not a consistent increase or decrease in removal efficiency for SSC on a gravimetric basis with increasing loading concentrations (from 100 to 300 mg/L as SSC) across the entire flow rate range for all tested diameters of unit. By comparison, the optimized "L-unit" results also showed that concentration in this same range did not influence the removal efficiency. However, this result might not be applicable in the situation that real rainfall-runoff is treated, where influent particle gradation and density and runoff flow rate are not constant but dynamically change within a single event and a high variation of constituents in terms of concentration and mass load can be found between events. In fact, our extensive database from eight "L-unit" rainfall-runoff treatment events revealed a new finding that urban rainfall-runoff with higher SSC tends to entrain more coarse particles than the one with lower SSC. The existence of this clear relationship between stormwater particle concentrations measured as SSC and removal efficiency of extended detention ponds provides new insights into why high initial concentration allowed 80-90 percent of TSS removal in Grizzard's study. This new finding will also be applied to treatment performance of any UOP that utilizes gravitational sedimentation entirely or as a part of their particle separation mechanisms. A greater understanding is expected to be gained through extensive database and analysis of discrete water-quality samples collected from a number of real storm "L-unit" treatment events in Baton Rouge, Louisiana.

Turbidity Removal

Turbidity removal efficiency for all tested PMSU20_20 configurations with a 2400 μm and 4700 μm screen for an NJCAT gradation were in the range from 13 percent to 47.3 percent noting that the unit was cleaned and dried out between each event. The results of turbidity are summarized in Table 7, Table 8, Table 9, and Table 10. Similar to SSC removal, as the flow rate increased, turbidity removal for the tested NJCAT gradation exhibited a decreasing trend from 15 to 45 percent, 15 to 40 percent, and 16 to 47 percent for the unit diameters of 60 in., 72 in., and 84 in., respectively under the specified operating range of flow rates and loading conditions.

The decreasing rate of turbidity removal as a function flow was not as rapid as decreasing SSC removal with the tested range of flow rates. This is attributable to the nature of NJCAT gradation that is mainly composed of fine particles since turbidity contributed by fine suspended particles in flow was relatively dominant compared to the reduction of turbidity

due to the separation of coarser sizes of particles by PMSU20_20. A significant fraction of these fine particles were in a suspended state and not captured by PMSU20_20 even under low flow rates. This result is a reminder that the same gravimetric mass of fine particles in a given sample would result in higher values of turbidity, from scattered light measurements in a turbidimeter, as compared to an equal mass of coarser particles.

Hydraulic Characteristics of PMSU_20 20

To identify the hydraulic response of 5.0-, 6.0- and 7.0-ft. diameter PMSU20_20 to various levels of influent flow rate during the entire duration of each treatment run, head loss data was measured by three pressure transducers installed at inlet channel, volute area, and screen area, respectively, in the PMSU20_20 unit. As illustrated in Figure 88, no statistically significant head differences were found across the unit until flow reached around 150 gpm. As the inlet throat began to be submerged under the influent flow in the inlet channel with increasing flow rate, H_I increased more rapidly than ΔH_S or ΔH_V.

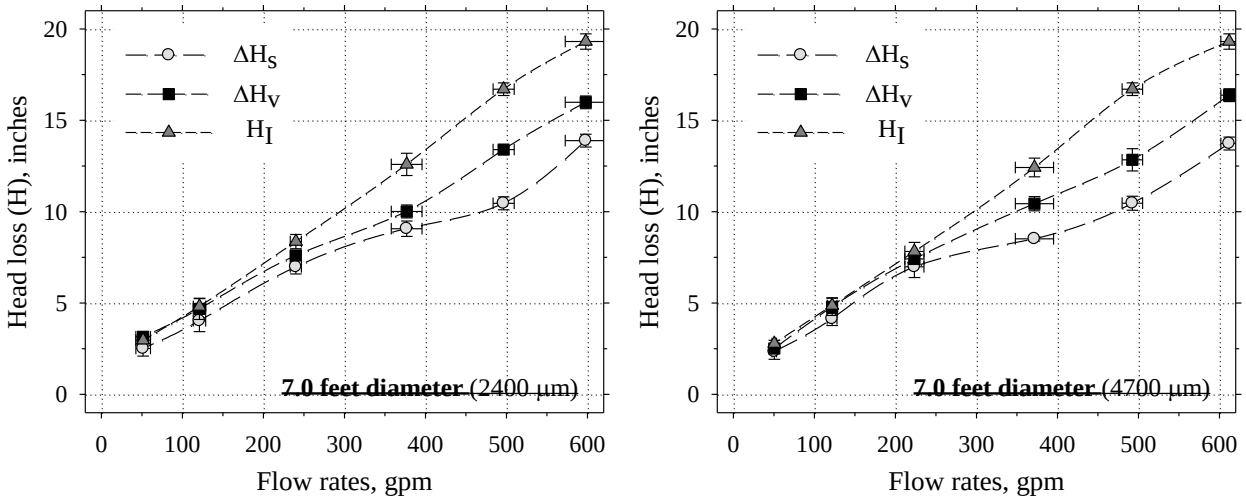

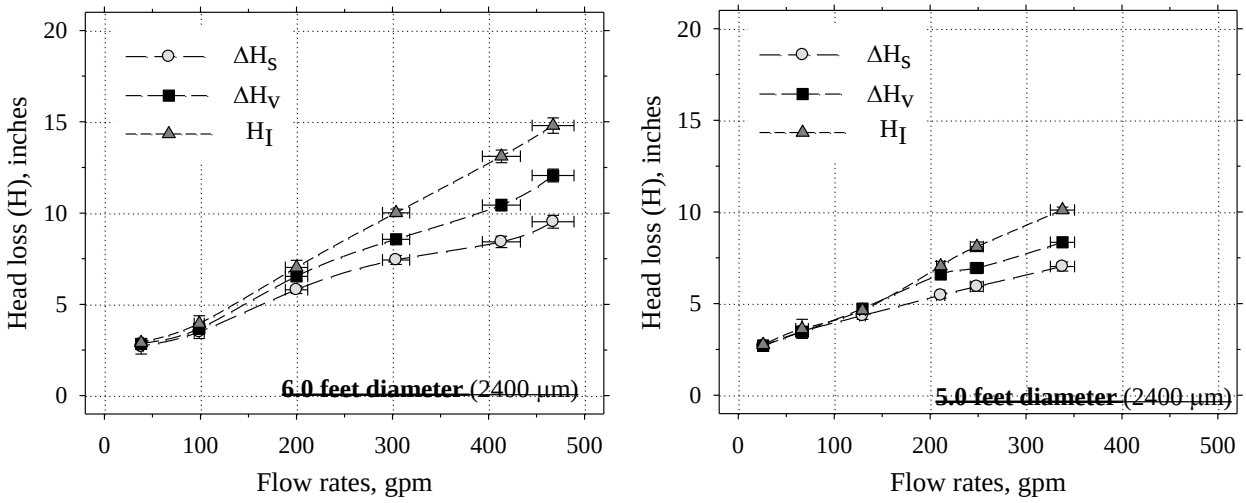

Figure 88
Head data for 5.0 and 6.0 ft. diameter PMSU20_20 treatment runs with the 2400 µm screen and for 7.0 ft. diameter PMSU20_20 with the 2400 µm and 4700 µm screen at various range of constant flow rates

ΔH_S = H_S (Pressure head from the invert of sump) - H_O
ΔH_V = H_V (Pressure head from the invert of volute chamber) - H_O
H_I = Pressure head in inlet open channel

Figure 12 illustrates the vertical and horizontal locations of two 2.5 psi pressure transducers for screen and volute area and one 1 psi pressure transducer for inlet channel of the 7.0-ft. diameter PMSU_20 20. The 2.5-psi transducer in the volute area was installed at the level of 17 in. (H_{DV}) above the invert of the volute chamber. The 2.5 psi transducer in the screen area was installed at the level of 35 in. (H_{DS}) above the invert of cylindrical sump. Since a pressure transducer was located at the center of the screen chamber where a slight vortex is established due to rotational flow, ΔH_S started to become lower than ΔH_V as the flow rate exceeded approximately 150 gpm. While trends exhibited some variability, results were consistent for each size of PMSU20_20. The head loss created by either the 2400 µm or 4700 µm screen was not considered to be significant below 50 percent of 1.1 cfs.

Design Option Results

Conventional: Design Option I

The resulting runoff hydrograph for the conventional design where three east and three west bound catchments are combined via piping and conveyed to each clarifier (east and west abutments) is shown in Figure 89. The circular clarifier at each abutment has two outflows systems: a V-notch weir and a 1-in. diameter siphon. The siphon in the clarifier permits slow drainage of the runoff stored in the clarifier between rainfall events without transporting PM. Both outflow systems route the collected rainfall runoff into a sand filter. The bottom of the clarifier was sloped for ease of sludge collection. The maximum overflow rate chosen was as 3 gal/ft2·min; corresponding to a settling velocity of approximately 2.0 mm/s. PM $\geq \sim 50$ μm were removed by discrete (Type I) settling in the clarifier. The shortest embankment area for the bridge is 36.5 ft. wide by 108 ft. long, thus the diameter of the circular clarifier could not exceed this width. The maximum overflow rate allowed for a diameter of 19.23 ft. The diameter chosen for the clarifier was thus 20 ft. The clarifier height was chosen as 5 ft. from the mean elevation of the sloped bottom to the notch of the weir. This minimized cost, improved safety, and eased maintenance. The height allowed for flow equalization. The full clarifier height with freeboard is 5.75 ft. The freeboard height was sufficient for the maximum head above the weir notch of 0.27 ft. The clarifier PM separation efficiency was 94 percent by mass. Figure 90 illustrates influent and effluent PSDs for the clarifier and filters. The high clarifier efficiency provides lower PM loading to the filters and lower filter maintenance.

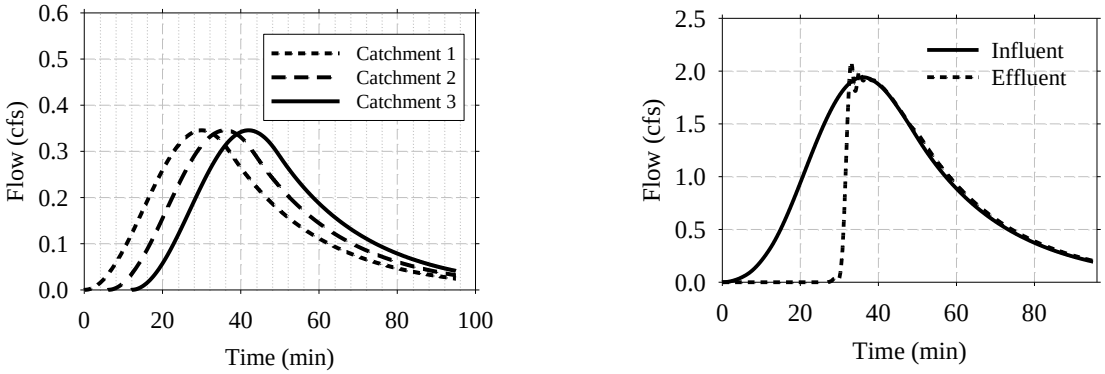

Figure 89
Influent 50-year, 1-hour hydrograph to the clarifier and resulting effluent hydrograph to filters

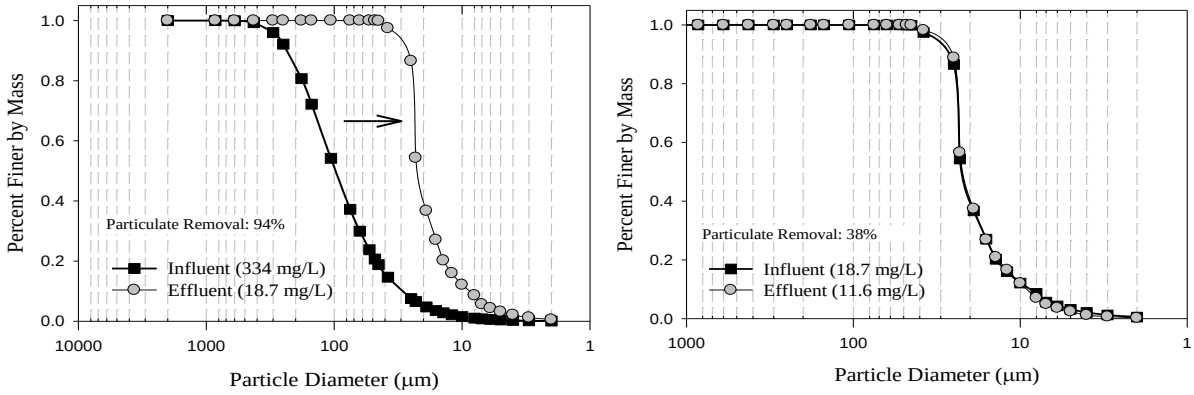

Figure 90
Influent and effluent PSDs for clarifier (left plot) and filters (right plot) for 50-yr. design storm

Head loss results based on the Ergun model demonstrated that in order to accommodate the full flow of the design storm at a maximum head loss of 3 ft., two filters were needed per clarifier. Each filter was designed with a 15-ft diameter, a media depth of 4 ft., a filter freeboard of 3 ft. and a media d50 diameter of 0.12 in. Two filters were used rather than just one in order to provide redundancy in the case of filter short circuiting or clogging. In addition, the use of a diffuser to distribute the flow evenly over the top of the filter reduced short circuiting. The use of 0.12-in. substrate provided sufficient particulate removal while allowing for rapid filtration and a porosity of 35 percent. Data from filtration using a similar clarifier and filter media combination at the I-10 bridge on April 29, 2006 event with a peak flow within 20 percent of the 50-year design storm was used as an unsteady physical model for this traditional design option loaded by the design storm. When this data was applied to the traditional filter influent (effluent from the clarifier), an efficiency of 38 percent was modeled. This low efficiency was a function of the small size of the influent PM.

For determining the maintenance frequency, based on head loss, rainfall data for 2008 input as a time series into SWMM was utilized to generate an annual runoff time series as shown in Figure 91. The clarification and filtration efficiency for each particle size of the influent PSD based on 19 historical storm datasets was applied. The resulting PM removal efficiency of the filter was 57 percent by mass on an annual basis. The PM removal efficiency for the clarifier and sand filters in series was 97 percent as shown in Figure 92. The clarifier removed 2,428 kg/yr and the associated filters removed 83 kg of PM. The table to the right of Figure 92 summarizes annual removal of PM and PM-bound constituents by the conventional treatment system. The system did not treat dissolved constituents as the specific and total surface area of the sand media was not sufficient to adsorb solutes.

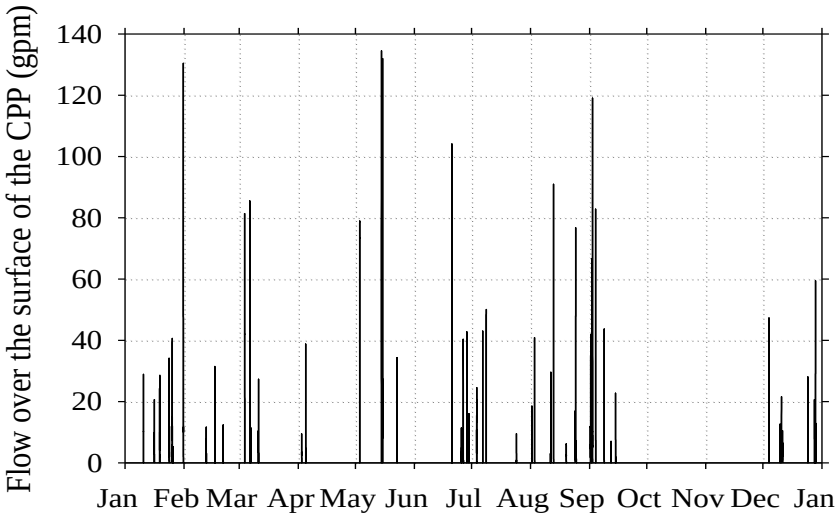

Figure 91
Time series of runoff flows for continuous simulation loadings (based on 2008 rainfall data)

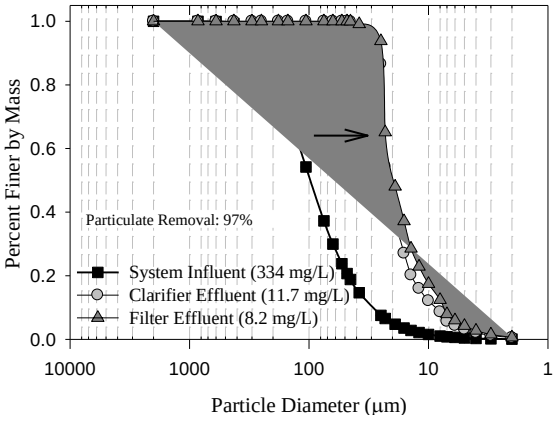

Constituent	Influent [mg/g]	Influent [µg/L]	Effluent [µg/L]	Mass Removed (kg/yr)
PM	1,000	334 mg/L	8 mg/L	2,511
TN	27.3	9,116	224	69
TP	0.78	261	6.4	2
Total Zn	0.38	128	3.15	1
Total Cu	0.05	15.4	0.379	0.1
Total Cd	0.001	0.334	0.008	0.003

Figure 92
Summary of median PSDs (left plot) based on annual continuous simulation loadings to the conventional design option. Annual mass removed for metals and nutrients are summarized in the table

Buoyant Adsorptive Media (BAM): Design Option II

In order to achieve an adsorption breakthrough time of greater than 2 years and a sludge maintenance interval of 1 year, the height of each BAM is 5 ft. and diameter is 3.3 ft. with a total volume of 43.8 cubic ft. The d50 of the uniform BAM media is 0.1 in., the porosity is 0.37 and the media specific gravity is 0.9 with oxide coatings (Liu et al., 2005a). The size of the BAMs and therefore media mass of MOPM and AOPM was based on providing a minimum of a 2-year solute breakthrough for phosphate and metals. Contact time for the floating filters at the peak flow of the 50-year design storm was calculated to be 116 seconds, longer than the 90-second contact time required for adequate solute adsorption (Liu et al. 2005b). Breakthrough capacity (X/M) is determined based on the Thomas model as shown in Figure 93 with the adjacent table summarizing system parameters.

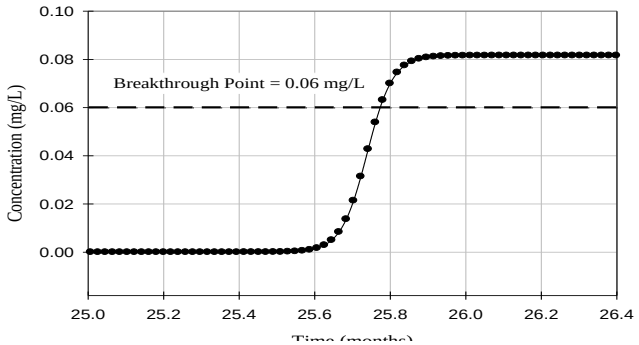

k (L/min-mg)	0.0082
Q_e [mg/g]	0.4497
Influent Conc. (g/L)	0.0816
Filter Cartridge Volume (L)	1034
Median Flowrate (L/min)	1.222
Breakthrough (months)	25.75

Figure 93
Breakthrough for phosphate for BAM design and associated Thomas model parameters

Through similar analysis utilizing the Thomas model and MOPM, physical model data, and continuous simulation rainfall-runoff data generated from SWMM, breakthrough times are shown for each metal and the combined (competitive) effect of the metals lowering the BAM breakthrough time.

Using physical model radial cartridge filtration data for 19 storms from the literature, removal efficiency for each particle was determined. These removal efficiencies were applied across the inflow PSD to calculate a removal efficiency of 89 percent by mass and an effluent PSD as shown in Figure 94. The PM removal rate and sludge production for each BAM are summarized in Table 24.

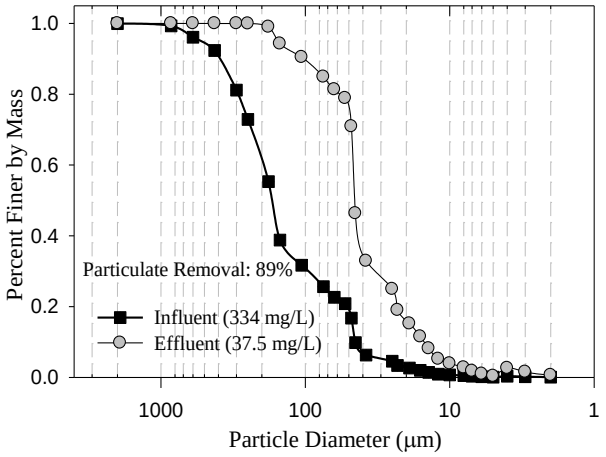

Time (years)	Flow Rate (m^3/s)	Porosity	Head Loss (m)
0	0.0590	0.37	0.34
2	0.0590	0.291	0.85

Constituent	Mass Removed (kg/yr)
PM	2,348
TN	63
TP	3
Total Zn	2
Total Cu	0.2
Total Cd	0.01

Figure 94
Influent and effluent PSDs for BAM (left plot) with head loss and annual mass removed based on continuous simulation of runoff loadings summarized in the two adjacent tables, respectively

Table 24
PM removal, sludge production, and sump volume

PM Removal per Volume of Inflow [g/L]	PM Removal Rate (L/yr)	Fraction Settled into Sump	Volume into Sump (L/yr)
0.305	140.9	0.25	35.2

Head loss through the BAM filter for the peak flow of the 50-year design storm was calculated for clean-bed conditions (time 0) and the end of the 2-year filter lifetime and summarized in the table in Figure 94. Head loss is reasonable considering the available head from the elevation difference of the bridge deck and the BAM filters. Results also demonstrate that breakthrough capacity (nominally at 2 years) controls BAM maintenance rather than filter clogging.

Cementitious Permeable Pavement (CPP): Design Option III

This design option replaces (by milling) the upper pavement surface of the impervious concrete bridge deck with a porous friction course of CPP. The placement of reinforcing steel restricts the CPP depth to 4 in. Therefore this design option provides a CPP depth of 2 in. and an option to increase this depth to four inches of CPP containing aluminum and manganese oxide as part of the water/cement ratio as admixtures. While the CPP with oxide admixtures has significant adsorptive capacity (greater than the BAMs), the CPP is a relatively thin (2-4 in. with a total porosity of 0.29) design element with lower hydraulic and volumetric capacity as compared to full-depth CPP. Therefore the 50-year design storm generates a significant level of runoff not infiltrated into the CPP, while infiltration and therefore potential treatment by the CPP is much greater for an annual time series as shown in Table 25.

Table 25

Hydrologic components for 50-year design storm and representative annual time series of rainfall

	50-year, 1-hour storm with 2 inches of CPP	50-year, 1-hour storm on impervious pavement	Representative year with 2 inches of CPP	Representative year on impervious pavement
Total precipitation (in)	3.2	3.2	58.1	58.1
Total evaporation (in)	0.03	0.03	4.9	7.5
Total infiltration (in)	0.52	0.03	17.8	2.8
Total upper zone ET (in)	0.01	0.000	2.9	0.000
Total runoff (in)	2.6	3.1	35.4	47.9
Peak runoff flow (gpm)	935	935	130	130
Runoff coefficient	0.82	0.98	0.61	0.83

CPP with oxide admixtures is a fixed-matrix adsorptive filter. As such, equilibria, kinetics, breakthrough, and filtration models can be applied to CPP. As utilized with sand and BAM filters, with CPP properties and physical modeling (Liu et al., 2005a, 2005b, Teng et. al., 2004, Kuang et. al., 2007), the treatment efficiency of CPP can be determined. Figure 95 and the associated table illustrate the annual removal by replacing 2-in. of the pavement with CPP.

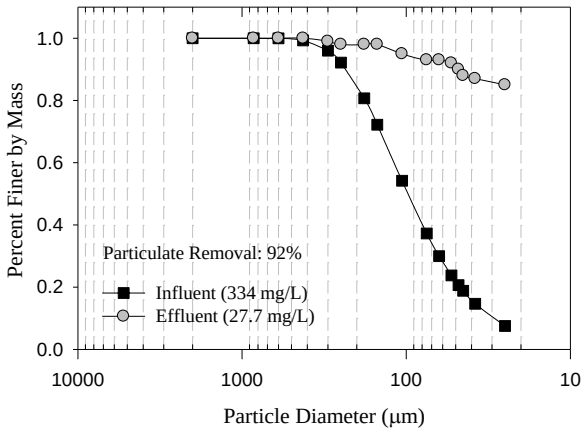

Constituent	Mass Removed (kg/yr)
PM	571
TN	16
TP	1
Total Zn	0.4
Total Cu	0.05
Total Cd	0.002

Figure 95
Summary of median PSDs (left plot) based on annual continuous simulation loadings to the two inch CPP design option. Annual mass removed for metals and nutrients are summarized in the table

CPP Combined with BAMs: Design Option IV

The CPP combined with the BAM filter network utilizes the same BAM filter dimensions and CPP depth of 2-in. as was the case for the earlier design options. However, the combination provides serial treatment (primary and secondary) for solutes, PM-bound constituents, and PM with an increase in adsorptive capacity and PM filtration lifetime for the BAMs. Using the fraction of runoff that infiltrates into the CPP before entering the BAM, and the runoff fraction that flows directly into the BAMs during a representative year, the combined behavior of this design option is evaluated. Phosphate breakthrough for this design option is shown in Figure 96 and Thomas model parameters shown in the adjacent table.

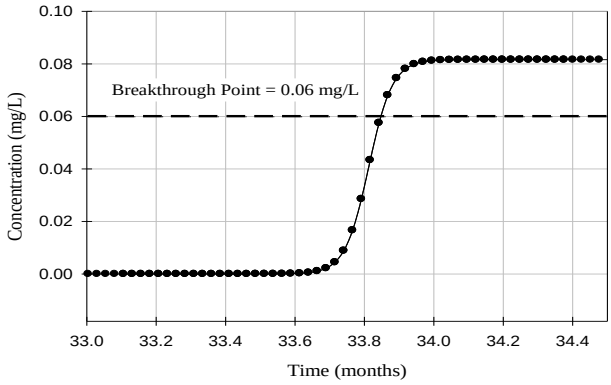

k (L/min-mg)	0.0082
Q_e [mg/g]	0.4497
Influent Conc. (g/L)	0.082
Filter Cartridge Volume (L)	1,034
Mean Flowrate (L/min)	0.93
Breakthrough Time (months)	33.9

Figure 96
Phosphorous breakthrough curve through BAM filter after CPP treatment

Through similar analysis utilizing the Thomas model and MOPM, physical model data, and continuous simulation rainfall-runoff data generated from SWMM; breakthrough times are shown for each metal and the combined (competitive) effect of the metals lowering the BAM breakthrough time. Results are shown in Table 26.

Table 26
Breakthrough time for metals in BAM filters

Metal Species	Co [mg/L]	Mass Inflow Rate (mg/year)	X/M [mg/g]	Breakthrough Capacity (g)	Breakthrough Time (years)
Zinc	0.0886	56,912	0.4	140.0	2.46
Copper	0.0111	7,130	0.56	196.0	27.5
Cadmium	0.0007	450	0.35	122.5	272.4
Total/Weighted	0.1004	64,492	0.417	146.1	2.26

A weighted PM removal efficiency of 89 percent by mass determined for the influent PSD after infiltration through the CPP. The influent and effluent PSDs are shown in Figure 97. This sludge volume collection rate is lower than that for the BAM filter alone option, so the sump dimensions from the BAM design option will be adequate for this design option. Results indicate that the CPP extends the BAM design life from two to three years.

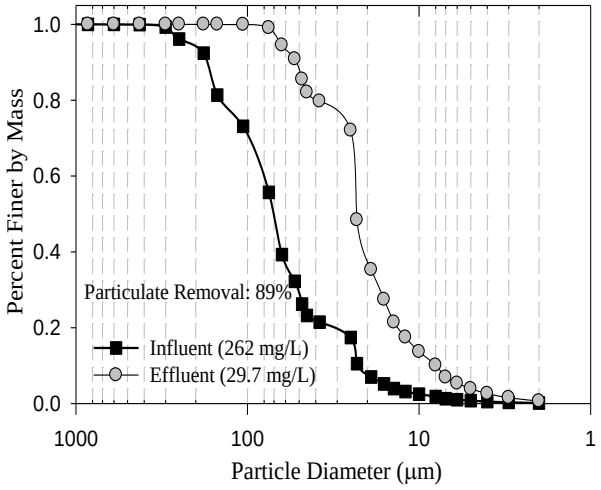

Time (years)	Flow Rate (m^3/s)	Porosity	Head Loss (m)
0	0.0526	0.37	0.29
3	0.0526	0.27	0.90

Constituent	Mass Removed (kg/yr)		
	From 2" CPP	From BAM	Total
PM	571	1,787	2,995
TN	36	49	85
TP	1.2	1.9	3.1
Total Zn	0.8	1.2	2.0
Total Cu	0.10	0.15	0.25
Total Cd	0.004	0.006	0.010

Figure 97
Influent and effluent PSDs to the BAM after CPP treatment (left plot) with head loss and annual mass removed based on continuous simulation of runoff loadings summarized in the two adjacent tables, respectively

Design Option Economics

Total design costs for each design option are presented in tabular form. These design option costs were developed from unit cost data, bridge resurfacing projects in Louisiana, costs from material suppliers such as Rinker Materials (Cemex) for CPP, general contractors, and property appraisal data obtained from Baton Rouge real estate appraisers. Operation and maintenance, demolition, and disposal costs are adjusted for cost increases over the project lifetime. For the design options with shorter lifetimes, replacement costs are adjusted for wage increases and inflation so that design options were compared for the same project life.

Conventional: Design Option I

Conventional treatment project costs are listed in Table 27. For this design option, a project life of 25 years was chosen with filter media replacements every 9 years based on head loss development as shown previously in the report. This lifetime approximately matches the

remaining bridge lifetime. The I-10 bridge lifetime is 50 years, but the bridge has been in place for approximately 25 years. A total project cost of approximately $2.8 million was estimated for the conventional design option.

Table 27
Conventional design option total project cost

Project Component	Description	Cost ($)
Capital Cost	Clarifier, Filters, Conveyances (piping)	1,535,990
Maintenance	Clarifier Cleaning	299,501
Replacements	Sand Filter Media	4,017
Demolition	Existing Concrete Appurtenances at Abutments	83,250
Disposal	Sub D Landfill	277,047
Contingency	10%	300,000
Engineering Fee	10%	300,000
Project Lifetime	25 years	
Total Project Cost		**2,799,804**

Cleaning is recommended twice a year to reduce sludge buildup and anaerobic conditions in the clarifier basin. Many clarifiers are only cleaned annually, but more frequent cleaning avoids many odiferous and vector concerns as well as repartitioning of metals and nutrients that arise from the buildup of sludge. When sludge is allowed to accumulate, not only does the sludge zone go anaerobic resulting in water chemistry changes, but in addition the potential for re-suspension and scour increases. Increasing scour will result in earlier clogging and replacement of the filter media. Under anaerobic conditions in the sludge zone, alkalinity will be consumed with a drop in pH with the potential to remobilize metals that have partitioned to the PM sludge. The filter replacement of every 9 years is based on bi-annual clarifier draining, cleaning, and maintenance.

Buoyant Adsorptive Media (BAM): Design Option II

A BAM lifetime of 10 years (filter cartridge, housing, and appurtenances) is utilized with oxide-coated buoyant adsorptive-filtration media replacements every 2 years. The initial total design cost for the BAM filters is $257,889. The total project cost is $1.1 million over the 25-year project lifetime. The media is replaced once the filter reaches a breakthrough concentration that exceeds the discharge limit for a constituent; for example 60 g/L for

phosphorus. Maintenance for the BAM filter design option maintenance is recommended annually. This involves using a pontoon boat to access the filters. A vactor hose fed through the pontoon boat from a shore-based vactor truck will be used to vacuum sludge on an annual basis. The hose must be supported by floats as it stretches across open water between the truck and pontoon. Given the shallow depth of the lake a pontoon is preferred but such a system is not feasible in more open water systems with long infrastructure spans. In deeper more open water with further distances from shore, such as for the Lake Pontchartrain Causeway, a shallow draft barge system with a vactor system or vehicle is more appropriate.

Cementitious Permeable Pavement (CPP): Design Option III

For CPP, a 10-year lifetime was specified for structural integrity, and breakthrough capacity of the CPP. Table 28 summarizes the costs associated with the 2 in. thickness of CPP. The cost of replacing the 2 in. of existing concrete bridge deck with 2 in. of CPP is $939,567 and the cost over the 25-year project lifetime is $4.4 million. Additionally, since the existing bridge condition can facilitate a 4 in. thickness of CPP, a 4-in. CPP option is also evaluated. Table 29 illustrates that the costs for 4 in. of CPP is $1,133,181 and a total project cost of approximately $5.3 million. In order to maintain the hydraulic conductivity of the CPP, it is recommended that the pavement is swept at least monthly with a vacuum- assisted street sweeper. The LADOTD has currently contracted all elevated portions of I-10 to be swept twice monthly with a vacuum assisted street sweeper (Hammock, 2010) for the existing impervious pavement. Since a bi-monthly schedule maintains the hydraulic conductivity of CPP, this cost and frequency were used in order to compare CPP with traditional pavement.

Table 28

CPP project cost (2 in. thickness)

Component	Description	Years 0-10 ($)	Years 11-20 ($)	Years 21-25 ($)
Capital, Demolition, Disposal	Mill with CPP added	796,870	1,280,634	1,682,533
Maintenance	Street Sweeping	15,291	23,073	15,624
Contingency	10%	63,703	96,126	145,050
Engineering Fee	10%	63,703	96,126	145,050
Design Lifetime	Years	10 years	10 years	5 years
Total Cost		939,567	1,495,958	1,988,257
Total Project Cost (25 yrs)				**4,423,782**

Table 29

CPP project cost (4 in. thickness)

Component	Description	Years 0-10 ($)	Years 11-20 ($)	Years 21-25 ($)
Capital, Demolition, Disposal	Mill with CPP added	963,795	1,548,895	2,034,983
Maintenance	Street Sweeping	15,291	23,073	15,624
Contingency	10%	77,048	116,262	175,434
Engineering Fee	10%	77,048	116,262	175,434
Design Lifetime	Years	10 years	10 years	5 years
Total Cost		1,133,181	1,804,492	2,401,476
Total Project Cost (25 yrs)				**5,339,149**

While impervious pavement combined with street sweeping (the existing condition) was not explored as a design option, replacement cost of this existing condition (impervious Portland cement concrete, PCC) was examined. This cost evaluation is also useful when weighing design options. Table 30 represents the costs to resurface the existing impervious PCC concrete bridge deck. The cost of $800,290 represents the replacement costs of the existing upper 2-in. of bridge deck. A 10-year lifetime is assumed for structural integrity. Street sweeping with a vacuum assisted mechanical sweeper is employed twice a month (Hammock, 2010). A total project cost of $3.8 million was estimated over a 25-year lifetime.

Table 30

Impervious pavement (existing condition resurfacing)

Component	Description	Yrs 0-10 ($)	Yrs 11-20 ($)	Yrs 21-25 ($)
Capital, Demolition, Disposal	Mill and replace with PCC	676,791	1,087,658	1,428,997
Maintenance	Street Sweeping	15,291	23,073	15,624
Contingency	10%	54,104	81,641	123,193
Engineering Fee	10%	54,104	81,641	123,193
Design Lifetime		10 years	10 years	5 years
Total Cost		800,290	1,274,013	1,691,006
Total Project Cost (25 yrs)				**3,765,310**

CPP and BAMs: Design Option IV

Table 31 and Table 32 list the project costs for 2 in. of CPP combined with the BAM filter network as well as 4 in. of CPP and BAM filter network design options, respectively. The total design cost for the 2-in. CPP and BAMs network combination is $1,190,369 with a total project cost of $5.5 million. The BAMs media must be replaced every three years for the 2-in. thickness of CPP and BAMs combination. The total design cost for the 4-in. CPP and BAMs network combination is $1,373,835 with a total project cost of $6.3 million for the 25 year project lifetime. The BAMs media must be replaced every five years for the 4-in. thickness of CPP and BAMs combination. Media replacements for the combination options are less frequent than for the BAMs alone because the CPP offers primary treatment, and the BAM filters are only being employed for secondary treatment.

Table 31

CPP (2 in. thickness) and BAM filter network project cost

Component	Description	Years 0-10 ($)	Years 11-20 ($)	Years 21-25 ($)
Capital and Demolition		905,713	1,455,553	1,912,348
Maintenance	Street Sweeping	15,291	23,073	15,624
	Filter Cleaning	109,062	164,571	111,439
Replacements	Filter Media	14,885	22, 461	23,185
Disposal	Sub. D Landfill	608	918	1,127
Contingency	10%	72,405	109,256	164,862
Engineering Fee	10%	72,405	109,256	164,862
Design Lifetime		10	10	5
Total Cost		1,190,369	1,885,087	2,393,447
Total Project Cost (25 yrs)				**5,468,903**

Table 32

CPP (4 in. thickness) and BAM filter network project cost

Component	Description	Years 0-10 ($)	Years 11-20 ($)	Years 21-25 ($)
Capital and Demolition		1,072,638	1,723,815	2,264,798
Maintenance	Street Sweeping	15,291	23,072	15,623
	Filter Cleaning	109,062	164,570	111,438
Replacements	Filter Media	4,738	7,148	0
Disposal	Sub. D Landfill	$08	917	1,127
Contingency	10%	85,749	129,392	195,247
Engineering Fee	10%	85,749	129,392	195,247
Design Lifetime	Years	10	10	5
Total Cost		1,373,835	2,178,309	2,783,482
Total Project Cost (25 yrs)				**6,335,625**

Cost Comparison Summary

To compare each design option, costs categories are summarized in Table 33. Combined with constituent removal efficiency the cost per unit mass ($/lb) are compared with each

other and with the median costs from the Florida Department of Environmental Protection, FDEP database for Florida BMPs. Table 34 lists the total project costs for each design option and variation. Since the existing condition (impervious PCC) requires replacement every 10 years, Table 34 utilizes the differential costs of replacing impervious PCC with CPP in the last column of the table for all design options using CPP. This was done to compare the design options on the same level of service. Since CPP functions as a pavement and a BMP, the cost associated with the pavement component was subtracted to yield a differential cost for treatment.

Table 33

BMP cost comparison for annual TN, TP, and PM removal

Treatment Design Option	Cost ($/lb/yr)		
	TN	TP	PM
Conventional (Clarifier + Filters)	743	25,893	20
BAM Network	310	8,010	8
4 inches of CPP	468	13,453	14
BAMs + 2 inches of CPP	363	9,896	10
2 inches of CPP	327	9,547	10
BAMs + 4 inches of CPP	522	14,581	15
FL Database of BMP	1,876	10,448	41

Table 34

Total project cost comparison without regard to treatment levels

Design Option	Capital Cost ($)	O & M ($)	Disposal ($)	10% Contingency ($)	10% Engineering Fee ($)	Total Project Cost ($)	Differential Cost ($)
Conventional	1,535,990	303,517	360,297	300,000	300,000	2,799,804	2,799,804
BAMs	426,136	452,707	2,653	42,614	42,614	1,066,136	1,066,136
4" CPP	3,687,442	53,987	n/a	368,744	368,744	5,339,149	1,573,839
2"CPP+BAMs	3,465,224	499,590	2,653	346,522	346,522	5,468,903	1,703,593
2" CPP	3,048,794	53,987	n/a	304,879	304,879	4,423,782	658,473
4"CPP+BAMs	4,103,873	450,946	2,653	410,387	410,387	6,335,625	1,703,593

Without accounting for differences in treatment levels of each design option in Table 34, it appears that the 2-in. CPP design option is the most economical followed by the BAM filter network. However, Table 34 does not factor in the level of treatment; and therefore load reduction for TN, TP and PM. For example, the BAMs have much higher constituent removals than the 2-in. CPP design option because of the lower hydraulic and volumetric capacity of this thin section of CPP. In order to account for the differences in the level of treatment, design options were compared as costs per year, per pound of TN, TP, and PM removed. The pounds per year and the percentage removal are listed in Table 35. Table 35 illustrates that the BAM filter network is more economical than the 2-in. CPP design option.

Table 35
Comparison of yearly TSS, TN, and TP removal and cost

Design Option	Cost Per Year ($/yr)	TN			TP			PM		
		% Removal	lb/yr	$/lb/yr	% Removal	lb/yr	$/lb/yr	% Removal	lb/yr	$/lb/yr
Conventional	111,992	80	151	743	74	4.3	25,893	97	5,522	20
BAM	42,645	74	138	310	92	5.3	8,010	89	5,170	8
4" CPP	62,954	58	135	468	65	4.7	13,453	64	4,502	14
BAM + 2" CPP	68,144	81	188	363	95	6.9	9,896	93	6,589	10
2" CPP	26,339	35	81	327	38	2.8	9,547	38	2,658	10
BAM + 4" CPP	102,813	84	197	522	97	7.1	14,581	96	6,791	15

CONCLUSIONS

This study examined the event-based performance of a screened hydrodynamic separator (HS) for particulate matter and phosphorus transported in actual rainfall-runoff from a 1088 m^2 source area paved urban watershed. Eight independent rainfall-runoff events were examined and the entire volume of runoff from each event was treated by the screened HS. A series of four additional unit designs were examined as preferred and viable solutions for the given loadings.

The screened HS with the effective volume of 412 L was capable of reducing the particulate matter load in highway rainfall-runoff by from 38 to 70 percent and reducing phosphorus from 8 percent to 49 percent. In spite of highly variable event hydraulic (flow rate) and hydrologic (duration and intensity) characteristics, the screened HS showed consistently good separation capability for sediment fraction (> 75 μm) of particulate matter for all eight monitored events in the range of 76 percent (June 30, 2005) to 94 percent while for settleable and suspended fractions, PSE was highly variable from 3 to 57 percent and 1 to 43 percent in terms of mass removal, respectively.

Particle separation performance for a BMP to treat rainfall-runoff can be evaluated on a mass or concentration basis. For events which generate high volume of runoff, results from these two methods were similar. However, for low-runoff volume events, the difference between mass removal (%) and concentration reduction (%) became important. It was observed that while the screened HS provided 51 percent of mass removal, the actual ΔEMC between influent and effluent particulate matter across the unit was only 9.8 percent. This result indicates that volumetric confinement of particulate matter made more significant contribution to overall mass removal by the screened HS.

The consistent trend was found that there are more increases in fractions of sediment and settleable particles (> 25 μm) than fraction of suspended particle fraction (1-25 μm) when the total mass of particulate matter in rainfall-runoff increases. It indicates that the gravimetric PSD of particulate matter tend to skew toward the coarser particles as particle concentration in runoff increases. This relationship between influent particle concentration and PSD has an important inference regarding effect of particle concentration on BMP efficiency. There is inconsistent effect of influent concentration on particle separation efficiency. The relationship identified here in this study provides experimental proof

explaining that higher removal efficiency with higher loading concentrations was mainly due to coarse influent particle sizes, not necessarily because of high concentration itself.

The results of sieve analysis for the screened HS particles illuminated the fundamental differences in the role of screened and volute area for overall particle separation performance of the screened HS. Screened area was mainly separating very coarse particles with wide variation of PSD while volute area captured coarse particles with more consistent PSD between events. This distinct difference in granulometry between screened and volute particles is mainly due to the unique hydraulic internal configuration of the screen HS that influent particles are treated in a sequential order of screened and volute area. Variation of particle PSD entering into the volute area is lessened because of pre-separation performance by screen area while influent PSD directly load the screen area.

It is understood that the hydrologic and hydraulic conditions of rainfall-runoff event not only affects the treatment performance of stormwater UOPs but also governs, to a certain extent, the transport process of particulate matter from the surface of pavement in highways during the event, which in turn affects particle size distribution in runoff flow. However, the results from this study clearly demonstrated that the particle separation performance of the tested screened HS was influenced by influent particle size distribution far more strongly than hydrologic and hydraulic conditions. Higher runoff flow rate did not always ensure the transport of coarser particles from the pavement of highway and conveyance system to the screened HS. It appears that PSD transported by runoff during an event is related to granulometric characteristics of sediment source available on the surface of catchment prior to the start of event.

The regression line for particulate matter indicates that separation performance of the screened HS described by EMC percent reduction does vary depending on influent EMC. Data support the notion that high particle concentration itself does not promote removal by the screened HS, but it reflects the interaction between the screened HS and influent hydraulic and granulometric characteristics (i.e., flow rate and PSD).

Caution should be practiced while implementing results from this work, especially when attempting to compare the performance of the screened HS to other structural UOPs, or to a screened HS with different internal configuration and/or unit dimension. The reasons are that watersheds have substantially different parameters such as runoff characteristics, sources of

particulate matter with different physical and chemical nature, and dissimilar hydrologic and hydraulic transport patterns, but primarily different particle properties combined with differing hydraulic loads. This would highlight the importance of influent particle size distribution analyses in order to make an accurate assessment of separation performance for any BMP of interest, especially for the ones whose separation mechanisms are largely or in part dependent on gravitational settling. Additionally, all tests were conducted with cleaned and washed screened HS units to eliminate all scour potential which is a major concern for screened HS units.

This study examined the influence of hydrology on stormwater metal element speciation at the upper end of an experimental urban watershed in Baton Rouge, Louisiana. Measured concentrations, mass and flow parameters, indicate high intra-event and inter-event variability. Unsteady rainfall intensity and the associated runoff flow rates during the events are the primary causes of this variation. High intensity events decrease the pavement residence time, decreasing partitioning time and resulting in higher f_d values. However, the increased flow energy associated with high intensity events increases transport of constituents, particularly across the rising limb of the hydrograph. Results indicate that the transport of ionic constituents governs the speciation and ultimately the toxicity of the aqueous metal species. Non-colloidal particulate-bound metals, while not potentially an acute threat, are a potential reservoir of metals in the environment and as such are a potential chronic source of toxicity. Ionic and weakly bound organic and inorganic species of metals pose the most direct threat due to their bioavailability. During high flow rates, Cd, Cu, and Zn tended to exhibit low f_d values due to a more pronounced diluting effect on dissolved metal concentrations and a more pronounced delivery of particulate-bound metals. In addition, increased flow rates resulted in an increase in transport of particulate-bound metal mass, sequentially decreasing f_d values. However, Pb was unaffected by flow rates and remained predominately particulate-bound for each of the events.

Understanding the partitioning and speciation of heavy metals, as a function of hydrology, is crucial in designing in-situ strategies to control these metals at the upper end of the watershed. Investigations into the pollutant contributions of rainwater revealed insignificant ionic concentrations when compared to the runoff. In atmospheric rainwater, Cd, Cu, Pb, and Zn were primarily ionic due to the relatively acidic nature of Baton Rouge rainwater and the lack of complexing agents in the medium. When modeling the pavement runoff, results from MINTEQ indicate that ionic forms of Cd and Zn comprises a significant portion of the

total dissolved metal content of the runoff at the experimental site in this study. Despite variations in hydrology during events and when making comparisons between events, speciation of Cd and Zn displays little variability. The ionic forms remained dominant throughout these events. However, these dominant phases became more pronounced during the peak of the hydrograph when concentration of sulfates and alkalinity decreased. Speciation of Zn and Cd were not influenced by pH primarily because there was little variability in pH. With the exception of SO_4^{-2}, other anions did not play a significant role in the overall speciation.

Ionic species are extremely mobile and should be removed via adsorption or precipitation. These free metal complexes are readily available to aquatic biota and can be detrimental to the recipient (in particular Cd). Available forms of Cd and Zn were significantly higher than in previously published research (Revitt and Morrison, 1987), comprising as much as 96 percent and 94 percent of the total aqueous concentrations, respectively.

Pb and Cu have greater potential to form complexes with organics and carbonates than Cd and Zn. The range of DOM concentrations present in runoff had some influence on speciation. These effects are amplified at elevated DOM concentrations exceeding typical Baton Rouge levels. The concentrations of the organic complexes were directly and significantly influenced by flow rate. Cu was predominately available as $CuCO_3$ with the exception of the intense event occurring on May 30, 2002. Carbonate and hydroxide washoff resulted in the dominance of CuDOM followed by Cu^{+2}. Cu^{+2} is potentially toxic to aquatic life and the bioavailability of this constituent is a potential concern. The behavior of Pb was similar to that of Cu. Decreases in organic-bound Pb gave rise to increases in lead hydroxide and carbonate concentrations in all but one event in which concentrations of Pb^{+2} were significantly increased as a result of carbonate and hydroxide washoff. Available forms of Pb and Cu were significantly higher than in previously published research (Revitt and Morrison, 1987), comprising as much as 26 percent and 40 percent of the total aqueous concentrations, respectively. The dynamic behavior of Cu during intense events makes it a difficult ion to treat because the dominant species varies significantly as a function of hydrology. Analysis of the output revealed that PO_4^{-3} did not form significant complexes with any of the four metals.

This study indicates that Cd, Cu, Pb, and Zn can predominate as a variety of complexes throughout the duration of an event. Effective control of stormwater metal elements will

require physico-chemical mechanisms that account for the ionic, complexed, and particulate-bound species as well as the hydrology at the upper end of the urban watershed. Results generated from this research can be used in developing control strategies that target potentially bioavailable species of aqueous metals while physically removing the particulate-bound species. The ionic metal species, such as Cd^{2+} and Zn^{2+}, could be removed through adsorptive mechanisms. Media encapsulated in a negatively charged oxide coating could provide sufficient surface charge for removing the free metal ions as well as weakly complexed metals. The metal elements prone to complexation could be removed by increasing pH and alkalinity, thus promoting precipitation and complexation. One possible strategy could incorporate complexation and adsorptive mechanisms into a single unit by coating cementitious media with an oxide coating. Again, the oxide coating would remove ionic and weakly bound species (Zn and Cd) while calcite crystals protruding through the coating could complex Cu and Pb species. Particulates could be removed through the physical straining and filtration mechanisms of the media itself. These treatment units could provide significant removal of the typical hazardous metal elements in rainfall-runoff.

Urban stormwater can exhibit acute toxicity, depending on the source, storm characteristics, timing during the storm, and overall drainage design. Sansalone and Buchberger (1997) reported that flow rate and duration controlled the yield and size of transported solids. Generally, the fine particles contribute most to the lethal and sublethal toxicity due to their larger specific surface area that allow more contaminants including metals bound with them. In addition, fine solids could suspend in a water column and increase the exposure time for an organism. The larger particles are considered mostly as a chronic effect after they settled down. It is generally accepted that larger particles (>75 μm) play a minor role in the determination of acute toxicity. First flush was considered most toxic during the storm event in most cases because accumulation of contaminants and high concentration of road salts, solids and metals all contribute to increased first-flush toxicity. Sampling efforts focusing on the first flush are likely to produce more toxic responses, but volumes and durations of such flows are relatively small.

In this study, the early life stage organisms are more sensitive to runoff samples. The possible routes for toxicant entry in fish include direct uptake across the gills, uptake by the skin, and through ingestion of particles. Postlarvae may ingest the proper size fine particles, which could cause second exposure through the intestine. For the juvenile and adult fish, ingestion is not likely as an exposure pathway for fine particles, but the epithelial tissues in

gills are able to trap the suspended particles, which are less than 30 μm. Generally, they are not acute toxic to juvenile and adult stage fish. The raw samples containing suspended and settleable solids could facilitate the toxicity, especially for the first flush. Dissolved metals also contribute a lot because of their high bioavailability. A dynamic partitioning process happened between dissolved and particulate phases all the time, and it is very difficult to separate them or consider each of them alone.

There was a reasonable linear relationship between oxygen consumption rate and total weight of test fish. It might be due to the greater gill surface area per amount of body mass for smaller individuals of a species. Fish exposed to the fine solid solutions and real stormwater runoff exhibited an increase in oxygen consumption that was possibly associated with any variation in gill function. Fine particles (< 25 μm) at sufficient high concentration could be trapped by gill filaments and result in mucus precipitation on gill surfaces. The increased metabolism energy demand will be reflected in the increased ventilation (like gas exchange) of the fish. An increase in oxygen consumption rate in real stormwater runoff tests might be associated to not only particles, but also dissolved fractions. Fish gill as a respiratory organ also played an important role in excretion and elimination process. Part of the dissolved heavy metals uptake by fish could be transferred by biotransformation and removed from body by excretion. Thus more oxygen and energy will be needed in this case. No difference of oxygen consumption rate between settled and unsettled runoff samples suggested that settleable and sediment particles was not sufficient to significantly impact on the gill function. This result will be helpful in selecting better BMPs for controlling the quality of stormwater runoff and unit operation and process design on toxicity reduction.

With the particle gradation specified in the New Jersey testing, the standard “L-Unit” with a 2400-μm screen performance ranged from 22 to 44 percent removal efficiency based on suspended sediment concentration (SSC). Performance behavior was stable over the entire operating range and this stability was observed for all three concentration levels. In addition, for the entire set of experiments, there was no indication of clogging of the screen. Whether real rainfall-runoff gradations and granulometric characteristics are similar to the gradation specified, or are coarser and more variable during an event with more variable specific gravities as is the case in many rainfall-runoff treatment applications, there are several system design recommendations for improved HS performance. The first recommendation is to use a 1200-μm or smaller screen as long as the potential for clogging is low. Given the

gradation specified in these tests, clogging potential is low. The second recommendation is to increase the sump capacity and change the sump design to reduce scour and to apply frequent clean-out schedules.

Given the PMSU20_20 configuration, three levels (100, 200, and 300 mg/L) of influent particle loading conditions, the separation efficiency of the 84-in. diameter with a 2400 μm screen ranged from 70 percent to 43 percent with the arithmetic mean of 52.9 percent, for tested flow rates that ranged from 50 gpm to 603 gpm, based on suspended sediment concentration (SSC). For the 60-in. diameter unit, SSC removal ranged from 67 percent to 35 percent with the arithmetic mean of 51.5 percent at the tested flow rates that ranged from 26 gpm to 338 gpm, while the 72-in. diameter provided 68 percent to 38 percent of SSC removal with the arithmetic mean of 52.0 percent for the range of flow rates tested (38 gpm to 467 gpm). At same flow rate within the tested range, the 84 in. diameter always performed the best followed by the 72-in. and 60-in. unit in terms of SSC removal efficiency, while performance differences between each diameter unit became minimized at the lowest operating flow rate. There was no indication of clogging of the screen but the same recommendations for the L-unit for sump design, scour and clean-out apply.

From the results presented in this report, it was re-emphasized that the fate of the performance level was determined mainly based on the size of unit since these are largely gravitational settling units (the size determines particle and hydraulic residence time), influent particle gradation (which affects settling velocity with particle density), operating flow rate, the use of a 1200 μm screen, and a sediment weir. Although SSC removal can be further improved by a series of optimization processes which might incorporate modification of internal geometry and/or configuration (i.e. SA/TA), screen aperture size, horizontal (central or eccentric) and vertical location of screen, inlet configuration (open channel or closed channel, and inlet area), and sump design (shear ring, volume, shape), the results with the specified NJCAT gradation demonstrated that there was not a consistent increase or decrease in removal efficiency for SSC on a gravimetric basis with increasing loading concentrations (from 100 to 300 mg/L as SSC) across the entire flow rate range for all tested diameters of unit.

It was indicated that using 2400 μm did improve overall SSC removal marginally (but still statistically significant). Such an improvement was mostly attributable to the enhanced

performance of the screen area (2 to 8 percent increase with respect to influent mass) when 4700 μm was replaced with 2400 μm. These results also infer that 2400 μm size of screen aperture will enhance the performance of the screen area and reduce the dependence on the volute area for overall SSC removal. It is important to recognize that particle separation performance by the screen area was independent on overall unit diameter, but it was only a function of surface overflow rate as long as the screen geometry and influent PSD were maintained constantly. The particle trap efficiency exhibited by the volute section of 5.0-ft. in diameter ranged from 50 percent to 67 percent with respect to total captured mass across the range of operating flow rates, from 25 gpm to 315 gpm.

Regarding the treatment of rainfall-runoff water, the management represents a significant challenge requiring economic resources equal to or greater than domestic wastewater. The complexity and challenges of urban stormwater management, beyond mitigating flooding, are now recognized as embodied in current debates over total maximum daily loads (TMDLs) and nutrient criteria. While managing stormwater from at-grade pavement systems is challenging, management of elevated pavement systems such as bridges represents an even more difficult challenge. Southeastern states, in particular coastal and the expansive inland receiving waters of peninsular Florida and South Louisiana, have been traversed by contemporary transportation infrastructure, often elevated with direct discharges to receiving waters. Nutrients, metals, and PM are directly discharged to receiving waters with the potential to generate acute and chronic toxicity. Conventional stormwater designs typically require detention/retention, are land-intensive and can be at odds with the context-sensitive nature of land-water interfaces that require innovative solutions.

The metrics that characterize the preferred treatment solution described in the previous chapter demonstrates that the selected option provides a significant reduction in TN, TP, and PM loading to the receiving water while meeting regulatory criteria at a lower cost/benefit ratio with respect to design alternatives. However, it is important to note that, in a popular recreational area, the aesthetic benefit of low footprint treatment options is also of significant value as a context-sensitive attribute. While BAM filters are preferred to CPP for economic reasons, BAM filters are also preferred to conventional treatment as they provide a smaller footprint. In addition, a portion of the BAM filters are hidden from view below the water surface. The CPP combined with the BAM filters provides both primary and secondary treatment adding redundancy to the system and providing a higher total treatment. The reduction in TP, TN and PM loading provided by the BAMs network closely followed by the

2 in. of CPP design options reduce eutrophication, turbidity and metal discharges to City Park Lake, thereby providing aesthetic and water chemistry benefits. In addition, the removal of nutrients will help return the lake towards the ecological diversity of Bayou Duplantier. Although this design illustrated results for TN and TP, the BAM and CPP are also effective adsorptive systems for dissolved metals. The integration of manganese oxide as a media coating for the BAMs and as an admixture in the CPP provided significant metal adsorption capacity as well as filtration by these design options. The adsorption of metals, such as Zn, Cu and Cd whether in the BAM filters or the CPP will benefit the ecology of the lake and prevents bio-magnification of metals. Detailed design options, feasibility, and costs are illustrated for the I-10 bridge over City Park Lake in this report. There are over 10,000 bridges in Louisiana of which over 80 percent of these bridges are over water; providing significant potential for extensibility of these design results to infrastructure crossing land-water interfaces across Louisiana.

RECOMMENDATIONS

Transport and in-situ treatment of source area particles metals and TP during the urban rainfall runoff is a complicated phenomenon because of wide gradation of particles and TP always dynamically partitioning between dissolved and particulate bound phase. Appropriate sampling strategy forms the corner stone to represent what was really occurring in the rainfall runoff. Manual sampling across the full flow direction through a wide open mouth container could capture even coarse particles representatively. In addition, the replicate sediment fraction was sieved and quantified by 12-L containers and duplicate settleable and suspended fractions were obtained from a 1-L quiescent settling test, which allowed the minimal experimental error by operating large volumes of solution and large concomitant values of particulate mass. Finally, the identification of three categories of particulate matter (sediments, settleables, and suspended) and P associated with would address the treatability and select the best unit operations and processes (UOPs).

After extensive testing of several screened hydronamic separators, results indicated that treatment and maintenance requirements were not sustainable for such units. Therefore four additional green infrastructure treatment designs were examined: (1) conventional clarification and filtration, (2) engineered oxide-admixture CPP (cementitious permeable pavement), (3) a network of BAM (Buoyant Adsorptive Media) filters in the lake, and (4) CPP and a BAM network. The high maintenance, scour potential, deteriorating inter-event water chemistry and lower inter-event treatment efficiency of the screened hydronamic separator units did not make such units viable treatment solutions compared to the four treatment designs illustrated. The metrics that characterize the preferred design treatment solution demonstrates that the selected option provides a significant reduction in TN, TP, metals, and PM loading to the receiving water while meeting regulatory criteria at a lower cost/benefit ratio with respect to design alternatives. However, it is important to note that in a popular recreational area the aesthetic benefit of low footprint treatment options is also of significant value as a context-sensitive attribute. Based on data analysis and process modeling, the BAM network is the most economical solutions, followed by CPP. Treatment and load reduction targets are achieved for the recommended BAM design and CPP with BAM network. Costs are lower than conventional treatment or current treatment databases. While BAM filters are preferred to CPP given the economics illustrated in Table 34, BAM filters are preferred to conventional treatment as they provide a smaller footprint. In addition, a portion of the BAM filters are hidden from view below the water surface. The CPP combined with the BAM filters provides both primary and secondary

treatment adding redundancy to the system and providing a higher total treatment. Given the current promulgation of nutrient criteria, Table 35 summarizes the treatment cost per kg of PM, TN, and TP for each treatment option. The reduction in TP, TN, and PM loading provided by the BAMs network, closely followed by the 2 in. of CPP design options, reduce eutrophication, turbidity, and metal discharges to City Park Lake, thereby providing aesthetic and water chemistry benefits. In addition, the removal of nutrients will help return the lake to the ecological diversity of Bayou DuPlantier. Although this design illustrated results for TN and TP, the BAM and CPP are also effective adsorptive systems for dissolved and particulate-bound metals. The integration of manganese oxide as a media coating for the BAMs and as an admixture in the CPP provided significant metal adsorption capacity as well as filtration by these design options. The adsorption of metals such as Zn, Cu, and Cd, whether in the BAM filters or the CPP, will benefit the ecology of the lake and prevent bio-magnification of metals. Detailed design options, feasibility, and costs are illustrated for the I-10 bridge over City Park Lake. There are over 10,000 bridges in Louisian of which 80 percent are over water. Thus, there is significant potential for extending these designs to infrastructure crossing land-water interfaces across Louisiana.

The major recommendation is to optimize the utilization of BAMS, or CPP in combination with BAMS, to capture more of the fractions of particulate matter, metals, and nutrients within an economic and context-sensitive design.

ACRONYMS, ABBREVIATIONS, AND SYMBOLS

BAM	Buoyant Adsorptive Media
BMP	Best Management Practice
Cd	Cadmium
Cl	Chlorine
CPP	Cementitious Permeable Pavement
CSO	Combined Sewer Overflow
$\overline{C}(t)$	Average concentration
Cu	Copper
Zn	Zinc
d_{50m}	Particle size finer than 50 percent in mass
DO	Dissolved oxygen
DOC	Dissolved organic carbon
DOM	Dissolved organic matter
f_d	Dissolved fraction
EMC	Event Mean Concentration
gpm	gallons per minute
GUI	Graphic User Interface
HS	Hydrodynamic Separator
ICP-MS	Inductive coupled plasma mass spectrometer
LT_{50}	The median lethal time
MB	Mass Balance
M_{in}	Total influent particle mass over entire event duration
MINTEQ	An equilibrium speciation model
M_{out}	Total effluent particle mass over entire event duration
MS4	Municipal Separate Storm Sewer Systems
$M_{screened}$	Dry particle mass of recovered from screened area
M_{volute}	Dry particle mass of recovered from volute area
n	Sample numbers coinciding with the last sample collection
NJCAT	New Jersey Corporation for Advanced Technology
NOET	No Observed Effective Time
NPDES	National Pollutant Discharge Elimination System
P	Phosphorus
Pb	Lead

PCC	Portland cement concrete
PM	Particulate matter
PMSU	Precast Manhole Stormwater Unit
PND	Particle Number Distribution
PR	Percent Removal
PSD	Particle Size Distribution
PSE	Particle Separation Efficiency
$\overline{Q}(t)$	Average flow rate
QA/QC	Quality analysis/Quality control
SLR	Surface Loading Rate
SSC	Suspended solids concentration
TDS	Total dissolved solids
TMDL	Total Maximum Daily Load
TN	Total Nitrogen
TOC	Total Organic Carbon
TP	Total phosphorous
TS	Total solids
TSS	Total suspended solids
TVC	Total volume concentrations
UOPs	Unit Operation and Processes
V_{O2}	Oxygen consumption rate
$\Sigma M(t)$	Total mass of particulate matter over entire event duration
$\Sigma V(t)$	Total runoff volume over entire event duration
ΔParticle	Particle separation efficiency (%)

REFERENCES

1. "A Review and Evaluation of Literature Pertaining to the Quality and Control of Pollution from Highway Runoff and Construction." Center for Research in Water Resources, Bureau of Engineering Research, University of Texas at Austin, 1993. 160 pp.

2. Akan, A. O., and Houghtalen, R. J., Urban Hydrology, Hydraulics, and Stormwater Quality: Engineering Applications and Computer Modeling. Hoboken, N.J.: J. Wiley & Sons, 2003.

3. Allison, J.D; Brown, D.S; and Novo-Gradac, K.J., "MINTEQA2/PRODEFA2, A Geochemical Assessment Model for Environmental Systems: Version 3.0 User's Manual." EPA/600/3-91/021, 1991. 115 pp.

4. American Public Health Association, American Water Works Association, and Water Pollution Control Federation, "Standard Methods for the Examination of Water And Wastewater" (19th ed.): Washington, D.C., American Public Health Association, 1995.

5. Ammann, A.A., "Speciation of Heavy Metals in Environmental Water by Ion Chromatography Coupled to ICP-MS." *Analytical and Bioanalytical Chemistry*, Vol. 372, No. 3, pp. 448-452, February, 2001.

6. ASTM. "Standard Practice for Dry Preparation of Soil Samples for Particle-Size Analysis and Determination of Soil Constants." *ASTM D 421-85*, West Conshohocken, Pa. Vol. 04.08, 1993. pp. 8-9.

7. ASTM, "Standard Test Method for Specific Gravity of Soil Solids by Gas Pycnometer." *ASTM D 5550-94*, West Conshohocken, Pa. Vol. 04.08, 1994. pp. 376-379.

8. Barrett, M.E., Zuber, R.D., Collins, E.R., Malina, J.F., Charbeneau, R.J. and Ward, G.H., "A Review and Evaluation of Literature Pertaining to the Quality and Control of Pollution from Highway Runoff and Construction." Center for Research in Water Resources, Bureau of Engineering Research, University of Texas at Austin, 1993. 160 pp.

9. Barrett, M.E; Malina, J.F; Charbeneau, R.J; and Ward, G.H., "Characterization of Highway Runoff in Austin Texas area." Center for Research in Water Resources, Bureau of Engineering Research, University of Texas at Austin, 1995. 35 pp.

10. Bent, G.C; Gray, J.R; Smith, K.P; and Glysson, G.D., Measuring Sediment in Highway Runoff: U.S. Geological Survey Open File Report 00-497, 2000. 51 pp.

11. Bertrand, J.L; Chebbo, G; and Saget, A. "Distribution of Pollutant Mass vs. Volume in Stormwater Discharges and the First Flush Phenomenon." *Water Res.*, 32(8), 1998. pp. 2341-2356.

12. Breault, R. and Granato, G., "A Synopsis of Technical Issues of Concern for Monitoring Trace Elements in Highway and Urban Runoff." U.S. Geological Survey Open File Report 00-422 Northborough, Massachusetts, 2000.

13. Chow, V. T., Maidment, D. R., and Mays, L. W., Applied Hydrology. New York: McGraw Hill. Chromatography Coupled to ICP-MS." *Analytical and Bioanalytical Chemistry*, Vol. 372, No. 3, February, 1988. pp. 448-452.

14. Cooper, P.I., The Absorption of Solar Radiation in Solar Stills. Solar Energy, 12(3), 1969. pp. 333-346.

15. Cristina C., Tramonte J., and Sansalone J.J., "A Process Design Selection Methodology for Separation of Traffic-Generated Sediments In Runoff," *Journal of Water, Air and Soil Pollution*, 136 (5), 33-53, May 2002.

16. Cristina, C., and Sansalone, J., Kinematic Wave Model of Urban Pavement Runoff Quantity Subject To Traffic Loadings. *ASCE Journal of Environmental Engineering*, 129(7), 2003. pp. 629-636.

17. Dean, C.M., Sansalone J.J., Cartledge, F.K., and Pardue, J.H., "Influence Of Hydrology on Rainfall-Runoff Metal Element Speciation," *Journal of Environmental Engineering*, 131 (4), April 2005. pp. 632-642.

18. Deletic, A.B. and Maksimovic, C.T., "Evaluation of Water Quality Factors in Storm Water Runoff from Paved Areas." *Journal of Environmental Engineering,* American Society of Civil Engineers, Vol. 124, No. 9, September, 1998. pp. 869-879.

19. DEQ, 2010. EPA recognizes DEQ's efforts to address wastewater concerns with stimulus money. DEQ Press Release. www.deq.state.la.us/-portal/portals/0/news/pdf/lettersfromEPA.pdf.

20. DeWiest, D., and Livingston, E. The Florida Stormwater, Erosion, and Sedimentation Control Inspector's Manual. Florida Department of Environmental Protection, Tallahassee, FL. http://www.dep.state.fl.us/water/nonpoint/erosion.htm, 2000.

21. Dura-Cast Products, Inc. Dura-Cast Products Inc, Home. Retrieved April 2010, from Dura-Cast Products: http://www.duracast.com/content/, 2003.

22. East Baton Rouge Landfill Tipping Fees. (D. Brooks, Interviewer). February 2010.

23. FDEP. TMDL Grants Cost per Pound. Florida Department of Environmental Protection, 2009.

24. FDOT, Application Assessment for the Florida Airports Stormwater Study, June 29, 2007. Retrieved from: http://www.florida-aviation-database.com/dotsite/pdfs/Application.pdf.

25. Federal Register, Nutrient Criteria Development; Notice of Ecoregional Nutrient Criteria, 68(3), 2003. www.epa.gov/fedrgstr/EPA-WATER/2003/January/Day-06/w176.htm.

26. Federal Register, Water quality standards for the state of Florida's lakes and flowing waters. Vol. 75, No. 16, 2010. (40 CFR Part 131) January 26, 2010.

27. Federal Reserve. Selected Interest Rates, from Federal Reserve Statistical Release: http://www.federalreserve.gov/releases/h15/data/htm, retrieved February 15, 2010.

28. Flores-Rodriquez, J.; Bussy, A.L; and Thevenot, D.R. "Toxic Metals in Urban Runoff: Physico-Chemical Mobility Assessment using Speciation Themes." *Water Science Technology*, Vol. 29, No. 1-2, pp. 83-93, 1994.

29. Florida Department of Transportation RCI Bridges, 2009. Retrieved February 15, 2010, from Florida Department of Transportation, http://www.dot.state.fl.us.

30. Freeze, R. A. c, and Cherry, J. A. Groundwater. Englewood Cliffs, N.J.: Prentice-Hall. 37, 1979.

31. Gallade Chemical. Chemical Distributer, 2007. Retrieved April 14, 2010, from Gallade Chemical: http://www.galladechem.com/.

32. Garton, E.R., Jr. The effects of highway construction on the hydrogeologic environment at Bowden, West Virginia. Hydrologic Problems in Karst Regions, Dilamarter, R.R., and Csallany, S.C., eds. Western Kentucky University, Bowling Green, 1977. pp. 439-449.

33. Gibbs, J. Easement Land Cost Appraisal Estimation Method. (H. Carter, Interview, April, 2010).

34. Gjessing, E.; Lygren, E.; Anderson, S. "Acute toxicity and chemical characteristics of moderately polluted runoff from highways." *Sci. of the Total Envir.*, 15(33), 1984. pp. 225-232.

35. Greenburg, A., Clesceri, L., and Eaton, A., eds. Standard methods for the examination of water and wastewater (19th Ed.) Am. Public Health Assn., Washington, D.C., 1995.

36. Grobler, E., Vuren, J.H.J.U.; and Dupreez, H.H., Routine oxygen consumption of Tilapia sparrani (Cichilidae) following acute exposure to atrazine. Comp. Biochem. Physiol. 93C(1), 1989. pp. 37-42.

37. Hammock, T. LADOTD Maintenance Costs for Elevated Portions of I10. (H. Carter, Interview, February, 2010).

38. Hartigan, J.P. Basis for design of wet detention basin BMPs. Design of Urban Runoff Quality Controls. ASCE. New York, NY, 1989. pp. 122-144.

39. Hayter A.J., Probability and Statistics for Engineers and Scientists (2nd Edition). Florence, KY: Duxbury Press, 2002. pp. 628-629; 657-658.

40. Hoins, U.; Charlet, L.; and Sticher, H. "Ligand Effect on the Adsorption of Heavy

Metals: The Sulfate – Cadmium – Geothite Case." *Water, Air, and Soil Pollution*. (68), Kulwer Academic Publishers, 1993. pp. 241-255.

41. Huber, W. "Contaminant transport in surface water." Handbook of hydrology, D.R. Maidment, ed., McGraw-Hill, New York, 1993, pp. 14.1-14.50.

42. Imbrium Systems Inc. (n.d.). Imbrium Home. Retrieved February 2010, from Imbrium Systems: http://www.imbriumsystems.com/.

43. James, R. "Solids in Stormwater Runoff." Water Resources Management, 1993. http://www.stormwaterauthority.org/assets/45solids.pdf, 1999.

44. Klein, C, and Hurlbut, C.S. Manual of Mineralogy. John Wiley & Sons, 1993.

45. Kobriger, N.P., & Geinopolos, A., "Sources and Migration of Highway Runoff Pollutants." Rep. FHWA/RD-84/059 (PB86-227915), U.S. Dept. of Transp., Fed. Hwy. Admin, Washington, D.C., 1984.

46. Kuang, X., Kim, J.Y., Gnecco, I., Raje, S., Garofalo, G., and Sansalone, J.J. Particle separation and hydrologic control by cementitious permeable pavement. *Journal of the Transportation Research Board 2025*, 2007. pp. 111-117.

47. Labye, Y., Design and Optimization of Irrigation Distribution Networks. FAO Irrigation and Drainage Paper, 44. Rome: Food and Agriculture Organization of the United Nations, 1988.

48. LADOTD. US 90 Deck Overlay Bayou Des Allemands Bid Tabs. Baton Rouge: LADOTD, 2008.

49. LADOTD. Department of Data Management, Highways and Major Roads, 2010.

50. Langston, W.J., Availability of Arsenic to Estuarine and Marine Organisms: A Field and Laboratory Evaluation. Mar. Biol., 80, 1984. pp. 143-154.

51. Lin, H., Ying, G. and Sansalone, J. "Granulometry of Non-colloidal Particulate Matter Transported by Urban Runoff," Water, Air, & Soil Pollution, Vol. 198, No. 1-4, 2009. pp 269-284.

52. Liu, B., Berretta, C., Gnecco, I., Ying, G. and Sansalone, J. “Control of Highway Stormwater during Event and Interevent Retention in Best Management Practices”, Journal of the Transportation Research Board, Vol. 2120, 2009. pp 115-122.

53. Liu, B., Sansalone, J., and Ying, G., Volumetric Filtration of Rainfall-Runoff: (I) Event-Based Separation of PM Fractions, 2010.

54. Liu, B., Ying, G., and Sansalone, J. “Volumetric Filtration of Rainfall-Runoff: (I) Event-Based Separation of Particulate Matter”, Journal of Environmental Engineering, 136(12), 2010. pp. 1321-1330

55. Liu, D., Sansalone, J.J., and Cartledge, F.K., Adsorption kinetics for urban rainfall-runoff metals by composite oxide-coated polymeric media. Journal of Environmental Engineering, 131, 2005A. pp. 1168-1177.

56. Liu, D., Sansalone, J.J., M.A.S.C.E, and Cartledge, F.K. Comparison of Sorptive Filter Media for Treatment of Metals in Runoff. Journal of Environmental Engineering, 131(8), 2005B. pp. 1178-1186.

57. Louisiana Department of Environmental Quality, Developing Nutrient Criteria for Louisiana, 2006. www.deq.louisiana.gov/portal/tabid/69/Default.aspx

58. Louisiana Department of Environmental Quality, DEQ Annual Report 2008-2009, 2009. http://www.deq.state.la.us/portal.

59. Ma, J., Ying, G. and Sansalone, J. “Transport and Distribution of Particulate Matter Phosphorus Fractions in Rainfall-Runoff from Roadway Source Areas”, Journal of Environmental Engineering, 136(11), 2010. pp. 1197-1205

60. Makepeace, D., Smith, D., and Stanley, S. “Urban Stormwater Quality: Summary of Contaminant Data.” *Critical Reviews in Environmental Science and Technology*, 25(2), 1995. pp. 93-139.

61. McBean, N.R.; Snodgrass, W.; and Mostrenko, I. “Sample Size Needs for Characteriza-tion Pollutant Concentrations in Highway Runoff.” *J. Enviro Engrg.*, ASCE, 123(10), October, 1997. pp. 1061-1065.

62. McCuen, R. Hydrology, FHWA-SA-96-067, Federal Highway Administration, Washington, D.C., 1996.

63. McKenzie, D. J., Irwin, G. A., Water-quality Assessment of Stormwater Runoff from a Heavily used Urban Highway Bridge in Miami, Florida – USGS 83-4153. U.S. Geological Survey and Florida Department of Transportation, 1983.

64. McKenzie, D.J.; and Irwin, G.A. Water-quality Assessment of Stormwater Runoff from a Heavily Used Urban Highway Bridge in Miami, Florida. USGS Water Resources Investigations Report 83-4153, Tallahassee, FL, 1983.

65. Mehta, P.K. Concrete Structure, Properties and Materials. New Jersey: Prentice-Hall Inc., 1986.

66. Montgomery, James M. Consulting Engineers, Water Treatment Principles and Design. New York: Wiley, 1985.

67. Morrison, G.M., Revitt, D.M. and Ellis, J.B. "Metal Speciation in Separate Stormwater Systems." *Water Science Technology*, Vol. 22, No. 10/11, 1990. pp. 53-60.

68. Morrison, G.M.; Batley, G.E.; and Florence, T.M. "Metal Speciation and Toxicity." *Chemistry in Britain*, August, 1989. pp. 791-796.

69. Muschack, W. "Pollution of Street Run-Off by Traffic and Local Conditions." *Science of the Total Environment*, 93, 1990. pp. 419-431.

70. Naghavi, B., Singh, V.P., Yu, F. X. LADOTD 24-hour Rainfall Frequency Maps and I-D-F Curves. Louisiana Transportation Research Center. Summary Report, No. FHWA/LA-91/236, 1991.

71. NCDC (National Climatic Data Center), 1979, September 1 to 2009, September 1. http://cdo.ncdc.noaa.gov/dly/DLY. Retrieved February 26, 2010, from Record of Climatological Web site: http://www7.ncdc.noaa.gov/CDO/cdo.

72. Office of Employment Security. 1988 Lousiana Employment and Wages. Baton Rouge: Lousiana Department of Labor, 1989.

73. Ormsbee, L.E. Rainfall Disaggregation Model for Continuous Hydrologic Modeling. Journal of Hydraulic Engineering, 115(44), 1989. pp. 507-525.

74. Pathapati S. and Sansalone J., "Combining Particle Analyses with Computation Fluid Dynamics Modeling to Predict Hetero-disperse Particulate Matter Fate and Pressure Drop in a Passive Runoff Radial Filter", ASCE J. of Environmental Engineering, 135(2), 77-85, 2009.

75. Paulsen, Janis. Verified Impaired Waters: Cycle NCDC (National Climatic Data Center), (1999, September 1 to 2009, September 1). http://cdo.ncdc.noaa.gov/dly/DLY. Retrieved April 01, 2010, from Record of Climatological Web site: http://www7.ncdc.noaa.gov/CDO/cdo.

76. Rawls, W.J., Brakensiek, D.L., & Miller, N. Green-Ampt Infiltration Parameters from Soils Data. ASCE Journal of Hydraulic Engineering, 109(1), 1983. pp. 62-70.

77. Reed Construction Data. RSMeans Building Construction Data 68th Annual Edition. Kingston, MA: RSMEANS, 2009.

78. Reemtsma, T., Gnirss, R. and Jekel, M. "Infiltration of Combined Sewer Overflow and Tertiary Treated Wastewater: An Integrated Lab and Field Study on Various Metals." *Water Environment Research*, Vol. 72, No. 6, November/December, 2000. pp. 644-650.

79. Reible, D.D., and McCutcheon, S.C. Fundamentals of Environmental Engineering. CRC Press, 2003.

80. Reich Associates, City Park/University Lake Management Plane Project No. 90-MP-EPA-0066 (Draft). City of Baton Rouge/Parish of East Baton Rouge Department of Public Works. Baton Rouge, Louisiana, 1991.

81. Representative, C. E. (2010, April 15). Vactor Service and Basin Cleaning Cost Estimates. (H. Carter, Interviewer)

82. Revitt, D.M. and Morrison, G.M. "Metal Speciation Variations within Separate Stormwater Systems." *Environmental Science and Technology Letters*, Vol. 8, 1987. pp. 373-380.

83. Reynolds, T. D., and Richards, P.A. Unit Operations and Processes in Environmental Engineering. PWS Publishing Company, Boston, 1995.

84. Sansalone, J., Kuang X., and Ranieri, V. Permeable Pavement as a Hydraulic and Filtration Interface for Urban Drainage. *ASCE Journal of Irrigation and Drainage*, 134(5), 2008. pp. 666-674.

85. Sansalone, J.J., Koran, J., Buchberger, S.G., and Smithson, J., "Physical Characteristics of Highway Solids Transported During Rainfall," *Journal of Environmental Engineering*, 124 (5), 427-440, May 1998.

86. Sansalone, J. Lin, H., and Ying, G., "Experimental and Field Studies of Type I Settling for Particulate Matter Transported by Urban Runoff*," Journal of Environmental Engineering*, Vol. 135, No. 10, 2009. pp 953-963.

87. Sansalone, J., and Ma, J. Parametric Analysis and Breakthrough Modeling of Stormwater Phosphorus from Al-oxide Filter Media, 2010.

88. Sansalone, J., Lin, H., and Ying, G. "Experimental and Field Studies of Type I Settling for Particulate Matter Transported by Urban Runoff," *Journal of Environmental Engineering*, 135(10), 2009A. pp. 953-963.

89. Sansalone, J., Liu, B., and Kim, J. Volumetric Clarifying Filtration of Urban Source Area Rainfall Runoff. Journal of Environmental Engineering, 135(8), 2009B. pp. 609-620.

90. Sansalone, J., Liu, B., and Ying, G. "Volumetric Filtration of Rainfall-Runoff: (II) Event-based and Inter-event Nutrient Fate," *Journal of Environmental Engineering*, 136(12), 2010. pp. 1331-1340.

91. Sansalone, J., Ying, G. and Lin, H. (2010). "Distribution of Metals for Particulate Matter Transported in Source Area Rainfall-Runoff," *Journal of Environmental Engineering*, Vol. 136, No. 2, 172-184.

92. Sansalone, J.and Ying, G. “Partitioning and Granulometric Distribution of Metal Leachate from Urban Traffic Dry Deposition Particulate Matter Subject to Acidic Rainfall and Runoff Retention,” Water Research, Vol. 42, No. 15, 2008. pp. 4146-4162.

93. Sansalone, J.J. “Physical and Chemical Nature of Urban Stormwater Runoff Pollutants,” in *Management of Wet-Weather Flows in the Watershed*, Fields, R. and Sullivan, D., (eds), CRC Press, Boca Raton, 2002. pp. 43-66.

94. Sansalone, J.J. and Buchberger, S.G. “Partitioning and First Flush of Metals in Urban Roadway Stormwater.” *Journal of Environmental Engineering*, American Society of Civil Engineers, Vol. 123. No. 2, February, 1997. pp. 134-143.

95. Sansalone, J.J., Hird, J.P., Cartledge, F.K., and Tittlebaum, M. E., Event-Based Stormwater Quality and Quantity Loadings from Elevated Urban Infrastructure Affected By Transportation. Water Environment Research, 77, 2005. pp. 348-65.

96. Sansalone, J.J., Hird, J.P., Cartledge, F.K., and Tittlebaum, M.E., “Event-based Stormwater Quality and Quantity Loadings from Elevated Urban Infrastructure Affected by Transportation” Water Environment Research, 77(4), 2005. pp. 348-365.

97. Sansalone, J.J., Koran, J.M., Smithson, J.A., and Buchberger, S.G. “Physical Characteristics of Urban Roadway Solids Transported During Rain Event” *Journal of Environmental Engineering*, ASCE, 124(5), 1998. pp. 427-440.

98. Savoy, H., Baton Rouge Easement Land Cost Estimation, March, 2010. (H. Carter, Interviewer).

99. Shaheen, D. G. “Contribution of Urban Roadway Usage to Water Pollution” EPA-600/2-75-004 U.S. Government Printing Office, Washington D.C., 1975.

100. Sheng, Y., Ying, G. and Sansalone, J. “Differentiation of Transport for Particulate and Dissolved Water Chemistry Load Indices in Rainfall–Runoff from Urban Source Area Watersheds,” *Journal of Hydrology*, Vol. 361, No. 1-2, 2008. pp. 144-15.

101. Snyder, S. H., Stormwater Measures for Bridges: Coastal Nonpoint Source Management in South Carolina. National Conference on Urban Runoff Management: Enhancing Urban Species of Heavy Metals in Highway Runoff." *Transportation Research Record* 1017, 1995. pp. 56-62.

102. Strecker, E.W.; Quigley, M.M.; Urbonas, B.R.; Jones, J.E.; and Clary J.K. "Determining Urban Stormwater BMP Effectiveness." *J Water Res. Pl.* ASCE, 127 (3), 2001. pp. 144-149.

103. Swartz, R. C.; Ditsworth, G. R.; Schults, D. W.; and Lamberson, J. O. Sediment Toxicity to a Marine Infaunal Amphipod: Cadmium and Its Interaction with Sewage Sludge. Environ. Res., 18, March, 1985a. pp. 133-153.

104. Sykes, C., Rinker Concrete Cost, March 29, 2010. (H. Carter, Interviewer).

105. Teng, Z., and Sansalone, J.J., "In-Situ Stormwater Treatment and Recharge through Infiltration: Particle Transport and Separation Mechanisms," *Journal of Environmental Engineering*, 130 (9), September 2004. pp. 1008-1020.

106. Tia, M. Concrete Mix Design, Lecture Notes. (2008). CE Materials. University of Florida, 2008.

107. U. S. Environmental Protection Agency (USEPA). National Water Quality Inventory-1996 Reports To Congress. Rep., Office of Water, USEPA, Washington, D.C., 1996.

108. U. S. Environmental Protection Agency. Overview of Impaired Waters and Total Maximum Daily Loads Program, 2010. http://www.epa.gov/owow/-tmdl/intro.html.

109. U.S. Environmental Protection Agency. City Park/University Lakes Management Plant: Existing Factors and Issues – Public Participation. EPA Project No. 90-MP-EPA-0066, 1991.

110. U.S. Environmental Protection Agency, Ecoregional Nutrient Criteria – Fact Sheet, 2002. www.epa.gov/waterscience/criteria/nutrient/ecoregions/.

111. U.S. EPA, Quality Criteria for Water. Office of Water Regulation and Standards, US Government Printing Office (PB81-226759), Washington, DC 20460. EPA 440/5-86-001, 1986.

112. Weather Underground, Inc. History for Baton Rouge, LA. Retrieved April 8, 2010, from http://www.wunderground.com/history/airport/KBTR/2008/1/1/CustomHistory.html?dayend=1&monthend=1&yearend=2009&req_city=NA&req_state=NA&req_statename=NA, 2008, January 1 to 2009, January 1.

113. Werner, E. Effects of Highways on Karst Springs: An example from Pocahontas County, West Virginia. In Environmental Karst, Dougherty, P.H., ed. Geospeleo Publications, Cincinnati, Ohio, 1983, pp. 3-13.

114. Wu, J.S., Allan, C.J., Saunders, W.L. and Evett, J.B. "Characterization and Pollutant Loading Estimation for Highway Runoff." *Journal of Environmental Engineering*, American Society of Civil Engineers, Vol. 124, No. 7, July, 1998. pp. 584-592.

115. Wu, K., Chen, B., Yao, W., and Zhang, D. Effect of Coarse Aggregate Type on Mechanical Properties of High-Performance Concrete. Cement and Concrete Research, 31(10), 2001. pp. 1421-1425.

116. Wu, T., Gnecco, I., Berretta, C., Ma, J. and Sansalone, J., "Stormwater Phosphorus Adsorption on Oxide-Coated Media," Proceedings of WEFTEC2008, Water Environment Federation, Chicago, IL, October 2008, 16 pages.

117. Ying, G. and Sansalone, J. "Granulometric Relationships for Urban Source Area Runoff as a Function of Hydrologic Event Classification and Sedimentation," Water, Air, & Soil Pollution, Vol. 193, No. 1, 2008. pp. 229-246.

118. Ying, G. and Sansalone, J. "Particulate Matter and Metals Partitioning in Highway Rainfall-Runoff", Frontiers of Environmental Science & Engineering in China, Vol. 4, No. 1, 2010. pp. 35-46.

119. Ying, G. and Sansalone, J., "Transport and Solubility of Hetero-disperse Dry Deposition Particulate Matter Subject To Urban Source Area Rainfall-Runoff Processes," *Journal of Hydrology*, Vol. 383, No. 3-4, 2010. pp. 156-166.

120. Yousef, Y.A.; Harper, H.H.; Wiseman, L.P.; and Bateman, J.M., "Consequential Species of Heavy Metals in Highway Runoff." Transportation Research Record 1017, 1985. pp. 56-62.